Molecular function of RIM1α: role of phosphorylation sites

Dissertation

zur

Erlangung des Doktorgrades (Dr. rer. nat)

der

Mathematisch-Naturwissenschaftlichen Fakultät

der

Rheinischen Friedrich-Wilhelms-Universität Bonn

vorgelegt

von

Johannes Alexander Müller

aus

Bonn

Bonn, Juli 2019

Angefertigt mit der Genehmigung der Mathematisch-Naturwissenschaftlichen Fakultät der Rheinischen Friedrich-Wilhelms-Universität Bonn.

1. Gutachter: Prof. Dr. Susanne Schoch McGovern

2. Gutachter: Prof. Dr. Thorsten Lang

Tag der Promotion: 09.10.2019

Erscheinungsjahr: 2020

Declaration:

Parts of this thesis are already published in:

Engholm-Keller K, Waardenberg AJ, **Müller JA**, Wark JR, Fernando RN, Arthur JW, Robinson PJ, Dietrich D, Schoch S, Graham ME. *The temporal profile of activity-dependent presynaptic phospho-signalling reveals long-lasting patterns of poststimulus regulation.* PLoS Biology 2019; 17(3): e3000170

Marvin JS, Scholl B, Wilson DE, Podgorski K, Kazemipour A, **Müller JA,** Schoch S, Quiroz FJU, Rebola N, Bao H, Little JP, Tkachuuk AN, Cai E, Hantman AW, Wang SS, DePiero VJ, Borghuis BG, Chapman ER, Dietrich D, DiGregorio DA, Fitzpatrick D, Looger LL. *Stability, affinity, and chromatic variants of the glutamate sensor iGluSnFR*. Nature Methods 2018; 15(11): 936-939

For a full list of publications, book chapters and conference presentations (also including works, that are not part of this thesis) please refer to section 11 (Publications).

Finally.

Index

List of Abbreviations

A	
A	alanine (mutation)
AMPA	α-amino-3-hydroxy-5-methyl-4-isoxazolepropionic acid
AP	action potential
approx.	approximately
a.u.	arbitrary unit
AZ	active zone
B	
BP	band pass
C	
$CaCl_2$	calcium chloride
CamK	calmodulin kinase
cAMP	cyclic adenosine monophosphate
CAZ	cytomatrix at the active zone
cDKO	conditional double knock-out
cm^2	square centimeters
Co^{2+}	cobalt
CO_2	carbon dioxide
ctrl.	control
°C	degree Celsius
D	
dCre	delta Cre-recombinase
DF/F	relative change in fluorescence
DG	dentate gyrus
DIV	days in vitro
DNA	deoxyribonucleic acid
E	
E	glutamate (mutation)
e.g.	example given
EM	electron microscopy
EM-CCD	Electron multiplying charge-coupled device
EPSP	excitatory postsynaptic potential
et al.	et alia
etc.	et cetera
F	
fEPSP	field EPSP
FRAP	fluorescence recovery after photobleaching
FRET	Förster resonance energy transfer
G	
GFP	green fluorescent protein
GST	glutathion-s-transferase
H	
h	hour
HEK293T	Human embyonic kindey 293 T cells
Hz	hertz
I	
i.e.	id est
IRES	internal ribosomal entry site
K	
K+	potassium
kDa	kilo Dalton
kDead	kinase dead
KCl	potassium chloride
KO	knock-out
L	
LB	Luria Bertani
LED	Light emitting diode
LP	long pass
LTD	long-term depression
LTP	long-term potentiation
M	
mA	milli ampere
mf	mossy fiber
µg	microgram
$MgCl2_2$	magnesium chloride
min	minute
minusC	deleted C-terminus
µl	microlitre
ml	millilitre
µM	mircomolar
µm	micrometre
mm	millimetre
mM	millimolar
ms	milliseconds
MS	mass spectrometry
mut.	mutation
N	
Na_2HPO_4	di-sodium hydrogen phosphate
NaCl	sodium chloride
nm	nano metre
NMDA	N-Methyl-D-Aspartate
NMJ	neuromuscular junction
ns	not significant

O	
OE	over-expression
P	
PBS	phosphate buffered saline
PCR	polymerase chain reation
PhD	philosophiae doctor
PKA	protein kinase A
PKC	protein kinase C
PP1	protein phosphatase 1
PSD	postsynaptic density
PTM	post-translational modification
p_{ves}	vesicular release probability
px	pixel
R	
RIM	Rab3-interacting molecule
RIM-BP	RIM binding protein
ROI	region of interest
RRP	readily releasable pool
RtP	Resting pool
S	
s	second
SDS	sodium dodecyl sulfate
shRNA	short hairpin RNA
SRPK	serine/arginine-rich protein kianse
SSA (SSB, SSC)	splicing site A (B, C)
struct.	structure
SV	synaptic vesicle
syn.	synaptic
T	
TBS	Tris buffered saline
TRP	total resting pool
TTX	tetrodotoxin
V	
V	volts
VGCC	voltage gated calcium channel
W	
WT	wild-type
Z	
Zn^{2+}	zinc

List of Figures

List of Tables

1 Summary

The chemical synapse is the central point of communication between cells in neuronal systems. The strength of individual synapses is constantly adapted in response to different levels of neuronal activity. This plastic adaptation happens in time scales of milliseconds to hours and even days. So far, the knowledge about the involved molecular processes is limited. Potential mechanisms that could contribute are post-translational modifications, such as phosphorylation. Post-translational modifications are chemical groups that are covalently attached to proteins and can change the proteins intrinsic properties (molecular interactions, folding, charge etc.).

A key player in synaptic transmission and synaptic plasticity is RIM1α, a multi-domain protein located in the cytomatrix at the active zone (CAZ). RIM1α is fundamentally involved in calcium channel clustering, vesicle to calcium channel coupling, vesicle docking, priming and synaptic plasticity. Additionally, it was proposed that RIM1α and protein kinase A (PKA) centrally participate in the generation of presynaptically mediated long-term potentiation. Here, we applied mass spectrometry (MS) together with phospho-enrichment, biochemical methods and live cell imaging to decipher the importance of phosphorylation of RIM1α for synaptic transmission.

We used different imaging tools (FM dye imaging and the glutamate sensor iGluSnFR) and developed assays to screen for phosphorylation sites in RIM1α with functional relevance for synaptic transmission. To this end we verified in FM dye imaging experiments that the knock-out of RIM1α or the ablation of all large isoforms of RIM lead to a reduced release probability that can be rescued by expression of a N-terminally GFP-tagged RIM1α (GFP-RIM1α) fusion protein. Using bioinformatics and phospho-proteomics of stimulated hippocampal neurons we identified a set of potential phosphorylation sites in RIM1α and mutated these to phospho-deficient and phospho-mimetic GFP-RIM1α variants. The mutated GFP-RIM1α variants were expressed in RIM1α knock-out or RIM1/2 conditional double knock-out (cDKO) neurons and rescue efficacy of synaptic release was investigated using FM dye imaging. In total we compared 17 different phosphorylation sites for functional relevance in synaptic transmission with the help of FM dyes. Three of these sites failed to rescue the reduced release probability when rendered phospho-deficient, while one site increased the synaptic release. Furthermore, we show that GFP-RIM1α variants that carry a release relevant mutation, are located in putative synaptic structures, but that their

persistence in the cytomatrix at the active zone is changed. This could point to altered protein-protein interactions at the active zone.

One protein that preferentially bound to phosphorylated RIM1α was Serine/Arginine-rich protein specific kinase 2 (SRPK2). A more detailed investigation of SRPK2 function revealed that this kinase is involved in modification of neurotransmitter release in a RIM dependent manner. We propose that the strength of synaptic transmission scales with the level of SRPK2 in the synapse. We identified three phosphorylation sites in RIM1α that could be necessary to act as phospho-switches to set the SRPK2 dependent synaptic release probability.

Taken together, our data suggest an essential function of phosphorylation of RIM1α for synaptic vesicle release. We could identify several functionally relevant phosphorylation sites in RIM1α and we have evidence that these potentially affect the dwell time of RIM1α in the CAZ, probably by changing protein-protein interactions. Finally, we identified SRPK2 as novel kinase in the presynapse that interacts with RIM1α and is involved in synaptic transmission.

2 Introduction

2.1 Synapses

The human brain is a huge network, composed of millions of neurons interconnected by a highly specialized structure: the chemical synapse. Synapses are formed by a presynaptic terminal and a postsynaptic compartment, separated by the synaptic cleft ([Schoch & Gundelfinger, 2006], see Figure 2.1). Information is passed on from one neuron to the next neuron, mainly unidirectional from pre- to postsynapse. The transmission of information from pre- to postsynapse is based on the fusion of vesicles with the presynaptic membrane leading to the release of neurotransmitters into the synaptic cleft [Südhof & Rizo, 2011].

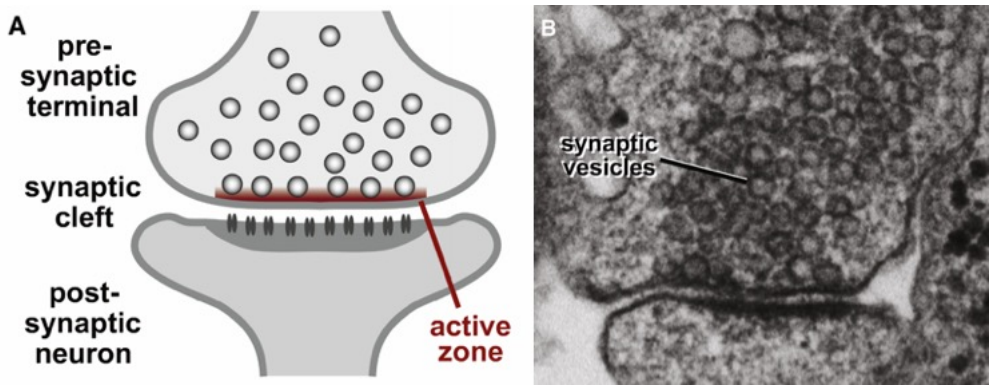

Figure 2.1: Gross architecture of the synapse. (A) Cartoon depicting the main compartments of a synapse. The presynaptic terminal is separated from the postsynaptic neuron by the synaptic cleft. The presynaptic compartment contains vesicles that are translocated to the active zone (AZ) and can release neurotransmitter in to the cleft. Postsynaptically neurotransmitters are sensed by specialized receptors that elicit ionotropic or metabotropic signaling. **(B)** Electron micrograph from a synapse in a cultured hippocampal neuron. The different parts of the synapse, such as vesicles, AZ and postsynaptic density can be clearly distinguished. (modified from [Südhof, 2012b, Kaeser et al., 2011]

Postsynaptically, these transmitters bind to receptors and elicit a metabotropic (second messenger mediated) or ionotropic (ion mediated) response that activate chemical or electrochemical signaling cascades [Smart & Paoletti, 2012]. The precise spatio-temporal release of neurotransmitters and their reception is dependent on a dynamic subset of proteins in the cytomatrix at the active zone (CAZ, presynaptic) as well as in the postsynaptic density (PSD). CAZ and PSD, are persistent over time, but are at the same

time highly dynamic and can be remodeled in response to physiologically relevant stimuli, a process that is called synaptic plasticity [Ziv & Arava, 2014]. Synaptic plasticity is usually bi-directional - synaptic connections can become stronger (larger postsynaptic response) or weaker (lower response)[Castillo, 2012].

2.2 The presynaptic terminal - a highly specialized subcellular compartment

The separation of synapses in a presynaptic and a postsynaptic terminal, that communicate via neurotransmitter diffusion in the synaptic cleft, is counterintuitive: Why is transmission slowed down by a passive diffusion process, when faster electrical signaling (i.e. via gap junctions [Rozental et al., 2000]) is possible? One potential reason is that chemical transmission, with the release of neurotransmitters, introduces several levels of control. This is necessary because any signal processing organism needs to filter an enormous amount of information from the environment and has to extract the essential fraction that is important for survival, only. The presynaptic terminal, in this context, acts as highly specialized filter-system. When an action potential (AP) arrives at the presynaptic terminal, voltage dependent Ca^{2+} - channels open and Ca^{2+} - influx is sensed to trigger the fusion of vesicles. This process is probabilistic - under baseline conditions it acts with a low probability, which means that an AP leads to the fusion of a vesicle only in 10 - 50 % of the cases (example from a hippocampal synapse as referred to in [Rosenmund et al., 1993]). In that way, a low frequency of APs, which might correspond to unrelevant information, is filtered by the presynaptic compartment. To this end the presynaptic terminal acts similar to an electric high-pass filter. The gross architecture (see Figure 2.1) of the presynapse is presetted for this: The pool of vesicles is separated into different sub-pools (for detailed explanations see section 2.4), so that only a fraction of vesicles can be released under baseline conditions at all. From the total amount of releasable vesicles only a tiny amount is ready for direct release upon AP arrival. The releasable vesicles are located at the active zone (AZ) were also Ca^{2+} - channels are located and clustered. The channel arrangement and the channel properties themselves set up microdomains of high Ca^{2+} concentrations ([Simon & Llinás, 1985, Serulle et al., 2007]), that can be sensed by a calcium sensor before Ca^{2+} diffuses away. Thus, the calcium sensor must be positioned in proximity to the Ca^{2+} - microdomains to initiate vesicle fusion. It is obvious, that a correct spatio-temporal arrangement of AP invasion, synaptic vesicle positioning at the AZ and Ca^{2+} - channel clustering is essential for vesicle fusion.

In the other direction, when important information is processed or in dangerous situations, when APs arrive with high frequencies, the presynaptic terminal rearranges itself to pass on information with high

reliability, which means that the release probability is increased (see Sections 2.7 and 2.6). The amount of releasable vesicles is increased, the replenishment of vesicles is assured and the modularities at the AZ (Ca^{2+} - channel number, synaptic vesicle to channel coupling etc.) are adapted.

In the following it will be discussed how vesicle availability is ensured, how the machinery that is responsible for positioning and release of vesicles works and which factors are elementary for the adaptation of the presynaptic terminal. One key player that will be focused on is Rab3-interacting molecule (RIM), that is of central relevance for this thesis.

2.3 Generation, fusion and recycling of synaptic vesicles

Synaptic transmission is highly dependent on the availability of synaptic vesicles that are able to fuse with the plasma membrane and release neurotransmitter into the synaptic cleft. In common agreement these vesicles are part of distinct vesicle pools that arguably harbor different properties with regard to mode of fusion (spontaneous or evoked, [Sara et al., 2005, Ramirez & Kavalali, 2011]) and organizational characteristics (reviewed in [Fowler & Staras, 2015], also see Section 2.4).

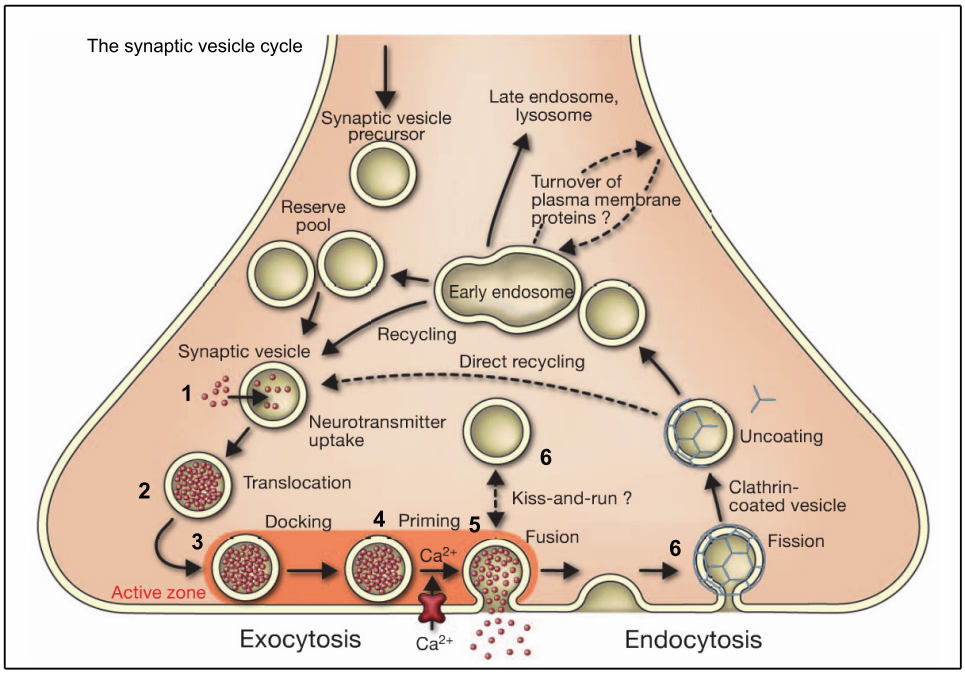

Figure 2.2: Illustration of the synaptic vesicle cycle. Vesicles are organizational separated into different pools. Vesicles that are part of the reserve pool can be translocated to the active zone and be rendered to become fusion competent. These vesicles undergo certain steps: (1) Neurotransmitter uptake, (2) translocation / tethering and (3) docking to the plasma membrane, (4) priming, (5) fusion and finally, (6) endocytosis / retrieval. Afterwards vesicles are directly recycled or are prepared for reuse via an endosomal pathway. Note, this is a simplified illustration. Different steps (e.g. retrieval), might involve different modes or variations. (modified from [Jahn & Fasshauer, 2012])

Even though the steps of a vesicle's lifetime are distinct and separated, the term vesicle cycle has been established and is commonly used [Südhof, 2004]. The steps in this pathway proceed in a distinct order (see Figure 2.2). After neurotransmitter uptake, vesicles are rendered towards a fusion-competent state, a process which is divided in tethering and docking, as well as priming. Afterwards, the actual fusion of vesicles with neurotransmitter release into the synaptic cleft takes place. Finally, the vesicles are internalized again and recycled to be reused in the release process. The main steps in the vesicle cycle and the vesicle pools are discussed in more detail below.

Before vesicles can be released in response to an action potential they need to be spatially positioned, which means that they need to be directed to the active zone to the sites of release. Different studies tried to resolve the ultrastructure of the active zone to get detailed information about the machinery that translocates SVs to the active zone [Pfenninger et al., 1972, Fernández-Busnadiego et al., 2010]. While some results suggested that the active zone is made up by electron dense projections that form a hexagonal grid with intercalated SVs, other results could not verify the existence of electron dense material, but identified "tethers" that connect SVs to the plasma membrane (5-20 nm) and "connectors" between SVs (10 nm). Even though there are differences, all studies propose structures that position SVs correctly spaced at the active zone. Evidence for the molecular nature of theses structures came from a newer study that used genetic knock-outs of CAZ proteins and analyzed the synaptosomes for changes in SVs positioning [Rubén et al., 2013]. Interestingly, the synaptosomes of RIM1α KO mice had significantly reduced synaptic vesicles proximal to the AZ, which points to an important function of RIM1α for tethering of synaptic vesicles.

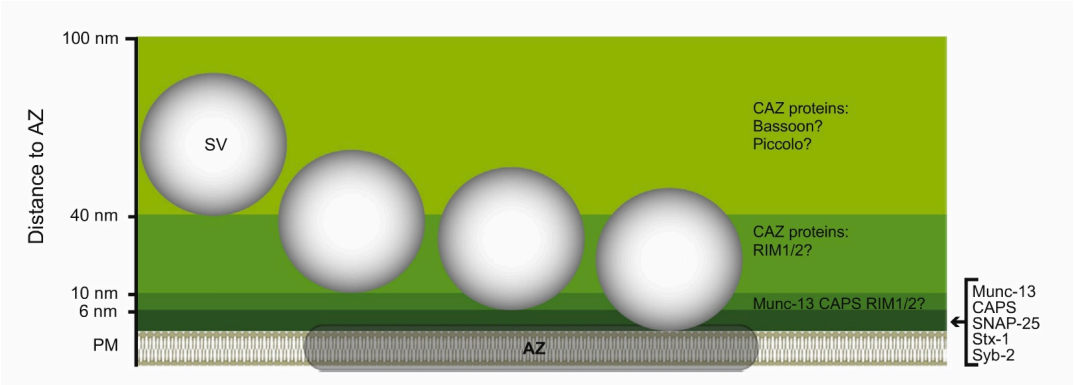

Figure 2.3: Vesicle tethering to the active zone is orchestrated by different proteins. The illustrated model is based on three-dimensional analysis of cryofixed slice cultures [Imig et al., 2014]. Many proteins are involved in a sequential tethering process, to finally place synaptic vesicles (SV) in proximity to the plasma membrane (PM) at the ative zone (AZ) where they can be primed for release. Vesicle size relative to y-axis: 50 nm. (from [Michel et al., 2015])

In 2014, Imig et al. systematically compared the consequence of the loss of key synaptic proteins for the sequential steps of tethering and docking of synaptic vesicles. The study proposes that vesicles

are recruited to the active zone by CAZ proteins (possibly by Piccollo and bassoon) and are tethered in close proximity to the AZ plasma membrane (up to 10 nm). Potential players involved in this step might be RIM1 and/or RIM2. Afterwards, vesicles are pulled even closer (up to 6 nm) by Munc13s, CAPS and potentially other CAZ proteins (Figure 2.3). In a final step the trans-SNARE complex formation takes place, a process also called priming.

Priming is the process that renders vesicles fusion competent. Upon calcium entry, these vesicles are able to fuse rapidly with the plasma membrane and release neurotransmitter in to the synaptic cleft. The key step in priming is the formation of the trans-SNARE complex at the active zone. The trans-SNARE complex is composed of three proteins: VAMP/Synaptobrevin is located on synaptic vesicles and Syntaxin1 as well as SNAP25 are proteins that are anchored to the plasma membrane [Sutton et al., 1998]. Sequentially, Syntaxin1 and SNAP25 bind to each other, forming a complex that is able to bind Synaptobrevin. Upon this formation the α-helices of the involved proteins partially zip up from N-termini to C-termini [Hanson et al., 1997, Becherer & Rettig, 2006].

It has been shown that the formation of the core trans-SNARE complex is dependent on, or facilitated by additional proteins, such as RIM1α [Betz et al., 2001], Munc13 [Augustin et al., 1999, Betz et al., 2001], Munc18 [Gerber et al., 2008] and Complexin1 [Chen et al., 2002]. Munc13 has an essential role in the formation of the trans-SNARE complex and priming since its interaction via its MUN domain with Syntaxin1 probably opens the closed form of SyntaxinI, which is necessary for efficient trans-SNARE complex formation. In Munc13 knock-out studies it has been shown that neurotransmitter release is almost completely abolished when all Munc13 isoforms are absent [Brose et al., 1995, Augustin et al., 1999, Varoqueaux et al., 2002, Varoqueaux et al., 2005].

Munc13a proteins form homodimers via the N-terminal C2A domain [Dulubova et al., 2005], which results in an inactive state of this protein. RIM1α's zinc-finger domain is able to disrupt the homodimerization by binding to the C2A domain, which activates Munc13a. This important function of RIM1α in the priming process was verified by investigation of RIM-deficient synapses, which showed a severe impairment in vesicle priming. The phenotype could be either rescued by expressing a N-terminal fragment of RIM1α or a Munc13 mutation that is constitutively monomeric [Deng et al., 2011].

When the action potential arrives at the synaptic terminal, voltage-gated calcium channels open, and the calcium influx triggers vesicle fusion via the calcium sensor Synaptotagmin1 which is located at the membrane of synaptic vesicles [Brose et al., 1992, Rafael et al., 2001, Chang et al., 2018]. The fusion process takes place within milliseconds after calcium entry [Chang et al., 2018]. The fusion itself does not necessarily need to be a full collapse of the vesicle into the plasma membrane. Also partial collapse, the so-called kiss-and-run, is a potential fusion mode ([Houy et al., 2013, Chanaday & Kavalali, 2017], see Figure 2.4). While in full collapse the vesicle melts to a large extend with the plasma membrane

and is later endocytosed with the help of a clathrin coat or as bulk endocytosis [Houy et al., 2013], in the kiss-and-run mode only a very small pore is opened, before the vesicle is directly internalized again [Alabi & Tsien, 2013]. The mode of fusion defines the endocytotic pathway of the vesicle and thereby the time-course of re-availability for synaptic transmission.

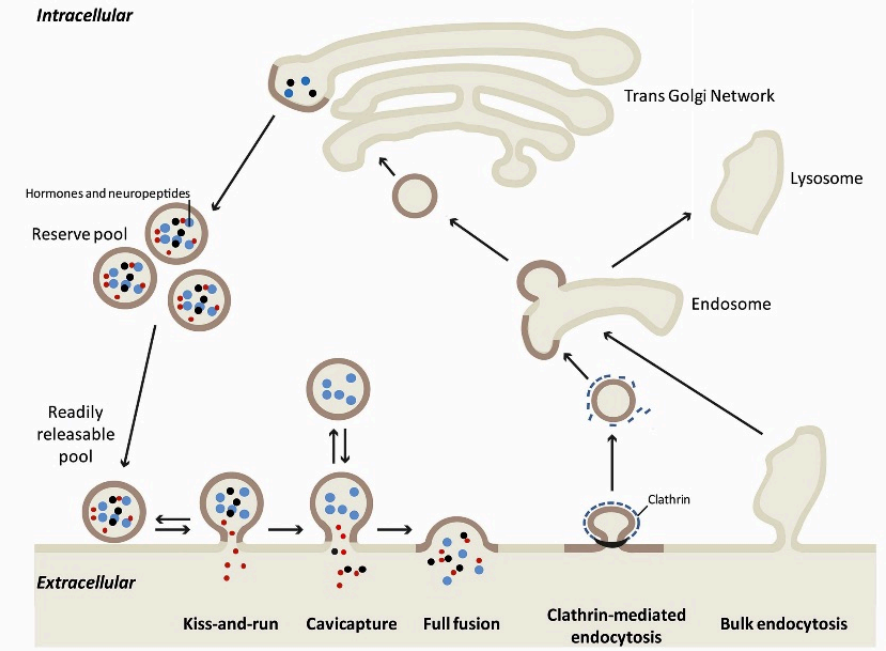

Figure 2.4: Different modes of vesicle exo- and endocytosis. To release neurotransmitters in to the synaptic cleft vesicles need to fuse partially or completely with the membrane. A very fast process is kiss-and-run fusion, where only a small pore is opened to release the neurotransmitter, before the vesicles are recycled. Slower fusion modes are partial or full fusion, which is followed by clathrin mediated or bulk endocytosis, via the endosomal pathway. (modified from [Houy et al., 2013])

The premise for the rapid fusion is a correct positioning of primed vesicles and calcium channels next to each other at the active zone [Wadel et al., 2007]. This is important since the calcium influx sets up a microdomain of high calcium concentration in direct proximity to the opening of the channels [Llinas et al., 1992, Serulle et al., 2007]. Synaptotagmin1 can bind five Ca^{2+} ions in total, but needs at least 3 to 4 Ca^{2+} ions to act in cooperativity to become active [Dodge & Rahamimoff, 1967]. As soon as Synaptotagmin1 senses the elevated Ca^{2+} concentration and binds enough Ca^{2+} ions, it is triggered to interact with the SNARE complex. It was speculated that Synaptotagmin1 could pull at the SNARE complex, which forces the SNARE complex to fully zip up and thereby disrupt the plasma membrane [Tang et al., 2006, Südhof, 2012a]. As a result the phospho-bilayers from the plasma membrane and the synaptic vesicle could fuse, so that the neurotransmitter cargo is released in the synaptic cleft. The fully zippered cis-SNARE complexes are afterwards disassembled by the ATPase NSF and alpha-SNAP [Söllner et al., 1993] and can be reused to prime new vesicles.

Vesicles that released neurotransmitter into the synaptic cleft are afterwards internalized and then re-

cycled, so that they can be re-introduced into the releasable pool of vesicles. Ongoing activity results in constant release of synaptic vesicles, however, synaptic transmission does not arrest under these conditions as the synaptic vesicle pool is not depleted completely [Tomás & Ryan, 2004]. Therefore, synaptic vesicles as well as their proteins and lipids, must be internalized efficiently and in reasonable timescales [Chanaday & Kavalali, 2018]. Many different studies tried to resolve the time course of vesicle retrieval and recycling. The first studies using EM experiments reported time-courses from 20 - 90 s [Miller & Heuser, 1984, Ryan et al., 1996] for the internalization process, whereas studies based on capacitance measurements and FM dye experiments proposed internalization times of about two seconds [Gersdorff & Mathews, 1994, Klingauf et al., 1998, Kavalali et al., 1999]. Newer estimates from improved capacitance measurements [Delvendahl et al., 2016] and fast-freeze EM [Watanabe et al., 2013] range from 100 - 500 milliseconds. What all of these studies lack, is the observation on the single vesicle level. A problem that was solved very recently using the genetically encoded vesicle release reporter vGlut1-pHlourin [Chanaday & Kavalali, 2018]. Using these reporters Chanday et al. (2018) proposed that there are at least three modes of vesicle endocytosis. They distinguish a slow (more than 20 seconds to retrieve vesicles), a fast (5-12 seconds) and an ultrafast (150-250 milliseconds) pathway for vesicle retrieval. The different kinetics of the pathways point to different mechanisms of retrieval. Ultrafast endocytosed vesicles show quantal retrieval - the same number of proteins that were fused are internalized again [Chanaday & Kavalali, 2018]. This is in line with the vesicle fusion mode “kiss-and-run” [Alabi & Tsien, 2013]). Alternatively (or additionally), it is possible that proteins and lipids from a fused vesicle remain clustered in the plasma membrane [Bennett et al., 1992, Willig et al., 2006, Opazo & Rizzoli, 2014]. The classical clathrin-dependent endocytosis via the endosomal pathway potentially applies for the fast and slow retrieval modes.

2.4 Heterogeneity of presynaptic vesicle pools

Though synaptic vesicles appear largely indistinct in electron micrographs (Figure 2.1, [Kaeser et al., 2011]) functional and organizational characteristics support the separation of vesicles in distinct vesicle pools [Fowler & Staras, 2015]. Starting from the whole population of morphological defined vesicles in a small hippocampal synapse (approx. 200, [Harris & Sultan, 1995, Schikorski & Stevens, 1997]) the first separation could be to divide the resting pool (RtP) and the total recycling pool (TRP) [Fowler & Staras, 2015]. The total recycling pool (5 - 23 % of all vesicles [Denker et al., 2011, Marra et al., 2012]) describes the population of vesicles that can be released by a sufficient long stimulation of the synapse, while the resting pool is made up by the remaining fraction which appear immobile even in saturating stimulation scenarios [Fowler & Staras, 2015]. Evidence exists that the TRP may be expanded at the expense of the

RtP [Jung et al., 2014, Fowler & Staras, 2015]. Interestingly, also in the context of this work, the transition from RtP to TRP has been shown to be, next to other mechanisms, kinase and probably phosphorylation dependent (e.g. CDK5, [Kim & Neuron, 2010]). The TRP may be further subdivided into the recycling pool (RP) and readily releasable pool (RRP). The latter has central relevance in rapid and immediate release. It has been estimated to be composed of only a few vesicles (5-15, [Stevens & Tsujimoto, 1995, Dobrunz & Stevens, 1997, Murthy & Nature, 1998]), that are ready for direct release upon action potential arrival. Released vesicles from the RRP are constantly replenished by vesicles from the RP [Guo et al., 2015], this ensures a constant availability of releasable vesicles. Again, it is notable that kinase activity (e.g. PKC, [Stevens & Neuron, 1998, Waters & Smith, 2000]) can expand the RRP and speed up replenishment of vesicles.

Vesicle populations may further be distinguished by whether they need an AP to be released or whether they fuse spontaneously with the plasma membrane (evoked and spontaneous pool, [Sara et al., 2005]). Initially it was proposed that evoked and spontaneous pools are strictly separated. This means that the spontaneous pool undergoes its own endocytic pathway and the evoked pool does the same. During the process pools are not mixed [Sara et al., 2002, Chung et al., 2010]. However, other studies propose at least partial overlap between the pools [Prange & Murphy, 1999, Wilhelm et al., 2010]. The separation of spontaneous and evoked pool applies for excitatory and inhibitory synapses. Even more, the separation is not limited to the presynaptic compartment, but also post-synaptic subpopulations of receptors are activated preferentially by evoked release or spontaneously fused vesicles [Atasoy et al., 2008].

2.5 The active zone

When researchers investigated synaptic terminals, it was obvious that the contact sites between pre- and postsynapse were special, since they appear as electron-dense thickenings in EM images that could be clearly distinguished from other parts of the plasma membrane (Figure 2.1). Presynaptically, this is the area were synaptic vesicles fuse with the plasma membrane and release neurotransmitters into the synaptic cleft. The area is called active zone (AZ) and is characterized by a specialized network of different proteins, known as the cytomatrix at the active zone (CAZ) [Schoch & Gundelfinger, 2006, Südhof, 2012b].

2.5.1 The molecular architecture of the cytomatrix at the active zone

The cytomatrix at the active zone builds a dense protein network that is important for regulated vesicle release (see section 2.3) and has been proposed to be the underlying structure that is responsible for

long-term stability of synaptic sites [Tsuriel et al., 2009, Arava et al., 2011]. While the CAZ in itself is very stable, it simultaneously allows for dynamic adaptions that are crucial for certain forms of plasticity [Mittelstaedt et al., 2010]. The highly enriched core CAZ proteins are RIM, Munc13, ELKS/CAST, RIM-BP, Liprin-α and Piccolo/Bassoon [Schoch & Gundelfinger, 2006, Südhof, 2012b]. Their interaction patterns are depicted in Figure 2.5. The central role of RIM is illustrated by its interaction with almost all core CAZ proteins.

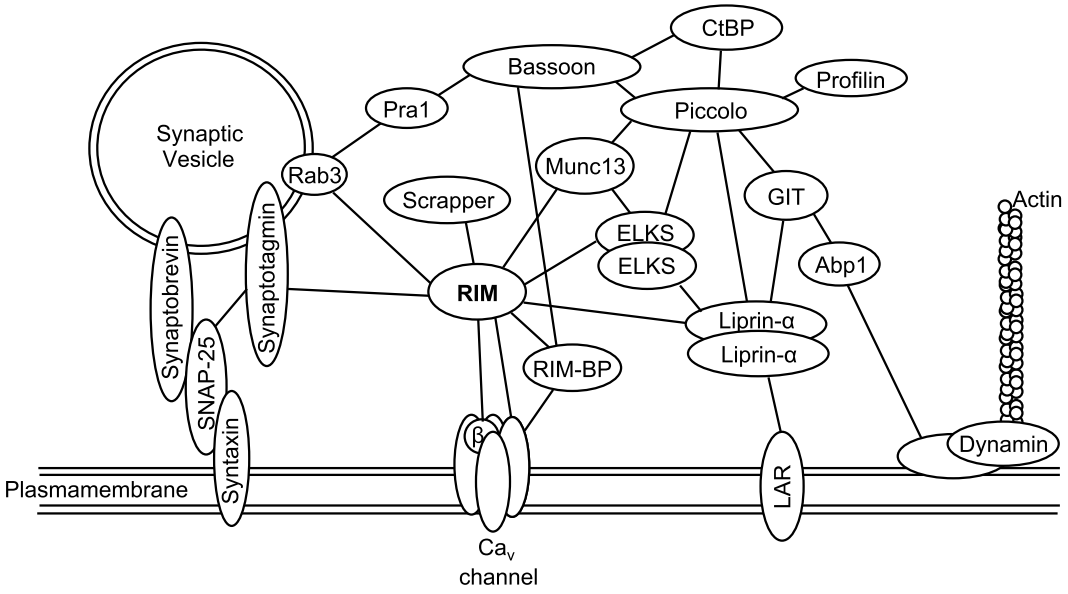

Figure 2.5: Organization of the cytomatrix at the active zone (CAZ). The cartoon illustrates the interactions of the proteins at the active zone. RIM is closely associated with the enriched core CAZ proteins, such as Bassoon, Munc13, ELKS and Liprin-α. Additionally, its function is dependent on binding to Rab3, Synaptotagmins, RIM-BPs and Ca^{2+} - channels (modified from [Mittelstaedt et al., 2010]).

2.5.2 RIM protein family

Rab3-interacting molecule 1 (RIM1) was first discovered as a putative effector of Rab3, a protein located on synaptic vesicles [Wang et al., 1997]. Since the discovery of RIM1 a multitude of studies have shown that the large RIM isoforms (RIM1 and RIM2) are key components of the CAZ (see below). But also the small γ-isoforms seem to play an important role in correct neuronal function, neuronal development and synaptic transmission.

Gene and molecular structure

The mammalian RIM protein family is encoded by four genes. In total seven members are expressed, but due to three splicing sites in the large isoforms [Wang & Südhof, 2003], the diversity of RIM1 and RIM2 is much higher. So far, the functions of alternatively spliced exons are not known. However, all

members of the RIM family share highly homologous domains (see Figure 2.6).

The largest isoforms, RIM1α and RIM2α, consist of a Zn^{2+} - finger domain, a PDZ-domain and two C_2-domains (from N-terminus to C-terminus). β-RIMs (RIM1β and RIM2β) are in principle composed similar but they lack different parts at the N-terminus (see Figure 2.6, [Mittelstaedt et al., 2010]). The shortest members of the RIM protein family are the γ-RIMs (i.e. RIM2γ, RIM3γ, RIM4γ), which only contain one C_2-domain flanked by unstructured, but within the RIM family conserved sequences and a preceding γ-RIM specific sequence [Wang & Südhof, 2003]. To date much data exist about the function of the large RIM isoforms (discussed below), but little is known about the γ-RIMs. However, it seems that RIM3γ and RIM4γ have distinct functions in neuronal development and arborization [Alvarez-Baron et al., 2013] as well as the ability to modulate Ca^{2+} influx [Uriu et al., 2010]. Unpublished data from our workgroup imply a major role in coordination of normal movement.

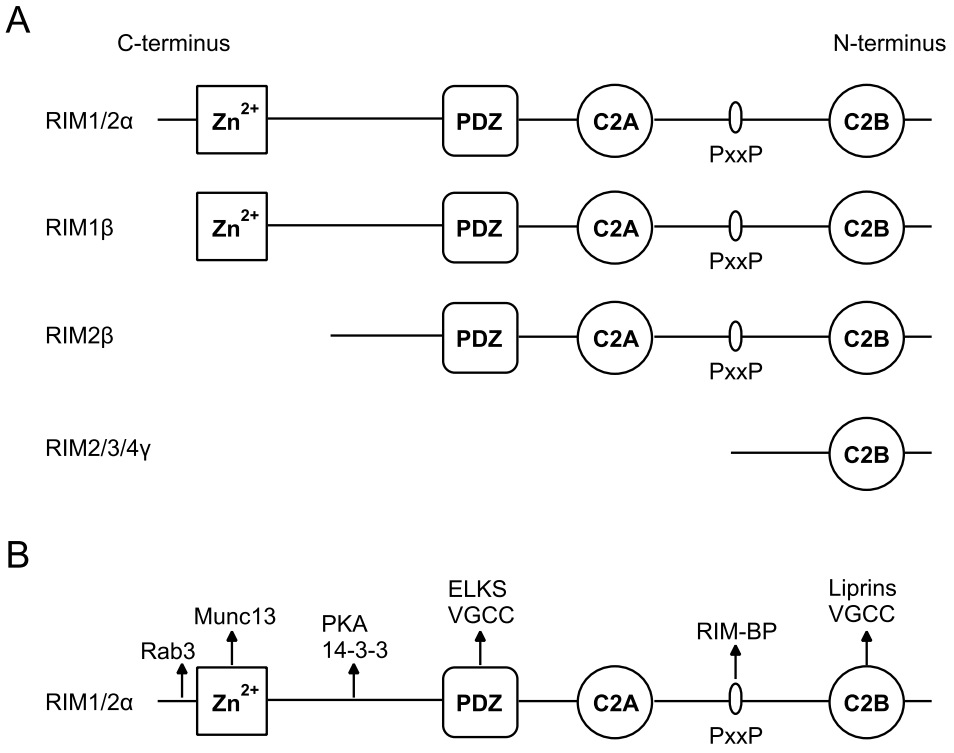

Figure 2.6: Domain structure of RIM protein family. RIM1α and RIM2α are the largest members and compose of all domains: Zn^{2+} - finger, PDZ, C2A and C2B domains. Between the C2 domains a proline - rich region is located. The shortest isoforms are the γ-RIMs which only consist the C2B domain and an isoform specific N-terminal sequences (modified from [Mittelstaedt et al., 2010]).

Interaction partners and molecular functions of RIM1α

RIM1α was named after the first interaction partner that was described, Rab3, a vesicular protein that interacts with a region in front of the Zn^{2+} - finger domain of RIM1α [Wang et al., 1997]. The interaction of Rab3 and RIM1α is of particular importance since it links SVs to Ca^{2+} - channels. Specifically, P/Q-type

and N-type channels probably interact with the PDZ domain of RIM1α [Kaeser et al., 2011]. Another important interaction that is frequently described is the binding to Munc13a [Betz et al., 2001]. Munc13a, as an essential priming factor needs the interaction with RIM1 to disrupt its homodimerization, which renders Munc13a active for vesicle priming [Deng et al., 2011]. RIM1 also interacts with Piccolo [Shibasaki et al., 2004, Etsuko et al., 2004], Bassoon [Etsuko et al., 2004], ELKS [Ohtsuka et al., 2002], RIM-BP [Wang et al., 2000] and Liprin [Schoch et al., 2002]. All of these interactions are believed to play a role in scaffolding. However, at least the interaction with RIM-BP additionally stabilizes the SV / Ca^{2+} - channel positioning, since RIM-BP itself is also able to bind Ca^{2+} - channels and Bassoon [Davydova et al., 2014]. The interaction with the large AZ protein Bassoon may influence vesicle tethering, which was supported by the finding, that less SVs are proximal to the active zone in RIM1α KO synaptosomes [Rubén et al., 2013]. It is remarkable that RIM1 interacts with all CAZ enriched proteins. Therefore, it is not surprising, that RIM1α KO and RIM1/2 DKO (which is lethal and can only be investigated as conditional knockout [Schoch et al., 2006, Kaeser et al., 2011]) neurons exhibit multiple deficits. Maybe the most often mentioned deficit, is a considerable reduction in release probability [Castillo et al., 2002, Schoch et al., 2002, Calakos et al., 2004, Lu et al., 2006, Fourcaudot et al., 2008, Kaeser et al., 2008b, Han et al., 2011]. This can be explained by a reduced vesicle to Ca^{2+} - channel coupling (RIM KO neurons show a reduction in calcium influx and calcium channel coupling, [Han et al., 2011, Fourcaudot et al., 2008, Kaeser et al., 2011]). Still, other reasons for the reduced release probability, such as an impairment of the release machinery in general, for example a decrease in Ca^{2+} sensitivity might exists [Han et al., 2011]. RIM1 depletion was also suggested to reduce spontaneous release events [Kaeser et al., 2008b].
RIM1α plays a crucial role in synaptic plasticity. While short-term plasticity is altered accompanied by the changed release probabilities [Schoch et al., 2002, Fourcaudot et al., 2008, Kaeser et al., 2008b], it is interesting that presynaptic long-term plasticity in different synapses can be abolished completely in the absence of RIM1α [Castillo et al., 2002, Chevaleyre et al., 2007, Pelkey et al., 2008, Fourcaudot et al., 2008, Lachamp et al., 2009]. This phenomenon has been shown to be PKA dependent [Castillo et al., 2002, Fourcaudot et al., 2008, Pelkey et al., 2008].
Notably, the above mentioned functions of RIM apply in most cases for excitatory and inhibitory synapses, likewise.

Post-translational modifications of RIM1α

To date most studies focused on the general function of RIM1. Our understanding of the effects of post-translational modifications on RIM1α and the molecular consequences are very limited. When it was shown that RIM1α and PKA are both essential for mossy fiber long-term potentiation (mfLTP) in the hippocampus [Castillo et al., 2002, Castillo, 2012] it was very tempting to assume that RIM1α's

phosphorylation is necessary for fast induction of plasticity [Lonart et al., 2003]. Indeed, it was proven that RIM1α is a substrate of PKA with two perfect consensus sites - one located between Zn^{2+}-finger and PDZ domain, and one located at the very end in direct proximity to the C-terminus (see Figure 2.7, [Lonart et al., 2003])

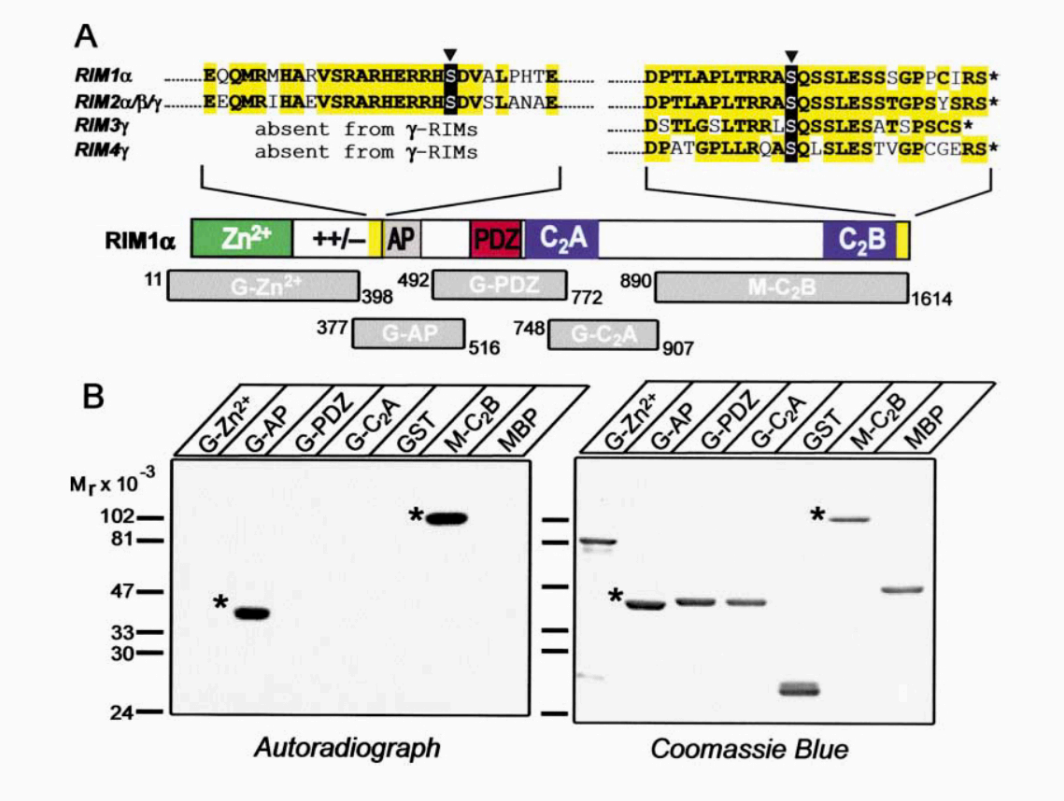

Figure 2.7: RIM1α contains two PKA consensus sites and is phosphorylated at both of them *in vitro*. **(A)** Alignment of RIM isoforms and illustration of the location of PKA consensus sites. The serine in the first consensus site is only conserved in RIM1 and RIM2. It is located between Zn^{2+}-finger and PDZ domain at position S413. The C-terminal serine is conserved in all isoforms and is located after the C_2B-domain almost at the end of the protein at position S1600 (Uniprot Accession No.: Q9JIR4) . **(B)** The RIM fragments were incubated with ATP and the catalytic subunit of PKA. Both fragments that contain the consensus sites are identified in the autoradiograph to be phosphorylated (*). [Lonart et al., 2003]

In vitro, PKA phosphorylates serine residues in both consensus sites of RIM1α (Figure 2.7 B) and subsequent experiments suggested that phosphorylation of S413, but not S1548 (S1600 in rat, uniprot.org accession number: Q9JIR4 as used in this study), has major implications for LTP in cerebellar mossy fiber synapses [Lonart et al., 2003]. The phospho-switch for RIM-dependent plasticity seemed to be found, but follow up studies failed to reproduce a S413 dependent plasticity [Kaeser et al., 2008a, Yang & Calakos, 2010]. Therefore, still no explicit phosphorylation site links RIM1 phsophorylation to the induction and maintenance of synaptic plasticity.

Next to phosphorylation, other post-translational modifications exist, that might influence the function of RIM. For example, SUMOylation of K502 in RIM1 has been shown to have relevance for presynaptic

vesicle release. SUMOylation of K502 appears independent of neuronal activity and does not contribute to normal distribution of RIM1 in neuronal structures. However, when K502 is mutated to arginine and can not be SUMOylated anymore, a marked decrease in evoked SV exocytosis was seen. The effect was linked to a reduction in calcium entry as result of impaired P/Q-type Ca^{2+}-channel clustering [Girach et al., 2013].

2.6 Ca^{2+}-channels and -influx are determinants of vesicle release

Fundamental to all communication between neurons is the release of vesicles at the chemical synapse. As already mentioned, the release of neurotransmitter is tightly controlled by an interplay of proteins in the presynaptic active zone and the localization and clustering of Ca^{2+} channels. The release of a vesicle is probabilistic, with a probability that one vesicle is released when an AP enters the synaptic terminal of around 10-50 % [Rosenmund et al., 1993]. The so-called synaptic release probability was set by Bernard Katz into a framework that is mainly defined by the probability that one vesicle is released (the so-called vesicular release probability) p_{ves} and the number of release sites N [del Castillo & Katz, 1954, Dittman & Ryan, 2019]. The synaptic release probability is highly variable when comparing different synapses, even at the same axon [Branco et al., 2008, Ermolyuk et al., 2012]. Another interesting phenomenon is that the trial-to-trial release probability in the same synapse is not set, but underlies stochastic effects [Dittman & Ryan, 2019].

p_{ves} is highly dependent on the influx of Ca^{2+} ions into the presynaptic terminal. In the 1930's T.P. Feng was able to show that already small changes in extracellular Ca^{2+} concentration led to serious changes in the postsynaptic responses at the neuromuscular junction [Dittman & Ryan, 2019]. The main Ca^{2+} sensor in the CAZ, Synaptotagmin1, triggers release on the cooperativity of three to four Ca^{2+}ions [Dodge & Rahamimoff, 1967]. On each vesicle there are around 15 Synaptotagmin1 molecules [Takamori et al., 2006], each with multiple C2 domains for Ca^{2+} binding [Chapman, 2008], creating the basis for the aforementioned necessity of Ca^{2+} cooperativity [Dittman & Ryan, 2019]. The high Ca^{2+} dependence of vesicle release might explain the stochastic fluctuations in trial-to-trial release, when there are certain variations in binding of $Ca^{2+}$to Synaptotagmin1 [Dittman & Ryan, 2019].

Since release probability is strongly connected to the presence of Ca^{2+}, it is obvious that localization of voltage gated Ca^{2+}-channels (VGCCs) in proximity to the release sites and the release machinery is a crucial factor. VGCCs are clustered at release sites and it was shown that the cluster number correlates with p_{ves} at this site [Scimemi & Diamond, 2012, Sheng et al., 2012]. The opening of VGCCs as response to an AP, builds up a very transient microdomain with a Ca^{2+} concentration elevated to 10-100 µM [Bollmann et al., 2000, Schneggenburger & Neher, 2000, Wang et al., 2008] which is large enough to

trigger synaptotagmin dependent SV release [Körber & Kuner, 2016]. The distance between SVs and VGCCs is a determinant of the p_{ves} since it decides, whether a SV (and the sensor on its membrane) is located within a Ca^{2+} microdomain. To date difference SV to VGCC distances were reported: they range from 5 nm (reported in some calyx of held preparations, [Chen et al., 2015]) to 75 nm (hippocampal mossy fiber synapses, [Vyleta & Jonas, 2014]). Clustering, localization and SV to VGCC coupling relies on proteins in the CAZ. Of central involvement for this process is RIM which on the one hand binds Rab3 on SVs [Wang et al., 1997] and on the other hand P/Q and N-Type VGCCs via its PDZ domain [Kaeser et al., 2011]. RIM itself therefore acts as molecular bridge between SVs and VGCCs. Additionally, RIM is supported by other proteins in the CAZ to set p_{ves}. RIM-BP is able to bind RIM and P/Q-type Ca^{2+} channels in a bassoon dependent manner. Loss of the RIM-BP/bassoon interaction replaces P/Q-type channels by N-type channels [Davydova et al., 2014]. Thus, the recruitment of specific channel sub-types depends on correct interactions between CAZ proteins.

Another modulator of the abundance of Ca^{2+}ions after AP arrival is the conductance of Ca^{2+} ions trough the Ca^{2+} channels. It can be distinguished between direct and indirect modulation of this parameter [Körber & Kuner, 2016]. Direct modulators within the CAZ for example are ELKS proteins [Südhof, 2012b] and Munc13a [Calloway et al., 2015], which do not affect the abundance of Ca^{2+}channels, but influence their functional properties. Additionally, the influx history of Ca^{2+} itself influences Ca^{2+} conductance. This phenomenon is associated with CaM, which binds to the C-terminus in a Ca^{2+} dependent manner and promotes channel inactivation during prolonged depolarization [Lee et al., 1999, Lee et al., 2000, Lee et al., 2002]. Another aspect, that determines the opening probability and thereby the conductance of the Ca^{2+}ions, is the surface charge density near Ca^{2+}channels. The surface charge density is set up by the ion distribution near the extracellular membrane. An increased amount of cations at the extracellular membrane leads to a more negative resting potential, which decreases the opening probability of Ca^{2+} channels.

In summary, the synaptic release probability is defined by the probability that a vesicle is released (p_{ves}) and the amount of release sites N. p_{ves} itself is highly dependent on the concentration of Ca^{2+} near the SV and Synaptotagmin1.

2.7 Presynaptic plasticity

In general plasticity is referred to a process that changes the current state of the brain, its neurons and the synapses. It is believed that synaptic plasticity is the underlying mechanism that allows to form memories and lead to adaptations in response to new experiences and environmental changes. Fundamentally, synaptic plasticity leads to a change in the strength of synaptic transmission. This change can last for

short time periods, in the millisecond range (short-term plasticity), or even persist over hours, days and weeks (long-term plasticity) [Citri & Malenka, 2007]. Synaptic plasticity is a phenomenon that can be observed at excitatory and inhibitory synapses [Castillo, 2012]. The modes of induction were shown to be presynaptic and / or postsynaptic and cover a wide range of changes in synaptic properties, such as changes in vesicle pool sizes, enlargement of the AZ, amount of Ca^{2+}influx, number of post-synaptic glutamate receptors, size of PSD and many more [Citri & Malenka, 2007]. Long-lasting changes in synaptic efficacy are often linked to changes in protein levels [Scharf et al., 2002], including the synthesis or degradation of proteins, depending on the type of plasticity. However, an intriguing possibility to initiate long-term changes instantaneously or maintain these changes over time are post-translational modifications (as partly discussed in section 2.5.2). Such protein modifications do not exclude the possibility of accompanied control of protein levels, because post-translational modifications themselves can be triggers for protein aggregation or degradation [Sambataro & Pennuto, 2017].
A thorough discussion of synaptic plasticity would exceed the scope of this thesis, therefore the following description aims to give an overview that sets a framework for the understanding of certain aspects of this thesis.

2.7.1 Short-Term Synaptic Plasticity

Changes in the strength of synaptic transmission that last only for milliseconds to seconds, mostly during ongoing transmission events are commonly referred to as short-term plasticity. The net effect of short-term plasticity is a transient change in neurotransmitter output [Regehr, 2012]. In general, it is differentiated between short-term facilitation and depression of synaptic release [Regehr, 2012].
Temporal very restricted changes in neurotransmitter release are direct adaptations of the presynaptic terminal to a certain set of activity. As discussed earlier, presynaptic terminals act under baseline conditions, when release probability is low, as high-pass filters. When synapses with low release probability are exposed to sustained activity (increased frequency) an effect known as facilitation takes place. Neurotransmitters are released with higher efficacy. However, this process is bi-directional: When release probability is high, sustained activity leads to a rapid depression [Abbott & Regehr, 2004]. Facilitation in case of low release probability and depression in cases with high release probability are commonly observed phenomena, which can be found to a certain extent during any ongoing synaptic transmission.

2.7.2 Presynaptic Long-Term Plasticity - LTP and LTD

Presynaptic long-term potentiation (LTP) is characterized by an increase in presynaptic neurotransmitter release, while presynaptic long-term depression (LTD) underlies the opposite, a long-lasting decrease

in neurotransmitter release [Castillo, 2012]. LTP and LTD can be formed at excitatory and inhibitory synapses (the later then called iLTP and iLTD). The induction mechanism, may be homosynaptic, entirely mediated by the presynapse or via a retrograde messenger from the postsynapse. But it could also be possible that the induction occurs heterosynaptically, where the signaling starts at the presynaptic or postsynaptic compartment from a entirely different synapse.

Presynaptic long-term potentiation is a phenomenon that can be observed in different parts of the brain, such as the dentate gyrus to CA3 synapse (DG-CA3) in the hippocampus [Nicoll & Schmitz, 2005], the cerebellum [Salin et al., 1996], the thalamus [Castro-Alamancos & Calcagnotto, 1999], the subiculum [Behr et al., 2009], the amygdala [Armentia & Sah, 2007] and the neocortex [Chen et al., 2009]. The molecular prerequisites for LTPs in these areas are very similar: the potentiation can be induced independent of NMDA receptors [Harris & Cotman, 1986], an increase in presynaptic Ca^{2+} concentration is needed [Zalutsky & Nicoll, 1990] and PKA / cAMP signaling is necessary [Weisskopf et al., 1994, Huang & Kandel, 1994]. Normally, Ca^{2+} influx at the presynapse, that is necessary for vesicle release, is mediated by N- and P/Q-type voltage gated Ca^{2+} - channels. However, in presynaptically mediated LTP it seems that R-Type channels are of central relevance, even though they do not contribute much to basal synaptic transmission [Breustedt et al., 2003, Dietrich et al., 2003]. It has to be mentioned, that albeit a presynaptical induction mechanism of these types of LTP has been proposed, evidence exists that retrograde signaling from the postsynapse might be involved or even necessary [Jaffe & Johnston, 1990, Kapur et al., 1998]. Mechanistically, a postsynaptic Ca^{2+} increase would mobilize a retrograde messenger that influences PKA activity in the presynaptic compartment [Castillo, 2012]. Retrograde messengers might include diffusible molecules such as (among others) arachidonic acid [Williams et al., 1989], platelet-activating factor [Kato et al., 1994] and BDNF [Inagaki et al., 2008, Fatma & Lonart, 2008, Meis et al., 2012]. Another possibility is that retrograde signaling is mediated by adhesion proteins spanning the synaptic cleft [Futai et al., 2007, Gottmann, 2008].

It is interesting that DG-CA3 synapses can express presynaptic LTP and LTD, since bi-directional expression of presynaptic LTP and LTD at the same synapse is not very common [Castillo, 2012]. LTD at the DG-CA3 synapse is NMDA receptor independent and was suggested to rely (at least partially) on presynaptic mGluR2 [Yokoi et al., 1996, Tzounopoulos et al., 1998]. Intriguingly, $G_{i/o}$ coupled mGluR2 activation decreases PKA activity [Castillo, 2012], which would point to a reversal mechanism with involvement of the same effector (PKA). However, more recent studies showed that mGluR2s are not sufficient nor necessary for induction of LTD in DG-CA3 synapses [Wostrack & Dietrich, 2009].

RIM1α is of central relevance for neuronal function (as discussed before, see Section 2.5.2 and subsections), but maybe the most striking involvement of RIM1α is its essential function in presynaptically mediated forms of LTP at the DG-CA3 synapse. It was shown that in RIM1α knock-out mice mfLTP was

completely abolished [Castillo et al., 2002]. The molecular, RIM - dependent pathway, is still not clearly resolved, but some other factors have been described that are essential. First of all Rab3A knock-out animals show a similar phenotype with absent mfLTP [Castillo et al., 1997]. Additionally, many forms of LTP, among them mfLTP, have been shown to be dependent on cAMP / PKA activity [Weisskopf et al., 1994, Huang & Kandel, 1994, Lonart et al., 2003]. Finally, Synaptotagmin12 and its phosphorylation site S97 are crucial for the induction of LTP in the mossy fiber synapse [Yea et al., 2013]. RIM1α and Syt12 (at S97) are a PKA substrates [Lonart et al., 2003], and RIM1 and Rab3 bind to each other [Wang et al., 1997], creating a molecular bridge between SV and Ca^{2+} - channels [Müller et al., 2012]. Moreover it was suggested that Syt12 phosphorylation might modulate the Ca^{2+}-triggered release mediated by Syt1 [Maximov et al., 2007]. Taken together, an interplay between all these molecules seem to be necessary for presynaptic mfLTP.

A simple sequential model of the induction of mfLTP might be the following: In a first step it is necessary to activate PKA. As described a potential initiation mechanism is the elevation of presynaptic Ca^{2+} concentration via R-type Ca^{2+} - channels [Dietrich et al., 2003, Breustedt et al., 2003]. The increased Ca^{2+} concentration activates adenylyl cyclase, which catalyzes the production of cAMP. The higher amount of cAMP molecules act on PKA, which becomes more active and phosphorylates RIM1α and other substrates, such as Syt12 which results in modulation of the release machinery or changes in the RRP and finally in an increase of the release probability. In the other direction, when PKA activity is decreased, and RIM1α is dephosphorylated by phosphatases, this would potentially lead to a synaptic depression in the DG-CA3 synapse [Castillo, 2012], which could explain the bi-directional expression of plasticity in the DG-CA3 synapse. However, while fragments of this pathway have been proven in the past, the missing link is a specific phosphorylation site in RIM1α and its molecular consequences on the release machinery that complete the picture of mfLTP and PKA-RIM1α dependence. For cerebellar mfLTP (similar induction and expression as hippocampal mfLTP) it was suggested that S413 in RIM1α is phosphorylated by PKA and that this allows the binding of 14-3-3 adaptor protein, which after all acts on the release machinery to increase the release probability [Lonart et al., 2003, Fatma et al., 2004]. However, these results were proven wrong by other studies that showed that S413 is not necessary for LTP [Kaeser et al., 2008a, Yang & Calakos, 2010]. Thus, the missing link between PKA and RIM1α remains unknown.

2.7.3 Homeostatic Plasticity

In general terms homeostatic plasticity is the ability of neurons to counterbalance destabilizing influences to move back towards the original functional state [Turrigiano, 2012, Fox & Stryker, 2017]. On the level of

synaptic transmission this means, that perturbations are rebalanced by scaling of neurotransmitter receptor expression or changing the amount of neurotransmitter release ([Davis, 2013], see Figure 2.8). The need for homeostatic signaling is obvious: How can memories, behaviors or constant signaling persist over time without mechanisms that stabilize neuronal function in an environment with daily experiential changes [Davis, 2013]?

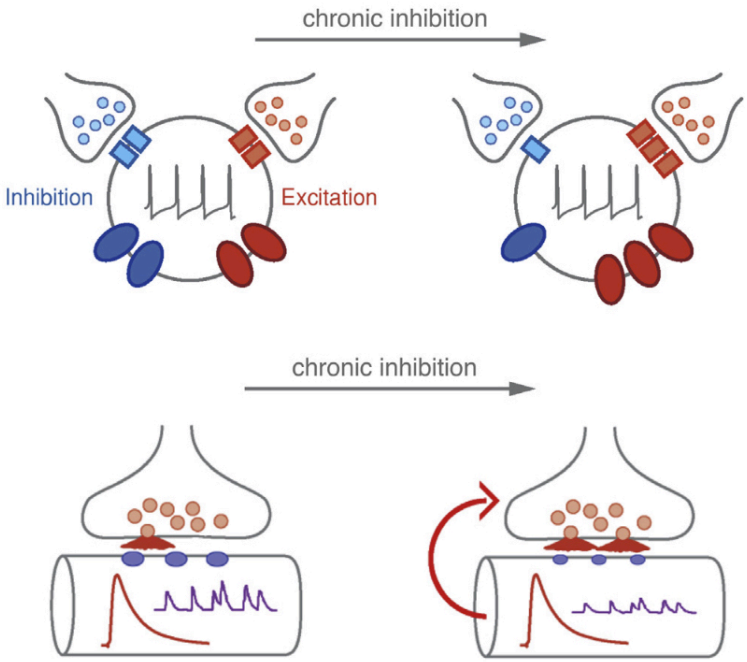

Figure 2.8: Homeostatic signaling offsets the change in neuronal excitability or synaptic transmission back to baseline. Top: When neurons are constantly inhibited, they rescale the ratio of depolarizing ion channels (red ovals) and ion channels that oppose depolarization (blue ovals). As a net result the neurons become more excitable and regain the same firing rate as they had prior to inhibition. Similarly, they may adjust the amount of inhibitory and excitatory postsynaptic receptors to re-balance their excitation state. Bottom: In presynaptic homeostasis, as often seen in the neuromuscular junction of Drosophila, a perturbation of post-synaptic receptors (bue ovals) leads to a retrograde signalling to the presynapse and subsequent increase in neurotransmitter output. As a result the net post-synaptic response (red traces) is set back to baseline, even though the post-synaptic response to individual release events is smaller (blue trace). The increase in neurotransmitter ouput is dependent on an increase in Ca^{2+} - influx and a higher number of release - ready vesicles. (modified from [Davis, 2013])

Some of the first evidence for synaptic scaling came from the neuromuscular junction, where the loss of muscle innervation increased the number of postsynaptic receptors [Berg & Hall, 1975, Sharpless, 1975]. Synaptic scaling has been studied manifold since the first observations in the neuromuscular junction and nowadays there is compelling evidence for synaptic scaling in central mammalian synapses. The first experiments that indicated synaptic scaling in mammalian central neurons were done in cell culture. Network activity was pharmacological pertubated and a compensation in synaptic strength was observed that restored baseline levels [Turrigiano et al., 1998]. In the synaptic scaling process AMPA and NMDA receptor expression and localization is regulated likewise [Watt et al., 2000, Pérez-Otaño & Ehlers, 2005]. The induction of this process takes some time (over hours to days, [Turrigiano, 2011]) and is dependent

on new protein synthesis, either by transcription or local translation processes [Sutton et al., 2006].

As mentioned, another way for homeostatic compensation is the control of presynaptic neurotransmitter release. Pioneer work in this area was done in the neuromuscular junction of *Drosophila melanogaster*, where genetically alterations of postsynaptic receptor expression or use of toxins to block these receptors lead to a homeostatic compensation, which could be linked to a change in presynaptic neurotransmitter release [Davis et al., 1997, Petersen et al., 2000, Müller et al., 2012, Müller et al., 2015]. In strong contrast to postsynaptic adaptation, this form of homeostatic plasticity is rapidly inducible (seconds to minutes) and does not need transcription or translation processes [Frank et al., 2006]. Presynaptically mediated homeostasis has also been observed in mammalian central synapses after alteration of postynaptic excitability [Burrone et al., 2002, Thiagarajan et al., 2005].

The exact modulation of transmitter release and / or receptor expression to precisely offset the perturbation of synaptic transmission is astonishing and raises the question, which mechanisms to sense changes in neuronal activity, exist in the cells. To date a distinct set of sensors that follow changes in neuronal activity remains to be discovered [Davis, 2013], but some potential players have been identified. First of all, calcium-dependent signaling is crucial, because it was shown that CamKK and CamKIV are required for synaptic scaling [Ibata et al., 2008, Goold & Nicoll, 2010]. Additionally, metabolic sensors have been proposed, such as eukaryotic elongated factor 2 (eEF2) [Sutton et al., 2004, Sutton et al., 2007] and TOR-dependent signaling downstream of AMPA receptor inhibition [Henry et al., 2012]. An important role for TOR signaling is supported by findings in the neuromuscular junction of *Drosophila melanogaster,* where block of TOR and S6 kinase pathway abolishes presynaptic homoeostasis [Penney et al., 2012]. Similar as for the sensors, the knowledge of potential effectors and their specific roles in homeostatic signaling remains incomplete [Davis, 2013]. However, some important effectors have been characterized among them RIM-BP [Müller et al., 2015], Rab3 [Müller et al., 2011] and RIM [Müller et al., 2012].

The role of RIM in presynaptic homeostatic plasticity has been studied in the neuromuscular junction of *Drosophila melanogaster* [Müller et al., 2012]. Specific mutations of the single RIM homolog in *Drosophila melanogaster* lead to a disruption of retrograde, homeostatic enhancement of presynaptic neurotransmitter release [Müller et al., 2012]. In general, two processes meet when vesicle release is potentiated in presynaptic homeostatic plasticity: Ca^{2+} influx is increased and the RRP size is enlarged [Davis, 2013]. Even though it is well established that RIM is important for normal presynaptic Ca^{2+} influx and channel clustering [Kiyonaka et al., 2007, Kaeser et al., 2011], it seems to be that the modulation of the RRP is the required function of RIM in homeostatic, retrograde signaling in the neuromuscular junction of *Drosophila melanogaster* [Müller et al., 2012]. An interesting point is, that the modulation of Ca^{2+} influx is still intact in the absence of functional RIM, which implies that other effectors are important

for this modulation. Interestingly, the molecules Rab3 and Rab3-GAP are also involved in presynaptic homeostasis in *Drosophila melanogaster* [Müller et al., 2011] and the interaction of RIM and Rab3 links SV to Ca^{2+} channels [Han et al., 2011, Kaeser et al., 2011]. Conclusively, this might represent a regulated scaffold that brings together the two essential events, of presynaptic homeostatic plasticity [Davis, 2013].

Evidence from mammalian central nervous system synapses propose a special role for RIM1α in presynaptic homeostatic scaling, too. In experiments, where network activity was blocked for 48 hours it was shown that RIM was redistributed to a subpopulation of synapses, which increased the level of RIM in these compartments and thereby elevating the synaptic efficacy after removal of activity blockage [Lazarevic et al., 2011]. This is especially interesting considering the fact that many CAZ components, such as Piccollo, Bassoon, Munc13 or ELKS/CAST were down regulated - an observation that stresses the importance of RIM availability in the homeostatic scaling process. However, RIM1 availability is only maintained, when synaptic function and general activity is possible. This was shown, when instead of inactivity (block of network activity and AP firing), synapses themselves were muted. In this case, RIM1 was degraded via the ubiquitin-proteasome system [Jiang et al., 2010]. Muting of synapses was prevented by previous overexpression of RIM1, giving additional evidence that RIM1 levels are important to specify which type of synaptic scaling (increase of synaptic efficacy or muting) is induced.

2.8 Phosphorylation: a molecular switch to control synaptic function

Proteins fulfill distinct tasks in their specific cellular environment. However, protein function is not static, but activity, enzymatic direction and interactions are highly dynamic and can be changed depending on biological prerequisites. An elegant, yet simple way for proteins to adapt quickly to the present needs are post-translational modifications (PTMs). PTMs are small chemical groups than can be attached or detached covalently by specific enzymes, to amino acid residues within synthesized proteins.

One major PTM, that is frequently linked to activation or deactivation of protein functions, is phosphorylation, were a phosphate group (PO_4) is attached by a kinase to serine, threonine or tyrosine residues within the protein. The phosphate group has a negative net charge, which allows for interaction or repulsion of other charged proteins or parts within the same proteins. This way conformational changes and / or alternation of binding partners are possible [Johnson & Barford, 2003, Xin & Radivojac, 2012, Nishi et al., 2011]. Kinases attach and phosphatases detach phosphate groups to proteins. Activation and inactivation of these enzymes are manifold: Some are constitutively active, while others are activated

by calcium or second messenger signaling [de Jong & Verhage, 2009]. Additionally, phosphorylation by other kinases or autophosphorylation are known mechanisms to change activity patterns of kinases [Nolen et al., 2004, Lučić et al., 2008].

Kinase activity and phosphorylation have been shown to play a major roles in synaptic transmission [Takahashi et al., 2003, Leenders & Sheng, 2005], in setting vesicle pool sizes [Verstegen et al., 2014], in changing the functional spectrum of the calcium sensor [de Jong et al., 2016] and in different forms of synaptic plasticity [Castillo et al., 2002, Sossin, 2007].

2.9 SRPK2 a novel player among presynaptic kinases

While pathways and implications for synaptic function of many common kinases have been topic of several studies, a relatively uninvestigated family of kinases are Serine/Arginine rich-protein specific kinases (SRPKs). The mammalian SRPK family consists of three members SRPK1, SRPK2 and SRPK3 [Gui et al., 1994, Wang et al., 1998, Nakagawa et al., 2005]. Each SRPK has a unique expression pattern (with partial overlap between the isozymes), with SRPK2 mainly expressed in the brain [Wang et al., 1998]. While all mammalian SRPKs have been described to have important functions in different cell types and also in different pathophysiological conditions, the following description focuses on SRPK function in neuronal tissue and disorders.

A initial step in the understanding of SRPK function in the neuronal context came from the neuromuscular junction (NMJ) of *Drosophila melanogaster,* were SRPK79D a homolog of mammalian SRPKs is expressed. Its kinase-domain is around 50-60 % identical with the mammalian variants [Nieratschker et al., 2009]. It was shown that SRPK79D has an important function in synapse formation, since its kinase function is necessary for correct *Bruchpilot* localization and to prevent premature T-bar formation in the peripheral axon [Johnson et al., 2009]. Furthermore, overexpression of SRPK79D negatively regulates synaptic transmission and leads to a substantial reduction of EPSPs at the neuromuscular junction [Johnson et al., 2009].

In mammalian cells SRPKs have been shown to phosphorylate different RNA-binding proteins [Gui et al., 1994, Wang et al., 1998] and thereby contribute to regulation of RNA splicing. However, mammalian SRPKs are also implicated in pathophysiological conditions such as tauopathies (e.g. Alzheimer's disease). For example, SRPK1 and SRPK2 have been shown to be able to initiate sequential hyperphosphorylation of tau by phosphorylating S214 [Hong et al., 2012], which enables stress-induced phosphorylation of T212 and T217 by protein kinase-4 and JNK2 [Yoshida & Goedert, 2006]. Hyperphosphorylation of tau leads to a destabilization of microtubules and an aberrant aggregation of tau, a hallmark of Alzheimer's disease [Grundke-Iqbal et al., 1986]. Interestingly, depletion of SRPK2 from APP/PS1 mice

(an Alzheimer's model), leads to an improvement of typical neuronal deficits of the model (LTP, memory formation and dendritic complexity, [Hong et al., 2012]).

So far, our knowledge of SRPK function is limited to the NMJ of *Drosophila melanogaster* and pathophysiological conditions such as Alzheimer's disease models. Future studies will show the implications of SRPK function in the healthy mammalian neuron.

2.10 Optical tools to measure neurotransmitter release

2.10.1 Membrane staining based methods

Since synaptic vesicles are membraneous structures with associated vesicular proteins, one approach to investigate specific release parameters are staining methods of the phospholipid bilayer or the proteins located in the same. A widely used method to investigate the amount of release and uptake of vesicles is the antibody uptake assay. For example an antibody against the luminal part of Synaptotagmin1 is washed in the extracellular medium and will bind to the sensor, as soon as vesicles fuse with the membrane. The antibody will be taken up, when the vesicles are internalized. Lastly, the bound antibody can be immunostained and the amount of fluorescence can be quantified to estimate the amount of release to a given stimulus [Davydova et al., 2014].

The antibody uptake is a static assay and dynamic experiments are difficult to perform. A more versatile experimental approach are styryl dyes (commonly known as FM dyes). These fluorescent probes are amphipathic and thereby intercalate loosely to cellular membranes. When neurons are stimulated in the presence of FM dyes vesicles that are endocytosed from the membrane will enclose the dye. In another stimulation event, the synaptic vesicles will fuse again with the membrane and the dye is lost to the extracellular space. FM dyes are brightly fluorescent when they are bound to membranes, but this fluorescence is quenched around 100-fold when they enter aqueous solution [Kavalali & Jorgensen, 2013]. Moreover, alteration of the length of the lipophilic tail of the dyes allow for different dissociation times and thus different types of experiments. In general, when stimulation leads to vesicle fusion and dye loss, the rate of the decrease of fluorescence in a region of interest can be approximated as synaptic release probability. FM dye imaging is a simple, yet powerful technique that can be used with different kinds of stimulation, such as potassium stimulation, electrical stimulation or osmotic stimulation (sucrose). FM dyes have been used to study release probability [Ermolyuk et al., 2012], vesicle pools [Sara et al., 2005], maturation of synapses [Mozhayeva et al., 2002] and vesicle cycling [Rizzoli et al., 2003].

2.10.2 pH - sensitive fluorescence reporters

Synaptic vesicles are small, in itself delimited structures with specific properties. One of these properties is the acidic lumen with a pH of approximately 5.5 [Kavalali & Jorgensen, 2013]. This feature is used by pHlourin-probes. pHlourins contain a ph-sensitive GFP variant, that is quenched in acidic pH and becomes bright in neutral pH. One of the first pHlourins was SynaptopHlourin (synaptobrevin-pHlourin) that was engineered by Gero Miesenböck and colleagues already in 1998 [Miesenböck et al., 1998]. pHlourins are attached to the luminal site of vesicular proteins, and are therefore exposed to the acidic lumen of the vesicle during resting periods. Activity leads to the fusion of vesicles and the exposure of the probe to the neutral extracellular space. The increase of fluorescence can be measured and used to read out release parameters. A main advantage of pHlourin probes is the molecular specificity of the signal [Kavalali & Jorgensen, 2013], which is defined by the vesicular protein, that is the carrier of the pHlourin. This way, specific types of synapses (inhibitory, excitatory, Cholinergic, Dopaminergic etc.) can be targeted. pHlourins are also useful to study the recycling of vesicular proteins and their reuse. For instance, synaptophysin and the vesicular glutamate transporter, when used as carriers for pHlourin, show very little surface fluorescence during rest and almost no lateral diffusion after stimulation [Balaji & Ryan, 2007, Granseth et al., 2007, Zhu et al., 2009]. An advantage of pHlourins is that the signal can be read out without changing the intrinsic state of neurons by pre-stimulation. Membrane based methods always need a pre-stimulation protocol for vesicles to take up the dyes. This pre-stimulation can be origin for plastic changes in synapses which influence measurements. This pre-stimulation step is not necessary when pHlourins are used. However, pHlourins have some drawbacks: the signal is mostly normalized to the total maximal fluorescence increase that can be achieved by application of NH_4Cl which neutralizes the membranous compartments and vesicles [Lazarenko et al., 2017]. The total fluorescence then might contain other sources than only the vesicles, which underestimates measurements. Depending on the experimental setup other problems might be signal-to-noise ratios, delays in reacidification of vesicles and toxicity of pHlourin expression by transient transfection or transduction of vectors [Kavalali & Jorgensen, 2013].

2.10.3 Neurotransmitter binding sensors

Early approaches to develop neurotransmitter detecting probes consisted of the generation of FRET (Förster resonance energy transfer) sensors with a glutamate binding protein and fluorescent probes fused to the termini [Okumoto et al., 2005]. Binding of glutamate would bring the fluorescent reporters in proximity and allow FRET. Major problems with the existing FRET based glutamate sensors are low dynamic ranges upon glutamate binding and difficult multiplex imaging due to the use of several wave-

lengths during excitation and acquisition [Marvin et al., 2013].

In 2013, Marvin and colleagues introduced an intensity-based glutamate-sensing fluorescent reporter (iGluSnFR). This single-wavelength indicator can detect increases in glutamate concentrations in the nM to µM range. The sensor is constructed from the *E.coli* GltI protein (periplasmic component of ABC transporter complex for glutamate and aspartate) fused to a circularly permuted eGFP. The protein is localized extracellularly by an IgG secretion signal and a PDGFR transmembrane domain. This way, the protein is present at all parts of the extracellularly exposed site of the cell membrane. Recent alterations of the sensor consisted of the replacement of the cpGFP to a superfolder cpGFP and different point mutations leading to more photo stable and different affinity variants [Helassa et al., 2018, Marvin et al., 2018]. The different affinity variants allow for detection of signals that are either temporally very restricted (low affinity sensor) or show only small increases in glutamate concentrations (high affinity sensor). Different experiments showed the usability of iGluSnFR probes *in vitro* and *in vivo.*

New developments include similar sensors for the detection of the neurotransmitters Dopamine [Patriarchi et al., 2018], GABA [Looger et al., 2018] and Acetylcholine (not published yet, but used in [Kazemipour et al., 2018]).

3 Aims of the Project

RIM1α is of fundamental relevance for synaptic processes such as synaptic transmission and synaptic plasticity. Many different studies investigated the general importance of RIM1α for synaptic function. However, the detailed molecular mechanisms, such as the influence of post-translational modifications, of RIM1α's involvement in synaptic transmission and synaptic plasticity are not resolved in detail to date. Here, we want to investigate the importance of specific phosphorylation sites of RIM1α for synaptic transmission. Therefore, we address the following aims in this study: (1) By means of bioinformatic analysis and phoshoproteomics, we will identify phosphorylation sites in RIM1α. (2) The identified sites will be tested for their functional relevance in synaptic transmission. To this end we will establish screening assays in cultured RIM1α knock-out and RIM1/2 conditional double knock-out neurons. The screening assays will rely on FM dyes and the glutamate reporter iGluSnFR to resolve the influence of phospho-deficient and phospho-mimetic mutations in RIM1α on synaptic release. (3) For phosphorylation sites that are found to be important for synaptic release we aim to resolve underlying mechanisms, such as protein-protein interactions and synaptic persistence. (4) Finally, it will be necessary to characterize specific kinases that are involved in the regulation of functional relevant phosphorylation sites in RIM1α. Accumulating evidence from our lab and from studies in *Drosophila melanogaster* point to a role for Serine/Arginine-rich protein-specific kinase 2 (SRPK2) in the mechanisms mediating presynaptic plasticity. Therefore, we want to probe the hypothesis that SRPK2 is a key protein for presynaptic plasticity and acts upstream of RIM1α in this process by potentially regulating its phosphorylation status.
Overall, this study aims to identify phosphorylation sites in RIM1α, to test their functional relevance for synaptic release, and to find regulating kinases of these sites.

4 Material and Methods

Chemicals were purchased from Sigma-Aldrich (Taufkirchen, Germany) or from the manufacturers and resellers indicated in the methods description. Used materials are mentioned in the text when necessary. List of used primers and antibodies can be found in section 9.9 (List of Antibodies and Primers).

4.1 Molecular Biology

4.1.1 Polymerase Chain Reaction (PCR) and site-directed mutagenesis

Amplification of all DNA in this work was done by standard polymerase chain reaction (PCR). PCR mix contained 100 - 500 ng sample DNA, 1 µl DNA polymerase (e.g. Phusion (Thermo fisher, Waltham, USA)), 1 x polymerase reaction buffer, 3 pM forward primer, 3 pM reverse primer and 3 pM dNTPs. PCR mix was filled up to 50 µl with PCR grade water. Reactions were carried out in a BioRad thermal cycler (Bio-Rad, California, USA). A typical PCR program consisted of initial denaturation (95°C, 30 s), denaturation (95°C, 10 s), annealing (50 - 60°C, 30 s), elongation (68-72°C, 30-600 s), final elongation (68-72°C, 600 s) and infinite hold at 4°C. The steps denaturation, annealing and elongation were sequentially repeated, typically up to 30 times. Amplified DNA was run on an agarose gel (1%), to separate desired DNA from unspecific fragments or source DNA. Afterwards DNA was purified and recovered with Zymoclean^{TM} Gel DNA Recovery Kit (Zymo Research, Irvine, USA).

Point mutations were introduced via site-directed mutagenisis using the above mentioned PCR (but only 18 cycles). For this purpose primers were designed with the desired mutation flanked by approx. 20 nucleotides up- and downstream. After PCR reaction, original vector without mutation (from the bacterial preparation) was digested with *DpnI* and 1x Tango-Buffer (Thermo Scientific, Waltham, USA) at 37°C over night. Finally, DNA was precipitated by solving the PCR mix in 100 % ethanol containing 100 mM sodium acetate. The solution was cooled for 1 hour at -80°C and then centrifuged at 15000 rcf for 1 hour at 4°C. The DNA pellet was washed with 70 % ethanol and centrifuged again for 30 minutes. Finally, the DNA pellet was solved in 5-10 µl water and transformed in to competent bacteria (see Section 4.1.3).

4.1.2 Restriction cloning of DNA fragments and fragmented cloning of RIM1

Restriction of DNA fragments and vectors for subcloning was performed by mixing 1 - 2 µg of DNA with 1 µl of restriction enzymes and appropriate amount of restriction buffer (depending on enzyme 1 or 2 x concentrated). The mix was filled up to 20 µl with PCR grade water. The restriction mix was incubated at 37°C for 3 hours. Vector backbones were additionally incubated with alkaline phosphatase (FastAP, Thermo Fisher) for 15 minutes, to dephosphorylate the vector, which avoids self-ligation. Restricted DNA was purified similar to PCR products as described in section 4.1.1. Restricted vector backbone (100 ng) and DNA to be inserted were mixed in molar ratios of 1:3 or 1:5. T4 DNA-Ligase and T4 Ligase-Buffer (Thermo Fisher) were added and volume was filled up to 20 µl with PCR grade water. The reaction was left over night at room temperature and was directly used for transformation of competent cells (see section 4.1.3).

Due to the size of RIM1α (rat: 1615 amino acids in full length) direct cloning is not feasible. Therefore, our cloning strategy modularized the sequence in four parts. To yield usable restriction sites, some of the junction positions of the four parts had to be changed as indicated in Table 4.1. This resulted in some point mutations. It was tried to obtain silent mutations or changes to amino acids which were conserved in other species at this position.

Table 4.1: Junction sites for cloning of RIM1α. Displayed are nucleotide positions of junctions, alterations of the nucleotide sequence and the kind of introduced mutation.

Junction Position	Orig. Seq.	New Seq.	Mutation	amino acid position
1196-1199	ATGCAC	ATGCAT	His to His, silent	400
2140-2145	CCTGAG	CCTAGG	Glu to Arg, conserved	715
3043-3048	GCCGAT	GTATAC	Ala to Val, conserved	1015
			Asp to Tyr, not conserved	1016

RIM1α fragments were amplified from rat cDNA (as indicated in Section 4.1.1) and cloned into lentiviral backbones.

All cloned DNA constructs were sequenced to verify correct insertion of DNA fragments or point mutations. Sequencing was performed by the company “Eurofins Genomics” (www.eurofinsgenomics.eu) according to the provided instructions.

4.1.3 Transformation of and DNA preparation from competent bacteria

DNA amplification of whole plasmid was done in competent bacteria. For viral vectors containing internal terminal repeats (ITRs) recombinase deficient bacteria were used (*E. coli* XL 10-gold, Agilent, Santa Clara, USA), for all other vectors *E. coli* DH5α bacteria (Thermo Fisher) were used. Bacteria were thawed on ice and 50 µl bacterial suspension was mixed with DNA. After incubating the mix on ice for 30

minutes, bacteria were heat-shocked at 42°C for 45 seconds and then shortly placed back on ice. 200 µl LB-medium was added and bacteria were incubated for 1 hour under constant shaking at 37°C . Bacteria were seeded on agar plates containing ampicillin and incubated over night. Finally, single colonies were picked and inoculated (LB-medium with 100 µg/ml ampicillin) over night for DNA preparation.
Depending on the amount and the purity of DNA, different DNA preparation kits were used (e.g. Endofree Plasmid Maxi Kit, Qiagen, Venlo, NL). All kits were used according to the manufacturers instructions. Note, endotoxin free DNA was needed for virus preparation and primary neuron transfection.

4.2 Cell culture

All cell culture techniques were performed in a workbench with laminar air flow to maintain sterile conditions. If not stated differently, cells were kept in humidified incubators at 37°C and 5 % CO_2.

4.2.1 Human Kidney Embryo (HEK) 293T cell culture

HEK293T cells were used for different purposes in this study (viral production, control expression of cloned plasmid etc.). HEK293T cells were cultured either in T75 flasks or on 10 cm petri dishes up to 80 % confluency. General culture medium was Dulbecco's modifed eagle medium (DMEM, Cat.No.: 41966, Life technologies, Van Allen, USA) containing 10 % FCS and 1 % Penicillin/Streptavidin. Note, HEK293T cells for lentiviral production were cultured in DMEM + Glutamax (Cat. No. 32430, Life Technologies) and 10 % FCS, supplemented with 300 µg/ml G418 (Invivogen, San Diego, USA). This is necessary to select cells for SV40 largeT antigen (expressed on plasmid with Neo-Casette), which is important to yield high virus titer. Prior to transfection, these cells were plated on 10 cm dishes and G418 was removed, because G418 is very toxic for cells without Neo-casette (e.g. neurons in later experiments).
When HEK293T cells reached 80 % confluency in flasks they were passaged by trypsination (5 minutes Trypsin-EDTA (Thermo Fisher) on cells to digest extracellular parts of adhesion proteins) and seeded 1:6 to a new flask.
For Western Blots, Pull-Downs and fluorescence expression controls, HEK293T cells were transiently transfected using the calcium-phosphate method. For lenti-viral particle production, HEK293T cells were transfected with GeneJet transfection reagent (SignaGen, Rockville, USA).

Transient calcium-phosphate transfection of HEK293T cells

Cells were cultured on 10 cm petri dishes and allowed to reach 60 % confluency. Culture medium was replaced by Iscove's modified Dulbecco's medium (IMDM, Cat.No.: 21980, Life Technologies) supple-

mented with 5 % FCS 4 hours prior to transfection. Transfection mix contained 1.1 ml cell culture grade H_2O, 145 µl $CaCl_2$ (2.5 M), 4-5 µg DNA and 1.6 ml Hepes Buffered Solution (HeBS Stock solution contained (in mM): 50 HEPES, 280 NaCl, 1.5 Na_2HPO_4, pH: 7.05). Transfection complex was accomplished by adding HeBS at last, in a drop-wise manner under constant shaking. The mix was added to the cells and incubated for 24 hours. Medium was changed to general DMEM culturing medium and cells could be harvested 48 hours post-transfection.

GeneJet transfection of HEK293T cells

One day prior to transfection 3*10^6 HEK293T cells were seeded on 10 cm cell culture dishes in high glucose DMEM medium (Cat. No. 32430, Life Technologies) supplemented with 10 % FBS. After 24 hours medium was replaced with 6 ml fresh medium containing 10 % FBS. Transfection mix containing 3 ml high glucose DMEM, 40 µl GenJet^{TM} transfection reagent (SignaGen, Rockville, USA) , 7.5 µg packaging plasmid (psPax2, addgene #12260), 5 µg pseudotyping plasmid (pMD2.G, addgene #12259) and 3-4 µg expression plasmid was added to each dish. After 12 hours cells were washed and fed fresh high glucose DMEM containing 10 % FBS.

4.2.2 Primary neuron culture

Preparation of primary neurons

Primary Neurons were isolated and cultured by Sabine Opitz and Lioba Dammer. The protocol to isolate neurons from mouse brains was described before [Woitecki et al., 2016] and consisted of the following steps: Mouse embryos were isolated at E16 - E19. Embryos were decapitated in ice-cold HBSS (Cat. No. 14170, Life Technology) supplemented with 20 % FCS. The meninges was removed and cortices or hippocampi were isolated. Tissue was cut into small pieces, washed 6 x in HBSS (with 20 % FCS) and incubated with 2.5 % trypsin (Thermo Fisher) at 37° C for 20 minutes. After washing (3 x in HBSS + 20 % FCS), 200 µl DNaseI (Sigma-Aldrich, Taufkirchen) was added and tissue was further dissociated by tituration until the solution was homogenous. Finally, BME (Cat. No. 41010, Life Technology) was added, cells were counted and plated on poly-D-Lysine (Sigma-Aldrich) coated coverslips. Medium was replaced after 24 h to neurobasal medium (Cat. No. 21103, Life Technology) and cells were kept in the same medium until use in experiments.

DNA delivery to neurons by transient transfection or viral transduction

Neurons were transfected at DIV2-6 as described before [Köhrmann et al., 1999]. Briefly, neurobasal culture medium was exchanged with pre-incubated (37° C, 5 % CO_2) minimum essential medium (MEM).

Old neurobasal medium was kept under steril conditions in the incubator. Transfection mix contained 60 µl $CaCl_2$ (250 mM), 4-5 µg DNA, 60 µl BES buffered saline (BBS stock contained in mM: 280 NaCl, 1.5 Na_2HPO_4, 50 BES, pH: 7.1). BBS was added slowly at last, while the mix was vortexed. Transfection mix was incubated for 1-2 minutes at RT and then added drop-wise to the cells. Cells were incubated for around 30 - 60 minutes at 37°C and 2.5 % CO_2 until precipitate of transfection complexes was visible. Thereafter, cells were washed twice with HBS buffer and old neurobasal medium was placed back on the cell.

Viral transduction of neurons was used to make sure that most of the cells express the gene of interest. If not stated differently, transduction was performed at DIV4-6 by resuspending 1 µl of viral suspension in approx. 500 µl cell medium. The mix was pipetted drop-wise to the cells.

4.3 Virus preparation

In this study two different types of viral particles were used. For large proteins, such as RIM1α, lenti-viral vectors in a 2 nd generation packaging system (Trono Lab) were used. For smaller or middle-sized proteins, such as SRPK2 or iGluSnFR, recombinant adeno-associated viral particles (rAAV) of serotype 1/2 were produced.

4.3.1 Lenti-viral particles

Production of lenti-viral particles was described before [van Loo et al., 2019]. Briefly, HEK293T cells were transfected as described in section 4.2.1. Cells were then incubated for 72 hours at standard incubation conditions. The supernatant from cells was collected and centrifuged at 3500 rpm for 10 minutes to remove cell debris and dead cells. Afterwards suspension was filtered through 0.45 µm PVDF membrane filters (GE Healthcare, Little Chalfont, UK) and collected in conical ultracentrifugation tubes (Beckmann & Coulter, Brea, USA). A 60 % iodixanol (Opitprep, Sigma-Aldrich) solution was pipetted at the bottom of each tube, to yield two separate layers. Supernatant was ultracentrifuged at 24000 rpm and 4°C for 2 hours in a SW-Ti32 swinging bucket (Beckmann & Coulter, Brea, USA). Afterwards the supernatant was discarded, without disturbing the lower phase and the layer of viral particles at its top. Tubes were filled with TBS-5 (containing in mM: 50 Tris-HCl, 130 NaCl, 10 KCl, 5 $MgCl_2$) buffer and the lower phase was gently mixed with the buffer.

Again suspension was ultracentrifuged as before. Supernatant was discarded completely and pellet was soaked with 50 - 100 µl TBS-5 buffer over night at 4°C. Finally, viral particles were resuspended in TBS-5 buffer, aliquoted and stored at -80°C until use.

4.3.2 Recombinant adeno-associated viral (rAAV) particles

Adeno-associated viruses were produced as described [van Loo et al., 2012]. Plasmid of interest, plasmids containing rep and cap genes (pRV1 and pH21), and adenoviral helper pFΔ6 (Stratagene, La Jolla, USA) were transfected in HEK293T cells as described in Section 4.2.1. Cells were harvested approx. 72 h after transfection. Cells were scraped from petri dishes and pelleted by centrifugation. Pellets were lysed in lysis buffer (50 ml PBS, 50 mM, 150 mM NaCl, 1 % Triton-X 100, 1 protease inhibitor tablet, pH: 7.4) supplemented with 0.5 % sodium deoxycholate (Sigma-Aldrich) and 50 units/ml Benzonase endonuclease (Sigma-Aldrich). Lysate was run on HiTrap^{TM} heparin columns (GE Healthcare) for purification of viral particles. The suspension was concentrated using Amicon ultra centrifugal filters (Millipore) to get a final stock in a volume of about 500µl. Virus purity was validated with Coomassie blue staining of SDS-polyacrylamide gels.

4.4 Biochemistry

4.4.1 Lysis of cells

Lysis of HEK293T cells for control of protein expression or protein-protein interaction experiments was done as follows: Cells were scraped from culture dishes with approx. 300 µl pre-chilled lysis buffer (containing in mM: 50 HEPES, 150 NaCl, 1 % Triton X-100, 1 x Complete Protease inhibitor tablet (Roche, Basel), pH: 7.4) and incubated afterwards for 1 hour on ice. Cell lysate was sonicated 3 x times with 10 second breaks on ice and then centrifuged at 14000 rcf for 5 minutes to pellet cell debris. The clear supernatant was used for further procession (SDS-PAGE, protein-interaction etc.).

4.4.2 Protein synthesis induction and purification

For GST-Pull down assays, bait proteins had to be expressed from a pGEX plasmid coding for glutathione-S-transerase (addgene #119756). pGEX plasmids were retransformed in *E. coli* BL21 DE3 bacteria (Thermo Fisher) and inoculated in LB-Medium (Sigma-Aldrich) supplemented with ampicillin up to a optic density (at 600 nm) of 0.6 to 0.8. Subsequently, protein expression from pGEX plasmid was induced by ITPG (1 mM, Sigma-Aldrich) and protein synthesis was allowed for 3 - 4 h at 37° C on a shaker. Bacteria were pelleted by centrifugation (4500 rcf for 3 h at 4° C) and lysed on ice in bacterial lysis buffer (PBS, 1 x complete protease inhibitor tablet (Roche), 0.5 mg/ml Lysozym (Sigma-Aldrich)) for 20 minutes. Suspension was sonicated and again centrifuged for 1 hour at 4500 rcf and 4° C. The supernatant contained the purified protein and could be used for GST-Pull down assays (see section 4.4.3). Protein induction

was controlled by SDS-PAGE (see section 4.4.4) and Coomassie staining.

4.4.3 GST-Pull down assay

Supernatant from protein purification (see section 4.4.2) was incubated with Glutathion-agarose beads (Sigma-Aldrich) for 1 hour and afterwards washed 5 - 6 x in PBS with protease inhibitor and 0.5 % Triton - X100. The fusion proteins were kept in a 50 % slurry with PBS. To pull down protein of interest, supernatant from HEK293T cell lysis (see section 4.4.1) was incubated with GST-agarose-fusion proteins for 2 hours at 4° C on a rotator. Proteins were pulled down by centrifugation at 1500 rcf and washed 5 x in PBS. Proteins were analyzed using SDS-PAGE and western blotting (see section 4.4.4).

4.4.4 Gel-electrophoresis and western blotting

Cell lysates, purified or isolated proteins were boiled for 5 minutes at 95° C in Leammli-buffer (4 % SDS, 20 % Glycerol, 120 mM Tris-Cl). Protein separation according to molecular weight was done by SDS-PAGE. The expected protein sizes determined the concentration of acrylamid in the separation gel. For example a 8 % running gel was prepared to separate RIM1α (180 kDa) from other proteins. Stacking gel was always prepared with 5 % acrylamid. Gels were run at 60 V while proteins were stacked and at 100 V when protein bands entered running gel. To identify specific proteins, western blotting was performed. Proteins were blotted on a nitrocellulose membrane (GE Healthcare) in a wet blot chamber, at 45 mA over night in a cooling room (4° C). Afterwards, membranes were blocked with 2 % fish gelatine (Sigma-Aldrich) for 90 minutes and primary antibodies (in blocking solution) were incubated for 1 hour. Membranes were washed three times and secondary antibody (1:15000 in blocking solution) was applied for 45 minutes. Finally, membranes were washed three times for 10 minutes and afterwards analyzed on a Odyssey Imaging System (Li-Cor, Lincoln, USA) .

4.5 Mass - spectrometry

Phospho - enrichment and mass spectrometry, as well as subsequent bioinformatical analysis (identification of phospho - sites, KinSwing analysis etc.) was performed by our collaboration partner Mark E. Graham from the Children's Medical Research Institute in Westmead, Australia. Detailed experimental procedures can be found in Engholm-Keller et al., 2019.

4.6 Bioinformatics

For consensus based identification of potential phosphorylation sites in RIM1α we used different websites and tools (GPS 2.1, KinasePhos 2.0, NetPhosK 1.0, PhosphoSitePlus and Scansite 2.0). Internet addresses and accession dates can be found in table 9.1 in the appendix. As reference amino acid sequence of RIM1α we used the rat sequence from uniprot.org (accession number: Q9JIR4). To assist in cloning and intron/exon identification of the cloned RIM1α protein we used ensembl.org genome browser.

4.7 Microscopy and image analysis

4.7.1 Confocal imaging

Some of the experiments (FRAP, FM with potassium stimulation, immunostainings) were performed with a Eclipse Ti confocal microscope (Nikon, Tokio, JP). In live cell imaging experiments a constant perfusion system was set up in the experimental chamber to generate a constant exchange of the imaging buffer (approx. 1 ml/min.). The confocal microscope was equipped with 10 x and 20 x air objectives as well as 40 x and 60 x immersion objectives and standard filters for DAPI, GFP, RFP and Cy5. Laserlines 405, 488, 561 and 658 were available. Detailed imaging settings are described in the appropriate sections.

4.7.2 FM imaging

If not otherwise noted, all FM experiments were carried out with primary hippocampal neurons at DIV13-21. Dye release experiments were performed in modified Tyrode's solution (containing in mM: 150 NaCl, 4 KCl, 2 $MgCl_2$, 2 $CaCl_2$, 10 D-Glucose, 10 HEPES, pH: 7.4). Due to technical and establishing reasons we performed FM experiments with potassium stimulation and with electrical field potential stimulation. Experiments with electrical stimulation were performed with buffer containing additionally 10 µM CNQX (Bio-Techne, Wiesbaden), and 50 µM DL-AP5 (Bio-Techne) to suppress recurrent network activity. During resting/washing steps and image acquisition, cells were constantly perfused with modified Tyrode's solution at 1 ml/min.

FM imaging with potassium stimulation

Loading was performed by stimulation with 90 mM K^+ solution (in mM: 64 NaCl, 90 KCl, 2 $MgCl_2$, 2 $CaCl_2$, 10 D-Glucose, 10 HEPES, pH: 7.4) containing 10 µM FM4-64 (Thermo Fisher) for 90 seconds. Afterwards cells were washed 5 times with modified Tyrode's solution to remove unspecific extracellular

membrane staining. Recording of FM fluorescence was done with the above mentioned confocal microscope. We imaged through the 60 x immersion objective (Plan Apo IR, 1.27 WI, Nikon). Laserline 561, together with a standard Cy5 filter was used to excite FM in the near red spectrum and to get a high photon yield from the long far red emission of FM4-64. Images were acquired at 0.016 Hz (= one image per minute). After 15 frames of baseline, 45 mM K^+ solution (in mM: 109 NaCl, 45 KCl, 2 $MgCl_2$, 2 $CaCl_2$, 10 D-Glucose, 10 HEPES, pH: 7.4) solution was perfused into the reaction chamber and dye loss was monitored for 35 minutes.

FM imaging with electrical stimulation

To load the vesicles with dye, 10 µM FM4-64 in modified Tyrode's solution was pipetted to the cells and dye uptake was induced by application of 900 pulses of low amplitude field stimulation for 90 seconds (10 Hz, 20 mA) with two large platinum/iridium electrodes submerged in the experimental chamber. Residual dye was washed out for approx. 9-10 minutes by constant perfusion before image acquisition was started. Images were acquired with an EM-CCD camera (ImagEM X2, Hamamatsu Photonics, Naka-Ku, JP) with 20 ms exposure time at 0.2 Hz acquisition rate. As light source a stabilized white LED filtered to 550 nm (Cairn, Edinburgh, UK) was used. Experiments were visualized through a 63 x immersion objective with 1.4 NA (Zeiss, Jena) and a custom made FM filter (Excitation: 550/49, Emission: 594 LP, Beamsplitter: 593 LP). After baseline acquisition for 2 minutes, ongoing stimulation (5 Hz, 80 mA) for dye release was triggered and applied for 5 minutes. In a final stimulation step a high frequency stimulation (5 x 100 Hz for 1 s with 10 s rest in between) was applied to verify responding synapses. The remaining fluorescence in regions of interest after final stimulation was defined as unspecific background to be subtracted in image analysis.

FM analysis: Bleaching correction

To estimate the amount of photo-bleaching we applied the following procedure (which was similar for experiments with potassium and electrical stimulation). First we performed experiments with low laser power or LED illumination (we selected intensities so that the FM puncta were just visible) and acquired 11 data points over the full time course of a typical FM experiment. Here, no stimulation challenge was applied. The assumption is that, the low laser power and the few images result a time course that does not contain photo-bleaching. The fluorescence loss over the time course of the experiment solely represents spontaneous dye release (to control that there is no photo-bleaching in this case, we did the same experiment in a very brief time period where we could detect virtually no photo-bleaching). 20 to 40 regions of interest (ROIs) were defined, corrected for the average background in the experiment and

normalized to the average of the data points 1 to 4 of each ROI. The time courses of one experiment were averaged and the mean traces of all experiments (n = 6) were averaged again and fitted to the function

$$f(t) = y_0 + (1 - y_0) * e^{(-\frac{t-t_0}{\tau})} \tag{4.1}$$

The equation represents a mono-exponential decay function, where the amplitude A is substituted to yield y_0 + A =1 and x_0 was fixed to 0. In the next step we acquired time courses with the experimental illumination settings, but again without stimulation. The resulting time course contains photo-bleaching and spontaneous dye loss. ROIs were defined as before and experiments (n=10) were averaged as described. The calculated mean traces ware divided by the fit from the experiments with the lower laser power. This results in a trace that represents the contribution of photo-bleaching to the fluorescence loss, only. Finally, the trace representing the photo-bleaching was fit to equation (4.1) with the parameters y_0 and x_0 fixed to 0. All following FM experiments were corrected for the estimated photo-bleaching by dividing the experimental curves by the fit of the photo-bleaching trace.

FM analysis: Fitting of dye loss with sum of two exponential decay functions

As discussed in section 2.4, vesicles in the presynapse may be subdivided into distinct vesicle pools. These vesicle pools are defined according to functional or organizational characteristics. Considering the pool of vesicles that can be released, a common distinction is the separation into vesicles that can be spontaneously released and vesicles that are released as response to action potentials (evoked release). Previous studies have proposed that these pools are strictly separated - which means that during recycling spontaneously released vesicles and vesicles that are released after stimulation do not intermix [Sara et al., 2002, Chung et al., 2010]. However, this view was partly revised and at least partial overlap of the two types of vesicles was proposed [Wilhelm et al., 2010].

Here, we consider the two pools to release vesicles independent of each other. However, from our data (during baseline acquisition there is a considerable loss of dye, but see Section 9.1), we assume an exchange of vesicles between the pools after loading. This means, that vesicles that are loaded by stimulation can afterwards become vesicles that are released independently and spontaneously and vice versa.

Taking into account the described two pool assumption, the FM dye loss can be explained by the sum of two exponential functions:

$$f(t) = F * (y_0 + A_{sp} * e^{(\frac{-t}{\tau_{sp}})} + (t - t_{ev} >= 0) * A_{ev} * e^{(\frac{-(t-t_{ev})}{\tau_{ev}})} + (t - t_{ev} < 0) * A_{ev}) \tag{4.2}$$

The first part of the equation describes the spontaneous loss, which is ongoing during the whole experiment and is mainly described by the Amplitude A_{sp} of the spontaneous pool and the exponential decay which is defined by the time constant τ_{sp}. The second part of the equation describes the evoked release. While the Amplitude A_{ev} of the evoked pool is constant before stimulation (t-t_{ev} < 0), the decay is exponential with the onset of stimulation (t-t_{ev} >= 0). As in the spontaneous decay, the evoked decay is defined by its Amplitude A_{ev} and the time constant. A_{sp} and A_{ev} together define the total pool and should sum up to 1 if all loaded vesicles can be released. The factor F at the beginning accounts for the absolute fluorescence of a ROI. y_0 is the final fluorescence level. If all dye can be released then this should approach zero. If dye retain in the synaptic structure this value levels above zero. The rates of release are calculated by $1/\tau$ and are direct read-outs for the synaptic release probability.

FM analysis: General procedure

Image analysis was carried out with Image J 1.51 (measurement of fluorescence values) and Igor Pro 7.0 Software (fitting of fluorescence decay). Image Stacks were registered with StackReg Plugin in ImageJ. Per experiment 20-40 (potassium experiments) or 40-80 (electrical stimulation) ROIs were selected. Background subtraction was performed by subtraction of the final fluorescent value (after 100 Hz stimulation) in electrical stimulation experiments. In the experiments with potassium stimulation background ROIs (positions with no fluorescence) were defined and their fluorescence values were averaged. The average background was multiplied by the size of individual synaptic ROIs and then subtracted from the summed fluorescent value at each time point in each individual ROI. Time-courses were bleaching corrected as described. The time course of each ROI was fitted with the described sum of two exponential decay functions to read-out the evoked and spontaneous release rate, as well as the absolute loading and relative contributions of vesicle pools. For details to bleaching correction and fitting procedure see Sections 4.7.2 and 4.7.2.

4.7.3 iGluSnFR Imaging

iGluSnFR image acquisition

iGluSnFR experiments were performed in the same setup as FM experiments with electrical stimulation (see Section 4.7.2). For iGluSnFR imaging a standard GFP filter cube (Emission: 470/40, Excitation: 525/50, Beamsplitter: 495 LP) and a blue LED (470 nm) were used. Imaging settings were 20 ms exposure time and 200 x EM gain. LED power was set in each experiment to yield good photon count and acceptable signal-to-noise ratio. A general iGluSnFR experiment contained of repetitive (depending on the experiment between 20 and 200) imaging trials with 30 to 40 frames each. During each trial the neu-

rons were stimulated once after frame 20 via field potentials to elicit one AP per trial, which eventually results in synaptic release.

iGluSnFR image analysis

Image analysis of iGluSnFR was performed with Image J 1.51 (automatic detection of response sites and measurement of fluorescent increase) and Igor Pro 7.0 Software (sorting of traces of individual trials and calculation of ΔF/F). Image stacks of each trial were registered to the first image of the first trial with StackReg Pro Plugin for ImageJ. For each trial a response image was calculated by subtraction of the baseline (average of 4 images before stimulation) by the response (average of two images after stimulation). Response images were filtered with a gaussian blur filter (2 pixel) and then projected for maximum intensity. Release sites were detected with auto local threshold method “phansalkar” in ImageJ. For detected particles a ROI set was generated and ROIs containing multiple synapses were deleted by eye. For the remaining ROIs average fluorescence intensity were measured and background subtracted. In our setup iGluSnFR signals mostly show a ΔF/F amplitude of 0.05 - 0.1, thus to avoid contamination of false positive signals caused by noise, we decided to include only ROIs, where the baseline noise did not exceed a ΔF/F of $\pm$ 0.05. Further selection was done by the rational that we only included ROIs in the analysis, in which at least on clear signal could be identified. The threshold of this signal was 4 x standard deviation of baseline noise. ROIs that passed all these criteria were used in the follow up analyses.

Quantification of general glutamate release with iGluSnFR

The amount of synaptic release is a fundamental parameter that defines the conversion of action potential generation to synaptic transmission. We wanted to develop an easy to use method to compare glutamate release between different conditions with the help of the genetically encoded glutamate sensor iGluSnFR. Our approach is simple: When a neuron is stimulated in repetitive trials, any synapse will release in some trials vesicles and in others not (depending on the synaptic release probability). Thus, a normalized average of all release events and failures, will represent the amount of the glutamate release and thereby the synaptic release probability and can be compared between conditions.
We calculated the ΔF/F trace for each selected synapse in each trial by

$$\Delta F/F = \frac{(F_t - F_{baseline})}{F_{baseline}} \tag{4.3}$$

$F_t$was the fluorescence at any given time point. $F_{baseline}$ was the average of 4 values before stimulation, to which the response signal is normalized. The ΔF/F traces were fitted with an iGluSnFR response

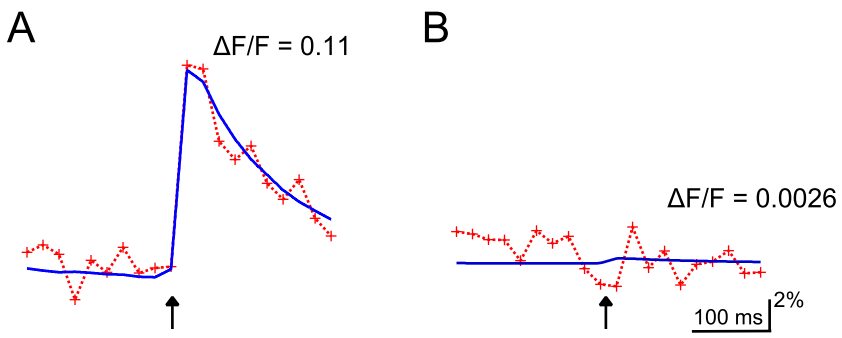

Figure 4.1: Template fit of iGluSnFR response to estimate $\triangle$F/F amplitudes. (A) Shown is an iGluSnFR response of one trial of one ROI (response is the red dashed line with markers). Blue trace indicates template, which was generated from the average of a typical iGluSnFR response over 30 trials. The template was fitted to the experimental response to estimate the $\triangle$F/F amplitude. **(B)** Example of a trial with no response after stimulation. Shown is another trial from the same ROI as in A, but this time the synapse did not release glutamate. The template fit in this case estimated $\triangle$F/F to be close to zero. Arrows in A and B indicate time points of field stimulation.

template, that was generated once from a representative iGluSnFR response (the template that was used to fit therefore was the same for all evaluated experiments and synapses, Figure 4.1 A blue trace). The resulting fit returned the $\triangle$F/F amplitude (Figure 4.1 A). Trials with no response were also fitted to the template, which resulted in a $\triangle$F/F close to zero (Figure 4.1 B). The amplitudes of all trials in one ROI were averaged to get the average $\triangle$F/F value for one synaptic structure. Finally, all synaptic structures in one experiment were averaged for comparison with other experiments.

4.7.4 Fluorescence recovery after photo-bleaching (FRAP)

We performed FRAP experiments with the confocal microscope described in Section 4.7.1. Frames were acquired at 0.1 Hz for up to 15 minutes. Neurons were kept constantly (without perfusion) in modified Tyrode's solution. GFP, GFP-RIM1α and mutated GFP-RIM1α variants were excited and bleached with a 488 nm laser, through a 60 x immersion objective (Plan Apo IR, 1.27 WI, Nikon) with 4 x zoom. Up to three bleaching positions were selected per field of view before the experiments were started. The positions were choosen by visual inspection of the GFP expression in the neurons. Laser intensity for bleaching was selected, such that the bleaching intensity was maximal 60 % of baseline intensity.
Acquired image stacks were registered with StackReg plugin in ImageJ and mean fluorescence values in bleached spots, up to five reference spots and three background areas were measured over the whole time of the experiment. Normalization and correction of fluorescent values was performed as described in the following:

1. Background areas were averaged and subtracted from reference spots and bleached spots.

2. Bleached spots were normalized for ongoing photo-bleaching and relative to baseline by the formula:

$$f(t) = \frac{ROI_t}{ROI_{baseline}} * \frac{REF_{baseline}}{REF_t} \tag{4.4}$$

   ROI_t is the mean value in the bleached ROI at each time-point t. $ROI_{baseline}$ describes the average intensity of the ROI during baseline acquisition. REF_t and $REF_{baseline}$ are the same for the means of the reference regions.

3. Traces were normalized to full scale for comparison by the formula:

$$f(t) = \frac{ROI_t - ROI_0}{1 - ROI_0} \tag{4.5}$$

   Where ROI_0defines the fluorescence intensity in the bleached ROI at the time-point of bleaching.

All spots of a condition that were normalized in this fashion were averaged and then fitted to a bi-exponential recovery function. For simplification our fitting procedure assumed full recovery (y_0 = 1). The bi-exponential fit allowed to read out the recovery time constants. Fitting of single spots was difficult due to bad signal-to-noise ratio. Therefore, to get a proxy for the turnover of GFP-RIM1α in synaptic structures, we decided for this procedure.
Additionally, we calculated the mean recovery after certain time points (150 or 500 seconds). We averaged five values at the named time-points per bleached spot and calculated an average recovery over all experiments in each condition for statistical comparison.

4.8 Statistics and data presentation

General statistics

Statistical data processing and analysis was performed with Microsoft Office Excel (Microsoft Corporation, Redmond, USA), Graphpad Prism 6.0 (Graphpad Software Inc.; La Jolla, USA) and Igor Pro 7.0 (Wavemetrics, Lake Oswega, USA). Statistical tests were used as indicated. Difference between conditions were assumed to be statistical significant at p-values < 0.05. If not stated differently, graphs show means with SEM as error bars.

Special considerations in statistical analysis of FM experiments with multiple comparisons

In the FM dye experiments we screened many different GFP-RIM1α mutants for functional release relevance. In general we aimed to compare 5-8 independent experiments per condition. Statistical comparison with the control conditions (WT and KO) would be necessary for each mutation. We decided to acquire a reasonable amount of experiments for the control conditions (24-25) and used random selection with returning for statistical comparison. This means: When we compared a specific condition with WT and KO conditions, we selected randomly eight independent experiments from the WT and KO experiments and statistically compared these with the specific mutation. Afterwards the experiments of the control conditions (WT and KO) were returned into the pool of all experiments for the next selection round. For the next condition again eight experiments from WT and KO were selected randomly (thus, individual experiments could be part of multiple comparisons).

5 Results

5.1 FM imaging to investigate vesicle fusion and neurotransmitter release

One of the main aims of this thesis was to identify phosphorylation sites in RIM1α that are necessary to set the basal release probability or even to increase synaptic vesicle fusion, as for example seen during different plasticity events. One of the techniques used to screen for these functional relevant phosphorylation sites was FM dye imaging. Due to technical reasons we started our screening experiments with high potassium (K^+) stimulation and later changed to electrical field potential stimulation. In the following, control and optimization experiments are described that verify and justify the use of FM dye imaging (the general experimental procedures can be found in Material and Methods Section 4.7.2).

5.1.1 FM imaging approach to resolve reduced release probability in cultured neurons

When perfusion with high potassium is used to stimulate neurons, a main concern is the inability to control the exact timing and extent of the stimulus during the experiment. To test whether our FM dye approach is comparable to an established and defined electrical stimulation setup, we compared the inhibition of synaptic release with 200 µM Cobalt (Co^{2+}) in field potential stimulation experiments and in the FM dye imaging approach with high potassium stimulation. In a first step we tested if and to which extend 200 µM of the unspecific Ca^{2+} - channel blocker Co^{2+} would inhibit fEPSPs in the CA1 region of hippocampal slices, after stimulation of the fibers in the CA3 region (the Schaffer Collateral pathway, Figure 5.1 A, stimulation in hippocampal slices was done by Sara Ferrando-Colomer). CA3 fibers were stimulated every 30 s and fEPSP responses in CA1 were recorded simultaneously. 200 µM Co^{2+} was perfused after baseline acquisition. The fEPSP response dropped by 40 % after Co^{2+} entering the experimental chamber (Figure 5.1 B). Next, we performed a similar experiment with the FM dye approach and 45 mM K^+ stimulation in hippocampal cultured primary neurons (DIV14-21). We started the experiment with or without 200 µM Co^{2+} in the solution and stimulated the neurons with perfusion of 45 mM K^+solution.

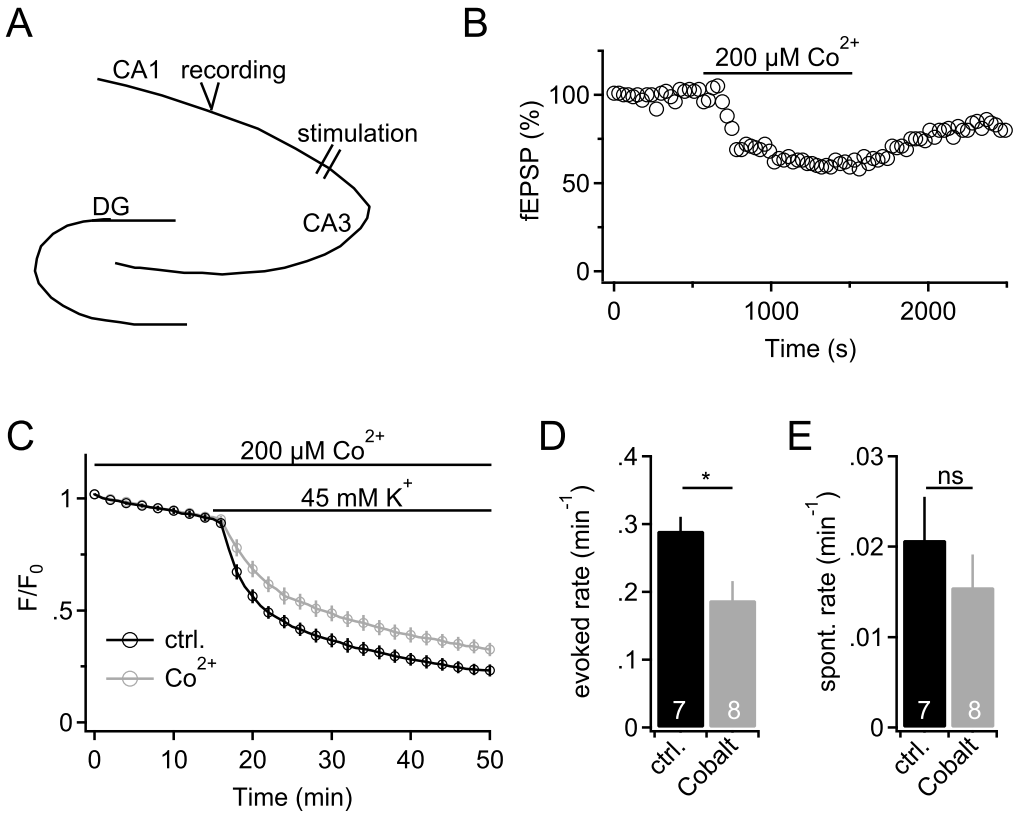

Figure 5.1: Ca^{2+}-channel blocker Co^{2+} proves sensitivity and usability of FM dye approach. To estimate the sensitivity of the FM dye approach we compared the reduction of the release in hippocampal slices when 200 µM of the unspecific Ca^{2+}-channel blocker Co^{2+} was applied and compared the effect of Co^{2+} application in cultured hippocampal primary neurons (DIV14-21) when probed with FM dye imaging. **(A)** Experimental setup in field potential experiments. Hippocampal slices were stimulated in the Schaffer Collateral pathway (fibers of the CA3 region) and the response was recorded in the CA1 region of the hippocampus. **(B)** Representative trace of remaining normalized fEPSPs amplitudes. When Co^{2+} is applied the fEPSP response in CA1 drops by 40 % compared to the baseline fEPSPs. **(C)** Average time courses of control experiments (black) and Co^{2+} application (grey). Note, the difference in the rate of fluorescence loss. **(D)** The evoked release rate is significantly reduced by 34.5 % when Co^{2+} blocked Ca^{2+} entry (evoked release rates were ctrl.: 0.29 $\pm$0.02 and Co^{2+}: 0.19 $\pm$0.028 min^{-1}). **(E)** Spontaneous dye loss is not significantly altered (ctrl.: 0.021 $\pm$0.005; Co^{2+}: 0.016 $\pm$0.004 min^{-1}). Data are presented as means ± SEMs (numbers in bars indicate numbers of experiments (= n)). Statistical significance was assessed by unpaired Student's t-test (*, p<0.05).

There is a clear difference in the speed of fluorescence loss as seen from the average time course of dye loss with the onset of perfusion of the high K^+solution (Figure 5.1 C). Quantification of the release rate shows that there is a significant reduction in the evoked release rate by 34.5 % (ctrl.: 0.29 $\pm$0.02 min^{-1}; Co^{2+}: 0.19 $\pm$0.028 min^{-1}, Figure 5.1 D), which is comparable to the result seen in experiments with electrical stimulation. The spontaneous dye loss, as it was estimated from the baseline, is not significantly changed (Figure 5.1 E). This is expected, as the non-evoked loss of dye in our experiments mainly consists of spontaneous release (see Sections 4.7.2 and 4.7.2 for details), which should not be dependent on AP induction or Ca^{2+} influx. This experiment also proves that the perfusion speed used in these experiments (1 ml/min) was fast enough to increase the K^+ concentration sufficiently to induce

and to investigate evoked neurotransmitter release.

Taken together these results indicate that the FM dye approach, even with a relatively uncontrolled stimulation paradigm such as K^+ stimulation, has comparable sensitivity as electrical field stimulation in brain slices.

5.1.2 Potassium induced vesicle fusion is Ca^{2+} dependent

Strong potassium stimulation of neurons represents an unphysiological stimulus, that leads to high release of synaptic vesicles. To exclude the possibility, that the potassium stimulation, which we wanted to use to screen for functional relevant phosphorylation sites in RIM1α, would lead to action potential and Ca^{2+} independent release, we performed FM dye experiments in buffers containing no Ca^{2+} and added 1 µM TTX to suppress action potential firing. If there would be release in these conditions, then this release should be likely caused by an unspecific Ca^{2+}source and this source would be activated independent of action potential generating sodium channels, or the strong membrane depolarization would directly lead to vesicle fusion.

We probed these conditions with the same protocol as before and used the adjusted (0 mM Ca^{2+} and 1 µM TTX) buffer for washing, during baseline acquisition and when high K^+ stimulation was applied. Using these conditions we could not detect any evoked release component in the experiment (Figure 5.2).

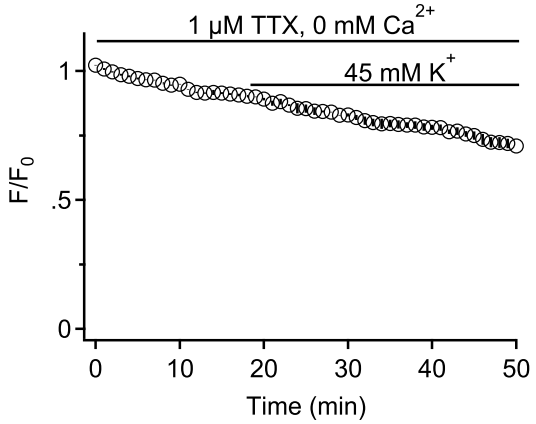

Figure 5.2: Ca^{2+} and action potential dependent release. FM loaded neurons were incubated with 1 µM TTX and 0 mM Ca^{2+} and challenged with 45 mM K^+. The K^+ stimulation did not lead to the induction of evoked release under these conditions, which under normal conditions would be visible with the onset of high K^+ application. The experiment was repeated in two biological replicates with similar results (N = 2).

The time course of the spontaneous release was similar as the release observed under normal conditions. This is expected since spontaneous release is not dependent on AP generating sodium channels or Ca^{2+} influx into the presynapse [Vyleta & Smith, 2011].

In a second set of experiments we tested whether the loading of FM dye with K^+ would be Ca^{2+} dependent. We performed the normal loading protocol, with 2 mM Ca^{2+} and compared the loading with an adjusted protocol using 0 mM Ca^{2+}. The control condition with 2 mM Ca^{2+} results in good FM loading into synaptic vesicles (Figure 5.3 A), while loading with 0 mM Ca^{2+} resulted in very weak, almost not detectable uptake of dye (Figure 5.3 B). Quantification of the loaded synapses showed that the residual fluorescence with 0 mM Ca^{2+} is 5.8 times weaker than under normal loading conditions (ctrl.: $5.68*10^4 \pm 0.3*10^4$ a.u.; no Ca^{2+}: $0.98*10^4 \pm 0.02*10^4$ a.u.). Residual loading is not unexpected, since vesicles can fuse spontaneously in a Ca^{2+} independent manner and take up dye. Additionally, unspecific labeling of membranous structures can not be excluded. Nevertheless, most of the loading which we saw in our experiments derives from stimulation and is Ca^{2+} dependent. Taken together, we conclude from these data that our protocol and the stimulation paradigm with potassium is usable to check for action potential induced and Ca^{2+} dependent synaptic vesicle fusion during the loading of FM dyes and during the measurement of synaptic release.

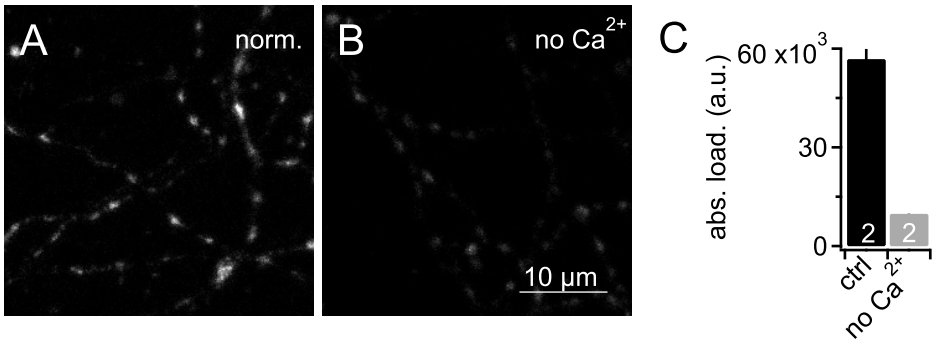

Figure 5.3: Loading of FM dyes into vesicles is Ca^{2+} dependent. (A,B) Representative images of synaptic structures loaded with (A) or without (B) Ca^{2+}. Both images were set to the same brightness range for comparison. **(C)** Quantification of synaptic structures as seen in A and B. The absolute loading was 5.8 times higher when Ca^{2+} was present (ctrl.: $5.68*10^4 \pm 0.3*10^4$ a.u.; no Ca^{2+}: $0.98*10^4 \pm 0.02*10^4$ a.u.). Experiments were repeated twice and were carried out at the same day and in direct succession to avoid day-to-day or time dependent variances. Number of experiments (n) as indicated in bar graphs. Error bars represent SEM.

5.2 iGluSnFR: a novel tool for the investigation of synaptic release parameters

We explored the usability of the genetically encoded glutamate reporter iGluSnFR for the investigation of different research questions. We compared responsiveness of different affinity variants in neuronal cultures and the ability of these variants to detect the position of release sites. Additionally, we probed whether the sensor can be used to estimate glutamate diffusion (spatial range and speed). Finally, we wanted to establish an approach to compare the amount of synaptic release between different conditions

and established a method to estimate the vesicular release probability of individual synapses. Parts of the results in this section may be published in Marvin et al., 2019.

5.2.1 Low affinity variant of iGluSnFR to resolve high stimulation frequencies

The original iGluSnFR had a K_d of 40 µM and one iGluSnFR response persisted for around 100 - 500 ms [Marvin et al., 2013]. While the affinity was suited to detect single release events in neuronal systems, high frequency events can not be resolved to a sufficient degree. We tested whether the newly generated low affinity variant SF.iGluSnFR.S72A [Marvin et al., 2018] was able to resolve glutamate release events at frequencies of 10 Hz in a paired pulse paradigm and at 20 Hz in train stimulation experiments. The original sensor, a new variant SF.iGluSnFR.A184V (original affinity with super-folder GFP) and the low affinity variant SF.iGluSnFR.S72A all could visibly report the release of glutamatergic vesicles upon electrical field potential stimulation (Figure 5.4 A - C). Obviously, and not surprisingly, the signal-to-noise ratio was better for the sensors with higher affinities (compare Figure 5.4 B with C). We probed the three variants in a paired pulse paradigm, with the two pulses elicited at 10 Hz. The faster off rate of the low affinity variant S72A allowed for more precise quantification of quantal release as response to the second pulse (Figure 5.4 D and insets). In the next experiment we adjusted the release probability and thereby the temporal depression or facilitation of release by application of different extracellular calcium concentrations (1 mM and 3.5 mM Ca^{2+}). It was obvious that SF.iGluSnFR.A184V and the original iGluSnFR could not distinguish clearly between the different temporal release patterns given by the modulated release probabilities during the stimulus train at 20 Hz (Figure 5.4 E and F). On the other side, the low affinity sensor (S72A) showed a clear difference in the response pattern and displayed the conversion of the facilitation at low Ca^{2+} concentration to a strong depression in high Ca^{2+} concentrations for individual responses during the whole stimulation train (Figure 5.4 E). We conclude that the low affinity variant SF-iGluSnFR.S72A is better suited to investigate short-term synaptic plasticity events, such as facilitation and depression, that occur in high frequency firing.

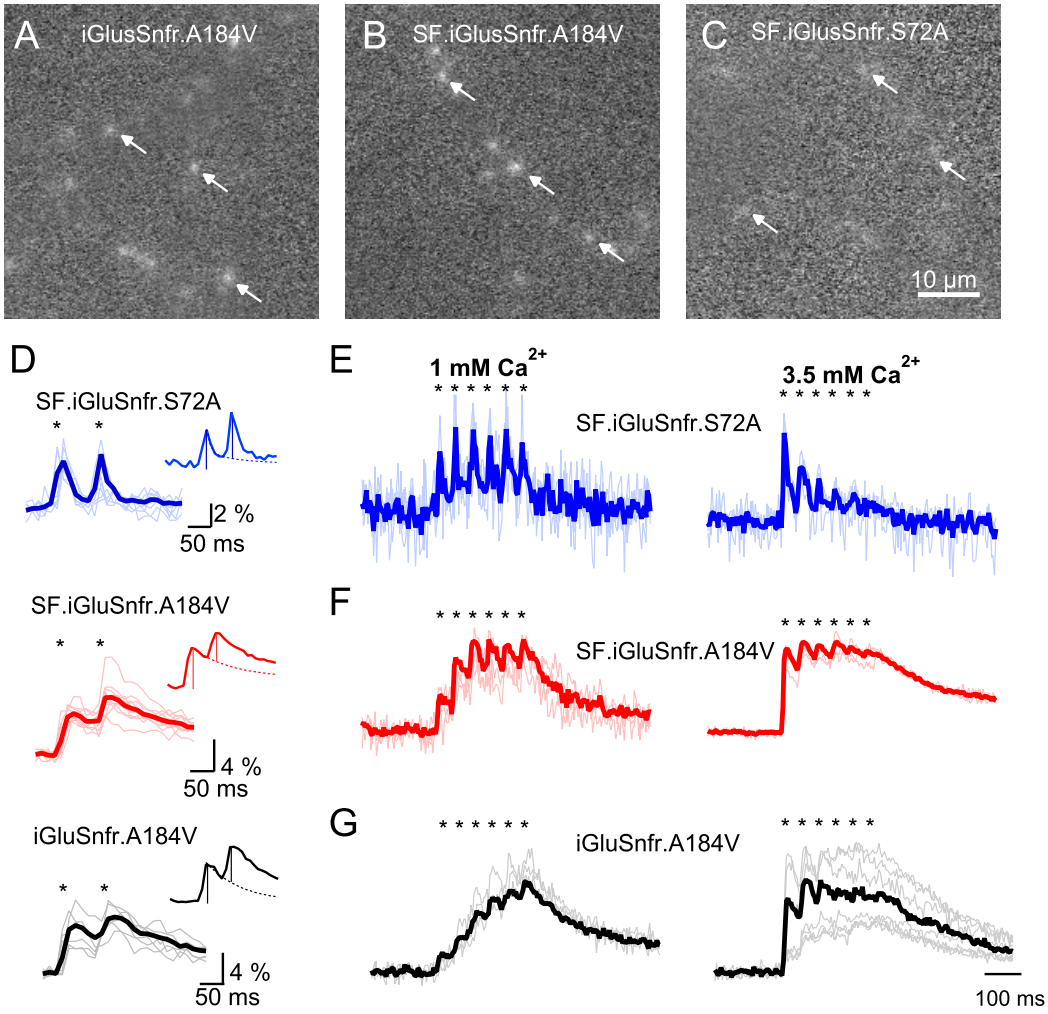

Figure 5.4: The low affinity iGluSnFR sensor is better suited to resolve high frequency events. (A-C) Representative single ΔF/F images of iGluSnFR responses for high affinity sensor (A), high affinity sensor with superfolder GFP (B) and low affinity sensor (C) for one single stimulation event. Note, the signal-to-noise ratio is considerably better for the high affinity sensors (A and B) than for the low affinity sensor (C). **(D)** Average (thick lines) and individual (light lines) paired pulse traces of different iGluSnFR affinity variants. Only the low affinity sensor (SF.iGluSnFR.S72A) was able to fully recover before the onset of the second stimulation. Inset show quantal releases for the first and second pulse. Even with single vesicle (quantal) release, the high affinity sensor, were not recovered back to baseline (n = 4-5 per iGluSnFR variant). **(E-G)** The conversion from low release probability to high release probability was better reported by the low affinity sensor. The high affinity sensors (F and G) were not able to accurately report the depression in high Ca^{2+} concentration. Only the low affinity sensor (E) showed a clear and detectable depression of vesicle release (n = 4-5 per iGluSnFR variant, the results are partly published in [Marvin et al., 2018]).

5.2.2 iGluSnFR sensors allow sub-µm localization of release sites

The faster off rate of the low affinity variant should restrict the temporal and the spatial spread of the iGluSnFR responses compared with the high affinity variants. Especially, the restricted spatial extend of

the low affinity sensor would make this sensor better suited to accurately estimate the release sites of repetitive release events. Therefore, we stimulated neurons in 10-20 repetitive trials and generated line profiles along the neurites for each response in each trial. We fitted the line profile to gaussians (Figure 5.5 A - C) and thereby estimated the center of the response sites (Figure 5.5 D). Afterwards all centers were averaged and the standard deviation of all centers from the mean was calculated (Figure 5.5 F).

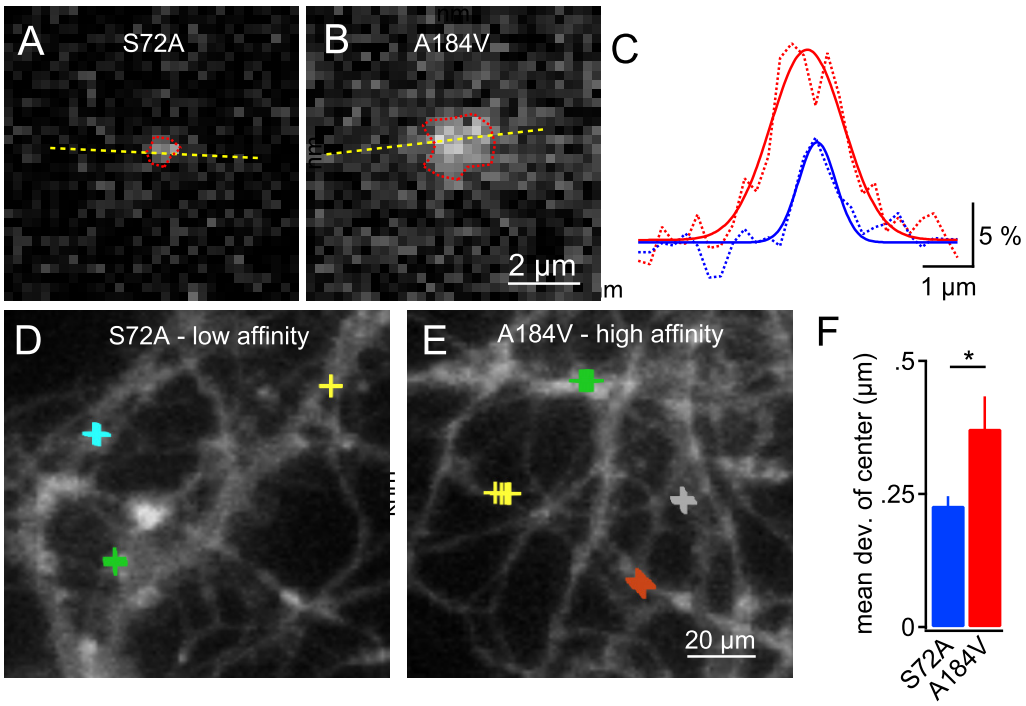

Figure 5.5: Detection of glutamate release sites is more accurate using a low affinity variant of iGluSnFR. **(A and B)** ΔF/F images from one release site for the low (iGluSnFR.S72A) and the high (iGluSnFR.A184V) affinity variant of iGluSnFR. The dashed yellow line indicates the direction of generated line profiles. The response sites are encircled by the red dashed lines. **(C)** Line profiles (dashed lines) of low affinity (blue) and high affinity (red) sensors were fitted to gaussians (straight lines) to determine the center of release sites. Note, that the low affinity response is smaller and narrower. **(D and E)** Representative images of low and high affinity iGluSnFR expression with trial-to-trial detected release sites (markers). Each marker indicates a release event and markers of the same color indicate release events of the same release site. Note, there is a higher deviation from trial-to-trial with the high affinity variant. **(F)** Quantification of the deviation (as shown in the examples in D and E). The low affinity sensor allows the detection of the release site with an accuracy below 250 nm (S72A: 0.23 ± 0.02 µm; A184V: 0.37 ± 0.06 µm), which is significantly more accurate than the high affinity sensor (For S72A n = 28 selected sites from 6 experiments and for A184V n = 53 selected sites from 8 experiments, unpaired Student's t-test (* $p < 0.05$) error bars are SEMs. The results are partly published in [Marvin et al., 2018])

This estimated how much the detection of the release site deviated from trial to trial. Even though the low affinity sensor had inferior signal-to-noise ratios, the detection of the release sites over many trials deviated significantly less around the calculated center (S72A: 0.23 ± 0.02 µm; A184V: 0.37 ± 0.06 µm, Figure 5.5 F) This result indicates a more accurate estimation of the position of the release sites. We could detect the center of a release site with an standard deviation below 250 nm when using the low

affinity sensor (Figure 5.5 F).

5.2.3 Estimation of glutamate diffusion speed in a given biological system

Glutamate diffusion, in temporal and spatial terms, is an important factor for neuronal signaling. The speed of diffusion defines how fast information can be passed on across synapses. The maximal distance of diffusion determines whether signaling is restricted to a single synapse or whether spillover of glutamate might activate juxtaposed synapses, as well. We wanted to know whether iGluSnFR sensors can be used to estimate the speed of glutamate diffusion in the extracellular space of cultured neurons in a reasonable manner. We stimulated neurons in 5-10 trials and calculated the spatial extension of iGluSnFR responses by fitting line profiles over the responses to gaussian and thereby estimating the width of a iGluSnFR response. This was done for 10 frames (in total 80 ms) after onset of iGluSnFR response. The spatial extension of the signal can be linearly followed for the high affinity sensor, but not for the low affinity sensor (Figure 5.6 A. Note, that the response from the low affinity sensor is not detectable anymore after the third frame). The diffusion speed of glutamate in this system was then calculated after plotting the linear broadening of the signal in width^2 over 4*t. The result was fitted to a line and the slope estimates the apparent diffusion coefficient (D_{app}). We found that glutamate extended with a D_{app} of 4.35 µm^2/s in this system (Figure 5.6 B).

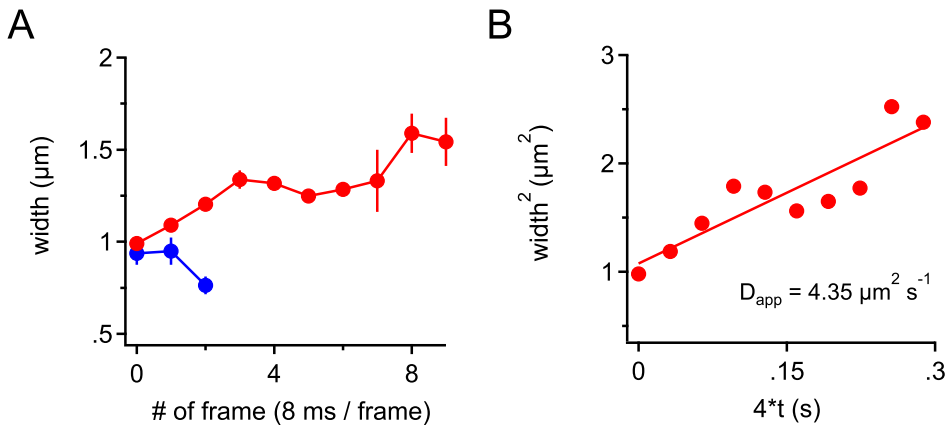

Figure 5.6: iGluSnFR sensors can be used to estimate diffusion speed of glutamate. **(A)** Signal of SF-iGluSnFR.A184V was measured as line profiles and fitted to gaussians. The response progressively broadened over time (red). The spread of the signal could not be followed with SF-iGluSnFR.S72A (low affinity variant), as there was no signal detectable anymore after 3 frames (24 ms). **(B)** The data from A were plotted as width^2 over 4*t. and fitted to a linear increase and the slope of the fitted line estimates the apparent diffusion coefficient (D_{app}) of synaptically released glutamate. This diffusion coefficient is slowed by glutamate binding to iGluSnFR (which acts as glutamate buffer). D_{app} in this system was calculated to be 4.35 µm^2/s. (Graph in A shows mean and SEM from n = 24 release sites in four experiments for SF-iGluSnFR.S72A (blue) and n = 19 release sites in three experiments for SF-iGluSnFR.A184V (red), the results are partly published in [Marvin et al., 2018])

This value is orders of magnitude smaller than the diffusion coefficient of free glutamate in aqueous solution (~600-700 $\mu m^2/s$), which is meaningful when considering that iGluSnFR itself acts as glutamate buffer and slows glutamate diffusion and that glutamate is firstly released in a synaptic cleft where glutamate diffusion is restricted.

5.2.4 Estimation of vesicular release probability with binomial release model

As described in Material and Methods (see Section 4.7.3) iGluSnFR can be used as a tool to measure the general amount of neurotransmitter release, which correlates with the synaptic release probability. The rational is to stimulate neurons in many trials and calculate the mean $\triangle$F/F of iGluSnFR responses. A higher average of $\triangle$F/F indicates more release events and therefore a higher synaptic release probability. This form of analysis investigates the synaptic release probability that by itself is defined by the vesicular release probability and the number of release sites, i.e. releasable vesicles per synapse. The synaptic release probability is a combination of both factors. The estimation of the synaptic release probability can not distinguish between these two parameters, for example: a synapse with many release sites but very low vesicular release probability might release with a similar synaptic release probability as a synapse with few release sites but very high vesicular release probability. However, the ability of iGluSnFR to detect release at the level of individual synapses is predestined for assessing quantal (single vesicle) release and vesicular release probability.

We stimulated neurons in 100 to 200 trials and detected the $\triangle$F/F signal of individual response sites in each trial by fitting to a template iGluSnFR response as described before (see Section 4.7.3). Usable response sites needed to be preselected, so that a response site represented glutamate release from one synapse only (multi-synaptic release would distort the analysis of quantal release and vesicular release probability). Criteria for usable synapses were a location distal from other release sites and individual responses needed to have a center of mass that did not deviate visibly from the average center of mass of all responses in a ROI. Additionally, a strong run-down in iGluSnFR response amplitude (due to photobleaching or other reasons) had to be avoided. The $\triangle$F/F values of single release sites were plotted in a histogram. From experimental observation, we guessed the $\triangle$F/F to be somewhere around 0.05 for one vesicle being released. Therefore, we selected a bin size of 0.01 to account for variability in iGluSnFR response signals. The resulting frequency distributions had multiple peaks, depending whether one, two or more vesicles are released simultaneously as response to one stimulation event. The positions of the maxima represent the quantal amplitudes of 1, 2, 3..... vesicles (Figure 5.7 A). The successful event of release can be approached as a binomial experiment, where n represents the amount of release sites and k represents the total number of releasable quanta. The plotted frequency distribution can be fitted

with the help of the binomial probability from these values and the assumption that the probability of all possible events (0, 1, 2 ... released vesicles) equals 1, which is the area under the curve of the whole fit. In other words: the area under the gaussian fits for each possible event must sum up to a probability of 1 (details to the fitting procedure can be found in Section 9.3 in the appendix). The number of release sites N (= n) was fixed and varied to test the quality of different fits. The best fit (lowest chisq), was used to determine the vesicular release probability (Figure 5.7).

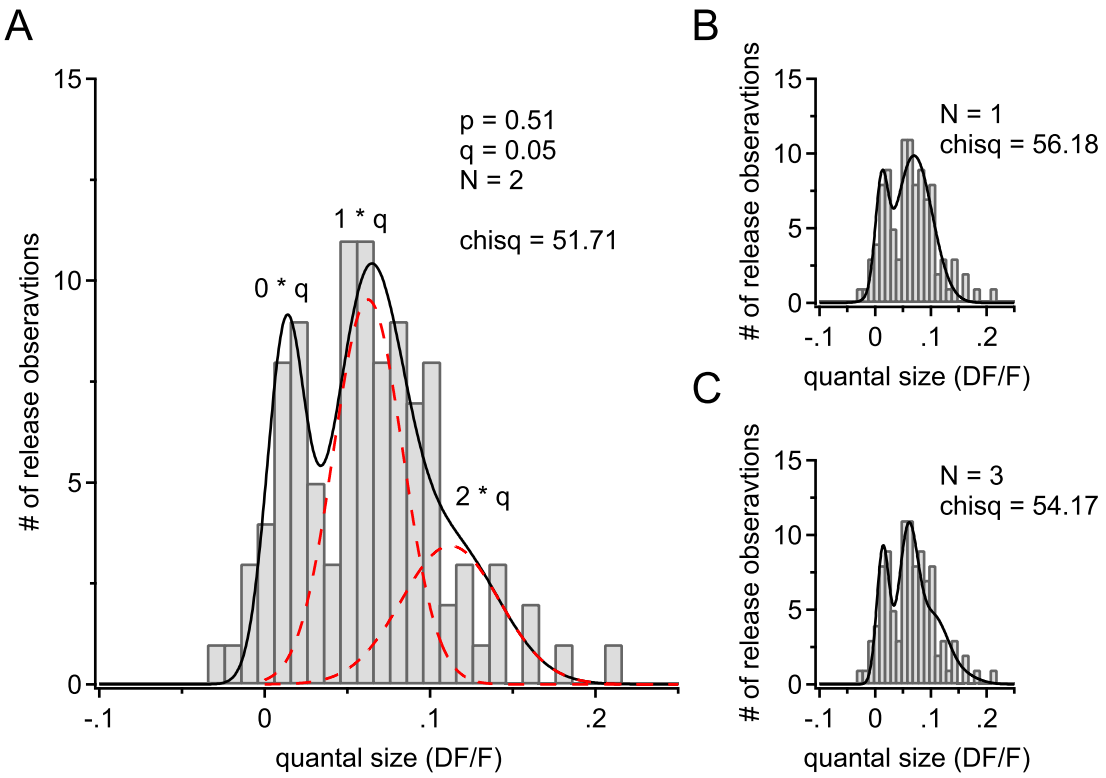

Figure 5.7: Fitting of frequency distributions of release events detected by iGluSnFR with a binomial release model to estimate vesicular release probability. (A) Sample frequency distribution of one release site in an iGluSnFR experiment. In 100 trials ΔF/F amplitudes of release events were detected and plotted in a histogram with 0.01 bin size. The resulting multi-peak graph was fitted to multiple gaussians with a fitting procedure that describes a binomial release model. The individual gaussians of release events are shown in dashed red lines. The black line is the complete fit (sum of individual gaussians). The gaussian for the noise (0 * q) is not shown. For this example the vesicular release probability was estimated to be p_{ves} = 0.51 with a quantal size of q = 0.05. The fit was produced with a fixed value of N = 2 release sites. **(B and C)** Same frequency distribution as in A, but fits were performed with fixed values for the release sites of N = 1 and 3. The chisq values were higher and indicated inferior fits.

5.3 Molecular rescue of RIM1α KO and RIM1/2 cDKO with GFP-RIM1α

In this thesis we aimed to identify functionally relevant phosphorylation sites in RIM1α. As already mentioned, RIM1α is centrally involved in synaptic release and release probability. The experimental strategy for the identification of release relevant phosphorylation sites was to use RIM1α KO or RIM1/2 cDKO neurons and try to rescue the changes in release parameters with phospho-deficient (mutation to alanine) or phospho-mimetic (mutation to glutamate) RIM1α constructs. In order to do this, it was necessary to characterize the release parameters, such as release probability, of RIM1α KO and RIM1/2 cDKO cells and to show that a re-expressed RIM1α WT variant is sufficient to rescue changes in these release parameters.

5.3.1 Stimulation strength is crucial to resolve reduced release probability

We loaded WT and RIM1α KO neurons in 90 mM K^+ solution with 10 µM FM4-64 for 3 minutes. Afterwards cells were washed extensively to remove unspecific labeling of cellular membranes (see Section 4.7.2for experimental procedure). This loading protocol resulted in a qualitatively and quantitatively comparable loading pattern (Figure 5.9 A and B). In a first attempt to compare the evoked dye release rate between the WT and RIM1α KO neurons, we tried a very common stimulation protocol: We induced synaptic vesicle fusion with 90 mM K^+ solution and quantified the evoked release rate by fitting the sum of the two exponential decay functions (see Section 4.7.2). The time courses of the dye release for the two genotypes were identical (Figure 5.8 A) and the fitting procedure resulted in indistinguishable evoked release rates of 0.75 $\pm$ 0.18 min^{-1} for WT neurons and 0.69 $\pm$ 0.11 min^{-1} for KO neurons, respectively (Figure 5.8 B).This result was puzzling, as the reduced release probability in RIM1α KO neurons has been reported before [Calakos et al., 2004, Kaeser et al., 2008b]. A main problem of the stimulation protocol could be that the high potassium concentration caused a strong membrane depolarization so that Ca^{2+} influx derived from different sources. This could have increased the Ca^{2+} concentration in the synaptic terminal to a degree, where the coupling of Ca^{2+} - channels and the vesicles, thus the dependence on the release machinery and RIM1α became less important. The Ca^{2+} levels would be elevated strong enough to override a deficient Ca^{2+} - channel to vesicle coupling or other deficits in RIM1α KO neurons. Indeed, Nimmervoll and colleagues (2013) showed exactly this phenomenon, when comparing different K^+ stimulation protocols to check which Ca^{2+} - channels are involved in synaptic release. They found K^+ concentrations above 60 mM to cause unspecific Ca^{2+} entry which voids the effects from Ca^{2+} - channel blockers Agatoxin or Conotoxin [Nimmervoll et al., 2013]. Therefore, we adjusted our

protocol to a K^+ concentration of 45 mM for induction of evoked release and again compared the release rates of primary hippocampal RIM1α WT and KO neurons (see Section 5.3.2).

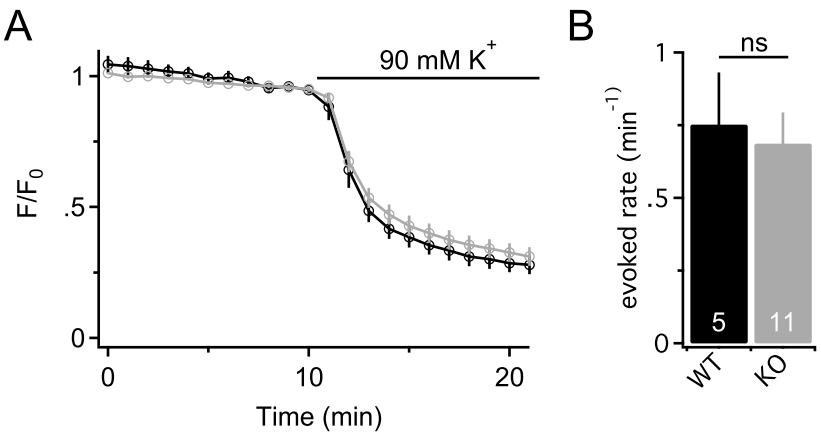

Figure 5.8: 90 mM K^+ stimulation obscured expected phenotype of RIM1α KO neurons. (A) The time courses of FM dye release of WT and RIM1α KO neurons when stimulated with 90 mM K^+ are identical. **(B)** Quantification of the evoked release rates from neurons stimulated with 90 mM K^+ showed no difference between WT (0.75 ± 0.18 min^{-1}) and RIM1α KO (0.69 ± 0.11 min^{-1}) neurons. Data are presented as means ± SEMs. Numbers in bars indicate numbers of experiments (= n). Statistical significance was assessed by unpaired Student's t-test (*, $p < 0.05$).

5.3.2 Release probability in RIM1α KO neurons is strongly reduced

Synaptic vesicles were loaded with FM4-64 and baseline was acquired for 15 minutes. Afterwards neurons were stimulated with 45 mM K^+ and dye release was acquired for 35 minutes (Figure 5.9 A-C). The qualitative and quantitative loading was similar for WT and RIM1α KO neurons (Figure 5.9 A,B, and F). The unloading pattern and the time courses of dye release between WT and RIM1α KO neurons showed a much slower loss for RIM1α KO neurons (Figure 5.9 A-C). It also seemed as if the spontaneous release was slightly reduced in RIM1α KO neurons (see baseline in Figure 5.9 C). Fitting and quantification of the release parameters revealed that the release rate was significantly reduced by 55.6 % in RIM1α KO neurons (WT rate was 0.27 ± 0.052 min^{-1}; KO rate was 0.11 ± 0.012 min^{-1}, Figure 5.9 D). A change in the spontaneous release rate could be assumed (WT: 0.022 ± 0.004 min^{-1}, KO: 0.014 ± 0.003 min^{-1}, Figure 5.9 E), but we could not detect statistical significance ($p = 0.1191$) . The absolute dye loading and the contribution of evoked and spontaneous release to the total amount of release were unchanged (Figure 5.9 F-H). It is expected that all vesicles, that are loaded with FM4-64, should be able to release the dye given enough time and an appropriate stimulus. Therefore, dye that was not unloaded could derive from unspecific loading, vesicles that did not re-enter the vesicle cycle or vesicles that were trapped and exhibited a very low individual probability to be released. Our fitting procedure also estimated the final residual dye in the synaptic structures. We found that in WT 5.82 % (± 1.03 %) of dye resided in

the structures, whereas this value was increased to 8.78 % ± 1.24 %) in KO neurons. The difference was not statistical significant (p = 0.0882), but the tendency might point to vesicles that were differentially recycled after release and retrieval.

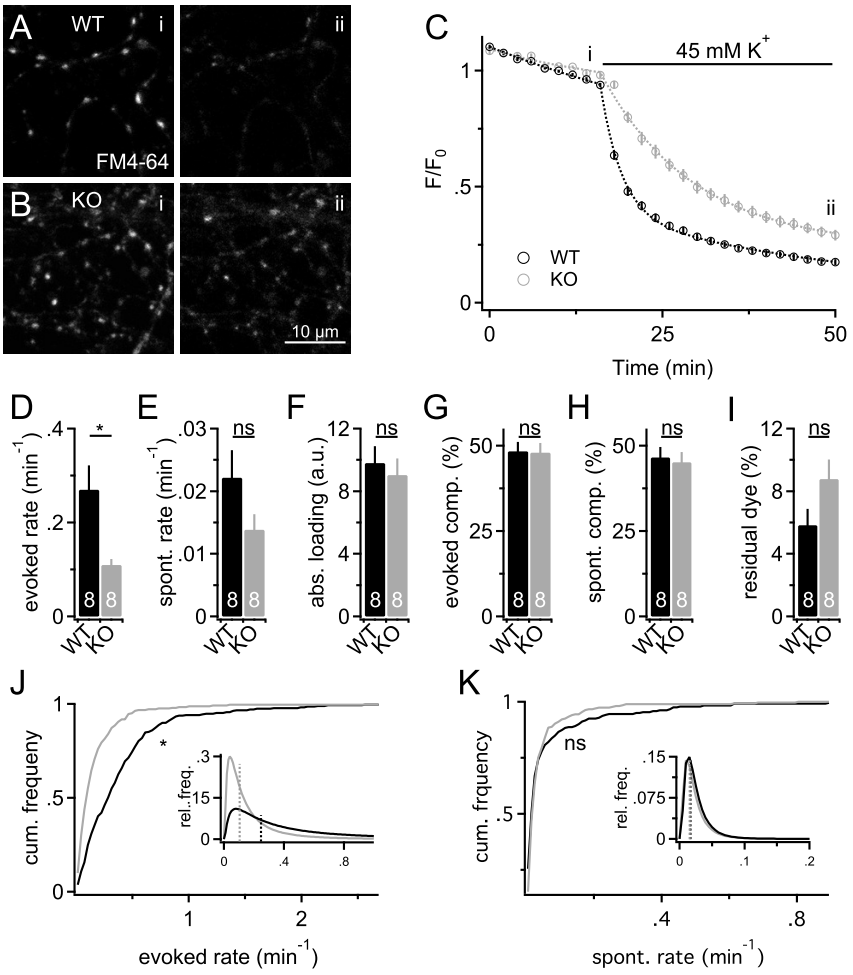

Figure 5.9: RIM1α KO neurons manifest strongly reduced synaptic release probability. (A and B) Representative FM4-64 images before (i) and and after (ii) unloading. The loadings of WT (A) and RIM1α KO (B) neurons were qualitatively and quantitatively similar. Unloading was reduced in KO neurons (B ii)**. (C)** Time course of the experiments shown in A and B. i and ii indicate the time-points as displayed in A and B. The evoked loss of fluorescence with the onset of 45 mM K^+ stimulation was steeper for WT neurons, indicating a faster dye loss. The spontaneous loss (in baseline) seemed to be a little slower for RIM1α KO neurons. Dashed lines indicate fit of trace shown as markers. Markers are average time-course values from experiments in A and B. **(D-I)** Quantification of release parameters from fitting of dye-loss curves. There was a significant decrease in the evoked release rate (D) by 55.6 % between WT and RIM1α KO neurons (WT: 0.27 $\pm$ 0.052 min^{-1}; KO: 0.11 $\pm$ 0.012 min^{-1}). The other parameters (spont. rate (E), abs. loading (F), fraction of evoked release (G), fraction of spont. release (H) and residual dye after unloading (I)) were not significantly changed. However, spontaneous release rate and residual dye seemed to have different mean values (WT: 0.022 $\pm$ 0.004 min^{-1}, KO: 0.014 $\pm$ 0.003 min^{-1}, no statistical significance). **(J)** Cumulative probability plot and fitted log-normal distributions (inset) of evoked release rates of single synapses. The distributions were significantly different and the RIM1α KO phenotype exhibited a loss of high release probability synapses. Dashed lines in inset indicate geometric means of log-normal distributions. **(K)** Same as in J for spontaneous release rates. There was no significant difference in the distributions and no change in the geometric means. Amount of synapses evaluated in cumulative frequency distributions: 269 (WT) and 242 (KO). Data are presented as means ± SEMs. Numbers in bars indicate numbers of experiments (= n). Statistical significance was assessed by unpaired Student's t-test for bar graphs and with Kolmogorov-Smirnov test for cumulative probability distributions (* p < 0.05).

To examine what happened to the release rates on the single synapse level, we plotted the evoked and spontaneous release rates of each single synapse as cumulative probability frequency distribution (Figure 5.9 J and K). It seemed that synapses with a high evoked release rate above 0.5 min^{-1} are lost in RIM1α KO neurons (Figure 5.9 J) and that the proportion of synapses with slower release rate increased (Figure 5.9 J inset). However, high release rate synapses were not completely absent, but merely strongly reduced in RIM1α KO neurons (Figure 5.9 J inset). The distributions of spontaneous release rates were not significantly shifted (Figure 5.9 K and inset).

5.3.3 Reduced release probability of RIM1α KO neurons is rescued by expression of GFP-RIM1α

Next, we wanted to investigate whether a cloned transcript of RIM1α with N-terminally fused GFP (Figure 5.10 A) can rescue the reduced synaptic release probability seen in the RIM1α KO neurons (Section 5.3.2). Therefore, RIM1α KO neurons were transduced with lenti-viral particles to express a GFP-RIM1α fusion protein (Figure 5.10 A-D). As described (Section 2.5.2) RIM1α has three splicing sites and hence is natively expressed in many different splicing variants. The cloned and used transcript, shown in Figure 5.10 A, is the longest variant we could identify and consisted of all exons, except of exons 20, 22 and 24 (exon 22 is retina specific and would therefore not be found in RIM1α that is transcribed in central nervous system synapses [Johnson et al., 2003]).

We repeated the FM dye imaging approach with RIM1α KO neurons expressing GFP-RIM1α fusion protein (Figure 5.10 B-D). There was clear co-localization between lenti-virally expressed GFP-RIM1α and FM4-64 puncta (Figure 5.10 B-D, arrows), indicating that the fusion protein was translocated correctly to putative synaptic structures. The time course of FM dye loss in GFP-RIM1α transduced KO neurons, was almost identical with the WT time-course and also the quantification of the evoked release rate indicated the rescue of the reduced synaptic release probability of RIM1α KO (Figure 5.10 E). The mean evoked release rate for WT neurons in these experiments was 0.35 min^{-1} ($\pm$ 0.06) and did not differ significantly from the evoked release rate of GFP-RIM1α expressing KO neurons (0.31 $\pm$ 0.04 min^{-1} , Figure 5.10 F). As mentioned before, it seemed that also the spontaneous release rate (WT: 0.026 $\pm$ 0.004 min^{-1}, KO: 0.016 $\pm$ 0.003 min^{-1}; Rescue: 0.026 $\pm$ 0.004 min^{-1}) and the residual dye (WT: 5.9 $\pm$ 1.2 %; KO: 8.7 $\pm$ 1.8 %; Rescue: 4.8 $\pm$ 1.1 %) in synaptic structures are changed between WT and KO neurons, but again we could no detect a statistical significance in these cases (also see Section 5.3.2). Interestingly, the GFP-RIM1α expression in KO neurons, also setted these parameters back to WT levels (Figure 5.10 G and H). We conclude that the GFP-RIM1α fusion protein, in the used splicing variant (Figure 5.10 A) is able to fully rescue the reduced evoked release rate (synaptic release probability) of

RIM1α KO neurons.

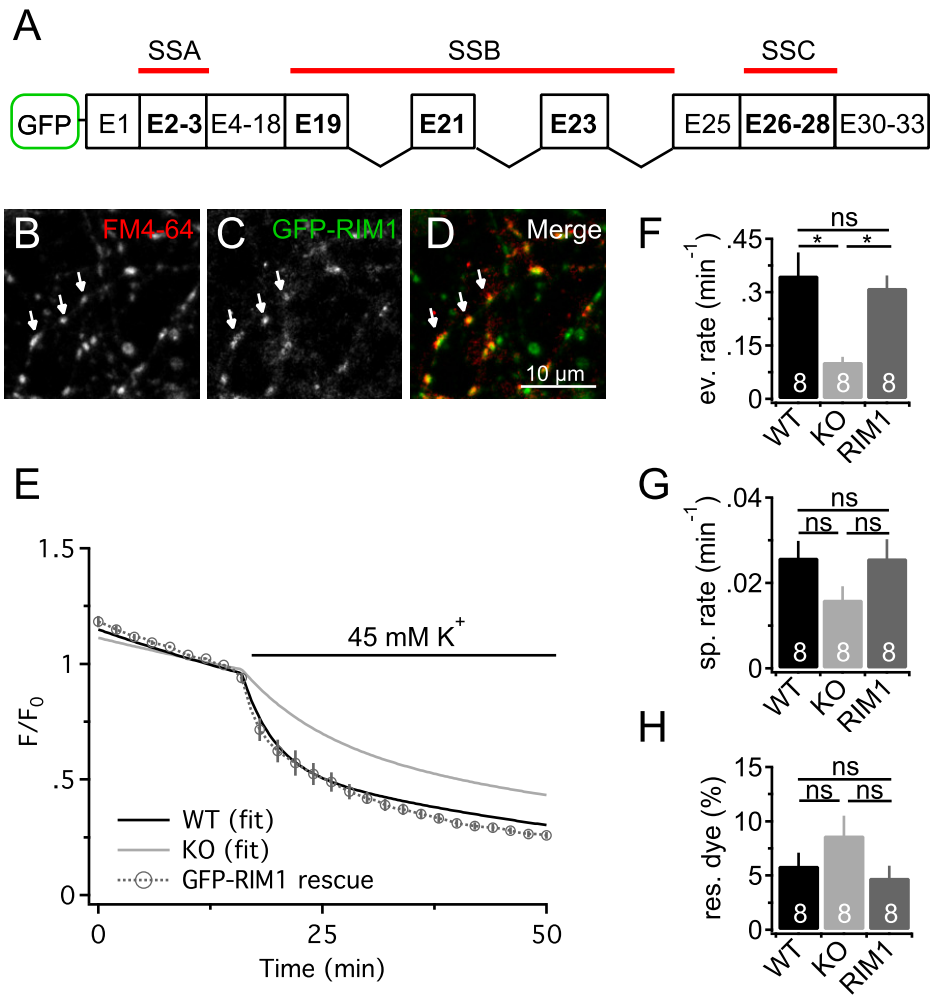

Figure 5.10: GFP-RIM1α fully rescued the reduced synaptic release probability of RIM1α KO neurons. (A) Exon structure of the splicing variant that was expressed for rescue. Only in splice site B (SSB) three exons (20, 22, 24) were missing from the full length transcript. GFP was fused N-terminally for protein detection in different experiments. **(B-D)** Representative images of lenti-virally delivered GFP-RIM1α expression in primary hippocampal neurons. FM4-64 (B) and GFP-RIM1α (C) co-localize (arrows). **(E)** Time course of FM dye release in the different conditions. GFP-RIM1α expressing RIM1α KO neurons showed identical loss of FM dye as WT neurons. For illustration reasons time courses of WT and KO dye loss are only indicated with their respective fits. The markers depict the average time course of the rescue condition over all experiments (± SEMs). **(F)** The evoked release rate was set back to WT levels when GFP-RIM1α was expressed in RIM1α KO neurons (WT: 0.35 $\pm$ 0.06 min^{-1}; KO: 0.1 $\pm$ 0.015 min^{-1}; Rescue: 0.31 $\pm$ 0.04 min^{-1}). **(G)** The spontaneous release rate of GFP-RIM1α expressing KO neurons resembled the WT levels WT: 0.026 $\pm$ 0.004 min^{-1}, KO: 0.016 $\pm$ 0.003 min^{-1}; Rescue: 0.026 $\pm$ 0.004 min^{-1}). **(H)** Residual dye in neurons after unloading was comparable between WT and rescued KO neurons (WT: 5.9 $\pm$ 1.2 %; KO: 8.7 $\pm$ 1.8 %; Rescue: 4.8 $\pm$ 1.1 %). Data are presented as means ± SEMs. Numbers in bars indicate numbers of experiments (= n). Statistical significance was assessed with One-way ANOVA with Tukey's post-hoc test (* $p < 0.05$).

5.3.4 RIM1/2 cDKO neurons phenocopy reduced synaptic release probability of RIM1α KO neurons

In another set of experiments we planned to perform similar rescue experiments with RIM1/2 conditional double knock-out (cDKO) neurons as with the RIM1α KO neurons. In these experiments we would use electrical field-potentials to stimulate neurons for neurotransmitter release. This stimulation paradigm resembles physiological conditions and would confirm and extend the results derived from potassium induced vesicle release. Therefore, the first step again was to characterize the phenotype of the used cells - in this case RIM1/2 cDKO neurons. We transduced primary hippocampal RIM1/2 $^{fl/fl}$ neurons with Cre - recombinases as described (Section 4.2.2) at DIV4 - 6 to delete the large RIM isoforms and to yield RIM1/2 cDKO neurons. As control we used untreated neurons from the same preparation or neurons treated with inactive dCre - recombinase (see Appendix Section 9.4 for verification of comparability of untreated and dCre treated neurons). Experiments were carried out at DIV14 - 21. We loaded vesicles with FM4-64 dye by application of 900 pulses at 10 Hz via field-potentials in the presence of 10 µM FM4-64. Afterwards unspecific extracellular membrane staining was washed out by constant perfusion with modified Tyrode's buffer for 10 min. This results in qualitatively and quantitatively similar staining for WT and cDKO neurons (Figure 5.11 A and B). To induce vesicle release and thus unloading of FM dye we applied ongoing field stimulation at 5 Hz. Similar to the RIM1α KO experiments a clear difference between the time-courses of dye release in WT (control) and RIM1/2 cDKO neurons was visible (Figure 5.11 C). Fitting of the dye loss of single synaptic structures and subsequent quantification showed that RIM1/2 cDKO neurons in this experimental paradigm had a significantly reduced evoked release rate (reduced by 43.1 %, WT: 0.72 $\pm$ 0.09 min^{-1}; cDKO: 0.41 $\pm$ 0.03 min^{-1}). The frequency distributions of the evoked release rates of single synaptic structures were significantly different and again it seemed that the high probability releasers (> 0.8 min^{-1}) were mostly absent in the RIM1/2 cDKO condition (Figure 5.11 G). Similar to what we found in the the K^+ stimulation paradigm with RIM1α KO neurons, we also saw a potential reduction in the spontaneous release rate in RIM1/2 cDKO (WT: 0.075 $\pm$ 0.014 min^{-1}: cDKO: 0.043 $\pm$ 0.018 min^{-1}) and an increase in the amount of residual dye (WT: 0.97 $\pm$ 0.36 %; KO: 3.8 $\pm$ 1.33 %). However, we did not detect statistical significance for these differences (spontaneous release rate p = 0.2 and residual dye p = 0.06).

We conclude that the RIM1/2 cDKO phenotype seen in our electrical FM dye approach is comparable with the phenotype of RIM1α KO neurons seen with potassium stimulation.

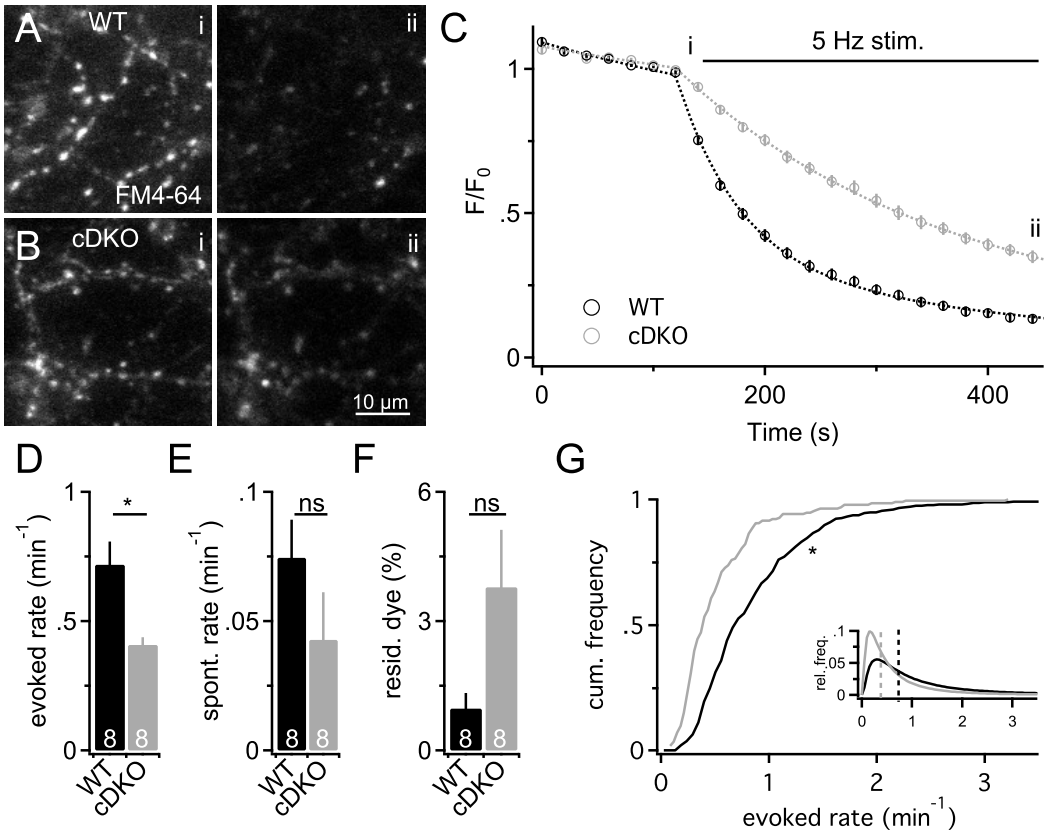

Figure 5.11: The main identified phenotypic hallmark of RIM1/2 cDKO synapses is the reduced evoked release probability. (A and B) Representative images of FM loading with electrical stimulation of WT (A) and RIM1/2 cDKO (B) neurons. i and ii indicate FM staining before stimulation (i) and at the end of 5 Hz stimulation (ii). **(C)** Average time-courses of the experiments shown in A and B. The loss of fluorescence was strongly slowed in RIM1/2 cDKO neurons when 5 Hz stimulation was triggered. i and ii indicate time points in A and B. Dashed lines are fits from the average time courses as indicated by the markers. **(D)** The evoked release rate of RIM1/2 cDKO neurons was significantly reduced by 43.1 % compared to WT neurons (WT: 0.72 ± 0.09 min^{-1}, cDKO: 0.41 ± 0.03 min^{-1}). **(E)** The spontaneous release rate of RIM1/2 cDKO neurons seemed to be reduced for RIM1/2 cDKO neurons but we could not detect statistical significance (p = 0.2, WT: 0.075 ± 0.015 min^{-1}, cDKO: 0.043 ± 0.018 min^{-1}). **(F)** The final level of the fit, which accounts for the residual dye in a synaptic structure, seemed to be higher for RIM1/2 cDKO, but the difference was not significant (p = 0.06, WT: 0.97 ± 0.36 %, cDKO: 3.8 ± 1.33 %). **(G)** Cumulative frequency distribution of evoked release rates from individual synaptic structures. The release rates of RIM1/2 cDKO neurons were significantly shifted to the left indicating lower rates. Rates higher than 0.8 min^{-1} were almost completely lost. Inset shows log-normal distribution of WT (black) and RIM1/2 cDKO (grey). Dashed line show geometric means of the distributions. Amount of synaptic structures analyzed in cumulative frequency distributions were 351 (WT) and 191 (RIM 1/2 cDKO). Data are presented as means ± SEMs. Numbers in bars indicate numbers of experiments (= n). Statistical significance was assessed by unpaired Student's t-test for bar graphs and with Kolmogorov-Smirnov test for cumulative probability distributions (* p < 0.05).

5.3.5 The vesicular release probability in RIM1/2 cDKO synapses is reduced compared to control neurons

Since we saw in RIM1α KO and in RIM1/2 cDKO a strong reduction in synaptic release probability, we asked whether this phenotype originated from fewer releasable vesicles or a reduced vesicular release

probability (or both). Therefore, we applied the introduced analysis for a binomial release model of vesicular release probability (see Section 5.2.4) to WT and RIM1/2 cDKO neurons. To this end we compared 3-4 synapses from 3 cultures each and estimated the vesicular release probability, the quantal content and the amount of release sites at each respective synapse with the help of iGluSnFR. We compared the iGluSnFR response amplitude frequency distributions of WT and RIM1/2 cDKO neurons and observed that WT neurons more often had multiple peaks (indicating multi-quantal release) and less failures (compare Figure 5.12 A and B).

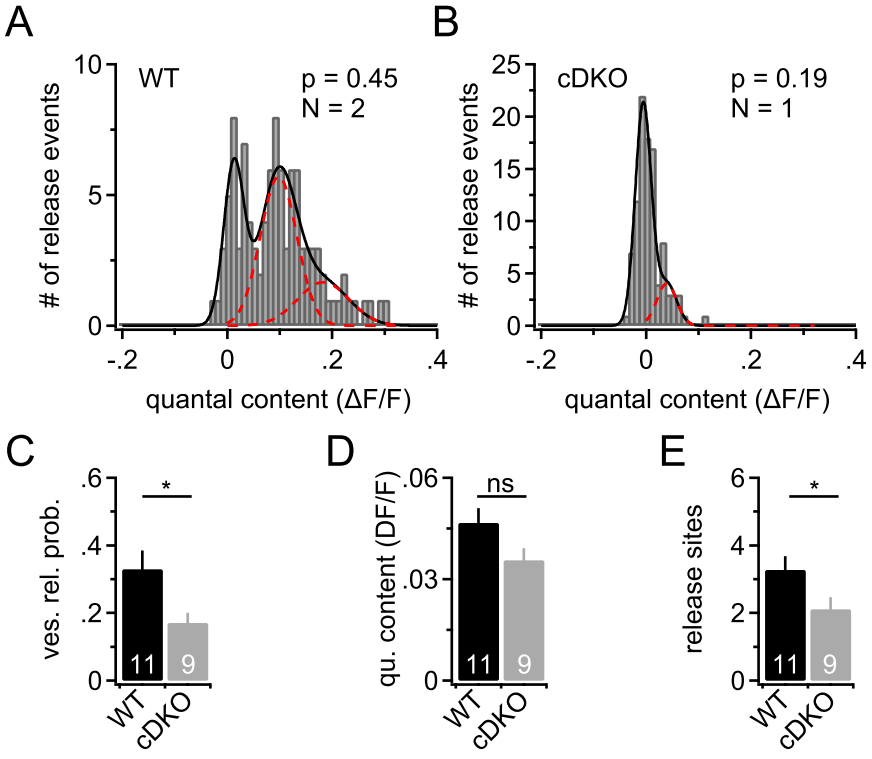

Figure 5.12: Vesicular release probability of RIM1/2 cDKO neurons was reduced compared to WT neurons. **(A)** Frequency distribution and best fit of a WT synapse. Black line indicates fit over whole frequency distribution. Red dashed lines are gaussian of single- and multi-quantal release. Fit of noise (Gaussian with peak at 0) is not shown. **(B)** Frequency distribution of release events of a RIM1/2 cDKO synapse. **(C)** Quantification of vesicular release probability. The vesicular release probability of RIM1/2 cDKO neurons was reduced by 49.4 %. **(D)** Quantification of quantal content measured as ΔF/F amplitude from release events. RIM1/2 cDKO neurons had quantal contents that were not significantly reduced compared to control neurons. **(E)** The amount of release sites per synapse was significantly reduced by 35.5 % in RIM1/2 cDKO neurons. Data in bar graphs illustrate means ± SEMs. Number of analyzed glutamate response sites (n) per condition as indicated in the bar graphs. Statistical significance was assessed by two-tailed unpaired t-test (* $p < 0.05$).

Fitting of the data showed that the vesicular release probability of cDKO neurons was significantly reduced by 49.4 % (WT: 0.33 ± 0.055; cDKO: 0.17 ± 0.03, Figure 5.12 C). Additionally, cDKO neurons had significantly less readily releasable vesicles (i.e. release sites) per synapse (reduced by 35.5 %; WT: 3.27 ± 0.4; cDKO: 2.11 ± 0.35; Figure 5.12_E). The quantal content per vesicle did not change significantly

(WT: 0.047 ± 0.004; cDKO: 0.036 ± 0.004; Figure 5.12 D). Taken together, the data indicate that the two parameters that define the synaptic release probability are reduced in RIM1/2 cDKO neurons.

5.3.6 GFP-RIM1α rescues synaptic release probability of RIM1/2 cDKO

After proving that the phenotype of RIM1/2 cDKO neurons resembled the phenotype of RIM1α KO neurons, we next examined whether our GFP-RIM1α splicing variant (Figure 5.10 A) was able to rescue the reduced release probability of RIM1/2 cDKO neurons in a similar manner as before (considering the fact that in RIM1/2 cDKO neurons all large isoforms are ablated). We co-transduced GFP-RIM1α with the Cre - recombinase or control virus at DIV4 - 6 and investigated the neurons at DIV14 - 21. Expression of GFP-RIM1α in cDKO neurons was clearly visible (Figure 5.13 B) and co-localized with FM puncta (Figure 5.13 C), which indicated synaptic localization of GFP-RIM1α in RIM1/2 cDKO neurons.

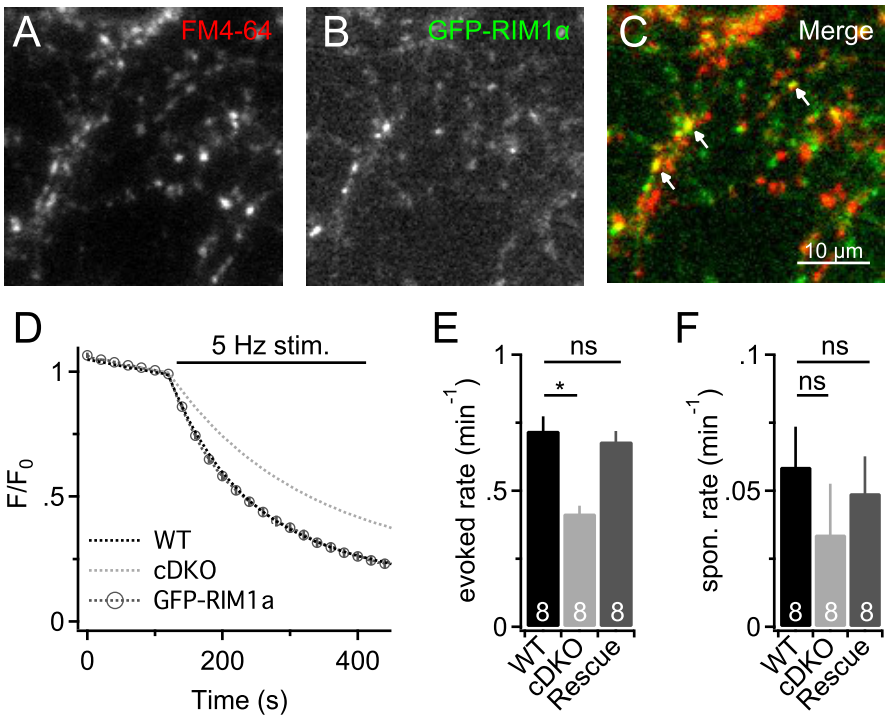

Figure 5.13: Reduced synaptic release probability in RIM1/2 cDKO neurons is rescued by lenti-viral expression of GFP-RIM1α fusion protein. (A-C) Representative images of FM4-64 staining (A) and GFP-RIM1α expression (B). The puncta from FM staining and GFP-RIM1α expression co-localize (C, arrows). **(D)** Time course of WT (black), RIM1/2 cDKO (grey) and GFP-RIM1α rescue in RIM1/2 cDKO (dark grey). The rescue setted the time course back to WT level, while the cDKO had a slower loss of fluorescence at stimulation onset. For illustration reasons WT and RIM1/2 cDKO are only shown as fitted data (dashed lines) and GFP-RIM1α rescue is indicated as means ± SEMs (markers). **(E)** The evoked release rate was set back to WT levels, when RIM1/2 cDKO neurons expressed GFP-RIM1α in the used splice variant (WT: 0.72 $\pm$0.05 min^{-1}, KO: 0.42 $\pm$0.03 min^{-1}, Rescue: 0.68 $\pm$0.04 min^{-1}). **(F)** The spontaneous release of GFP-RIM1α expressing cDKO neurons was similar as in WT neurons (WT: 0.059 $\pm$0.015 min^{-1}, KO: 0.034 $\pm$0.018 min^{-1}, Rescue: 0.049 $\pm$0.028 min^{-1}). Data are shown as means ± SEMs. Statistical significance in bar graphs was tested with One-Way ANOVA and Tukey's Post-Hoc test (* $p < 0.05$). Amount of experiments per condition (n) as indicated in bar graphs.

Stimulation of GFP-RIM1α transduced RIM1/2 cDKO neurons with 5 Hz ongoing field potentials resulted in a time course of dye release that was identical with WT neurons (Figure 5.13 D). Quantification of the evoked release rate showed that the RIM1/2 cDKO release deficits were fully rescued by introduction of this single RIM1α isoform (Figure 5.13 E, evoked release rates were: WT: 0.72 $\pm$ 0.05 min^{-1}, KO: 0.42 $\pm$ 0.03 min^{-1}, Rescue: 0.68 $\pm$ 0.04 min^{-1}). Again we also tested the spontaneous release and found that (even though no significance was detected) the rescue condition elevated spontaneous release, which resembled the WT condition (Figure 5.13 F).

5.4 Identification of phosphorylation sites in RIM1α

RIM1α has been shown to be a phosphoprotein [Lonart et al., 2003, Mahdokht et al., 2016]. However, even though it is assumed that phosphorylation of RIM1α is involved in synaptic release and plasticity it has not been clearly proven so far. Here, we tried to identify kinases that are evidently involved in RIM1α phosphorylation, investigated the effect of RIM1α phosphorylation on synaptic release and plasticity and to name the relevant phosphorylated amino acid residues in RIM1α. In a first step we sought to identify candidate phosphorylation sites and responsible kinases by means of bioinformatic tools and mass spectrometry based analysis.

5.4.1 Bioinformatic identification of RIM1α phosphorylation sites

The consensus sites for many kinases are known and can be used to get a first selection of potential phosphorylation sites in proteins. We used different databases and consensus analysis tools to predict phosphorylation sites in RIM1α. We mainly considered sites that were likely to be phosphorylated by PKA, CamKII, PKC and MAP kinases since these are kinases that have been linked to synaptic plasticity and release. As sequence template for RIM1α, the sequence from rat RIM1α was used (uniprot entry no.: Q9JIR4).

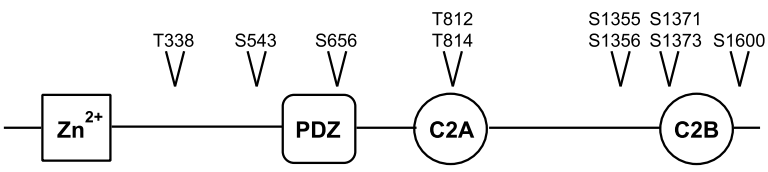

Figure 5.14: Potential phosphorylation sites in RIM1α protein sequence identified by means of bioinformatic tools. Cartoon illustrates RIM1α domain structure and the positions of potential phosphorylation sites that were point-mutated to alanine and glutamate for analysis in later release assays. For sites in direct proximity (e.g. T812/814) double-mutants were generated.

Predicted phosphorylation sites were ranked for top hits and the ten most likely sites were mutated to phospho-deficient point mutations (mutation to alanine) to check functional relevance in later *in vitro* experiments. We excluded S413 which was ranked very high in all of the used tools, since it had already been studied and shown not to be important for mossy fiber long-term potentiation [Yang & Calakos, 2010, Kaeser et al., 2008a]. In cases of sites close to each other we generated double mutations (e.g. T812/814). Interestingly, all selected phosphorylation sites are highly conserved among species. Figure 5.14 includes bioinformatically identified sites and their relative position within the RIM1α domain structure.

5.4.2 Activity regulated phosphorylation helps to identify phosphorylation sites of RIMα

An alternative, evidence based approach was performed in collaboration with Mark E. Graham (Children's Medical Research Institute in Westmead, Australia). Synaptosomes or cultured neurons were depolarized with 20 and 76 mM K^+ or mock-stimulated with 4.7 mM K^+ for 10 s. Afterwards the synaptic phospho-proteome was analyzed with phospho-enrichment and mass spectrometry over a time course of 900 s (Figure 5.15 A). This protocol leads to a strong regulation of phosphorylation sites in proteins in the presynaptic compartment. The protein with the largest changes in phosphorylation was Bassoon, which appears to be a major target of phospho-signaling in the presynapse. Additionally, RIM1α was among the proteins with high magnitude changes in phosphorylation. In the synaptosomal preparation 17 significantly regulated phosphorylation sites were identified in RIM1α, whereas in the neuronal preparation this number was much higher (around 40). From all significantly regulated sites we mutated 12 high ranking amino acid residues (Figure 5.15 C) for further investigation in later release assays (detailed results can be found in [Engholm-Keller et al., 2019]).

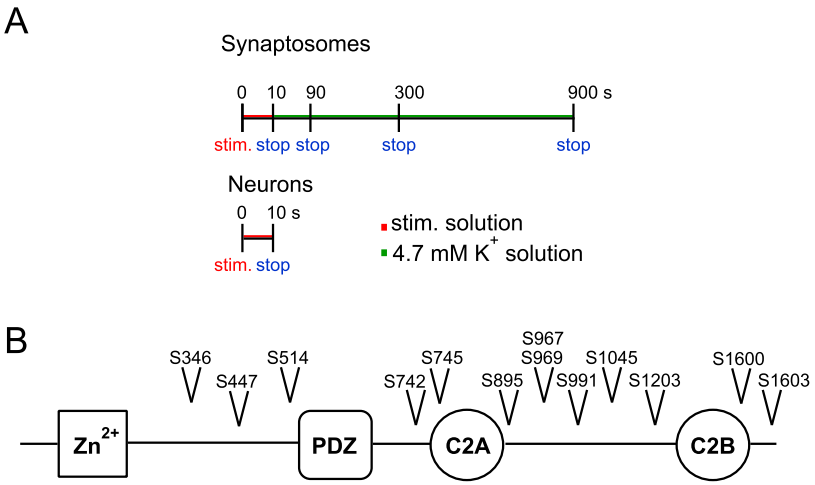

Figure 5.15: Phospho-enrichment and mass spectrometry analysis for the identification of phosphorylation sites in RIM1α. (A) Protocols for synaptosome and neuron stimulation. Preparations were stimulated with 4.7, 20 or 76 mM K^+ for 10 s. Afterwards solution was switched to 4.7 mM K^+ and preparations were lysed at the indicated stop-time-points. Lysed preparations were further processed for mass spectrometry as described in Engholm-Keller et al., 2019. **(B)** Regulated phsophorylation sites in RIM1α that were mutated to phospho-deficient (S to A) or phospho-mimetic (S to E) variants. The results are partly published in [Engholm-Keller et al., 2019].

5.4.3 Depolarization of neurons activates different kinases and phosphatases

The phosphorylation and de-phosphorylation of proteins in an activity dependent manner, as seen in Section 5.4.2, requires the activation/inactivation of kinases and phosphatases. Which kinases are activated to which extend at which time-points can be assessed by investigation of the sequence of phosphopeptides at different time points after neuron or synaptosome depolarization. These sequences can be compared with known or very likely consensus sites of kinases and the frequency of detection of respective sequences can be used to calculate the activity of a kinase at the given time point. Our collaborators Mark E. Graham and Caspar Engholm-Keller (Children's Hospital, Westmead, Australia) introduced the KinSwing analysis (Figure 5.16 A), which uses this rational to calculate the activity of a kinase at a given time point in the mentioned experimental paradigm (for further details see Engholm-Keller et al., 2019). From this analysis it became evident that after 10 s of 76 mM K^+ stimulation especially CamKII and PKA were among the most active kinases. This was similarly seen in synaptosomal preparations and in neuronal preparations, which indicates a high preservation of distinct pathways in the different preparations. We experimentally verified the increased activity of CamKII after 10 s stimulation with 76 mM K^+ using a known CamKII phosphorylation site in SynapsinI, one of the best characterized phosphoproteins in the presynapse. SynapsinI is evidently phosphorylated by CamKII at position S603 [Wang, 2008]. We used lysates from neurons stimulated according to the described experimental paradigm and analyzed the phosphorylation of S603 using a phospho-specific anti-SynapsinI antibody (Rockland, Limerick, USA).

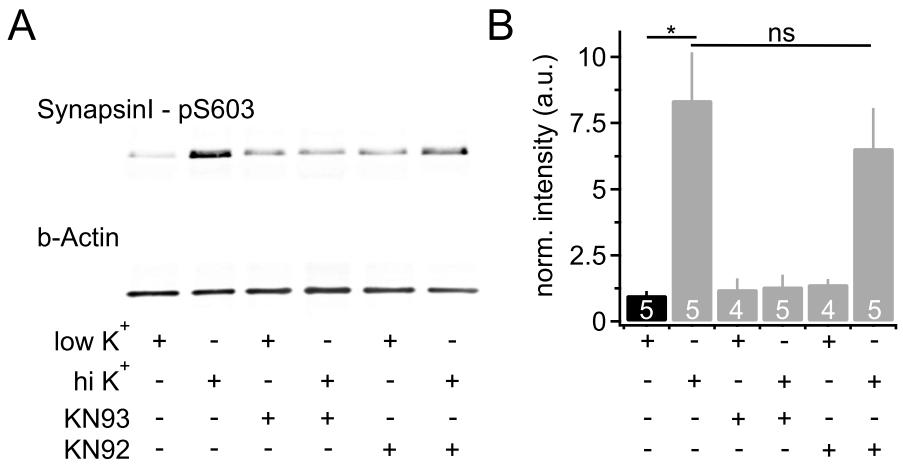

Figure 5.16: CamKII is activated when neurons are depolarized. (A) Verification of activity of CamKII with the known substrate SynapsinI^{S603}. Stimulated Neurons were lysed and phosphorylation of SynapsinI at S603 was investigated via Western Blot with an anti-SynI^{pS603} antibody. (low K^+ = 4.7 mM, hi K^+ = 76 mM, KN93 and KN92 applied at 20 µM) **(B)** Quantification showed a significant increase in phosphorylated S603 upon stimulation, which could not be achieved when CamKII was inhibited with KN93. The inactive analogue KN92 did not lead to a significant reduction of pS603. Data are presented as means ± SEMs. Number of experiments (n) as indicated in the bar graph. Statistical significance in B was assessed with One-way ANOVA and Tukey's Post-hoc test (* $p < 0.05$).

To confirm that the phosphorylation was really mediated by CamKII and not another unknown or unspecific kinase we applied the CamKII inhibitor KN93 (Tocris, Bristol), or as control the inactive analogue KN92 (Tocris, Bristol). After 10 s stimulation with 76 mM K^+ phosphorylation of S603 in SynapsinI was significantly increased around 8-fold compared to mock-stimulation with 4.7 mM K+ (Figure 5.16 A and B). Inhibition of CamKII with KN93 failed to induce the strong increase in phosphorylation of S603. Application of KN92 did not significantly affect the phosphorylation of SynapsinI after neuron depolarization. The down-regulation of phospho-sites in the late time points of the mass spectrometry experiments [Engholm-Keller et al., 2019] suggested that the stimulation of neurons not only activated kinases, but also phosphatases. An interesting phenomenon of the short, but strong neuron stimulation was that the release probability of stimulated neurons was reduced 900 s post-stimulus, compared with untreated control cultures [Engholm-Keller et al., 2019]. Accompanied with this reduction in release probability, was a reduction in substrate phosphorylation and kinase activity, which indicates that in the late phase of the experiment phosphatases might be activated, which could lead to a reduction in vesicle release. We tested whether Protein Phosphatase 1 (PP1) might be involved in decreasing the release probability. We performed FM dye imaging with pre-stimulated neurons and applied Tautomycetin, a PP1 inhibitor to test whether this would rescue the initial release probability (Figure 5.17 A). While the initial stimulation alone leaded to a reduction of the release rate by 28.6 %. The release probability was rescued when 0.6 µM Tautomycetin was applied to the neurons (Figure 5.17 B and C). Interestingly, application of Tautomycetin without pre-stimulus also resulted in a significant reduction of the release probability (Figure

5.17 C), which indicates that under basal conditions PP1 is involved in setting the steady-state release probability.

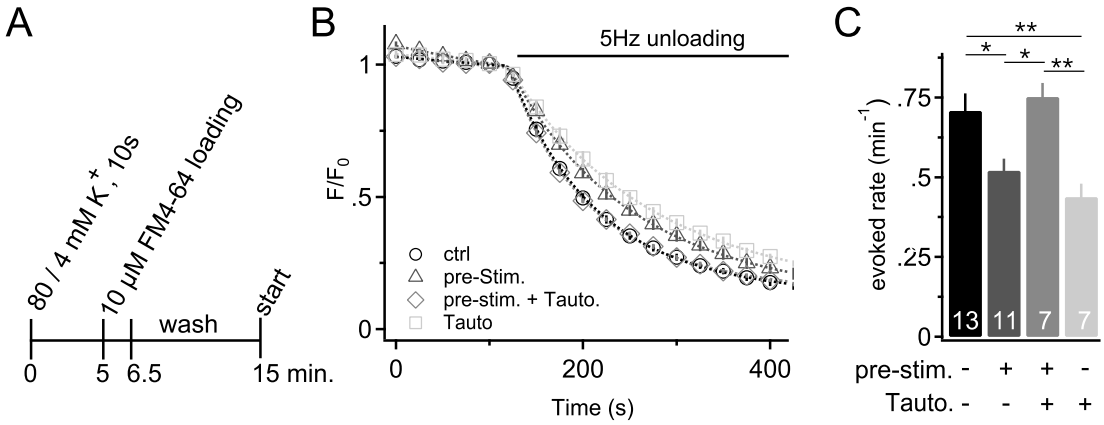

Figure 5.17: Protein phosphatase 1 (PP1) is responsible for reduced release probability in the late phase of the experimental paradigm. (A) Experimental procedure. Neurons were pre-stimulated with 80 mM K^+ or mock-stimulated with 4 mM $K^+$and after 5 minutes of rest FM dye was electrically loaded. Acquisition was started 15 min (900 s) after application of the pre-stimulus, which copies the experimental paradigm of the mass-spec experiments. **(B)** Time courses of dye loss of different conditions. Pre-stimulated neurons did not release FM dye as fast as control neurons. The release rate can be rescued when pre-stimulated neurons are pre-treated with 0.6 µM tautomycetin. Note, tautomycetin alone (without pre-stimulation), also lead to a reduced release rate. Traces show means ± SEMs of different experiments. **(C)** Quantification of B. The release probability was reduced by 28.6 % when neurons were pre-stimulated with high K^+ (ctrl. 0.71 ± 0.05 min^{-1}; pre-stim.: 0.52 ± 0.04 min^{-1}). The effect could be rescued by application of the PP1 inhibitor tautomycetin (tauto.: 0.75 ± 0.04 min^{-1}). Shown are means ± SEMs. Statistical significance was assessed by One-way ANOVA with Tukey's Post-hoc test ($p < 0.05$). Amount of experiments (n) as indicated in bar graphs.

5.5 Phosphorylation sites in RIM1α that are relevant for basal release

In the bioinformatic analysis and in the mass spectrometry experiments we identified a subset of phosphorylation sites which might be potentially important for synaptic release (Sections 5.4.1 and 5.4.2). To examine which sites affect synaptic vesicle release we generated lenti-viral vectors of GFP-RIM1α with point-mutations that render the protein deficient for phosphorylation at specific serine or threonine residues. We expressed these mutants in RIM1αKO or RIM1/2 cDKO neurons and tested for rescue of the already described reduction in release probability (see Section 5.3.3 and 5.3.6). For technical reasons we started with RIM1α KO neurons stimulated with K^+ and the potential phospho-sites identified via consensus analysis.

5.5.1 Mutations of T812/814 and S1600 to alanine are not able rescue the reduced release probability of RIM1α KO neurons

Potential phospho-sites selected from the bioinformatic analysis were point-mutated to generate phospho-deficient RIM1α mutants. After expression of the constructs in RIM1α KO neurons, we investigated whether the reduced release rate was rescued back to WT levels (Figure 5.18). The parameter that was compared was the evoked release rate, because this was the primary phenotypic hallmark we could identify in the RIM1α KO neurons with our FM dye approach. Almost all phospho-deficient mutants rescued the reduced release probability. Only two constructs failed to rescue the evoked release rate - T812/814A (Figure 5.18 D) and S1600A (Figure 5.18) G). The mutants had release rates of 0.15 min^{-1} ($\pm$ 0.016, T812/814A) and 0.146 min^{-1} ($\pm$ 0.013, S1600A), which were comparable with the RIM1α KO release rates of 0.12 - 0.13 min^{-1}. Even though we could not detect a significant change of spontaneous release between WT and RIM1α KO condition, we constantly saw a reduction in this parameter in the RIM1α KO neurons (for example see Figure 5.9). Interestingly, this reduction was always set back to WT level when GFP-RIM1α constructs were expressed in the RIM1α KO neurons (data not shown). The results point to a functional relevance of the phosphorylation sites T812/814 and S1600 for evoked synaptic release.

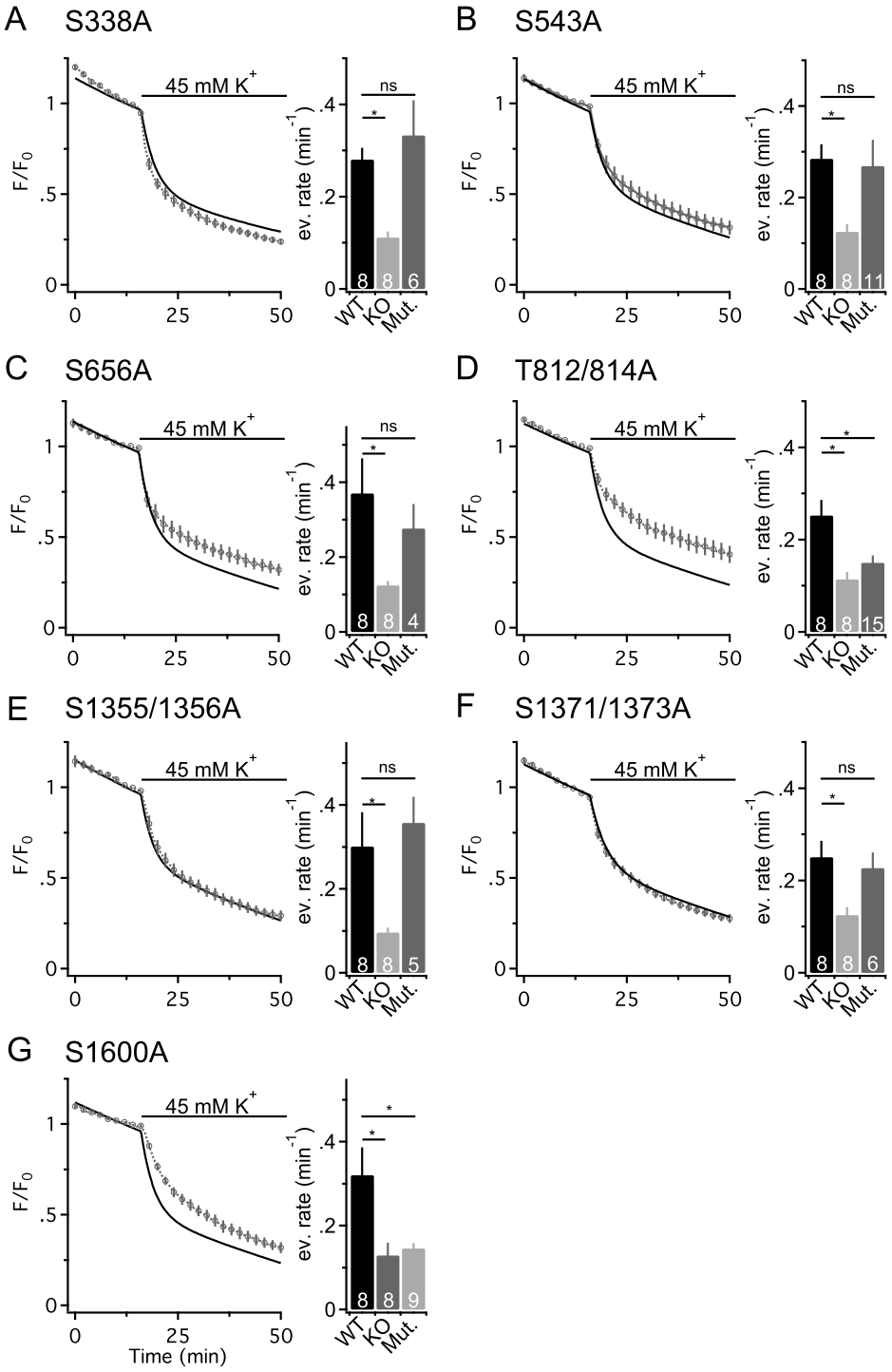

Figure 5.18: RIM1α KO rescue screening of phospho-deficient GFP-RIM1α constructs. (A-G) Different mutants where lenti-virally expressed in RIM1α KO neurons and FM dye imaging was used to screen for their rescue capability. Only the mutants T812/814A (D) and S1600A (G) showed a significant lack of rescue in the dye release assay. The evoked release rates of T812/814A ($0.15 \pm 0.016\,\mathrm{min}^{-1}$) and S1600A ($0.146 \pm 0.013\,\mathrm{min}^{-1}$) are significantly reduced compared to WT ($0.3 - 0.37\ \mathrm{min}^{-1}$) and are on level with the RIM1α KO phenotype ($0.12 - 0.13\ \mathrm{min}^{-1}$). Black traces in release graphs show fitted time course of WT experiments. Dark grey traces with markers indicate mean time courses ± SEMs of mutations. For visualization reasons only SEM for mutants are indicated and KO time-courses were not plotted. Data in bar graphs depict means ± SEMs. Statistical significance was assessed by One-Way ANOVA with Dunnet's correction for multiple comparisons (* $p < 0.05$). Amount of experiments (n) as indicated in bar graphs.

5.5.2 S991A, T812/814A and S1600A fail to rescue reduced release probability when physiologically stimulated

To confirm and extend the data from Section 5.5.1 we wanted to investigate the phosphorylation sites found in mass spectrometry experiments (see Section 5.4.2) for release deficiency. This time we used RIM1/2 cDKO neurons and a physiological stimulation approach with electrical field potentials delivered at 5 Hz for the induction of evoked vesicle release. We co-transduced Cre - recombinase and GFP-RIM1α mutants at DIV4 - 6 in hippocampal RIM1/2$^{fl/fl}$ neurons and performed the experiments at DIV14 - 21. As control we used WT neurons or neurons transduced with an inactive dCre - recombinase. As before, most mutants completely rescued the evoked release rate in RIM1/2 cDKO neurons. However, expression of GFP-RIM1α with the mutation S991A was not able to rescue the phenotype back to control levels and lead to a significantly reduced evoked release rate (WT: 0.67 $\pm$ 0.05 min^{-1} ; GFP-RIM1α(S991A): 0.48 $\pm$ 0.05 min^{-1}).

Another interesting result was seen with GFP-RIM1α carrying the mutation S514A. In this case the phospho-deficient mutation significantly increased the evoked release rate compared to control, suggesting a gain of function mutation (WT: 0.66 $\pm$ 0.07 min^{-1} ; GFP-RIM1α(S514A): 0.89 $\pm$ 0.08 min^{-1}). This indicates that some phosphorylation sites in RIM1α promote and some sites inhibit synaptic vesicle release.

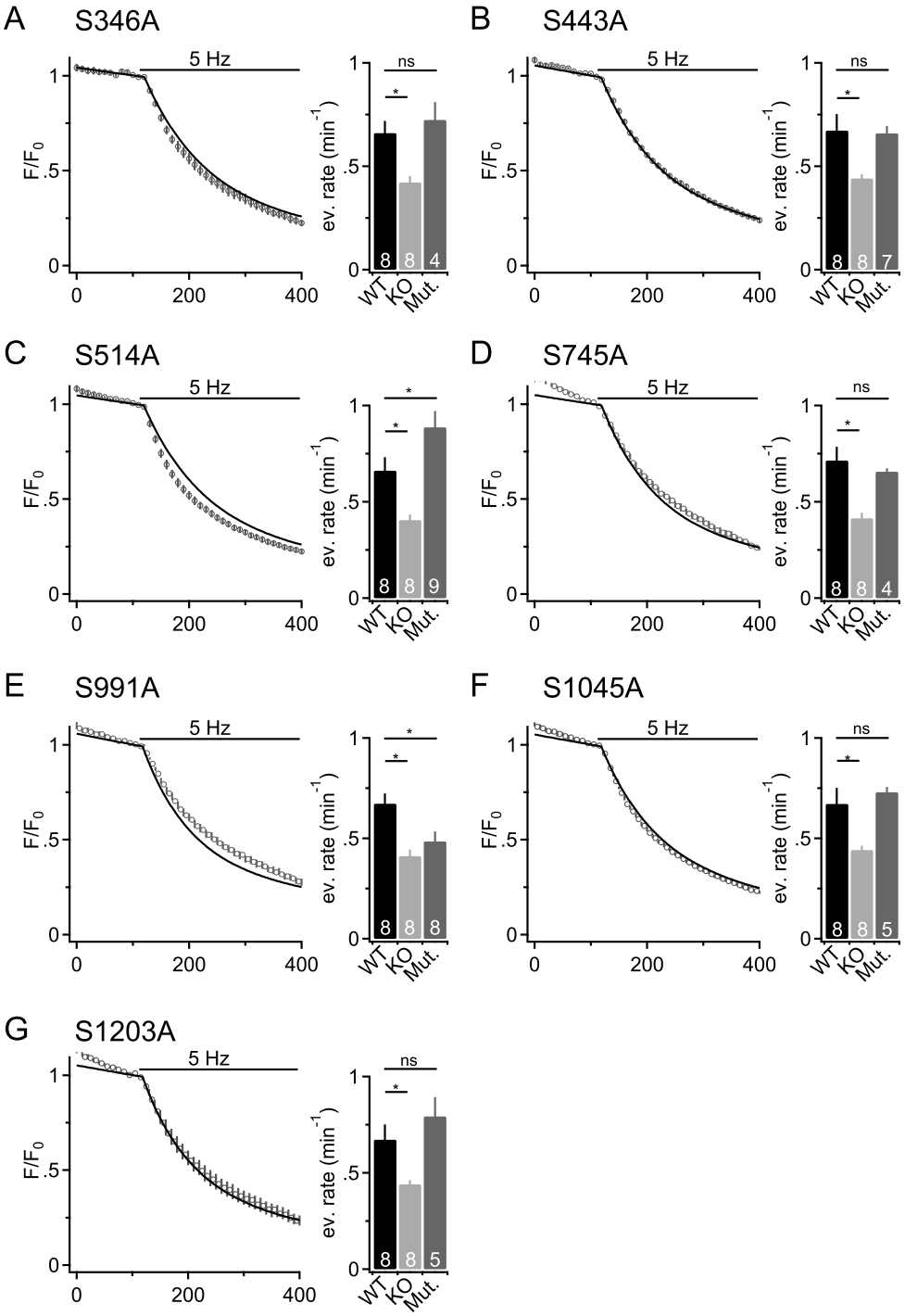

Figure 5.19: RIM1/2 cDKO rescue screening of phospho-deficient GFP-RIM1α constructs with physiological stimulation protocol. (A-G) Different mutants were lenti-virally expressed in RIM1/2 cDKO neurons and FM dye approach with field potential stimulation was used to screen for rescue of reduced release probability. The mutation S991A (E) showed a significant reduction in the evoked release rate compared to control neurons (WT: 0.67 $\pm$ 0.05 min^{-1} ; GFP-RIM1α(S991A): 0.48 $\pm$ 0.05 min^{-1}). Additionally, S514A resulted in a gain of function (WT: 0.66 $\pm$ 0.07 min^{-1} ; GFP-RIM1α(S514A): 0.89 $\pm$ 0.08 min^{-1}), leading to a significantly increase in the evoked release rate (C). All other tested phospho - deficient mutations did rescue the evoked release rate to similar levels as control conditions. Black traces in time-courses show fitted WT experiments. Dark grey traces with markers show mutations. For visualization reasons only SEM for mutants are indicated and cDKO time-courses are not plotted. Data are presented as means ± SEMs. Statistical significance was assessed by One-Way ANOVA with Dunnet's correction for multiple comparison (* p < 0.05). Number of experiments (n) as indicated in bar graphs.

We also retested the two mutations T812/812A and S1600A with electrical field-potentials to confirm the results from the experiments with K^+ - stimulation. In both cases the release deficiency of the mutations was confirmed in RIM1/2 cDKO neurons (Figure 5.20).

Taken together, we found three sites (T812/T814, S991 and S1600) which cannot rescue the reduced release probability of RIM1α KO and RIM1/2 cDKO neurons. Moreover, we have strong evidence, that the site S514 leads to a gain of function, when it is rendered phospho-deficient.

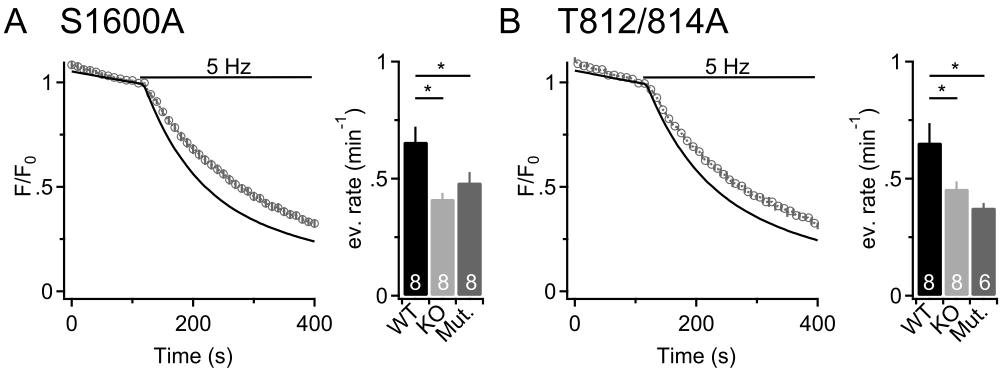

Figure 5.20: Confirmation of release deficiency of RIM1α mutants S1600A and T812/814A using electrical stimulation. The mutants S1600A and T812/814A failed to rescue the reduced release probability of RIM1α KO in former experiments with high K^+stimulation. This was confirmed by electrical stimulation in RIM1/2 cDKO. The time courses of the mutations S1600A (A, left) and T812/814A (B, left) showed a slower dye loss compared to WT. The evoked release rates were significantly reduced for S1600A (A, right, WT: 0.66 $\pm$ 0.06 min^{-1}, KO: 0.41 $\pm$ 0.03 min^{-1}; Mut.: 0.48 $\pm$ 0.04 min^{-1}) and for T812/814A (B, right, WT: 0.65 $\pm$ 0.08 min^{-1}, KO: 0.46 $\pm$ 0.03 min^{-1}; Mut.: 0.38 $\pm$ 0.02 min^{-1}). Data in bar graphs show means ± SEMs. Statistical significance was assessed by One-Way ANOVA with Dunnet's correction for multiple comparisons (* p < 0.05). Amount of experiments (n) as indicated in bar graphs. Black traces in time courses show fitted WT experiments. Dark grey traces with markers show mutations. For visualization reasons only SEM for mutants are indicated (very small) in time courses and cDKO time courses are not plotted.

5.5.3 Phospho-mimicry rescues release deficiency

A point mutation of serine or threonine to alanine renders a potential phospho-site deficient for phosphorylation. In contrast, mutations from serine or threonine to glutamate or aspartate are considered to mimic a constant phosphorylation of the specific amino acid residue [Maciejewski et al., 1995]. An important question was whether phospho-mimicry could rescue the release deficiency of the sites found in the former sections. We mutated S991 and S1600 to glutamate and repeated the FM experiments as before (T812/814 was not checked by this procedure, so far). We introduced GFP-RIM1α with mutation S1600E in RIM1α KO and RIM1/2 cDKO neurons and checked for rescue efficiency with potassium stimulation and electrical field-potentials. We found that in both cases the release deficiency was set back to WT levels (Figure 5.21). We did see identical time courses of FM dye loss between rescue and WT in both experimental paradigms (Figure 5.21 A and B). The evoked release rates did not differ significantly

from the WT (control) conditions (Figure 5.21 A and B bar graphs).

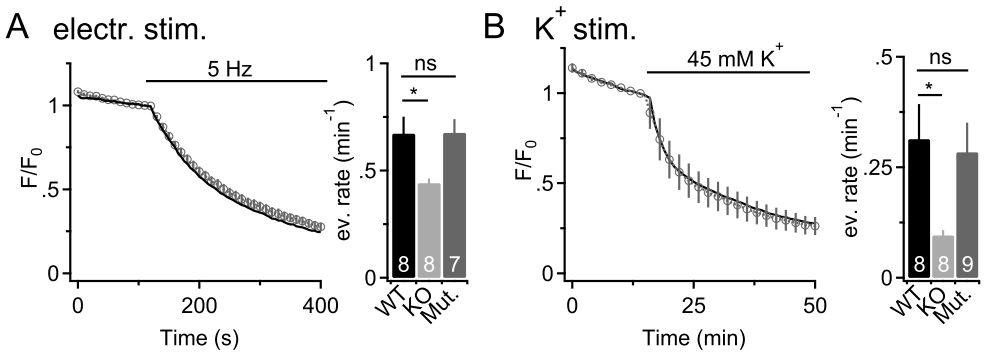

Figure 5.21: Phospho-mimicry at position S1600 rescued the reduced release rate of RIM1α KO and RIM1/2 cDKO neurons. (A) GFP-RIM1α(S1600E) was transduced in RIM1/2 cDKO neurons and rescue of reduced release rate was measured with FM dye imaging and electrical stimulation. GFP-RIM1α(S1600E) rescued the release probability to identical levels as control conditions (WT: 0.67 $\pm$0.08 min^{-1}; KO: 0.44 $\pm$0.021 min^{-1}; Mut.: 0.68 $\pm$0.06 min^{-1}) **(B)** Same as in A, but with RIM1α KO neurons and K^{+}stimulation. Again the reduced release probability was rescued (WT: 0.31 $\pm$0.08 min^{-1}; KO: 0.1 $\pm$0.012 min^{-1}; Mut.: 0.28 $\pm$0.07 min^{-1}). Data in bar graphs show means ± SEMs. Statistical significance was assessed by One-Way ANOVA with Dunnet's correction for multiple comparisons (* p < 0.05). Amount of experiments (n) as indicated in bar graphs. Black traces in time courses show fitted WT experiments. Dark grey traces with markers show mutations. For visualization reasons only SEM for mutants are indicated in time courses and cDKO time courses are not plotted.

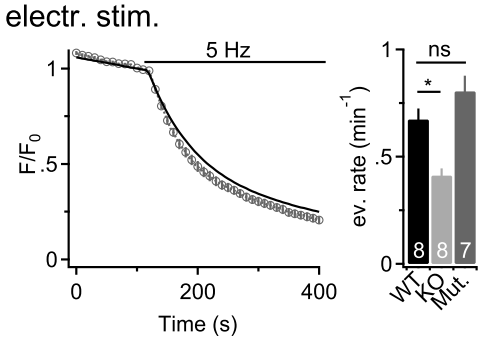

Figure 5.22: Phospho-mimicry at position S991 rescued reduced release rate of RIM1/2 cDKO. GFP-RIM1α(S991E) was transduced in RIM1/2 cDKO neurons and rescue ability was measured with the FM dye approach and electrical stimulation. The phenotype was fully rescued and, although not significant, the evoked release rate seemed to be increased by 15.9 % (WT: 0.69 $\pm$0.08 min^{-1} vs Mut.: 0.80 $\pm$0.07 min^{-1}). Data in bar graphs show means ± SEMs. Statistical significance was assessed by One-Way ANOVA with Dunnet's correction for multiple comparisons (* p < 0.05). Amount of experiments (n) as indicated in bar graphs. Black traces in time courses show fitted WT experiments. Dark grey traces with markers show mutations. For visualization reasons only SEMs for the mutation are indicated (very small) in time courses and cDKO time course is not plotted.

Rescue potential of GFP-RIM1α with mutation S991E was only tested in RIM1/2 cDKO cells with field potential stimulation paradigm. The average time course of fluorescence loss of cDKO cells expressing GFP-RIM1α(S991E) was comparable with the time course of WT cells (Figure 5.22). The quantified release rate (estimated by single ROI fitting) seemed to be increased by 15.9 % compared to WT, but we could not detect statistical significance (WT: 0.69 $\pm$0.08 min^{-1} vs Mut.: 0.80 $\pm$0.07 min^{-1}, Figure

5.22). These results indicate that phosphorylation of the sites S991 and S1600 is necessary for basal neurotransmitter release.

5.6 Localization and mobility of GFP-RIM1α variants in synaptic structures

5.6.1 GFP-RIM1α with release relevant mutations are present in synaptic terminals

A prerequisite for RIM1α to be functional is the correct transportation to and localization in the presynaptic terminal. Especially, for the mutations that can not rescue the reduced synaptic release probability the question came up, whether these GFP-RIM1α variants are located in synaptic terminals, or whether the mutations lead to transportation and localization deficiencies. We immunostained primary hippocampal neurons for Bassoon as a synaptic marker or loaded vesicles with FM dye and checked whether our GFP-RIM1α fusion proteins, that carry the mentioned mutations, are co-localized. GFP-RIM1α fusion proteins with point mutations S1600A or T812/814A were co-localized with FM4-64 in synaptic terminals (Figure 5.23) indicating synaptic transportation of these variants.

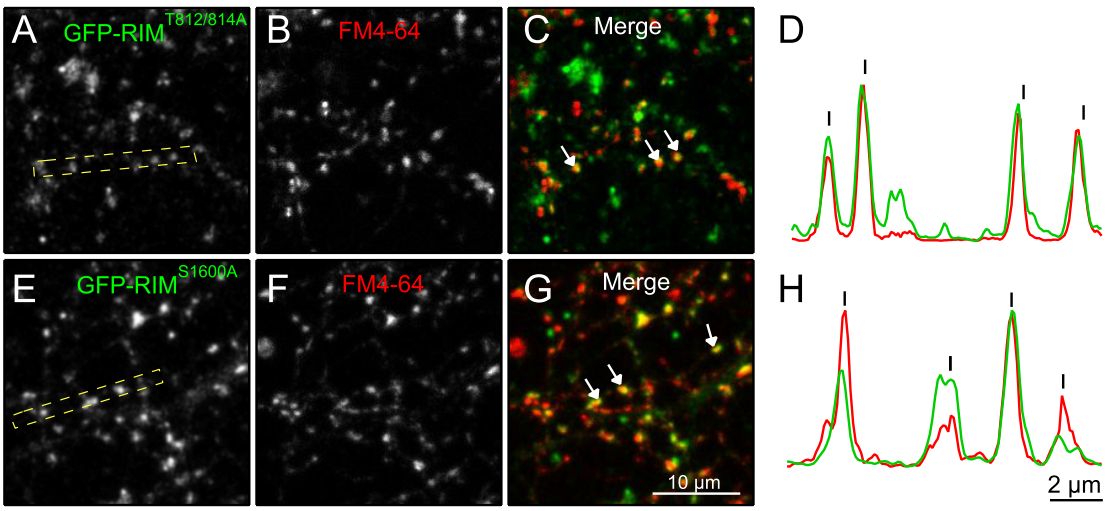

Figure 5.23: GFP-RIM1α(T812/814A) and GFP-RIM1α(S1600A) are localized in putative synaptic structures as identified by FM4-64. Representative images of neurons expressing GFP-RIM1α(T812/814A) **(A-D)** and GFP-RIM1α(S1600A) **(E-H)**. Synaptic vesicles in these neurons were loaded with FM4-64. There is good co-localization of GFP-RIM1α and FM4-64 (examples are marked with arrows). **(D and H)** Intensity profiles of the two channels in marked areas of (A) and (E). Intensity peaks of FM4-64 and GFP-RIMα match to a high degree (indicated by vertical line markers).

GFP-RIM1α with mutations S991A or S991E was also located in synaptic structures as seen by co-localization with Bassoon immunostaining (Figure 5.24). Nevertheless, even though we saw a high degree of synaptic localization, there was also a considerable proportion of unspecific signal in the cytoplasm in all transfected and lenti-virally expressed GFP-RIM1αvariants (Figure 5.24 A and E).

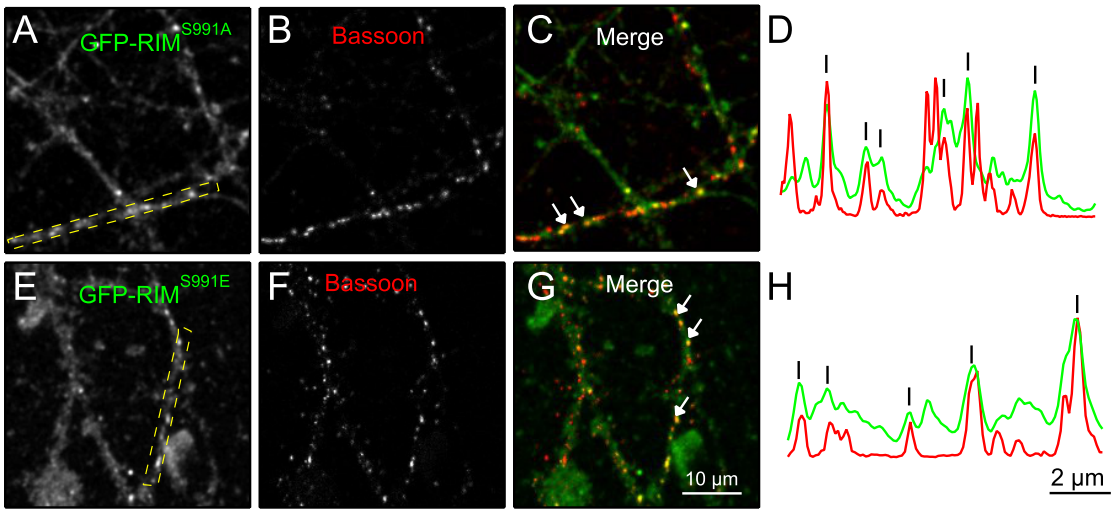

Figure 5.24: GFP-RIM1α(S991A) and GFP-RIM1α(S991E) are localized in synaptic structures. Representative images of neurons expressing GFP-RIM1α(S991A) **(A)** and GFP-RIIM1α(S991E) **(E)**. Neurons were immunostained for Bassoon **(B and E)** to identify putative synaptic structures. The colocalization of GFP-RIM1α and Bassoon indicated correct transportation of the RIM1α mutants to synaptic structures (examples are marked with arrows). **(D and H)** Intensity profiles of the channels in the marked areas in A and E. Intensity peaks of Bassoon staining and GFP-RIMα signal match to a high degree (indicated by vertical line markers).

5.6.2 GFP-RIM1α(S1600A) shows altered persistence in CAZ

Next to synaptic localization, the ability of RIM1α to be integrated into the CAZ to become a part of the release machinery, is crucial for its function in synaptic release. We used fluorescence recovery after photo-bleaching (FRAP) to investigate whether GFP-RIM1α(S1600A/E) fusion proteins were integrated in the CAZ and whether the strength of this integration would be altered in the different mutations. The rational behind this approach is the following: GFP-RIM1α that is integrated in the CAZ should retain longer at the AZ as free floating GFP or unbound GFP-RIM1α. Therefore, the recovery of bleached fusion proteins that are integrated in the CAZ should be slower compared to cytoplasmic proteins. If the mutation of a certain amino acid residue leads to a change in the strength of protein-protein binding, or even cause changed binding partners, this might influence the strength of GFP-RIM1α integration in the CAZ. A changed retention time could be the result and should be visible by altered recovery of fluorescence. We transduced or transfected hippocampal WT neurons with lenti-viral vectors to express

fluorescence proteins at DIV4 - 6 and performed FRAP experiments at DIV14 - 21, when synaptic structures were mature.

In a first step we tested whether GFP-RIM1α(WT) was integrated in the CAZ, by comparing the fluorescence recovery with transfected or transduced GFP that freely diffuses in the cytoplasm. The recovery of GFP-RIM1α was considerably slowed down, whereas GFP recovery took place within a few seconds (Figure 5.25 A). The reduced retention time of GFP-RIM1α itself is not necessarily evidence for integration in the CAZ, since unspecific interactions with other proteins or other GFP-RIM1α molecules (due to the overexpression) could slow down fluorescence recovery. Therefore, we tested whether the recovery of GFP-RIM1α at a position, that was likely no synapse (dendrite, soma) would also be slower compared to cytoplasmic GFP recovery (Figure 5.25 B). We found that GFP-RIM1α at cytoplasmic sites recovered at the same speed as GFP and much faster than GFP-RIM1α at putative synaptic structures.

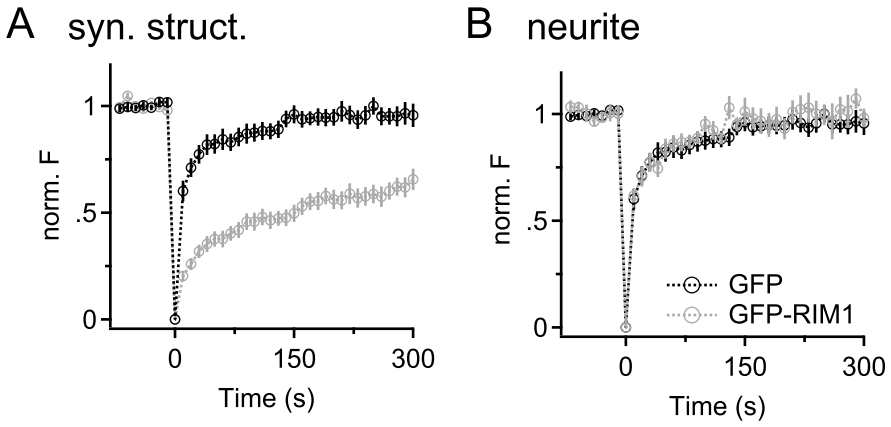

Figure 5.25: The expressed fusion protein GFP-RIM1α was integrated into the CAZ. (A) GFP-RIM1α and GFP were bleached in selected synaptic structures and fluorescence recovery was measured over time. GFP-RIM1α recovered considerably slower than GFP in the cytoplasm, which almost recovered completely back to baseline within a few seconds. **(B)** GFP-RIM1α recovery is not slowed down by unspecific protein-protein interactions. GFP-RIM1α was bleached at positions, likely not to be synaptic structures and fluorescence recovery was identical with GFP. Shown are mean recovery curves ± SEMs. We bleached 16 (GFP), 21 (synaptic GFP-RIM1α) and 13 (GFP-RIM1α on neurite) structures, respectively.

Since GFP-RIM1α seemed to be integrated in the CAZ, we asked whether the phospho-mutations change the turnover of GFP-RIM1α in the protein network.

We tested the mutations GFP-RIM1α(S1600A) and GFP-RIM1α(S1600E) and compared these to GFP-RIM1α(WT). To verify that the structures investigated were putative CAZ networks in synapses, we prestained cultures with FM4-64. We found that GFP puncta co-localize with FM4-64 in the majority of cases (see 5.26 A-C, but also see Figure 5.23). We double normalized recovery curves from individual bleached spots for ongoing photobleaching and to offset the recovery start point to zero. Next, we calculated an average recovery curve from all bleached structures in one condition. Afterwards, we fitted the average curve to a double exponential with full recovery (i.e. $y_0 = 1$) to read-out the fast and the

slow time-constants of the fluorescence recovery time course. Interestingly, theRIM1α mutant S1600A, a mutation that failed to rescue the reduced release probability, had longer retention times in the CAZ (τ_{fast} = 81.2 s, τ_{slow} = 3192.2 s) and significantly lower recovered fluorescence levels (40.03 $\pm$ 5.2 %) after 500 s, compared to GFP-RIM1α without mutation (τ_{fast} = 48.9 s, τ_{slow} = 1330 s, recovery = 61.6 $\pm$ 8.7 %, Figure 5.26 E, F and H). In contrast, GFP-RIM1α with the mutation S1600E had a similar turnover in the CAZ as the WT variant (τ_{fast} = 47.5 s, τ_{slow} = 1470 s, recovery = 54.6 $\pm$ 3.6 %, Figure 5.26 E, G and H). Nevertheless, all constructs (WT and mutations) retain relatively long in the active zone, which points to a general ability to be integrated in the active zone, independent of the named point mutations.

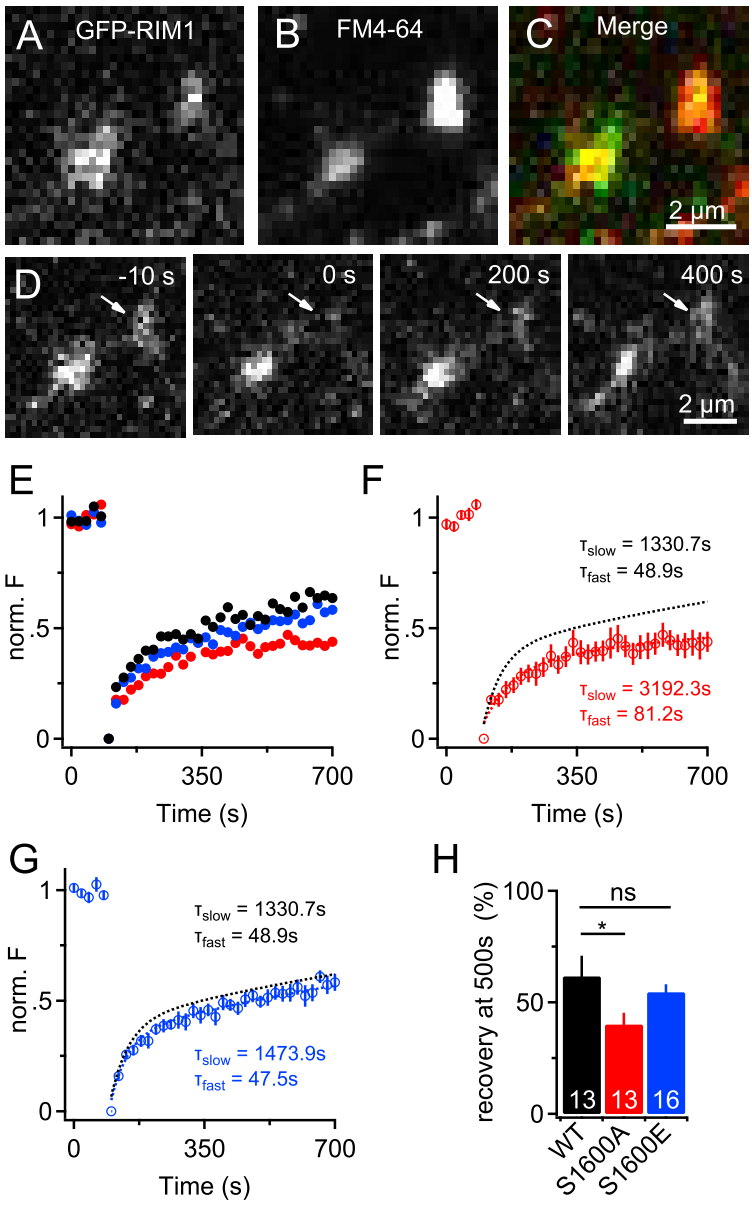

Figure 5.26: Phospho-deficiency of S1600 increased retention time of GFP-RIM1α in the CAZ. (A-C) Representative images showing co-localization (C) of GFP-RIM1α (A) and FM4-64 loading (B). **(D)** Example of bleaching and recovery of GFP-RIM1α (marked by arrows) in a putative synaptic structure at indicated time points. Note, proximal GFP spot was not bleached, pointing to a restricted bleaching to the selected area. **(E)** Comparison of average recovery of GFP-RIM1α(WT) (black markers), GFP-RIM1α(S1600A) (red markers) and GFP-RIM1α(S1600E) (blue markers). WT and S1600E recovery were similar, while S1600A recovered slower. No error bars are shown for illustration reasons **(F)** Illustration of double exponential fit (dashed red line, τ_{fast} = 81.2 s, τ_{slow} = 3192.2 s) of S1600A data (red markers) compared to WT fit (dashed black line, τ_{fast} = 48.9 s, τ_{slow} = 1330 s). The difference between the recovery is clearly visible. **(G)** Same as in F, but for S1600E (data: blue markers, fit: dashed blue line, τ_{fast} = 47.5 s, τ_{slow} = 1470 s). Almost no difference compared to WT (dashed black line, τ_{fast} = 48.9 s, τ_{slow} = 1330 s) was visible. **(H)** Average recovery of bleached spots after 500 s. GFP-RIM1α(S1600A) recovered significantly less compared to WT variant. GFP-RIM1α(S1600E) recovered to similar levels as wild-type GFP-RIM1α (recovery of WT: 61.6 $\pm$8.7 %; S1600A: 40.03 $\pm$5.2 %; S1600E: 54.6 $\pm$3.6 %). Bars indicate means of all bleached spots ± SEMs. Number of bleached spots (n) as indicated in bar graph. Statistical significance was assessed with One-Way ANOVA with Dunnet's correction for multiple comparisons (* $p < 0.05$).

5.7 The importance of the C-Terminus for synaptic release and CAZ integration

We saw that GFP-RIM1α with a mutation at S1600 to alanine lead to a reduced synaptic release probability and that this mutation increased the retention time of the fusion protein in CAZ. Therefore, we wondered whether there is a general importance of the C-terminal part of RIM1α for normal function of this protein.

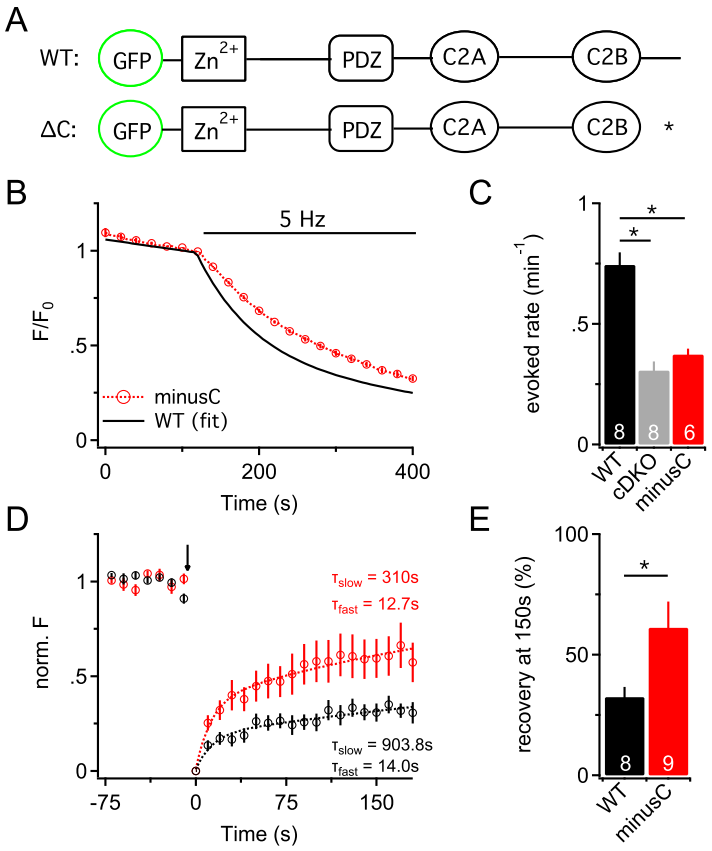

Figure 5.27: The C-terminus of RIM1α is important for synaptic release and integration of RIM1α in the CAZ. (A) Domain structure of GFP-RIM1α(WT) and GFP-RIM1α(ΔC). The truncation mutation lacks the C-terminal part, which succeeds the C2B domain (deleted amino acids: 1564-1615, marked by *). **(B)** Average time course of FM dye loss of control (illustrated as fit, black line) neurons and RIM1/2 cDKO neurons transduced with GFP-RIM1α(ΔC) (red markers). The evoked dye loss was slower in RIM1/2 cDKO with GFP-RIM1α(ΔC) compared to WT (for visualization reasons time course of RIM1/2 cDKO is not displayed, error bars as SEM are only shown for the truncation construct). **(C)** Quantification of evoked release rate in the different conditions. The evoked release rate of RIM1/2 cDKO expressing GFP-RIM1α(ΔC) was significantly reduced by 50.7 % compared to WT (WT: 0.75 $\pm$ 0.05 min^{-1}; KO: 0.31 $\pm$ 0.04 min^{-1}; ΔC: 0.37 $\pm$ 0.03 min^{-1}, One-Way ANOVA with Dunnet's correction for multiple comparisons (* p < 0.05). **(D)** Fluorescence recovery after photobleaching of GFP-RIM1α(WT) and GFP-RIM1α(ΔC) in synaptic structures of primary hippocampal neurons. The recovery of GFP-RIM1α(ΔC) was faster compared to GFP-RIM1α(WT), indicating weaker integration in the CAZ (markers indicate average data points of all bleached structures in one condition, error bars are SEMs, dashed lines are double exponential fits of data points, τ_{slow} of WT: 903.8 s, τ_{slow} of ΔC: 310 s). **(E)** The truncation mutation missing the C-terminus recovered significantly more after 150 s (WT: WT: 32.4 $\pm$ 4.2 %; minusC: 61.2 $\pm$ 10.8 %). Number of bleached spots as indicated in bar graph. Unpaired t-test (* p < 0.05).

To test this, we generated a truncated fusion protein that lacks the C-terminal part that succeeds the C2B domain (amino acids: 1564-1615, GFP-RIM1α(ΔC) or minusC, Figure 5.27 A). We used this truncation mutation in our FM dye approach and in FRAP experiments to investigate its ability to rescue the synaptic release probability in RIM1/2 cDKO and the integration of RIM1α in the CAZ. Similar to GFP-RIM1α(S1600A), the truncated GFP-RIM1α was not able to rescue the reduced release probability of RIM1/2 cDKO. The evoked release rates resembled RIM1/2 cDKO values (WT: 0.75 $\pm$ 0.05 min^{-1}; KO: 0.31 $\pm$ 0.04 min^{-1}; ΔC: 0.37 $\pm$ 0.03 min^{-1}, Figure 5.27 B and C). When we compared the recovery time of photo-bleached GFP-RIM1α(WT) and GFP-RIM1α(ΔC) in synaptic structures of cultured hippocampal neurons, we saw that the truncation mutation recovered faster compared to the WT fusion protein (τ_{slow} WT: 937 seconds, ΔC: 310 seconds, Figure 5.27 D) and had significantly higher fluorescence levels after 150 s of recovery (WT: 32.4 $\pm$ 4.2 %; minusC: 61.2 $\pm$ 10.8 %, Figure 5.27 D).
Taken together these results point to an important function of the C-terminus of RIM1α for integration and anchoring of the protein in to the CAZ and for synaptic release.

5.8 Phospho-dependent protein interactions of RIM1α

A former PhD student (Ana-Maria Oprisoreanu) in our lab investigated the interactome of RIM1α with emphasize on phospho - dependent protein binding. Experimentally, crude synaptosome from mouse brains were incubated with flag tagged fragments of RIM1α, that were treated with the kinase inhibitor staurosporine or the phosphatase inhibitor phoSTOP while expressed in HEK293T cells (as negative control methanol treatment was used). Proteins that interacted with RIM1α fragments were co-immunoprecipated via the flag tag and investigated with mass spectrometry. Four proteins were identified as promising new interaction partners of RIM1α: SRPK2, ULK1/2, VAP-A and Copine6. All four proteins interacted with a fragment of RIM**1**α containing the C2A and C2B domains and flanking regions. Interestingly, SRPK2 was detected with higher scores in mass spectrometry experiments, when samples were pre-treated with phoSTOP (a mix of phosphatase inhibitors), which causes higher levels of phosphorylation. Therefore, it was suggested that SRPK2 preferred phosphorylated RIM1α for interaction.
RIM1α(T812/814A) was one of the mutations we identified that could not rescue the reduced release probability of RIM1α KO neurons in the FM dye assay (Section 5.5.1). T812/T814 is located centrally in the C2A domain of RIM1α (Figure 5.14). We therefore tested whether the new interaction partners found in the mass-spectrometry experiments, that specifically bound to the C2A-C2B fragment, would show impaired binding with a RIM1α fragment containing the mutation T812/T814A. To this end we performed pull-downs of purified GST-C2A protein fragments with co-incubated lysates from HEK293T cells expressing the respective proteins. Copine6 and ULK1/2 did not show obvious changes in the

ability to be bound and pulled down by WT or mutated C2A fragments of RIM1α (data not shown). In case of VAP-A (and VAP-B) we detected a considerably reduced interaction with the C2A domain of RIM1α, when T812 and T814 were mutated to alanine (Figure 5.28).

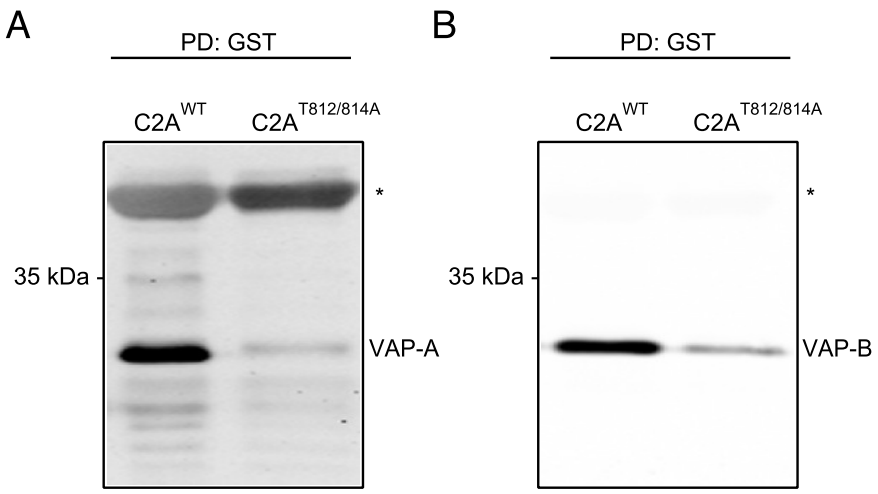

Figure 5.28: Impaired binding of VAP proteins to RIM1α(T812/814A). (A) Pull-down of VAP-A with GST-C2A fragment of RIM1α. Compared were the abilities of WT variant and the mutation T812/814A to pull-down VAP-A from HEK293T cell lysates. VAP-A bound obviously weaker to the mutated variant, as seen from the much weaker imunno-detected band below 35 kDa. The amount of used GST-C2A was comparable (GST-C2A band indicated by *). **(B)** Same experiment as in A, but VAP-B was pulled down and detected in WB. VAP-B also bound weaker to the mutated fragment of RIM1α. The experiment was repeated in N = 3 independent biological replicates with similar results.

5.9 Synaptic vesicle release correlates with the protein levels of SRPK2

When we were looking for new phospho-dependent RIM1α interaction partners in mass spectrometry experiments, one very interesting candidate was Serine/arginine - rich protein - specific kinase 2 (SRPK2). Interestingly, SRPK2 seemed to bind stronger to phosphorylated RIM1α (Section 5.8, performed by Ana-Maria Oprisoreanu). The role of SRPK2 in synaptic function has not been studied in mammalian neurons so far. Therefore, we investigated SRPK2's influence on synaptic release properties and the relevance of its binding to RIM1α.

5.9.1 SRPK2 over-expression increases and knock-down decreases synaptic release probability

It was previously shown that SRPK2 is a direct interaction partner of RIM1α (see Section 5.8, described in PhD Thesis of Ana-Maria Oprisoreanu). The binding was probably mediated by the C2A - and / or

the C2B - domain of RIM1α. Given the fact that RIM1α has important roles in neurotransmitter release, we asked whether changes in SRPK2 levels and thereby potential changes in the phosphorylation state of RIM1α would alter the release properties of cultured neurons. We transduced primary hippocampal mouse neurons either with pAAV-U6-shSRPK2-GFP or pAAV-CMV-SRPK2-GFP (as control pAAV-U6-GFP was transduced). The two constructs would decrease (shRNA mediated knock-down) or increase SRPK2 (overexpression) levels, respectively. We controlled the knock-down and over-expression efficiency and found that the knock-down reduced SRPK2 levels to around 20 - 50% of WT levels and overexpression increased SRPK2 amount to 300 - 400% over endogenous expressed SRPK2 (data not shown, performed by Julia Betzin). To assess the release properties of neurons with altered SRPK2 levels we applied the already described FM dye imaging approach (see Sections 4.7.2). We loaded the cells with FM4-64 and washed unspecific staining out while cells were left for a rest period of 9-10 minutes. Afterwards 2 minutes of baseline without stimulation was recorded, before 5 Hz ongoing field stimulation was applied for 5 minutes. As described earlier, this resulted in a time course that can be described by the sum of two exponential decay functions. We subtracted the background (see Section 4.7.2) and corrected for photo-bleaching (see Section 4.7.2). Finally we fitted the induced dye loss as described (see Section 4.7.2). The first exponential represents the spontaneous release and the second exponential defines the evoked release (see Fig. 5.29 D).

We found that when SRPK2 was over-expressed the evoked release rate is significantly increased by 32.1 % (OE rate was 0.074 $\pm$ 0.008 s^{-1}), whereas knock-down of SRPK2 reduced the release rate by 18.8 % (shRNA rate was 0.046 $\pm$ 0.004 s^{-1}) compared to control (WT rate was 0.056 $\pm$ 0.004 s^{-1}) (Fig. 5.29 E). We did not detect any difference in the relative contribution of evoked release to the total dye loss (Fig. 5.29 F) indicating that the relative distribution of vesicle pools was unchanged.

Taken together these results indicate that the SRPK2 amount and thus the potential level of RIM1α phosphorylation by SRPK2 correlates with amount of neurotransmitter release. More SRPK2 increases the synaptic release probability and less SRPK2 decreases the synaptic release probability.

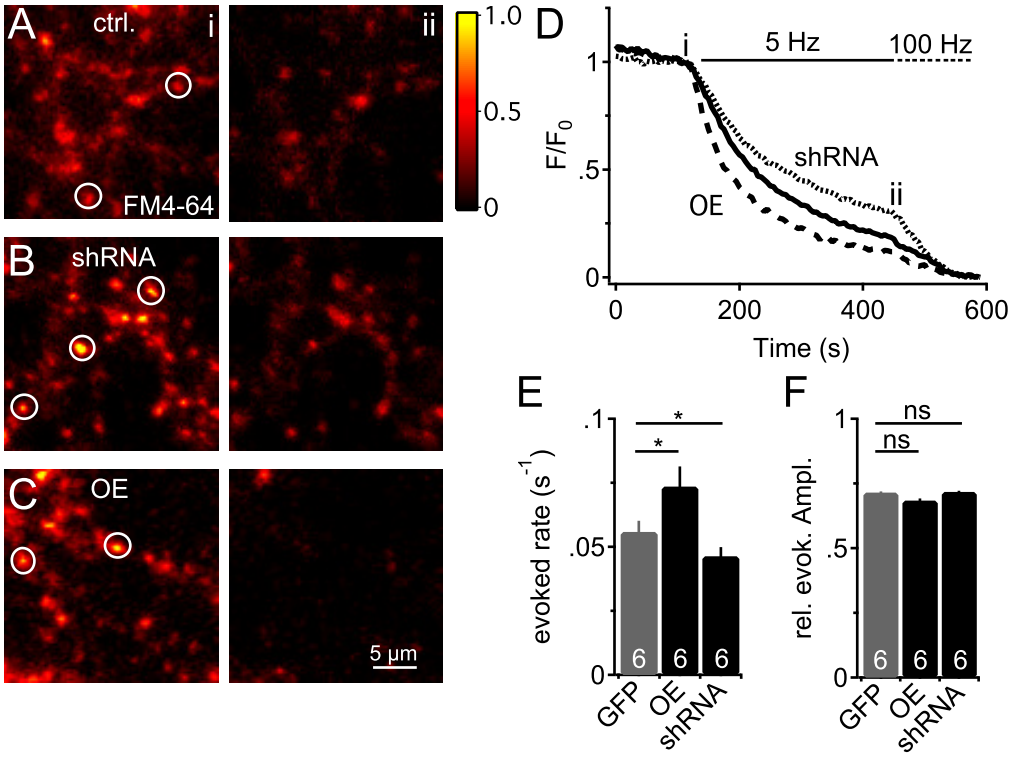

Figure 5.29: Neurotransmitter release scales with the expression level of SRPK2. (A-C) Representative images of loaded synapses (pseudo-colored) in neurons transduced GFP (= control), shRNA and SRPK2 overexpression construct. Marked regions indicate example ROIs that were used for later analysis. (D) Average time course of experiments shown in A-C. After onset of field-stimulation with 5 Hz there was a sharp drop in dye loss indicating release of synaptic vesicles. Note, that the evoked dye loss was faster when SRPK2 is over-expressed and slower when it was knocked down. (F) Quantification of the release rates of all experiments as shown in D. The evoked release rate was significantly increased in neurons with SRPK2 overexpression and decreased in neurons in which SRPK2 levels were reduced (ctrl. $0.056 \pm 0.004\,s^{-1}$; OE: $0.074 \pm 0.008\,s^{-1}$; shRNA: $0.046 \pm 0.004\,s^{-1}$). (G) Quantification of the relative evoked amplitude indicated that there is no difference in the fraction of releasable pools. Statistical significances in bar graphs were assessed by matched One-Way ANOVA with Holm-Sidak Post-hoc test (* $p < 0.05$). Number of experiments (=n) as indicated in bar graphs.

5.9.2 SRPK2 OE fails to increase glutamate release when RIM1 and RIM2 are ablated

Next, we wanted to know whether the presence of RIM is necessary or even mandatory for the increased synaptic release probability after SRPK2 overexpression. Therefore, we transduced RIM1/2$^{fl/fl}$ cells with pAAV-CBA-Cre to generate cDKO cultures and probed the amount of neurotransmitter release with the genetically encoded glutamate sensor SF-iGluSnFR.V184A (short: iGluSnFR) [Marvin et al., 2018]. The sensor is expressed extracellularly on the cell membrane and increases in fluorescence upon glutamate binding (see Section 2.10.3). First, we overexpressed SRPK2 in WT neurons to investigate whether we could reproduce the increased synaptic release seen in the FM experiments, when tested with the iGluSnFR sensor. We observed an increase in synaptic release by 56 % ($\Delta F/F$ of ctrl: 0.024 ± 0.003

;OE: 0.04 $\pm$ 0.003, Figure 5.30 E and I), which confirmed the results from the FM dye assay (see Section 5.9.1).

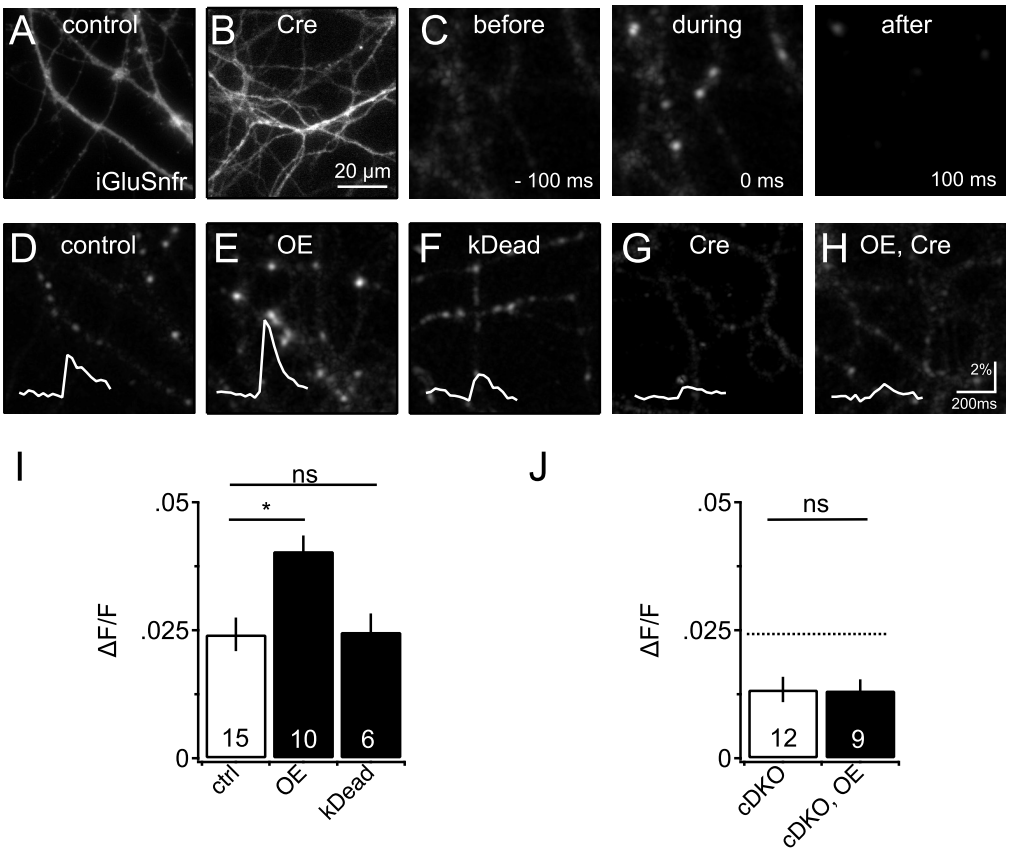

Figure 5.30: Changes in neurotransmitter release of RIM1/2 cDKO neurons investigated with the glutamate reporter iGluSnFR. (A and B) Expression of iGluSnFR in control neurons (A) and RIM1/2 cDKO neurons (B). **(C)** ΔF/F images before, during and after stimulation. Shown is a maximum intensity projection of 30 trials, where neurons were stimulated once per trial. The images were filtered with a gaussian filter (2 px) for data presentation. **(D-H)** Calculated response sites (ΔF/F) of iGluSnFR in neurons with the different conditions. Insets show average ΔF/F iGluSnFR responses of selected release sites in the shown experiments. **(I)** Quantification of the amount of neurotransmitter release is indicated as average ΔF/F. SRPK2 OE increased release by 56 %, while SRPK2 overexpression in a kinase dead variant (kDead) could not increase the release probability compared to control neurons. Shown are mean values with SEM. Statistical significance was assessed with One-way ANOVA and Holm-Sidak correction for multiple comparisons (* $p < 0.05$). **(J)** SRPK2 over-expression effect is RIM dependent. RIM1/2 cDKO neurons revealed a reduced amount of neurotransmitter release compared to control neurons (dashed line indicates average ΔF/F of WT/control neurons). SRPK2 over-expression in RIM1/2 cDKO did not elevate neurotransmitter release as the SRPK2 overexpression in control neurons did. Shown are means ± SEMs. Unpaired student's t-test (* $p < 0.05$).

Next, we checked whether the kinase activity of SRPK2 is important for the increased release, by overexpression of a kinase dead (kDead) variant of SRPK2 in untreated RIM1/2$^{fl/fl}$ cells. This variant was not able to increase the release (ΔF/F kDead: 0.025 $\pm$ 0.004, Figure 5.30 F and I), which indicated that the kinase activity of SRPK2 is mandatory for the elevated release probability mediated by SRPK2 overexpression. Finally, we tested whether SRPK2 overexpression in RIM1/2 cDKO neurons would lead to an

increase in synaptic release. When we compared the average ΔF/F values of RIM1/2 cDKO neurons and RIM1/2 cDKO neurons overexpressing SRPK2, we could not detect any difference (ΔF/F cDKO: 0.013 $\pm$ 0.002, cDKO+OE: 0.013 $\pm$ 0.002, Figure 5.30 G and H insets and J). which indicated that the SRPK2 overexpression mediated increase of neurotransmitter release was RIM dependent. In the SRPK2-RIM signaling cascade SRPK2 probably acts upstream of RIM, which means that SRPK2 directly or indirectly phosphorylates RIM proteins, which sets the release probability of the synapse.

5.9.3 SRPK2 overexpression mediated increase of neurotransmitter release depends on phosphorylation sites in RIM1α

If SRPK2 directly or indirectly phosphorylates RIM proteins, which results in a change of neurotransmitter release, the intriguing question is, whether we can identify the specific phosphorylation site or sites that are responsible for this effect. To this end, we screened different potential phosphorylation sites in RIM1α for an effect in neurotransmitter release dependent on SRPK2. The sites were selected from experiments were SRPK2 was overexpressed or knocked-down and regulation of phosphorylation sites was investigated by phospho-enrichment and mass spectrometry experiments (data not shown, performed by Julia Betzin and Mark E. Graham). We mutated the amino acid residues to alanine or glutamate to render them phospho-deficient or phospho-mimetic. We expressed GFP-RIM1α containing the different mutations and overexpressed SRPK2 in cDKO cells and tested whether the selected mutations were able to rescue the increased release that is mediated by SRPK2 over-expression (Figure 5.31). Of all mutations, only S991A and S1045 showed a significant difference in neurotransmitter release, when compared to SRPK2 overexpression in control neurons (Figure 5.31 E and F, also compare H and I). On the other site, the mutations S991E and S1045E both elevated neurotransmitter release to SRPK2 overexpression levels. This indicates that the respective sites in RIM1α are important to mediate the SRPK2 overexpression effect on synaptic release. It should be mentioned that the mutations S745A/E and S1078E did not potentiate release, as well (Figure 5.31 C and G) . However, we could not detect a significant difference of these mutations compared to SRPK2 overexpression condition.

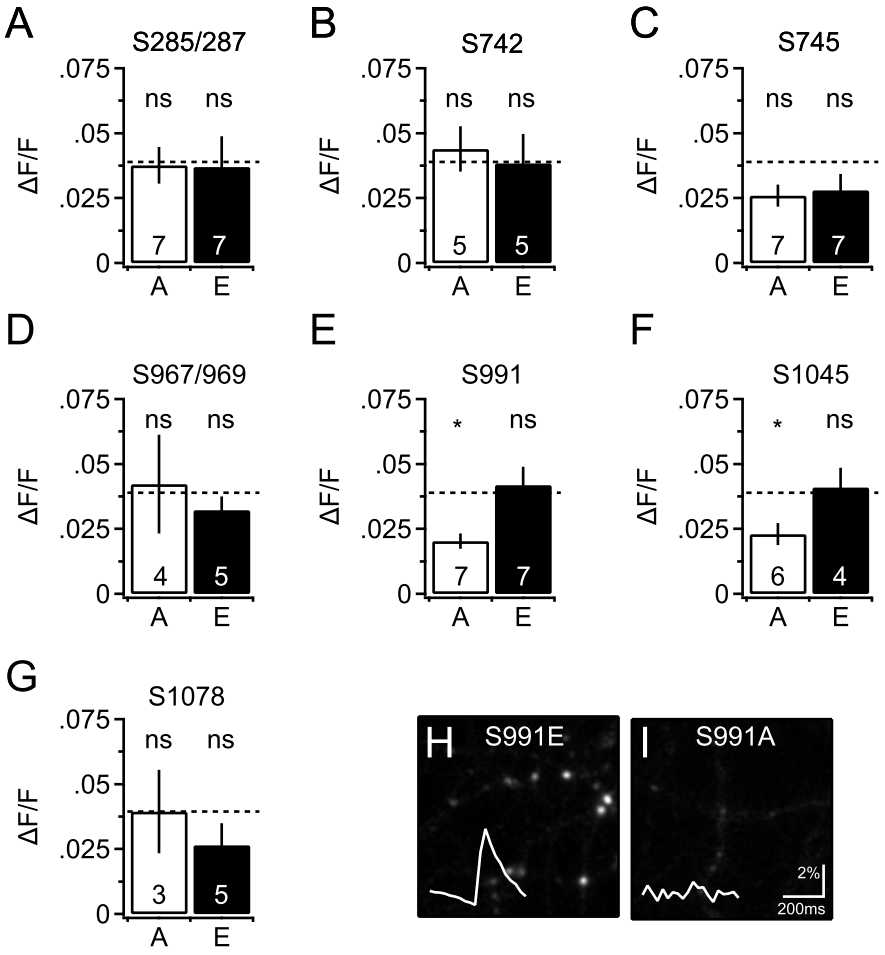

Figure 5.31: Screening for phosphorylation sites with relevance for SRPK2 overexpression mediated increase of synaptic release. (A-G) Different phospho-mutants were tested for changes in neurotransmitter release in experiments were SRPK2 was overexpressed in RIM1/2 cDKO neurons. The expression of the GFP-RIM1α mutations S991A and S1045A failed to increase the synaptic release, when SRPK2 was overexpressed. Experiments with these mutations showed a significant reduction of synaptic release compared to SRPK2 overexpression in control neurons (average ΔF/F of SRPK2 OE in WT: 0.04 ± 0.004; S991A: 0.015 ± 0.003; S1045A: 0.025 ± 0.001). S745A/E also seemed to reduce synaptic release compared to SRPK2 overexpression in control neurons, although we could not detect statistical significance (dashed lines indicate amount of neurotransmitter release, as measured by average ΔF/F iGluSnFR signal in SRPK2 overexpression condition. Number of experiments (n) as indicated in bar graphs. Statistical significance was assessed by One-Way ANOVA with Holm-Sidak correction for multiple comparisons against SRPK2 OE in control neurons, * $p < 0.05$). **(H and I)** Comparison of iGluSnFR response of GFP-RIM1α(S991E) and GFP-RIM(S991A) in SRPK2 overexpressing RIM1/2 cDKO neurons. S991E increased release, while S991A seemed to reduce release, even though SRPK2 was overexpressed. Insets show average ΔF/F of iGluSnFR signal of the illustrated experiments.

If phsophorylation of the sites S991 and S1045 (and also S745) in RIM1α would be important for the SRPK2 overexpression mediated increased release, phospho-mimicry at these positions might elevate synaptic transmission without additional need for SRPK2 overexpression. We expressed the different phospho-mutants of GFP-RIM1α in RIM1/2 cDKO neurons by lenti-viral transduction and tested the amount of neurotransmitter release by measuring the average ΔF/F of the iGluSnFR signal as before.

This time without additional overexpression of SRPK2. Mutations of RIM1α at position S745 did not alter the release compared to WT levels Figure 5.32 A. However, phospho-mimicry at positions S991 and S1045 significantly elevated the synaptic release compared to WT levels (Figure 5.32 B and C).

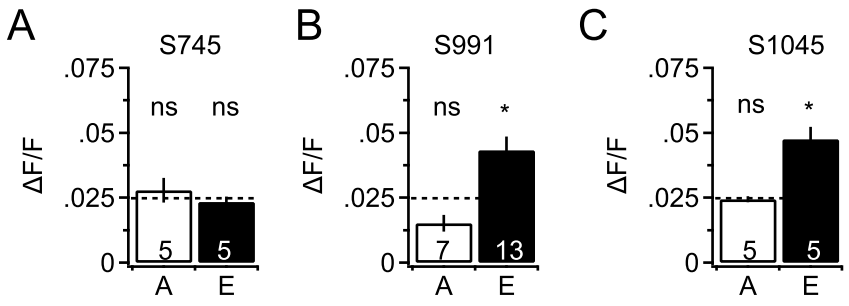

Figure 5.32: Effect of phospho-deficient and phospho-mimetic sites of RIM1α in RIM1/2 cDKO neurons without additional overexpression of SRPK2. (A) S745A and E did not lead to a change of the neurotransmitter release compared to control neurons. **(B)** S991E significantly increased the neurotransmitter release in RIM1/2 cDKO neurons compared to WT levels, even though SRPK2 was not expressed additionally (average ΔF/F of WT: 0.024 ± 0.003; S991E: 0.043 ± 0.005). **(C)** Similar effect of S1045E as in B (for S991E). The phospho-mimetic mutation of S1045 increased synaptic release similarly to SRPK2 OE in control neurons (average ΔF/F of S1045E: 0.047 ± 0.005). S1045A did not change neurotransmitter release compared to control neurons (dashed lines indicate amount of neurotransmitter release in WT (control) condition, One-Way ANOVA with Holm-Sidak against control neurons, * $p < 0.05$).

5.9.4 When SRPK2 is overexpressed, neurons fail to induce presynaptic homeostatic scaling

Homeostatic plasticity is the ability of neurons and synapses to adjust release and activity to perturbations that interfere with normal conditions. When release is inhibited, for example by suppressing AP firing, reshaping of synaptic structures take place that counteract the reduced release. On the contrary hyperexitability and increased release, lead to a reduction of release efficacy (see Section 2.7.3 for details). Here, we tested whether SRPK2 overexpression has an influence on presynaptic homeostatic scaling. We overexpressed SRPK2 in hippocampal primary neurons and suppressed neuronal firing with 1 µM TTX at DIV 13-14 for 30 - 48 hours. At DIV15 - 16 TTX was washed out for 10 minutes and homeostatic scaling was investigated by assessing the release probability with iGluSnFR at 2 mM Ca^{2+} by measuring ΔF/F amplitudes. If synaptic release was upscaled it is expected that synaptic release probability is increased from untreated to TTX treated neurons.

In WT neurons that did not overexpress SRPK2, synaptic scaling was clearly visible after TTX treatment (Figure 5.33 A), as seen by the increase in the average ΔF/F from untreated control neurons to the TTX treated condition (Figure 5.33 A and C). The relative increase of release was 63.5 % (Figure 5.33 C). When we overexpressed SRPK2 and probed presynaptic homeostatic scaling, we saw that no increase

of release was induced (Figure Figure 5.33 B and C). The results point to an interference of SRPK2 over expression with presynaptic scaling.

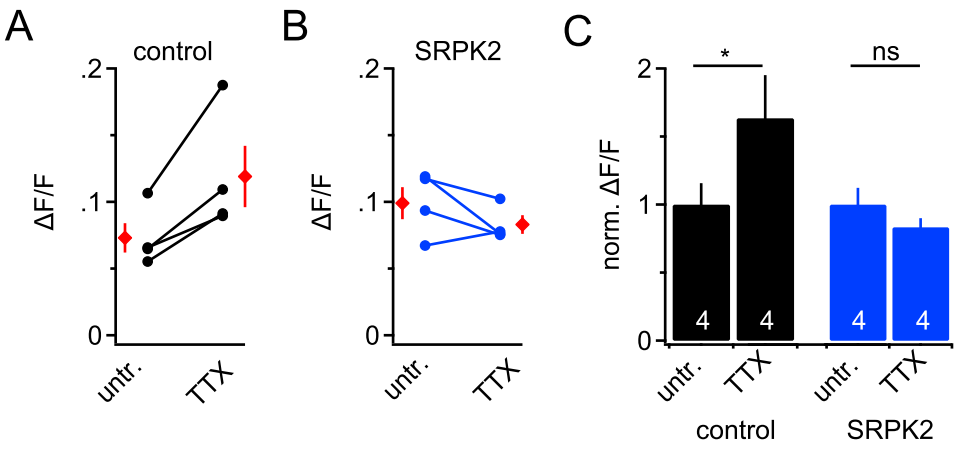

Figure 5.33: SRPK2 OE interferes with presynaptic homeostatic scaling. (A) Control neurons exhibit a clear presynaptic scaling effect after treatment with 1 µM TTX for 30 - 48 hours (average ΔF/F of untr.: 0.073 ± 0.011; TTX: 0.11 ± 0.023). **(B)** Neurons that overexpressed SRPK2 failed to induce presynaptic scaling (average ΔF/F of untr.: 0.099 ± 0.012; TTX: 0.083 ± 0.006)**. (C)** Relative scaling effect in control neurons and in SRPK2 OE neurons. TTX treatment of WT (control) neurons for 30 - 48 hours induced an increase of presynaptic neurotransmitter release by 63.5 % (black bars). When neurons overexpressed SRPK2 no homeostatic presynaptic scaling could be detected (blue bars). Data in bar graphs are presented as normalized means ± SEMs. Statistical significance was assessed by ratio paired t-test (* $p < 0.05$). Number of experiments (n) as indicated in bar graphs.

5.9.5 Homeostatic scaling is dependent on RIM and its phosphorylation state

As seen before homeostatic scaling cannot be induced when SRPK2 is overexpressed in neurons. Therefore, we wanted to know, whether phosphorylation sites in RIM1α that were important for the SRPK2 OE effect (increased synaptic release probability) influence the ability of the presynaptic compartment for homeostatic scaling. We applied 1 µM TTX for 48 hours to RIM1/2 cDKO neurons, that were previously transduced with iGluSnFR and different GFP-RIM1α mutants. We measured presynaptic homeostatic scaling as before by estimation of ΔF/F amplitudes from untreated and TTX treated neurons.

First of all, homeostatic scaling can not be induced in RIM1/2 cDKO neurons (Figure 5.34 A). This is in line with observations from Drosophila, where presynaptic homeostatic scaling in the neuromuscular junction is dependent on functional RIM [Müller et al., 2012]. Next, we tested whether homeostatic scaling can be induced in RIM1/2 cDKO transduced with GFP-RIM1α(S991E). This mutant had the same effect on the synaptic release probability as SRPK2 OE (see Section 5.9.2). Interestingly, we did not see a clear scaling effect, but comparable ΔF/F values before and after TTX treatment (Figure 5.34 B). Finally, we investigated the RIM1α mutations S1045A and S1045E for presynaptic homeostatic scaling. As described before, GFP-RIM1α(S1045E) expression in RIM1/2 cDKO neurons had the same effect as SRPK2 OE

in otherwise untreated neurons. On the other side, GFP-RIM1α(S1045A) expression failed to induce increased synaptic release with or without elevated SRPK2 levels. Strikingly, GFP-RIM1α(S1045E) failed to induce presynaptic homeostatic scaling (similar as SRPK2 OE and GFP-RIM1α(S991E), Figure 5.34 D), whereas GFP-RIM1α(S1045A) was able to induce a strong homeostatic scaling effect as seen before in WT neurons (Figure 5.34 C).

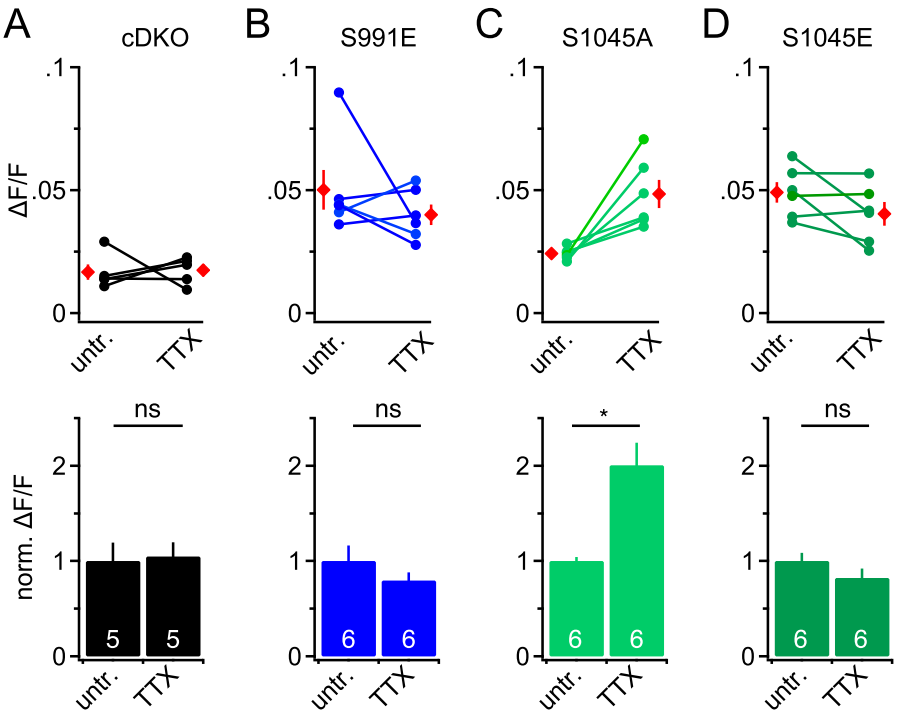

Figure 5.34: Homeostatic scaling depended on RIM and its phosphorylation. **(A)** There is no homeostatic scaling in RIM1/2 cDKO neurons. TTX treated and untreated RIM1/2 cDKO neurons show the same presynaptic neurotransmitter release (average ΔF/F of untr.: 0.0166 ± 0.003; TTX: 0.0174 ± 0.003). **(B)** Expression of GFP-RIM1(S991E) in RIM1/2 cDKO neurons does not lead to any scaling effect after TTX treatment (average ΔF/F of untr.: 0.050 ± 0.01; TTX: 0.04 ± 0.004). **(C)** Rescue of RIM1/2 cDKO neurons with GFP-RIM1(S1045A) allows presynaptic homeostatic scaling as in WT neurons. Glutamate release is increased by almost 100 % after TTX treatment (average ΔF/F of untr.: 0.024 ± 0.001; TTX: 0.049 ± 0.006). **(D)** This scaling capability is abolished when S1045 is mutated to glutamate, which mimics constant phosphorylation (average ΔF/F of untr.: 0.049 ± 0.004; TTX: 0.04 ± 0.005). Bar graphs on lower panel illustrate normalized ΔF/F to quantify relative changes of homeostatic plasticity. Red markers in upper graphs indicate means and SEM of paired data. Statistical significance was assessed by ratio paired t-test (* $p < 0.05$). Number of experiments (n) as indicated in bar graphs.

We also tested the mutations S745A and S745E for the ability of homeostatic presynaptic scaling in similar experiments but did not see any scaling effect with these mutations (performed by Annika Mayer, data not shown). Taken together, the data indicate that neurons that overexpress SRPK2 or RIM1α variants that mimics phosphorylation at sites which lead to increased neurotransmitter release do not scale their neurotransmitter release to adapt to silencing by TTX treatment.

6 Discussion

Presynaptic neurotransmitter release is of crucial relevance for communication in neuronal networks. Fusion of synaptic vesicles in response to action potential arrival at the synaptic terminal is orchestrated spatially and temporally precisely to allow for extremely fast synaptic vesicle fusion and synaptic transmission. The process of synaptic release is highly plastic and can be potentiated or depressed depending on the current needs for synaptic communication. The multi-domain protein and CAZ member RIM1α functionally regulates different steps during synaptic transmission.

In this study, we demonstrated that RIM1α is dynamically phosphorylated dependent on neuronal activity. By a combination of bioinformatical tools, mass spectrometry experiments and live-cell imaging, our study provides for the first time a systematic analysis of functional relevance of phosphorylation sites in RIM1α. By means of a FM imaging assay and the genetically encoded glutamate sensor iGluSnFR we characterized a reduced synaptic release probability as one of the hallmarks of ablation of RIM1α and RIM2. We demonstrated that this phenotype can be rescued with N-terminally GFP-tagged RIM1α and that this rescue strategy fails when RIM1α is mutated to alanine at the positions T812/814, S991 and S1600. Phospho-mimicry with a glutamate mutation reseted the release probability back to WT levels (or even increased release) in these cases. On the contrary, mutation of S514 to alanine boosted the synaptic release, pointing to positive and negative regulation of release by phosphorylation of RIM1α depending on the site that is phosphorylated. Finally, we identified a novel kinase, SRPK2, in the presynaptic terminal that regulates synaptic release in a RIM1/2 dependent manner. The effect of SRPK2 on synaptic release is dependent on its kinase activity and needs the phosphorylation sites S991 and S1045 (and potentially S745) in RIM1 for increasing glutamate release.

6.1 GFP-RIM1α fully rescues reduced synaptic release probability in RIM1α KO and RIM1/2 cDKO neurons

The screening for release relevant phospho-mutants in this work relied on rescue experiments, in which endogenous RIM1α and/or RIM2α was/were ablated and the fusion protein GFP-RIM1α in the longest

transcript was expressed via lenti-viral vectors. The experimental design could harbor different problems. Firstly, so far no RIM1α KO phenotype rescue experiment has been described, where a RIM1α fusion protein with a fluorescent tag was used. All complete rescue experiments described to date, used untagged RIM1α variants with independent expression of a fluorescent marker or without fluorescent marker at all. For example Yang and Calakos (2010) generated an expression construct of RIM1α and GFP with an IRES between the two proteins to rescue mfLTP in hippocampal slices of RIM1α KO mice. In another study RIM1α with a point mutation at S413 to alanine was knocked-in to investigate rescue efficacy of this mutation on presynaptic plasticity. Again no fluorescent protein was fused to RIM1α [Kaeser et al., 2008a]. Here, we decided for a fusion protein, because serval follow up experiments need a tagged RIM1α variant (e.g. FRAP for synaptic persistence of RIM1α mutants). The second issue involved be the splice variant. To date there are no data about the implications of the different splice variants of RIM1α for its multiple functions in the synaptic terminal. We initially cloned RIM1α in five different splice variants (not shown) and selected the longest transcript we could identify, which only lacks three exons. Nevertheless, the three missing exons could be of critical function. In 2013, Spangler and colleagues failed to rescue a Liprin1α KO mediated, but RIM1α dependent, release phenotype by overexpressing a shorter RIM1α splice variant. The question whether, the phenotype could not be rescued because Liprin1α was essential or whether the used RIM1α splice variant missed intrinsic properties due to the missing exons remained unresolved. Another possibility is that the exons could be essential for protein interactions, that mediated the RIM1α dependence.

Here, we demonstrated that the strategy to rescue the reduced synaptic release probability of RIM1α KO and RIM1/2 cDKO neurons with a GFP-RIM1α fusion protein in the described splice variant is successful in our hands. In all cases lentiviral expression of GFP-RIM1α was able to completely reset the release probability back to WT levels. We also saw that the spontaneous release rate (though not statistically significant) changed between WT an KO neurons and that this parameter was also set back to WT values, when GFP-RIM1α was expressed.

In addition to the functional evidence, we also saw mechanistically proof that GFP-RIM1α is fully functional in RIM1α KO and RIM1/2 cDKO neurons. Firstly, it was correctly localized to putative synaptic structures as seen by FM and bassoon co-stainings. Secondly, the long persistence of GFP-RIM1α in synaptic structures, as seen in FRAP experiments, points to an integration or at least an interaction in the CAZ. Finally, in Co-IPs with the GFP-tag of the fusion protein, we were able to identify known interaction partners of RIM1α, which suggests that the overall structure of RIM1α was intact (performed by Mark E. Graham, data not shown).

In this study we used two different mouse lines to prepare neurons. We used the originally described RIM1α KO mouse line [Schoch et al., 2002] and the later developed RIM1/2$^{fl/fl}$ mouse line [Kaeser

et al., 2011] from which RIM1/2 cDKO neurons were prepared. The consequences of RIM1α and RIM1/2 ablation on neurotransmitter release have been studied extensively before. For example RIM1α KO release probability was shown to be reduced by 50 % in different studies [Calakos et al., 2004, Kaeser et al., 2008b]. Hippocampal slices from RIM1/2 cDKO mice exhibited a reduction of EPSC amplitudes by 80 % compared to WT [Kaeser et al., 2011, Kaeser et al., 2012]. However, in another study the reduction of the release probability in RIM1/2 cDKO slices was found to be aprrox. 30 % compared with WT (measured at the calyx of held) [Han et al., 2011].

In general, cells from both mouse lines showed a strong reduction in synaptic evoked release probability in our imaging experiments. In both cases also the spontaneous release and the level of residual dye showed changes, even though we could never detect statistical significance for these parameters. Somewhat surprising, the release rate seemed to be more strongly affected in RIM1α KO neurons (reduction by 55.6 % compared to WT), when we applied K^+ stimulation, compared to RIM1/2 cDKO with electrical stimulation (reduction by 43.1 %). In the RIM1α KO cells RIM2α could compensate for the ablation of RIM1α, at least to a certain extent [Schoch et al., 2006], but in the double knock-out all RIM1/2 isoforms are deleted. Therefore, without a potential compensation one might expect a stronger phenotype. There are several explanations why we did not detect a stronger reduced synaptic release probability in RIM1/2 cDKO neurons than in RIM1α KO neurons. First of all, the phenotype of the RIM1α KO neurons was investigated with FM dyes and potassium stimulation, while the phenotype of the RIM1/2 cDKO neurons was measured with FM dyes and electrical stimulation. Stimulation strength and experimental paradigm influence the visibility and measurement of potential phenotypes. This phenomenon was seen in this study (see Section 5.3.1) and has already been described and published [Nimmervoll et al., 2013]. Secondly, the 5 Hz stimulation paradigm in experiments with electrical field potential stimulation might lead to a facilitation in synapses with low release probability (such a low release probability is expected RIM1/2 cDKO neurons). The facilitation of release would increase the estimated release probability seen in our experiments.

Furthermore, it needs to be considered that a constitutive knock-out of both large α-RIM isoforms is postnatally lethal [Schoch et al., 2006], therefore RIM1 and 2 were ablated via Cre - recombinase to produce a conditional double knock-out (while the RIM1α KO is constitutive). Nine days after transduction of Cre - recombinase no RIM is detectable anymore in WB from cultured hippocampal RIM1/2$^{fl/fl}$ neurons [Kaeser et al., 2011]. Therefore, we incubated the neurons at least for this time period after transduction with viral Cre-vectors before we performed the experiments. However, viral transduction, even though it is considered to have a high efficacy, probably not always targets 100% of the cultured cells. As a consequence the results might be contaminated by neurons that were not recombined. Additionally, the Cre recombinase results in a loss of newly synthesized RIM, only. Already, produced RIM proteins need

to be degraded via cellular protein degradation pathways, such as the proteasome. This implicates, that RIM must be accessible for this pathway. When molecules are strongly integrated in the CAZ, a structure which can be stable over days or even weeks [Ziv & Arava, 2014], individual RIM molecules might "survive" for longer time scales. These minute amounts of RIM molecules can be sufficient to falsify the phenotype, since only a handful of RIM molecules (38 - 39) were estimated to be present at a native synapse [Wilhelm et al., 2014] and probably less at individual active zones.
Nevertheless, the phenotypes of RIM1α KO neurons and RIM1/2 cDKO neurons we observed in this study showed a significant reduction in synaptic release probability in both cases and can be used to investigate the rescue efficacy of GFP-RIM1α variants with phospho-deficient or phospho-mimetic mutations..

6.2 The importance of RIM1α phosphorylation in synaptic function

For the analysis of the phospho-proteome in the presynapse and especially phosphorylation of RIM1α, we applied a ten second stimulus (high potassium) to cultured neurons to induce activity. We saw that this relatively short stimulation (even though very strong), induce a high regulation of phosphorylation in many different synaptic proteins. A similar study has been performed two years ago, where the stimulation was performed for two minutes, with direct lysis of cells afterwards to analyze the regulation of the phospho-proteome [Mahdokht et al., 2016]. Even though, the above mentioned study also identified many different proteins to contain several regulated phospho-sites, it has two problems: (1), the stimulation paradigm was rather long and unphysiological. The presence of high potassium for two minutes is under physiological conditions unlikely and toxic and therefore might induce unphysiological changes in the samples. (2), only one time point after the stimulus was analyzed. This is difficult to interpret, especially with the knowledge of our data, where we could see that the phospho-pattern is under constant change after the stimulation, because different kinases and phosphatases are activated with different time courses [Engholm-Keller et al., 2019]. While our experimental approach also used a very strong and unphysiological stimulus, the stimulation time was rather short and a 10 s high-frequency electrical stimulation protocol, that produced identical phospho-signalling responses for several proteins (as we found in our study) was previously published [Smillie & Cousin, 2012]. Additionally, we followed the phospho-pattern for up to 15 minutes post-stimulus. Therefore, we can follow a specific phosphosite and correlate this to the activity of a specific kinase via the KinSwing Analysis. Interestingly, the highly sophisticated phospho-pattern was correlated to an overall decrease of synaptic release probability, as seen in the FM dye approach. Thus, the reduction in release could in theory be correlated with the phospho-pattern of release relevant proteins.

RIM1α was identified as one of the major hubs for phosphorylation, which means that it was one of the proteins with most regulated phospho-sites in response to the stimulation (for details also see [Engholm-Keller et al., 2019]). This is interesting since it means that the phosphorylation of RIM1α is adjusted to a large extent after stimulation. The amount of adjustable phospho-sites could define the complexity of the signal integration of a protein in a synapse. What does this mean? A protein that has many different functions in the synaptic terminal, will need, dependent on the current activity level, ways to control its involvement in different processes. The more sites in a protein can be phosphorylated, the more different functions can be adopted by the protein. Every single phosphorylation or dephosphorylation by itself could lead to a specific functional change, but it is also possible, that the pattern of the phosphorylation in a protein defines its current function. This would be coded similar to a binary code. However, most likely it is a combination of both, like a weighted binary code, where the pattern defines the function, but individual phospho-sites can override the overall pattern, when necessary. This study showed that RIM1α has multiple phosphorylation sites. Phosphorylation and dephosphorylation of these sites and creation of distinct phospho-patterns might be necessary so that RIM1α can take over different tasks in the synapse at the same time.

We identified several phospho-sites in RIM1α that are activity regulated and we could link 4 of them to a functional relevance in synaptic release. This is the first systematic analysis of functional and release relevant phosphorylation sites in RIM1α.

A previously studied phosphorylation site is S413, which was proposed to be crucial for LTP in the cerebellum [Lonart et al., 2003], but studies using acute and constant in vivo rescues were not able to reproduce these results [Kaeser et al., 2008a, Yang & Calakos, 2010]. Maybe the most striking proof that S413 is not relevant for presynaptic forms of long-term plasticity was a study performed by Keaser and colleagues (2008), where a mouse model with RIM1α(S413A) knock-in was generated to test the functional relevance of this amino acid residue for presynaptic plasticity and synaptic efficacy. The study verified that RIM1α with phosphorylated S413 preferentially bound 14-3-3 adaptor protein, as it was suggested to be important for the induction of LTP in the cerebellum [Fatma et al., 2004], but apart from that, no effect on several forms of presynaptic plasticity, such as mfLTP, or deficits in behavioral tasks could be identified. Moreover, the study supported their data with an experiment were RIM2α was ablated to show that the lack of an effect of the S413A mutation of RIM1α is not due to compensational mechanisms, as mfLTP was still present [Kaeser et al., 2008a]. The authors concluded that phosphorylation of S413 is not relevant for synaptic transmission or presynaptic plasticity.

In general the lack of information about phosphorylation sites in RIM1α and their function is rather surprising, because the central roles of RIM1α and PKA in presynaptic LTP have been known for almost 20 years [Castillo et al., 1997, Castillo et al., 2002]. The abundance of potential phosphorylation sites

in RIM1α and the multitude of functions of RIM1α makes it difficult to link phosphorylation of RIM1α to distinct molecular functions. In our systematic analysis, we used a consensus site approach and phospho-enrichment in combination with mass spectrometry to delimit candidate phosphorylation sites to a number which could be screened with a suitable screening assay.

One of the most interesting phosphorylation sites identified, that showed functional relevance for synaptic release, was S1600 at the C-terminus of RIM1α. This site has been shown to be a perfect consensus site for PKA, which is *in vitro* phosphorylated by the kinase, but was proposed to have no relevance for presynaptic LTP [Lonart et al., 2003]. The fact that S1600 is a PKA substrate and the larger picture of our results make this phosphorylation site an intriguing candidate for central functions of RIM1α, maybe even the missing link to presynaptic LTP. Even though the protein interaction experiments and analysis are not finished, yet, we could already identify some proteins that significantly prefer to bind S1600E. Among these proteins we could name the priming factor Munc13 and the presynaptic protein Liprin, both important proteins for synaptic release (Mark Graham, unpublished). Additionally, among the top hits were isoforms of the adaptor protein 14-3-3, which, as already mentioned, was implied to be important for presynaptic LTP [Fatma et al., 2004]. We showed that the basal release is impaired when RIM1α is mutated at S1600 to alanine and that this is rescued back to WT levels with a mutation to glutamate. If this site was important for presynaptic potentiation one could expect a boost (similar to an increase in potentiation) in release with S1600E which we did not see. This might be explained, by the fact that the interplay with other molecular factors could be important or that glutamate mutations only have a 60 % resemblance to genuine phosphorylation.

The mutated variants GFP-RIM1α(S1600A) and GFP-RIM1α(S1600E) were tested for their localization in the presynapse and both co-localize with presynaptic markers (i.e. FM dyes). This points to structural integrity of the mutations since transportation is intact and they are correctly located to the presynaptic terminal. RIM1α is tightly integrated in the CAZ through its interactions with many CAZ components. Our FRAP results emphasize this fact. GFP-RIM1α recovery after photo-bleaching is considerably slower than GFP. Interestingly, this persistence is even increased when S1600 is mutated to alanine, while S1600E has a similar turnover as GFP-RIM1α(WT). In general, this points to changed protein-protein interactions within the CAZ in dependence on the phosphorylation site S1600. This is not surprising and is supported by other results in this study. An interesting point is, that the alanine mutation of S1600 is more strongly bound to the CAZ, even though it leads to a reduction in release. This is kind of counter-intuitive: Why should a strongly integrated RIM1α be less functional than a RIM1α with higher turnover? The strength of integration is mainly determined by the level of interaction. It could be that the unphosphorylated RIM1α (which is similar to the alanine mutation) is interacting with specific proteins that keep the RIM1α molecule closely located to the active zone and does not allow it to escape from the CAZ.

When the release event takes place, these RIM1α molecules might be directly available, be phosphorylated and then act in normal or increased release. This is not possible when serine is mutated to alanine and the described release phenotype can be seen. On the other side, the phospho-mimic, might not be as strongly integrated, because it needs some flexibility in movement to change from the "resting" position to the "active" position. Another explanation could be that a higher turnover might be necessary to exchange old RIM1α with new RIM1α, which is only possible in the phosphorylated variant.

Our results for the turnover of the different RIM1α variants are in line with a previously published study, that showed that synaptic efficacy is reduced, when a large proportion of the RIM1α pool becomes relatively immobile [Spangler et al., 2013]. An interesting fact is, that in the the mentioned study, Liprin-2α knock-down caused a decrease in RIM1α protein levels, a reduced mobility of RIM1α in the synapse and a significant reduction of synaptic release efficacy. It is known that Liprins bind to the C-terminal part of RIM1α, exactly were S1600 is located. Moreover, our preliminary interaction data from Co-IPs and mass spectrometry indicates that Liprin prefers the interaction with GFP-RIM1α(S1600E) (Mark Graham, unpublished).

In general, the C-terminus and potential phosphorylation of amino acid residues in this part of RIM1α seem to be important for anchoring RIM1α in the presynapse and for normal synaptic release. This was shown by our FM experiments in RIM1/2 cDKO neurons transduced with the truncated variant of RIM1α (GFP-RIM1α(ΔC), where we could show that this truncation mutation can not rescue the reduced synaptic release probability of the RIM1/2 cDKO neurons. Additionally, the FRAP experiments with the truncation mutation showed, that this RIM1α variant is not as strongly integrated in the CAZ as wild-type RIM1α. Different interactions of RIM1α that are dependent on the C-terminus have been described. For example Liprins and subunits of VGCCs have been proposed to bind in proximity to or at the C2B domain [Mittelstaedt et al., 2010]. A potential mechanism could be folding of the C-terminus to the body of the protein as result of the phosphorylation, which could inluence the ability of RIM1α to interact with distinct proteins (a potential mechanism which is currently under investigation in our lab).

T812/814 was one of the mutations in RIM1α that was identified by consensus analysis and showed a reduced synaptic release probability in the FM dye release assay with K^+ stimulation. For several reasons T812/814 must be viewed critically, but nevertheless can be considered to be of special interest. First of all, in this mutation two serine residues were mutated to alanine, which makes RIM1α containing this mutation more susceptible for irregular folding. We do not think that the seen release phenotype is a result of structural aberrations, because the localization (which implies transport and integration of the protein) is correct and we were able to pull down proteins that specifically bind to this part of RIM1α (i.e. the C2A domain). Secondly, while S991 and S1600 have been found in our mass spectrometry and phospho-enrichment experiments, as well as in other studies [Mahdokht et al., 2016, Engholm-

Keller et al., 2019], T812/814 has never been mentioned before and we did not detect it in the mass spectrometry approach. This is an interesting fact, since it either points to very low amounts of RIM1α molecules to be phosphorylated at this site or a very transient nature of the phosphorylation (or a false positive). Thirdly, T812/814 is located in the C2A domain in direct proximity to R844. A mutation at R844 to H is linked to CORD7 a retinal dystrophy [Johnson et al., 2003]. We have experimental evidence (data not shown) that the release probability is increased in R844H. The area of the mutation might be of central relevance to general vesicle release. Finally, we showed that the C2A domain containing the mutation T812/814A has a reduced ability to bind VAPA and VAPB. To date, the function of VAP proteins in synaptic release is not resolved, but there is evidence that VAP proteins contribute to normal release, since their occupancy by antibodies resulted in reduced vesicle release [Skehel et al., 1995]. So far, we did not test the effect of T812/814E on synaptic release. It would be interesting to know whether the synaptic release probability is not rescued (which might point to a structural phenomenon), whether the release is rescued to WT levels (which would indicate that the site is important for basal release) or whether release is even increased (this would strongly point to a potential for synaptic plasticity).

It is expected that phosphorylation events can lead to a reduction or gain of protein function. Therefore, it is not surprising that we found a phosphorylation site in RIM1α that increased release when rendered phospho-deficient. The mutation of S514 to alanine showed a significant increase in synaptic release probability by 20 %, when introduced in RIM1/2 cDKO neurons, compared to control cells. GFP-RIM1α(S514), was identified in the activity dependent mass spectrometry experiments. The abundance of phosphorylated S514 peptides of RIM1α showed a strong increase after the stimulation compared to control (mock stimulated) synaptosomes [Engholm-Keller et al., 2019]. So far, we did not test the effect of S514E on release. Nevertheless, one might expect that phosphorylation of S514 has a negative effect on release. If this assumption turns out to be true, it would be in line with the observation we made in the release experiments accompanying the mass spectrometry experiments. In these we pre-stimulated neurons in culture and saw that there is a synaptic depression in later FM experiments. S514 is located upstream of the PDZ domain, interestingly, directly next to K502 which is a known SUMOylation substrate with release relevant function in Ca^{2+} channel recruitment [Girach et al., 2013]. Although this might be a coincidence, it could also point to the existence of hot-spots of PTMs that regulate functions of RIM1α on the molecular levels. A conceivable scenario would be that sumoylation of K502 results in normal synaptic release by recruitment of Ca^{2+} channels, while the phosphorylation of S514 can reduce this release like a molecular brake that protects the neuron from hyperexitability.

It remains to be tested whether the phosphorylation of S514 (because of its position) directly inhibits the PDZ domain dependent interaction with VGCCs [Kaeser et al., 2011] or whether other molecular entities play a role in this regulation. In general, a potential mechanism of phosphorylation sites to be involved

in setting the synaptic release probability is to alter protein interactions and thereby either changing the state or amount of releasable vesicles (as for examples seen with complexin in the process of super-priming [Yang et al., 2010], which influences the amount of primed vesicles) or the coupling of vesicles to VGCCs.

6.3 SRPK2, a novel kinase in the presynaptic terminal, regulates neurotransmitter release and influences presynaptic homeostatic scaling

When we overexpressed SRPK2 in WT neurons we identified an increase of synaptic release probability by aprrox. 32 %. This result was seen in FM dye imaging and we could also reproduce an increased synaptic release with iGluSnFR. So far, no function for SRPK2 in the mammalian presynaptic terminal has been described. Therefore, we propose a novel function for SRPK2 to be involved in the regulation of synaptic transmission and setting the release probability. Our results extend findings from *Drosophila melanogaster* where the SRPK2 homolog SRPK79D was investigated [Johnson et al., 2009]. SRPK79D is necessary for correct development of the NMJ of *Drosophila melanogaster* since mutations in the protein lead to aberrant accumulation of Bruchpilot (homolog of CASK/ELKS in *Drosophila melanogaster*) in axons and premature T-bar assembly which are not correctly located to the synaptic terminal. Overexpression of SRPK79D in *Drosophila melanogaster* lead to a decrease in synaptic release by around 50 %, which opposes the increased neurotransmitter release we quantified, when we overexpressed SRPK2 in hippocampal neurons. Possible explanations for this difference are manifold. First of all, SRPK2 and SRPK79D are not identical but only homologs. SRPK79D shares approx. 54 % sequence homology with SRPK2 [Nieratschker et al., 2009]. This difference by itself already might explain different functions. For example Protein kinase C family in mammalian cells consists of eleven major isoforms and the function of these isoforms are different [Sossin, 2007]. Second, the NMJ of *Drosophila melanogaster* and the mammalian central nervous system synapses are different structures with different architectures of active zones. The different architectures and also different compositions of active zone proteins (e.g. more RIM1 isoforms in mammalian cells) point to different requirements for the involved proteins.

Furthermore, our findings are supported by ongoing experiments in our lab, which show that SRPK2 OE leads to a significant increase of RIM1α on the cellular level and also in synaptic terminals (Julia Betzin, unpublished). Additionally, super-resolution microscopy analysis point to an increase of RIM1α nanoclusters (Julia Betzin, unpublished). It has been shown before that the increase in synaptic release probability, is correlated with an increase in synaptic RIM1α levels [Lazarevic et al., 2011]. Additionally,

it was shown that the number of nanoclusters represent the number of release sites [Tang et al., 2016]. Taken together, our findings of increased release probability after SRPK2 OE is strongly supported by the reproducibility with different techniques and the accompanied increase of RIM1α proteins levels and the amount of nanoclusters.

Our results from experiments in RIM1/2 cDKO neurons implicate that the SRPK2 OE effect (i.e. increased release probability) can only take place, when RIM is present and S991 as well as S1045 (and possibly S745) can be/are phosphorylated. There are different modes of action to be considered: (1), SRPK2 directly phosphorylates these sites to adjust the release probability. (2), phosphorylation of different sites facilitate the binding of SRPK2, which phosphorylates RIM1α at other sites, which eventually lead to an increased release probability. (3), SRPK2 phosphorylates RIM1α and thereby facilitates its own binding, which leads to the phosphorylation of other sites. (4), the phosphorylation of different sites is necessary for RIM1α to be able to interact with another target. This target protein is the actual SRPK2 substrate. It is obvious, that potential modes of action can in reality be arbitrarily complex.

Our current view is that S991 is not directly phosphorylated by SRPK2 but allows the binding to RIM1α. Several indications point towards this: Firstly, the initial identification of SRPK2 as RIM1α interaction partner was phospho-dependent. Phosphorylated RIM1α bound more strongly to SRPK2 than dephosphorylated RIM1α. Therefore, a certain degree of phosphorylation is probably necessary for efficient SRPK2 binding. Preliminary, pull-down experiments point to stronger binding of SRPK2 to a RIM1α fragment containing the C2A domain carrying a mutation at S991 to glutamate, compared to the alanine mutation (Julia Betzin, data not shown). Moreover, S991 was not phosphorylated *in vitro* with purified SRPK2 (Julia Betzin, data not shown). Lastly, mass spectrometry experiments and KinSwing analysis suggest that S991 is a direct CamKII target (Mark Graham). The assumption that CamKII is involved in a process that positive regulates synaptic transmission is reasonable since many studies provided evidence for this (reviewed in [Wang, 2008]). Moreover, we have some experimental evidence supporting the involvement of CamKII in synaptic release: We performed FM experiments with the CamKII inhibitor KN93 that point to a reduced release when CamKII is not active (see Appendix Section 9.6). Additionally, we did some initial experiments with co-overexpression of SRPK2 and CamKII and saw further increase in release probability. In contrast, expression of a dominant negative variant of CamKII in SRPK2 OE neurons resulted in a decrease in synaptic release probability (the results from these preliminary experiments can be found in Appendix Section 9.6).

Taken together we propose the following novel kinase pathway with RIM1α involvement: In an early step S991 in RIM1α is phosphorylated by a yet unknown kinase, which might be CamKII. As a result, SRPK2 can bind to RIM1α and may walk along the polypeptide chain to phosphorylate other sites in the protein, such as S745 and S1045. Phosphorylation of these sites allow RIM1α to adapt its functional-

ity, by changing its binding partners, its abundance and stability in the synaptic terminal or modulating the amount of readily releasable vesicles and calcium channel clustering. The final net outcome is an increased release probability.

The increase of synaptic release probability when SRPK2 is overexpressed harbors the potential for different forms of synaptic plasticity or upscaling. The rational is simple: when the presynaptic terminal undergoes a plastic process it can increase or decrease the level or modulate the activity of SRPK2 and thereby regulate the synaptic release probability. Therefore we tested the effect of SRPK2 OE on synaptic upscaling as homeostatic adaptation to silencing of neuronal activity by TTX application. This phenomenon has already been established and described in literature and we were able to reproduce a considerable upscaling of release in silenced WT neurons as it was shown before [Murthy et al., 2001, Lazarevic et al., 2013]. Curiously, neurons that overexpressed SRPK2 failed to induce homeostatic upscaling of the synaptic release probability. Since SRPK2 increased the release probability, the potential for increase might be exhausted, but we saw further increase in WT and in SRPK2 OE neurons, when we increased release probability by elevating the extracellular Ca^{2+} concentration (see Appendix Section 9.6). It was proposed that two events meet when presynaptic scaling is induced - increasing the RRP and modulation of the calcium influx [Davis, 2013]. RIM was shown to be involved in the enlargement of the RRP when presynaptic homeostatic scaling is induced [Müller et al., 2012]. Mechanistically this could mean, that in our experiments, the SRPK2-RIM dependent increase of synaptic release mainly relied on adding vesicles to the RRP. The maximum amount of vesicles in the RRP was reached (also compare slot model of vesicles in the RRP [Frank et al., 2010]), when SRPK2 has been overexpressed. As a consequence, we could not see additional increase in RIM dependent homeostatic scaling in our experiments with SRPK2 overexpression, as no further enlargement of the RRP was possible. The enlarged release in experiments, where the extracellular Ca^{2+} was increased, could be explained by an increased, but RIM independent, Ca^{2+} influx and a subsequent enlargement of Ca^{2+} microdomains, which would allow the release of vesicles at more distal positions.

Another potential explanation for no additional scaling in SRPK2 overexpressing neurons, could be found in the constitutive nature of SRPK2. Neurons were transduced at DIV4-6 with AAVs to overexpress SRPK2. Therefore it can be assumed, that SRPK2 is highly abundant for many days before the experiments were started. When it is supposed that SRPK2 OE constantly increases the release probability, than this could lead to homeostatic downscaling, as it has been proposed for hyperactive neurons before [Lazarevic et al., 2013]. Indeed this possibility would imply other speculations: (1), when the SRPK2 OE neurons already downscaled the SRPK2 effect, this would mean that the still increased release probability is an already attenuated response. An acute up-regulation of SRPK2 might be much more dramatic. (2), SRPK79D OE in the NMJ has a contrary effect than SRPK2 OE in murine neurons. The question

arise whether this contrary effect is the actual effect of SRPK79D or whether this is the output of an homeostatic scaling effect. Induction of homeostatic plasticity in NMJ of Drosophila is very fast and happens in time scale of minutes [Müller et al., 2012, Davis & Müller, 2015], while the protocol to induce presynaptic homeostatic scaling in mouse neurons include the application of TTX for 24-48 h. This could imply that the NMJ is more prone to any scaling effect than the murine central nervous system neuron, which could lead to a reduced release probability. However, homeostatic plasticity in Drosophila normally exactly offsets the amount of perturbation, which means that a homeostatic downscaling, would set release back to WT levels. (3), finally in SRPK2 OE neurons a downscaling machinery would be opposed by the TTX silencing which activates an upscaling machinery. Possibly both machineries balance each other, which would result in no visible net effect of TTX application. Our findings that presynaptic scaling is not detectable in SRPK2 overexpressing neurons, were supported by our experiments with phospho-mutants of the sites in RIM1α that mediate the increased release probability after SRPK2 overexpression. Phospho-mimicry at sites S991 and S1045 failed to induce presynaptic homeostatic scaling after TTX application. Both sites increased synaptic release similar to SRPK2 overexpression when mutated to glutamate under basal conditions, but did not further elevate synaptic release as response to silencing. On the other site, when S1045 was mutated to alanine, we observed a strong homeostatic scaling effect. The observation that presynaptic homeostatic scaling is possible in this phospho-deficient mutation of RIM implies, that if phsophorylation is necessary for homeostatic scaling, probably other sites than S1045 would mediate the effect.

Taken together, we conclude that phosphorylation and dephosphorylation of SRPK2 target sites in RIM1α functionally regulate synaptic transmission and influence presynaptic homeostatic scaling effects. The role and potential of SRPK2 in regulating different types of synaptic plasticity events is intriguing and will open the path to many interesting research questions.

6.4 General implications of the results for presynaptic plasticity

RIM1α is tightly involved in many forms of presynaptic plasticity. The most prominent example would be the key role of RIM1α in purely presynaptic LTP, as it can be found in the mossy fiber synapses of the hippocampus [Castillo, 2012], in the cerebellum [Salin et al., 1996], in the thalamus [Castro-Alamancos & Calcagnotto, 1999], in the subiculum [Behr et al., 2009], in the amygdala [Armentia & Sah, 2007] and in the neocortex [Chen et al., 2009]. Furthermore, RIM is involved in homeostatic plasticity in Drosophila [Müller et al., 2012] and short-term plastic events [Schoch et al., 2002]. On the other hand, some of these plasticity processes are dependent on kinases. PKA is of central relevance for mossy fiber LTP and CamKII is involved in short-term plasticity and was suggested to be a potential player in homeostatic

plasticity [Kim & Hayashi, 2014]. When this study was started, the initial idea was to bring these facts together: Is RIM phosphorylated to play a role in presynaptic plasticity, and if yes, where, how and when? Even though we did not answer all of these questions completely, we want to frame some thoughts about our results in the context of synaptic plasticity.

While post-synaptically mediated plasticity mostly involves protein synthesis or protein trafficking, presynaptic plasticity was suggested to be induced fast and without initial synthesis of new proteins [Frank et al., 2006, Castillo, 2012], while in the later phases proteins might be newly synthesized [Böhme et al., 2019]. Therefore, molecular switches such as PTMs create a perfect toolkit for fast induction of presynaptic plasticity. Even more, the plastic process could be rapidly changed in both directions via PTMs (e.g. addition of PTM could increase release and removal could decrease the release). In this study we found several phosphorylation sites in RIM1α with direct effects on synaptic transmission. Three of these sites are positive regulators (T812/814, S991 and S1600) when phosphorylated (probably), while one site could be a negative regulator (S514). Two other sites might be mediators of kinase effects, that increase release when phosphorylated, but does not affect basal release when dephosphorylated (S745 and S1045). It is very likely, that more sites in RIM1α, or combinations of sites exists, that have an effect in synaptic transmission. It is obvious, that this manifold of relevant phosphorylation sites create many levels of control by many different kinases with different functions. For example, when a kinase becomes activated and phosphorylates a positive regulator, it could be that after some time the release must be slowed down to prevent depletion of vesicles or cytotoxic hyperactivity. However, the first kinase might be still active and at some point activates a second kinase, which phosphorylates RIM1α at a negative regulating site, which induces a reduction in synaptic neurotransmitter release. The interplay and combination of different phsophorylation events in RIM1α would define the actual strength of release and should theoretically allow an adjustment in any direction, depending on the plastic event that was induced.

The finding that SRPK2 OE increased the release introduces a novel RIM1α dependent pathway with importance for the regulation of synaptic transmission. As mentioned, presynaptic plasticity can be induced very fast and without the need for protein synthesis. Nevertheless, long lasting changes of synaptic transmission eventually lead to an increase in specific proteins (e.g. RIM1α levels go up with synaptic scaling, [Böhme et al., 2019]) or their functional spectrum is modified (e.g. different interactions). Therefore, when synaptic strength is increased, the activity of SRPK2 could be modulated to keep the elevated synaptic transmission intact for many hours to days.

The involvement of RIM1α in synaptic plasticity is commonly accepted. The molecular prerequisites for this involvement are not resolved in detail so far. We hypothesized that phosphorylation of RIM1α is involved in the process of plastic events in the presynapse. In this study we provide evidence that

phosphorylation of RIM1α is powerful, versatile and regulates synaptic neurotransmitter release and thereby harbor the ability to induce and regulate presynaptic plasticity.

6.5 Experimental and technical considerations

We present two technical approaches to investigate synaptic release with different read-outs. The FM dye approach allows to measure several synaptic release parameters, such as release rates and vesicle pools. iGluSnfr imaging delivers estimates of synaptic release probability and can be used to calculate the vesicular release probability and the amount of release sites per synapse on the basis of a binomial probability model. Both methods present different advantages and pitfalls that are discussed in the following sections.

Accuracy and reliability of the FM dye approach

FM dye imaging is a well established method that has been used since the mid of the 90's (some examples are [Mozhayeva et al., 2002, Klingauf et al., 1998, Waters & Smith, 2000, Ryan et al., 1996, Deák et al., 2004]). Questions around synaptic release and vesicles pools have been investigated and different read-outs have been described. In this study, we introduce a new and unpublished way to analyze FM data. We describe the dye loss in a typical FM experiment as the sum of two exponentials. This model implies the existence of two vesicles pools: a spontaneous releasable and an evoked releasable pool of vesicles. This concept is not new, but it was suggested that these pools are strictly separated [Ramirez & Kavalali, 2011, Sara et al., 2005]. What does this mean? A vesicle that belongs to the spontaneous pool, is released spontaneously and therefore would be loaded with FM dye in a spontaneous manner, whereas the vesicles from the evoked pool only fuse with the plasma membrane in an activity dependent manner and thus are only filled with FM dye after stimulation. Subsequent, unloading of the distinct vesicles would follow in the same way as the loading. In our study we used loading protocols (potassium or electrical) that last 90 - 180 s. Our data indicate that these loading protocols result in similar loading of synaptic vesicles for WT and RIM1α KO neurons, suggesting a high degree of dye loading of the synaptic vesicle population, overcoming the reduced synaptic release of RIM1α KO neurons. We fitted individual synaptic structures to measure the dye loss. The spontaneous and evoked release rates between individual synapses showed a high degree of variation, which is somehow expected and was described before [Ermolyuk et al., 2012]. In several cases the spontaneous component of release was considerably high and fast. This would be surprising in the context of the model which proposes strict separation of spontaneous and evoked synaptic vesicle pools and the fact that our short loading proto-

cols should not lead to a high degree of loading of the spontaneous synaptic vesicle pool. We can rule out the possibility that the spontaneous loss is contaminated by high photo-bleaching, because we developed a method to correct for bleaching and saw that the bleaching was in both FM protocols very low. Another possibility would be, that vesicles and/or neurons in our experiments leak, which would allow dye to escape and be washed out or that unspecific membrane staining was not washed long enough and the spontaneous dye loss we observe, is the loss of this unspecific dye rather than spontaneous release. This possibility is questionable, since we saw a clear punctate staining pattern and the rate and amount of spontaneous dye loss exhibited also high variability (some show almost no spontaneous release and some show a high amount of spontaneous release). If the dye loss resulted from unspecific staining, we would always expect a high spontaneous rate and fraction of dye loss. For two reasons we still tend to account "true" spontaneous release for this loss of dye in our experiments. On the one site we collected some experimental evidence, that support this model (see Appendix Section 9.1) and on the other site previous studies from other labs also found a mixing of spontaneous and evoked vesicle pools [Wilhelm et al., 2010].

In our analysis we excluded bad fits and not fittable structures. This was mostly the case when structures showed no or very little release. This is a critical point of the FM approach with fitting individual FM stained structures. If these structures are genuine synapses with an extremely low release probability, the overall release probability is overestimated since the low releasers are excluded. However, it can not be excluded that these structures are completely silenced synapses or not synapses at all and thus would not be relevant in the evaluation. With respect to our phenotype and the rescue experiments we consider this not to be problematic, since the amount of not fittable structures was always comparable or higher in KO neurons and in non-rescuing GFP-RIM1α variants than in WT and rescuing variants (see Appendix Section 9.5). The RIM1α phenotype, namely the reduced synaptic release probability, and the non-rescuing GFP-RIM1α mutations would therefore, if at all, be underestimated.

The estimated release parameters in the FM dye approach always have to be considered as relative values within the specific experimental context. This is something we already saw in our experiments, when we compared experiments stimulated either with potassium or electrically with field-potentials. Therefore it is hard to to compare FM dye experiments in absolute numbers between different labs or maybe even between experimenters in the same lab. However, the relative reduction in the release rate (which correlates to the synaptic release probability) should be comparable.

Finally, it has to be mentioned, that the FM dye approach was mainly developed as a screening experiment, that should allow to investigate many different conditions (here different phospho-mutations) with regard to synaptic release in an easy manner and in reasonable time scales. Interesting results were always supposed to be verified by additional experiments and with other methods.

Possibilities and limitations of iGluSnFR sensors

The introduction of the genetically encoded glutamate sensor iGluSnFR in variants with different affinities opens up new possibilities in neuronal imaging. While electrophysiology allows high temporal resolution, it is often not possible to locate the origin of the synapse, because the measured postsynaptic potentials integrate many synaptic inputs (exceptions would be direct patching of mossy fiber boutons or calyx of held synapses). Indeed it is possible to back calculate single inputs by deconvolution, but still this is an indirect method and the real source is unknown. On the other side imaging techniques such as the FM dye release assay exist. They allow to locate single synapses but they lack the temporal resolution to investigate single vesicle release at high frequencies. In our FM dye approach for example, we needed to stimulate continuously at 5 Hz to approximate the release rate. iGluSnFR and other neurotransmitter sensors combine positive aspects of both approaches. The different affinity variants of iGluSnFR allow a high temporal resolution of the detection of release events up to 100 Hz [Helassa et al., 2018] and measurements can be done at the single synapse level due to the good signal to noise ratio of the sensors. Future improvements of the sensor may allow the imaging of release events at even higher frequencies. We showed that iGluSnFR can be used to investigate different research questions. It is useful to estimate the spatial range and diffusion speed of glutamate (Section 5.2.3), it can be used to investigate presynaptic short-term plasticity (Section 5.2.1, but also see [Helassa et al., 2018]), it can be used to compare general release probabilities between genotypes or conditions (Section 4.7.3) and even to estimate the vesicular release probability of single synapses (Section 5.2.4).

While neurotransmitter sensors open up a wide range of opportunities for the investigation of release parameters on the single synapse level, there are some limitations and problems that should be kept in mind: iGluSnfr imaging is prone to photobleaching as every other imaging approach as well. While electrophysiological recordings, such as MEA measurements or LTP protocols, are performed in time-scales of hours to days, constant illumination of iGluSnFR over these time periods would not be feasible (bleaching of the sensor and photo-toxicity to the cells). It remains to be seen, whether comparable experiments can be shortened or redesigned to use iGluSnFR for similar research questions. A good example is the measurement of spontaneous release events - so-called mini release events. A major problem with the detection of miniature release is the fact, that it is not predictable where and when a release event will occur. Therefore, to measure the appearance of minis with iGluSnFR a specimen must be illuminated constantly for reasonable timescales (at least minutes).

iGluSnFR is predestined for quantal analysis, thus the measurement of single release events. The pre-requisite for accurate measurements would be to look at single synapses (i.e. close synapses might appear as one synapse and must be excluded). While our strategy involved visual inspection of release

sites (response sites should not a have center of mass that deviates much from a mean center of mass) other studies using glutamate sensors do not even mention the problem [Helassa et al., 2018] or only considered synapses that were located distal to other release sites [Sakamoto et al., 2018]. For accurate measurement and justified selection, a defined selection procedure should be established. Such efforts are currently ongoing in our lab. Our procedure of the analysis of vesicular release probability is in a preliminary state. We showed that we can measure parameters such as the amount of releasable vesicles and vesicular release probability, but we face several issues. A main problem is a strong run down we see in several experiments, when we image over many trials (probably due to photo-bleaching). This run down makes the comparison of a quantal release event at the beginning of the experiment and at the end of the experiment difficult. At both time points one quantum would be released, but they would show different $\triangle$F/F values and a higher scatter. A less clearly distributed multi-peak histogram would be the result. Fitting the data would become harder or impossible. Another problem is the bin size of the histogram. We stated that we expect one quantal amplitude to be approx. 0.05 ($\triangle$F/F) and thereby selected an appropiate bin size. However, if the value of the quantal content is not accurate the bin size may be too large or to small.

The release and the clearance of neurotransmitters include different pathways. Released neurotransmitters are cleared by enzymes, transporters and astrocytes and are finally brought back to the neurons for refilling vesicles [Scimemi et al., 2009]. The nature of iGluSnFR allows only the measurement of the release of glutamate and what happens to glutamate after the release (such as diffusion). Thus, iGluSnFR can not be used for acquiring information about the internalization process of vesicles (as for example pHourins could). Finally, iGluSnFR in its current design does not tell anything about the nature of the release sites. While we assume that all released glutamate that is detected by iGluSnFR comes from genuine synapses, we can not exclude the possibility that many synapses are clustered at these sites or even more that glutamate is released unspecifically at non-synaptic structures. A potential improvement of the sensor would be a selectively synaptic localization by fusion of the sensor to a synaptic targeting sequence (e.g. neurexin (presynaptic) or neuroligin (postsynaptic)). It remains to be seen, whether such a strategy is successful (problems of delivery and expression might occur).

Comparison of iGluSnFR and FM dye imaging in the context of this work

iGluSnFR as well as FM dye imaging allow to measure release relevant parameters. While our FM dye approach, with the resulting fluorescence decay with two exponential components, can quantify different release parameters, such as release rate and fraction of the vesicle pool that can be released by stimulation, the iGluSnFR imaging mainly returns a $\triangle$F/F value that can be used as estimate of the

amount or release, when comparing different conditions. Although the FM dye experiments have a higher output of parameters that can be directly compared between different conditions and that partly help to validate the experimental approach, iGluSnFR has the main advantage that no pre-stimulation is needed to load the vesicles. The importance of this, is stressed by the experiments in Section 5.4.3 (see Figure 5.17). In the presented experiments an applied pre-stimulus changed the release probability measured in the following FM dye experiment, which is a form of synaptic depression. Therefore, in any FM experiment it needs to be considered that by the application of the first stimulus, that is needed to load the vesicles with FM dye, plasticity events might be activated that could change the output in the later experiments. For example it could be possible, that a phenotype has its origin in a lack of presynaptic plasticity which normally would lead to an increase of release probability. As a result we would see a reduced release probability with the FM dyes (compared to a WT condition, where plasticity is still possible), which is the symptomatic expression of the phenotype but not the real source of the phenotype. Vice versa, it might be possible that plastic changes override a potential release phenotype that would be seen under basal release conditions. iGluSnFR needs no pre-stimulation and allows to read out the release probability from a basal state (where basal is relative, since parameters, such as culture density, age, amount of glia cells etc. change the basal state, and can even under controlled conditions, vary to some extend). However, iGluSnFR is an artificial protein in the cell that needs to be expressed some time before the experiments. The process of DNA delivery results in considerable stress to the specimen, that also might change intrinsic properties that are relevant to the readout. An interesting example that showed how strong a different expression mode might influence the following experiment was published by Jackmann and colleagues in 2014 (Journal of Neuroscience), where it was demonstrated that the transduction of the same optogenetic tool with AAVs in different serotypes resulted in strongly different experimental outcomes regarding short-term plasticity. While the expression strategy was the same (using AAVs), the mode of infiltration with the use of different epitopic receptors (different serotypes of viruses) already changed intrinsic properties that modified the experimental output [Jackman et al., 2014]. Another problem with iGluSnFR might be the high amount and ubiquitous expression on the cell membrane which might lead to cytotoxicity.

A cachet for any scientific result is its reproducibility in other experiments, therefore a short comparison between the different techniques in this study seems to be reasonable. When we compare the RIM1/2 cDKO phenotype that we measured with FM dyes (Section 5.3.4) and with iGluSnFR (Section 5.9.2) we see in both cases a significant reduction of the release probability of approximately 30 - 40 % which points to a good reproducibility of the phenotype and comparability of the methods at least in the context of this work. Additionally, the failed rescue efficacy of GFP-RIM1(S991A) was reproduced with both techniques.

7 Outlook

This study identified four distinct phoporylation sites in RIM1α (S514, T812/814, S991, S1600) with functional relevance for basal synaptic release. We started to identify potential underlying mechanisms that influence synaptic release in dependence on these sites. A main hypothesis is altered protein-protein interactions. Even though we already found some candidate proteins with changed binding to RIM1α, it will be necessary to identify additional protein interactions. Of special interest will be the interaction of RIM1α with Liprins and the functional consequences, which might contribute to the induction of presynaptic plasticity. Possible functional changes that need to be investigated would be vesicle to calcium channel coupling distances, changes in the amount of the readily releasable pool of synaptic vesicles or changes in the release machinery which influence synaptic release.

SRPK2 was identified as novel player in synaptic release. Its function in this process is RIM1α dependent. Many questions concerning the RIM1α and SRPK2 interaction are still open and are currently being investigated: Does SRPK2 change the amount of RIM1α in the neuron and in the synapse? Is the synaptic nano-architecture changed in dependence on SRPK2? While S991 is probably a phospho-switch that allows SRPK2 efficient binding to RIM1α, what are the direct phosphorylation sites of SRPK2 in RIM1α (maybe S745 and S1045?) and what is their functional relevance? Are there other SRPK2 substrates that contribute to synaptic function?

Finally, we will need to close the circle with the initial question: Is RIM1α phsophorylation important for synaptic plasticity, specifically presynaptically mediated LTP in the mossy fiber synapse of the hippocampus? To solve this question, LTP experiments in hippocampal slices from RIM1α KO or RIM1/2 cDKO mice will acutely be rescued with GFP-RIM1α, mutated at the identified release relevant phosphorylation sites.

8 Contributions

Contributions are mentioned in the text in the appropriate sections. Additionally an overview of contributions can be found below:

- measurements of fEPSP in hippocampal slices in Section 5.1.1 was performed by Sara Ferrando-Colomer (former PhD Student in Dirk Dietrich's laboratory)
- Phospho-dependent interaction of RIM1 and SRPK2 was investigated by Ana-Maria Oprisoreanu (former PhD Student in Susanne Schoch's laboratory)
- KinSwing analysis, phospho-enrichment and mass spectrometry were performed by Mark E. Graham, and Ashley Waardenberg form the Children's Medical Research Institute, Westmead, Australia
- testing of overexpression and knock-down of SRPK2 in neuronal cultures was done by Julia Betzin (PhD Student in Susanne Schoch's laboratory)
- testing of SRPK2 binding to RIM1 and RIM1 expression levels after SRPK2 OE (data not shown) was performed by Julia Betzin (PhD Student in Susanne Schoch's laboratory)
- homeostatic scaling experiments with GFP-RIM1(S745A/E) (data not shown) was performed by Annika Mayer (PhD Student in Susanne Schoch's laboratory)

9 Appendix

9.1 Experimental data support two-pool model

In our FM dye approach we describe the dye release as the sum of two exponential decay functions, one for spontaneous loss and one for evoked fusion events (see Section 4.7.2). This model assumes that the spontaneous loss and the evoked release derive from two independent pools. While the spontaneous release is ongoing and present at all times, evoked release has its onset, with the onset of the stimulation. To validate the two pool model, we used this rational: at any given time-point after the loading of FM dye into the vesicles the absolute evoked dye release should be comparable with other time points. However, the absolute dye loss coming from spontaneous release should be lower if the time point of measurement is delayed, because ongoing spontaneous release leads to a constant reduction of fluorescence of the spontaneous pool. We performed experiments were we waited less than 20 and more than 30 minutes after dye loading, before the recording started.

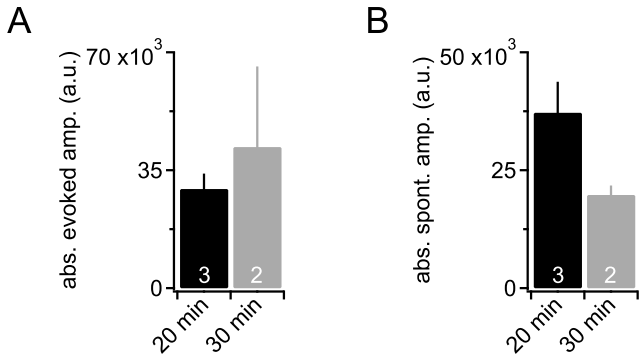

Figure 9.1: Smaller absolute spontaneous amplitude after delayed start of experiment supports two independent pool model. FM dye experiments were started with 20 or 30 minutes delay and absolute amplitudes of evoked and spontaneous release were quantified. **(A)** The evoked release amplitude stayed within the same range (20 min: $2.9*10^4 \pm 0.4*10^4$; 30 min: $4.5*10^4 \pm 2.4*10^4$ a.u.). **(B)** The absolute spontaneous amplitude was clearly smaller, when the start of the experiment was delayed to 30 minutes after loading, compared to 20 minutes after loading (20 min: $3.7*10^4 \pm 0.65*10^4$; 30 min: $1.97*10^4 \pm 0.2*10^4$ a.u.). Number of experiments n as indicated in bar graphs. Error bars represent SEM.

We fitted the data as described in Section 4.7.2 and quantified the absolute dye loss amplitude for each

component (spontaneous and evoked). As we wanted to compare absolute numbers, we performed these experiments on the same day to exclude technical or experimental day-to-day variance. The amount of absolute evoked dye loss seemed to stay in the same range in both time points (although there is a high variance visible, Figure 9.1 A), while the spontaneous loss decreased the longer the delay between loading and experiment took (Figure 9.1 B). These data support the working model of two independent vesicle pools.

9.2 FM analysis

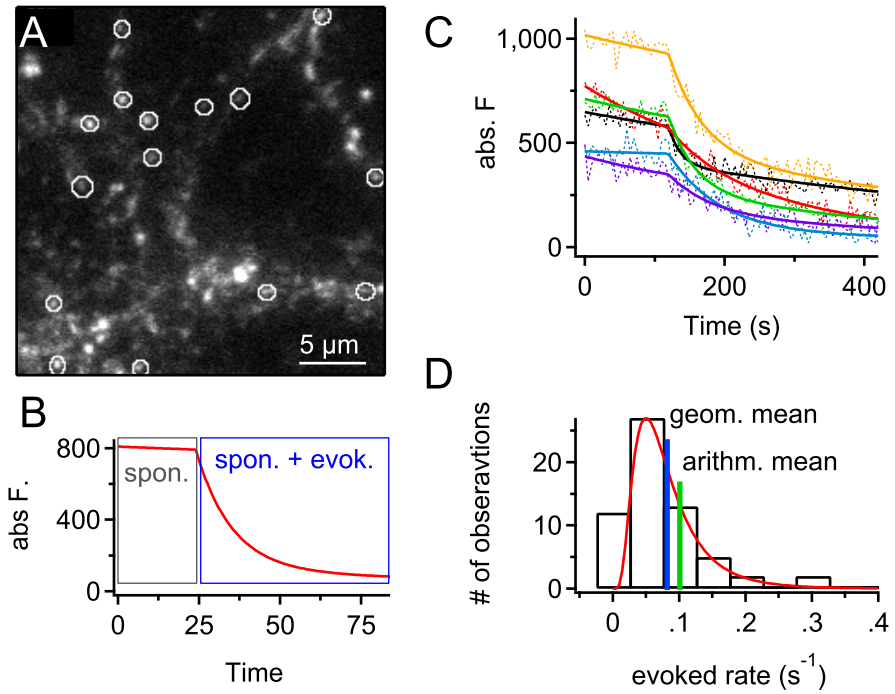

Figure 9.2: General procedure for the analysis of a typical FM experiments. (A) The image stack containing the acquired data, is registered and 40 (in K^+ stimulation experiments) or 80 (in field potential stimulation experiments) synaptic structures were selected in the first frame of the image stack (ROIs). Requirements for a structure to be selected were a clear center of mass, low background around the ROI and no clustering with other structures. Fluorescence values were measured in each frame of the stack for each ROI. Time-courses were background subtracted and bleaching corrected (see Sections 4.7.2 for details). Shown is a reprasentaitive (zoomed) image of a FM experiment with field potential stimulation. Circles mark ROIs as used in the evaluation. **(B)** The time-course of each ROI can be described as the sum of two exponentials according to the described formula (see Section 4.7.2). Shown is the fit of one sample ROI. The first part (baseline) purley consists of spontaneous dye loss (grey box). The second part, with the onset of stimulation, is a combination of evoked and spontaneous dye loss (blue box). **(C)** All ROIs in an experiment are fitted to the sum of the two exponentials to estimate the different release parameters (evoked release rate, spontaneous release rate, absolute loading, fraction of spontanoues dye loss, fraction of evoked dye loss, final fluorescence level (residual loading)). **(D)** Evoked release rates are not normal, but log-normal distributed. The best measure of location is therefore the geometric mean. The arithmetic mean should not be used, as it overvalue high release rates which can occur, but are rare compared with the the majority of release rates.

9.3 Fitting procedure for binomial analysis of vesicular release probability

The fitting procedure for vesicular release probability analysis with a binomial release model was performed considering the following assumptions and criteria:

1. The curve fit needs to return the parameters q, s, s_{noise}, n, p (q = ΔF/F of quantal amplitude, s = standard deviation of quantal distribution, s_{noise} = standard deviation of non-release, n = number of releasable vesicles, p = vesicular release probability)

2. It is assumed that the area under the curve is 1, which is the sum of the gaussian fits of 0, 1, 2... vesicles released. The area is defined by the binomial probability for each event and sets the amplitude A for each individual gaussian by:

$$A = \frac{area}{s * \sqrt{2\pi}} \tag{9.1}$$

The first step of the fitting was the calculation of the gaussian for the noise / failures of release. The binomial probability was calculated by:

$$P_x(n) = \binom{n}{k} * p^k * (1 - p^{(n-k)}) \tag{9.2}$$

In the next step the fit of the gaussian to the experimental data was calculated:

$$gauss(x) = e^{-\frac{1}{2}*(\frac{x-off)}{s_{noise}})^2} \tag{9.3}$$

Where *off* defining the offset to account for failures not being 0 ΔF/F. Finally, the amplitude of the gaussian was scaled to the binomial probability, so that the integral of the whole fit was equal to 1 at the end:

$$f(x) = \frac{P_x(0)}{s_{noise} * \sqrt{2\pi}} * gauss(x) \tag{9.4}$$

The procedure was repeated for each individual peak in the histogram, depending on n (releasable vesicle / release sites) with slight modifications:

$$f(x) = \frac{P_x(n)}{\sqrt{k} * s * \sqrt{2\pi}} * e^{-\frac{1}{2}*(\frac{x-off)-k*q)}{\sqrt{k}*s})^2} \tag{9.5}$$

The fit was repeated for each k und all gaussians were summed up. n was varied as long as the best chisq value was reached.

9.4 Pooling of WT/dCre and Cre/GFP-Cre experiments

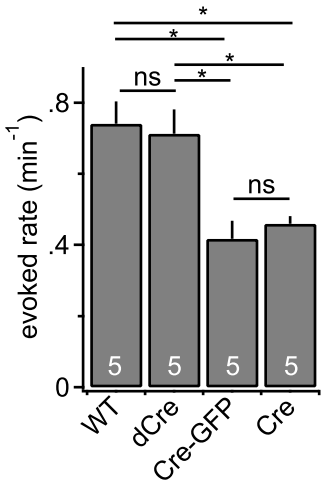

Figure 9.3: Comparison of evoked release rates from untreated RIM1/2$^{fl/fl}$ (WT) neurons to neurons transduced with inactive Cre (dCre) and RIM1/2 cDKO neurons, generated either with Cre-GFP or Cre virus. Five experiments for each condition were randomly selected and compared. The evoked release rates between WT and dCre transduced cells were similar and the evoked release rates from Cre-GFP and Cre treated cells were similar. The results justified pooling of WT and dCre experiments, as well as experiments with Cre-GFP and Cre treatment. (One-way ANOVA with Tukey's multiple comparison, * $p < 0.05$).

9.5 Amount of not fittable structures in different conditions

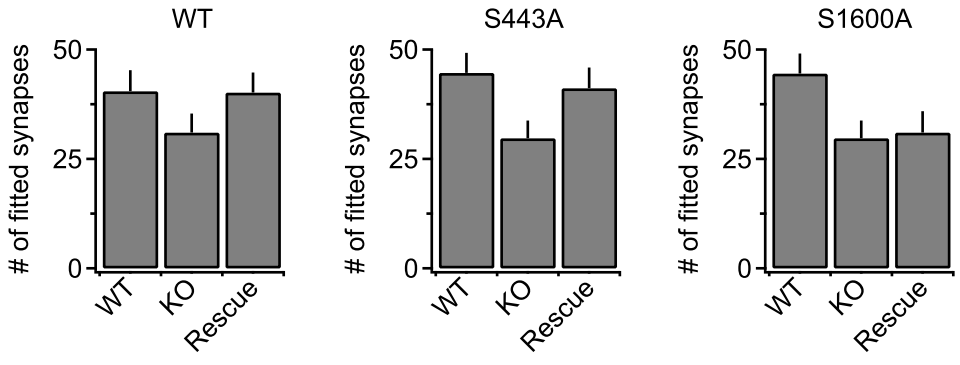

Figure 9.4: Amount of selected ROIs that could be fitted in FM dye approach. Shown are three examples: rescue with GFP-RIM1α (WT), with GFP-RIM1α(S443A) and with GFP-RIM1α (S1600A). Bar graphs indicate the amount of fitted structures of experiments in the specific conditions. Fluorescence traces in ROIs could not be fitted either, when there was almost no dye loss or when the fluorescence trace did not follow two exponential decay functions. These bad fits were discarded. Fittable structures were always less in KO neurons or in non-rescuing mutations (S1600A). Rescuing mutations had a similar amount of fittbale synapses as WT (compare WT with S443A). Since structures that could not be fitted were mostly low releasers (very slow evoked rate), the actual phenotype, if at all, is underestimated. Shown are means, error bars indicate SEM.

9.6 Involvement of CamKII in SRPK2-RIM signaling cascade

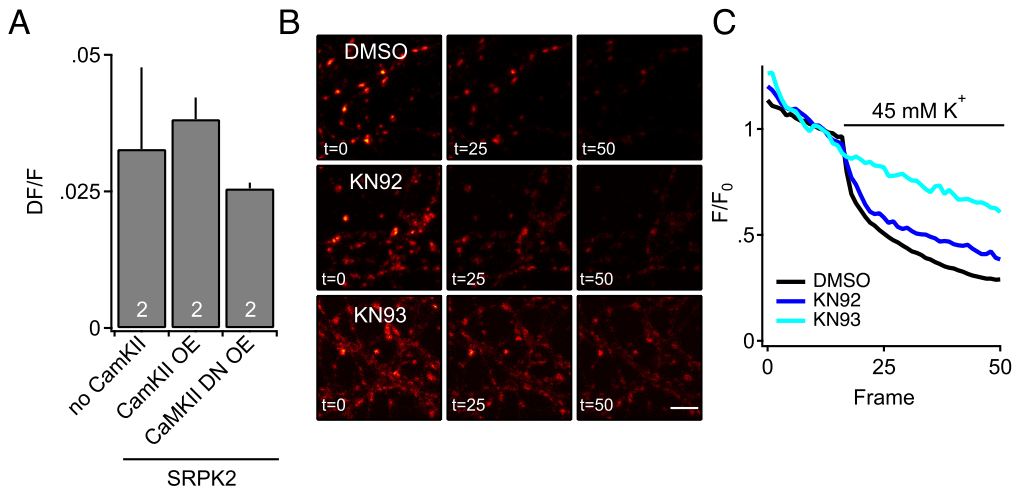

Figure 9.5: CamKII might be involved in the SRPK2-RIM pathway that increase synaptic release probability and is involved in basal vesicle release. (A) Hippocampal neurons were transduced with SRPK2 overexpression vector and iGluSnFR at DIV4-6. Additionally, CamKII or a CamKII dominant negative (DN) variant was co-transduced. iGluSnfr experiments were performed as described before. SRPK2 OE without CamKII resulted in a similar level of release as before. CamKII OE leads to a slight increase in the average release as it is indicated by a higher mean $\Delta F/F$ value. Expression of the DN variant of CamKII decreased the release probability. The experiments are preliminary (n = 2 and high SEM in no CamKII condition). **(B)** To test for the importance of CamKII in bsal release we performed FM experiments with potassium stimlation and inhibited CamKII activity with 10µM KN93 (pre-treated for 20 minutes and present during the experiment). As control DSMO and the inactive analogue of the CamKII inhibitor, KN92 was used. Images are normalized to the brightest pixel. The loss of FM dye from neurons treated with DSMO or KN-92 is clearly visible, whereas KN93 release is hardly visible. **(C)** Average dye loss traces from experiments seen in (B). While DMSO and KN92 treated neurons showed clear induced dye loss with the onset of potassium stimulation, KN93 treated neurons virtually show no release above spontaneous release and photobleaching. This indicates that the activity of CamKII might be important for basal neurotransmitter release. The result are preliminary.

9.7 Elevated Caclium conentration further increased release probability of neurons that overexpressed SRPK2

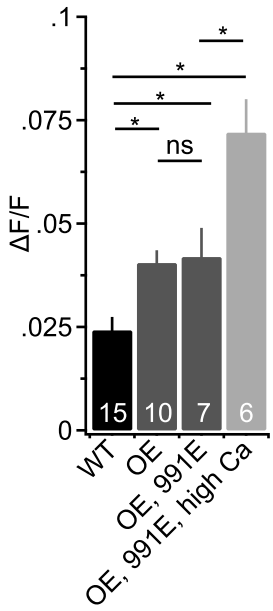

Figure 9.6: Elevated calcium concentration can increase release probability after SRPK2 overexpression. SRPK2 overexpression (OE) significantly increased synaptic release measured with iGluSnFR compared to control (WT) condition (mean ΔF/F in WT: 0.024 $\pm$0.003; OE: 0.041 $\pm$0.003). The amount of synaptic release is not further increased, when GFP-RIM1(S991E) is overexpressed together with SRKP2 (OE, 991E: 0.042 $\pm$0.007). However, when the release probability was increased by elevating the extracellular calcium concentration to 4 mM an increased release was visible (OE, 991E, high Ca: 0.072 $\pm$0.008). Thus while the the SRPK2 mediated increase in release seemed to be limited, this limit could be overcome by increasing the calcium concentration. Data are presented as means ± SEMs. Statistical significance was assessed by One-Way ANOVA with Holm-Sidak correction for multiple comparison (* $p < 0.05$). Number of experiments (n) as indicated in bar graphs.

9.8 Websites and Tools for Bioinformatics

Table 9.1: Websites, databases and tools that were used to identify phsophorylation sites in RIM1α via consensus motives.

Name	Web Address	Accession Date
GPS 2.1	http://gps.biocukoo.org/	May 2013
KinasePhos 2.0	http://kinasephos2.mbc.nctu.edu.tw/	May 2013
NetPhosK 1.0	http://www.cbs.dtu.dk/services/NetPhosK/	May 2013
PhosphoSitePlus	http://www.phosphosite.org	May2013
Scansite 2.0	http://scansite.mit.edu/	May 2013

9.9 List of Antibodies and Primers

Materials, chemicals, disposables and devices used in this thesis are mentioned in the text when appropriate. Some materials (like primers) could not be mentioned always explicitly and are listed below.

Antibodies and dyes

Table 9.2: List of antibodies that were used in this thesis. IC = immunocytochemistry, WB = western blot. RIM antibody was produced in a collaborating lab.

Name	Host	Use	Dilution	Source of supply
α-Bassoon	mouse	IC	1:200	Enzo, Firmingdale, USA
α-RIM1/2	rabbit	IC	1:600	
α-RIM1/2	rabbit	WB	1:1000	
α-Mouse, IRDye 680	goat	WB	1:15000	Li-Cor, Nebraska, USA
α-Rabbit, IRDye 680	goat	WB	1:15000	Li-Cor, Nebraska, USA
α-Mouse, IRDye 800	goat	WB	1:15000	Li-Cor, Nebraska, USA
α-Rabbit, IrDye 800	goat	WB	1:15000	Li-Cor, Nebraska, USA
α-GFP	mouse	WB	1:1000	SantaCruz Biotech., USA
α-Flag	mouse	WB	1:5000	Sigma, Taufkirchen
α-HA.11	mouse	WB	1:1000	Covance, Princeton, USA
α-Mouse, Alexa568	goat	IC	1:400	Invitrogen, Karlsruhe
α-Rabbit, Alexa488	goat	IC	1:400	Invitrogen, Karlsruhe
α-SynapsinI(pS603)	rabbit	WB	1:1000	Rockland, Limerick, USA

Oligonucleotides

Oligonucleotides were synthezised by Invitrogen (Karlsruhe). No special purification methods in addition to standard desalting were applicated.

Table 9.3: List of primers that were used for cloning. Index refers to the internal numbering system.

Index	Sequence (5' to 3')	DNA	Direction	Restr. Enzyme
c43	gcggaattccgaggccttctatttctgttatttc	RIM1α, C2A for pGex	Fw	*EcoRI*
c45	gcgctcgagtcaaggctgaggcagaggtag	RIM1α, C2A for pGex	Rev	*XhoI*
c68	gcggaattctatgtcctcggccgtggg	RIM1α, 1st fragment	Fw	*EcoRI*
c114	acacccgggcatgcatgcgcatctgc	RIM1α, 1st fragment)	Rev	*NsiI*
c115	gcagatgcgcatgcatgcccgggtgt	RIM1α, 2nd fragment	Fw	*NsiI*
c116	gatgggaactcctagggatcctgggg	RIM1α, 2nd fragment	Rev	*AvrII*
c117	ccccaggatccctaggagttcccatc	RIM1α, 3rd fragment	Fw	*AvrII*
c118	tggatctgtggtataccgggcttcgg	RIM1α, 3rd fragment	Rev	*BstZ17I*
c119	ccgaagcccggtataccacagatcca	RIM1α, 4th fragment	Fw	*BstZ17I*
c169	gcgcatatgtcatgaccggatgcagggagg	RIM1α, 4th fragment	Rev	*NdeI*
c180	gcggtgcgcataccatggtgagcaagggcgag	GFP	Fw	*FspAI*
c181	gcggaattccccggccccggcttgtacagctcgtccatg	GFP	Rev	*EcoRI*

Table 9.4: List of primers that were used for the mutation of RIM1α. Index refers to the internal numbering system.

Index	Sequence (5' to 3')	DNA	Direction
c620	ggaggcaagagacgtcagatggcggtgagcagctcggaggaggag	S543A	Fw
c621	ctcctcctccgagctgctcaccgccatctgacgtctcttgcctcc	S543A	Rev
c612	ggtggaaagaaacgaagagccgccctgagcgccaaagtggtagcc	S1355A, S1356A	Fw
c613	ggctaccactttggcgctcagggcggctcttcgtttctttccacc	S1355A, S1356A	Rev
c614	gagaggaaagagaggcgggaagcccgcaggttggagaaagggcgc	T338A	Fw
c615	gcgccctttctccaacctgcgggcttcccgcctctctttcctctc	T338A	Rev
c616	gcgacaaaagtaaaaggagagccaaagcagtaaagaaacttctag	T812A, T814A	Fw
c617	ctagaagtttctttactgctttggctctccttttacttttgtcgc	T812A, T814A	Rev
c618	caccaaagtaaagaagggcgccctggcagacgtcgtcggacac	S656A	Fw
c619	gtgtccgacgacgtctgccagggcgcccttctttacttttg	S656A	Rev
c620	ggaggcaagagacgtcagatggcggtgagcagctcggaggaggag	S543A	Fw
c621	ctcctcctccgagctgctcaccgccatctgacgtctcttgcctcc	S543A	Rev
c622	caagaacgcaccgacaaggagccccaacccagtctcctccagc	S1175A	Fw
c623	gctggaggagactgggttggggctccttgtcggtgcgttcttg	S1175A	Rev
c804	gtctcgaagaagcagggccacggcacagctcagccagacagagtcg	S1371A, S1373A	Fw
c805	cgactctgtctggctgagctgtgccgtggccctgcttcttcgagac	S1371A, S1373A	Rev
c1438	gcgcatatgtcacggagggaacaatttatac	minusC	Rev
c1440	gctcccctgacccgccgggctgcccaatcatctctggaaagttcg	S1600A	Fw
c1441	cgaactttccagagatgattgggcagcccggcgggtcaggggagc	S1600A	Rev
c1444	gctcccctgacccgccgggctgaacaatcatctctggaaagttcg	S1600E	Fw
c1445	cgaactttccagagatgattgttcagcccggcgggtcaggggagc	S1600E	Rev
c1503	aggttggagaaagggcgcgcccaggactactcagaccgg	S346A	Fw
c1504	ccggccaccgccagggtcgctcccccggaggccccgcgcgcacgcgcggcg	S443/447A	Fw
c1505	agcatgctgcggaacgacgcgctgagctccgatcagtcc	S514A	Fw
c1507	ccttctatttctgttattgctccaaccagccctggagct	S742A	Fw
c1508	tctgttatttctccaaccgcccctggagctctgaaagat	S745A	Fw
c1510	acacatcaccgctcacgtgccgtggctcctcatcgcggcgatgat	S967/969A	Fw
c1511	aatgtgccattacagagggccttagatgaaattcatcca	S991A	Fw
c1512	agagcaaaacgaggacgagctgcagaaagcctacacatg	S1045A	Fw
c1513	ccagatactagtttgcatgcaccagaacgagaaaggcac	S1078A	Fw
c1518	ccggtctgagtagtcctgggcgcgcccttctccaacct	S346A	Rev
c1519	cgccgcgcgtgcgcgcggggcctccgggggagcgaccctggcggtggccgg	S443/447A	Rev
c1520	ggactgatcggagctcagcgcgtcgttccgcagcatgct	S514A	Rev
c1522	agctccagggctggttggagcaataacagaaatagaagg	S742A	Rev
c1523	atctttcagagctccaggggcggttggagaaataacaga	S745A	Rev
c1525	atcatcgccgcgatgaggagccacggcacgtgagcggtgatgtgt	S967/969A	Rev
c1526	tggatgaatttcatctaaggccctctgtaatggcacatt	S991A	Rev
c1527	catgtgtaggctttctgcagctcgtcctcgttttgctct	S1045A	Rev
c1528	gtgcctttctcgttctggtgcatgcaaactagtatctgg	S1078A	Rev
c1533	aggttggagaaagggcgcgaacaggactactcagaccgg	S346E	Fw
c1534	ccggccaccgccagggtcgaaccccggaggaaccgcgcgcacgcgcggcg	S443/447E	Fw
c1535	agcatgctgcggaacgacgagctgagctccgatcagtcc	S514E	Fw
c1537	ccttctatttctgttattgaaccaaccagccctggagct	S742E	Fw
c1538	tctgttatttctccaaccgaacctggagctctgaaagat	S745E	Fw
c1540	acacatcaccgctcacgtgaagtggaacctcatcgcggcgatgat	S967/969E	Fw
c1541	aatgtgccattacagagggaattagatgaaattcatcca	S991E	Fw
c1542	agagcaaaacgaggacgagaagcagaaagcctacacatg	S1045E	Fw
c1543	ccagatactagtttgcatgaaccagaacgagaaaggcac	S1078E	Fw

Index	Sequence (5' to 3')	DNA	Direction
c1548	ccggtctgagtagtcctgttcgcgccctttctccaacct	S346E	Rev
c1549	cgccgcgcgtgcgcgcggttcctccgggggttcgaccctggcggtggccgg	S443/447E	Rev
c1550	ggactgatcggagctcagctcgtcgttccgcagcatgct	S514E	Rev
c1552	agctccagggctggttggttcaataacagaaatagaagg	S742E	Rev
c1553	atctttcagagctccaggttcggttggagaaataacaga	S745E	Rev
c1555	atcatcgccgcgatgaggttccacttcacgtgagcggtgatgtgt	S967/969E	Rev
c1556	tggatgaatttcatctaattccctctgtaatggcacatt	S991E	Rev
c1557	catgtgtaggctttctgcttctcgtcctcgttttgctct	S1045E	Rev
c1558	gtgcctttctcgttctggttcatgcaaactagtatctgg	S1078E	Rev
c1980	gaacagaagcaggcatcaagagcaagagccgagccaccgagggaaaggaag	S285/287A	Fw
c1981	cttcctttccctcggtggctcggctcttgctcttgatgcctgcttctgttc	S285/287A	Rev
c1982	gaacagaagcaggcatcaagagaaagagaggagccaccgagggaaaggaag	S285/287E	Fw
c1983	cttcctttccctcggtggctcctctctttctcttgatgcctgcttctgttc	S285/287E	Rev

Table 9.5: List of primers that were used for sequencing. Index refers to the internal numbering system.

Index	Sequence (5' to 3')	DNA	Direction
s32	aagttcgagggcgacacc	GFP	Fw
s16	atggtcctgctggagttc	GFP	FW
s18	ggttcattctcaagcctc	Ef1α, promotor	Fw
s46	caggcggaccccagg	RIM1α, C2A	Rev
s47	gtcgaaagcaacaagaaatc	RIM1α, Zn	Fw
s48	gggaaacgtcgcctatcag	RIM1α, PDZ	Fw
s49	gagagctccagcaaaaagc	RIM1α, exon 16	Fw
s50	gaacttgaccacgagcaat	RIM1α, exon 26	Fw
s51	ccaccccggccatggg	RIM1α, C2B	Fw
Topo_Fw	gcctgaacaccatatccatcc	Topo Inserts	Fw
Topo_Rev	gcagctgagaatattgtaggagatc	Topo Inserts	Rev
pGex_Fw	gggctggcaattggtg	pGex Inserts	Fw
pGex_Rev	ccgggagctgcagagg	pGex Inserts	Rev

10 References

[Abbott & Regehr, 2004] Abbott, L. & Regehr, W. G. (2004). Synaptic computation. *Nature*, 431(7010), nature03010.

[Alabi & Tsien, 2013] Alabi, A. & Tsien, R. (2013). Perspectives on Kiss-and-Run: role in exocytosis, endocytosis, and neurotransmission. *Annu Rev Physiol*, 75(1), 393–422.

[Alvarez-Baron et al., 2013] Alvarez-Baron, E., Michel, K., Mittelstaedt, T., Opitz, T., Schmitz, F., Beck, H., Dietrich, D., Becker, A., & Schoch, S. (2013). RIM3γ and RIM4γ are key regulators of neuronal arborization. *J Neurosci*, 33(2), 824–839.

[Arava et al., 2011] Arava, F., Zeidan, A., Stern, M., Garner, C. C., & Ziv, N. E. (2011). Use dependence of presynaptic tenacity. *J Neurosci*, 31(46), 16770–16780.

[Armentia & Sah, 2007] Armentia, M. & Sah, P. (2007). Bidirectional synaptic plasticity at nociceptive afferents in the rat central amygdala. *J Physiology*, 581(3), 961–970.

[Atasoy et al., 2008] Atasoy, D., Ertunc, M., Moulder, K. L., Blackwell, J., Chung, C., Su, J., & Kavalali, E. T. (2008). Spontaneous and evoked glutamate release activates two populations of NMDA receptors with limited overlap. (pp. 10151–10166).

[Augustin et al., 1999] Augustin, I., Rosenmund, C., Südhof, T. C., & Brose, N. (1999). Munc13-1 is essential for fusion competence of glutamatergic synaptic vesicles. *Nature*, 400(6743), 22768.

[Balaji & Ryan, 2007] Balaji, J. & Ryan, T. (2007). Single-vesicle imaging reveals that synaptic vesicle exocytosis and endocytosis are coupled by a single stochastic mode. *Proc National Acad Sci*, 104(51), 20576–20581.

[Becherer & Rettig, 2006] Becherer, U. & Rettig, J. (2006). Vesicle pools, docking, priming, and release. *Cell Tissue Res*, 326(2), 393–407.

[Behr et al., 2009] Behr, J., Wozny, C., Fidzinski, P., & Schmitz, D. (2009). Synaptic plasticity in the subiculum. *Prog Neurobiol*, 89(4), 334–342.

[Bennett et al., 1992] Bennett, M., Calakos, N., Kreiner, T., & Scheller, R. (1992). Synaptic vesicle membrane proteins interact to form a multimeric complex. *J Cell Biology*, 116(3), 761–775.

[Berg & Hall, 1975] Berg, D. & Hall, Z. (1975). Increased extrajunctional acetylcholine sensitivity produced by chronic acetylcholine sensitivity produced by chronic post-synaptic neuromuscular blockade. *J Physiology*, 244(3), 659–676.

[Betz et al., 2001] Betz, A., Thakur, P., Junge, H. J., Ashery, U., Rhee, J., Scheuss, V., Rosenmund, C., Rettig, J., & Brose, N. (2001). Functional interaction of the active zone proteins munc13-1 and RIM1 in synaptic vesicle priming. *Neuron*, 30(1), 183–196.

[Böhme et al., 2019] Böhme, M. A., W, M. A., Grasskamp, A. T., Beuschel, C. B., Goel, P., Jusyte, M., Laber, D., Huang, S., Rey, U., Petzoldt, A. G., Lehmann, M., Göttfert, F., Haghighi, P., Hell, S. W., Owald, D., Dickman, D., Sigrist, S. J., & Walter, A. M. (2019). Rapid active zone remodeling consolidates presynaptic potentiation. *Nat Commun*, 10(1), 1085.

[Bollmann et al., 2000] Bollmann, J. H., Sakmann, B., & Borst, G. J. (2000). Calcium sensitivity of glutamate release in a Calyx-Type terminal. *Science*, 289(5481), 953–957.

[Branco et al., 2008] Branco, T., Staras, K., Darcy, K. J., & Goda, Y. (2008). Local dendritic activity sets release probability at hippocampal synapses. *Neuron*, 59(3), 475–485.

[Breustedt et al., 2003] Breustedt, J., Vogt, K., Miller, R., Nicoll, R., & Schmitz, D. (2003). α1e-containing ca2+ channels are involved in synaptic plasticity. *Proc National Acad Sci*, 100(21), 12450–12455.

[Brose et al., 1995] Brose, N., Hofmann, K., Hata, Y., & Südhof, T. C. (1995). Mammalian homologues of caenorhabditis elegans unc-13 gene define novel family of c2-domain proteins. *J Biol Chem*, 270(42), 25273–25280.

[Brose et al., 1992] Brose, N., Petrenko, A., Sudhof, T., & Jahn, R. (1992). Synaptotagmin: a calcium sensor on the synaptic vesicle surface. *Science*, 256(5059), 1021–1025.

[Burrone et al., 2002] Burrone, J., Michael, O., & Murthy, V. N. (2002). Multiple forms of synaptic plasticity triggered by selective suppression of activity in individual neurons. *Nature*, 420(6914), 414.

[Calakos et al., 2004] Calakos, N., Schoch, S., Südhof, T. C., & Malenka, R. C. (2004). Multiple roles for the active zone protein RIM1α in late stages of neurotransmitter release. *Neuron*, 42(6), 889–896.

[Calloway et al., 2015] Calloway, N., Gouzer, G., Xue, M., & Ryan, T. A. (2015). The active-zone protein munc13 controls the use-dependence of presynaptic voltage-gated calcium channels. *Elife*, 4, e07728.

[Castillo, 2012] Castillo, P. E. (2012). Presynaptic LTP and LTD of excitatory and inhibitory synapses. *Csh Perspect Biol*, 4(2), a005728.

[Castillo et al., 1997] Castillo, P. E., Janz, R., Sdhof, T. C., Tzounopoulos, T., Malenka, R. C., & Nicoll, R. A. (1997). Rab3A is essential for mossy fibre long-term potentiation in the hippocampus. *Nature*, 388(6642), 590–593.

[Castillo et al., 2002] Castillo, P. E., Schoch, S., Schmitz, F., Südhof, T. C., & Malenka, R. C. (2002). RIM1α is required for presynaptic long-term potentiation. *Nature*, 415(6869), 327–30.

[Castro-Alamancos & Calcagnotto, 1999] Castro-Alamancos, M. A. & Calcagnotto, M. E. (1999). Presynaptic Long-Term potentiation in corticothalamic synapses. *J Neurosci*, 19(20), 9090–9097.

[Chanaday & Kavalali, 2017] Chanaday, N. & Kavalali, E. (2017). How do you recognize and reconstitute a synaptic vesicle after fusion? *F1000research*, 6, 1734.

[Chanaday & Kavalali, 2018] Chanaday, N. & Kavalali, E. (2018). Optical detection of three modes of endocytosis at hippocampal synapses. *Elife*, 7, e36097.

[Chang et al., 2018] Chang, S., Trimbuch, T., & Rosenmund, C. (2018). Synaptotagmin-1 drives synchronous ca2+-triggered fusion by C2B-domain-mediated synaptic-vesicle-membrane attachment. *Nat Neurosci*, 21(1), 33–40.

[Chapman, 2008] Chapman, E. R. (2008). How does synaptotagmin trigger neurotransmitter release? *Annu Rev Biochem*, 77(1), 615–641.

[Chen et al., 2009] Chen, H., Jiang, M., Akakin, D., & Roper, S. N. (2009). Long-Term potentiation of excitatory synapses on neocortical Somatostatin-Expressing interneurons. *J Neurophysiol*, 102(6), 3251–3259.

[Chen et al., 2002] Chen, X., Tomchick, D. R., Kovrigin, E., Araç, D., Machius, M., Südhof, T. C., & Rizo, J. (2002). Three-Dimensional structure of the Complexin/SNARE complex. *Neuron*, 33(3), 397–409.

[Chen et al., 2015] Chen, Z., Das, B., Nakamura, Y., A, D. D., & Young, S. M. (2015). Ca2+ channel to synaptic vesicle distance accounts for the readily releasable pool kinetics at a functionally mature auditory synapse. *J Neurosci*, 35(5), 2083–2100.

[Chevaleyre et al., 2007] Chevaleyre, V., Heifets, B. D., Kaeser, P. S., Südhof, T. C., Purpura, D. P., & Castillo, P. E. (2007). Endocannabinoid-Mediated Long-Term plasticity requires cAMP/PKA signaling and RIM1α. *Neuron*, 54(5), 801–812.

[Chung et al., 2010] Chung, C., Barylko, B., Leitz, J., Liu, X., & Kavalali, E. T. (2010). Acute dynamin inhibition dissects synaptic vesicle recycling pathways that drive spontaneous and evoked neurotransmission. *J Neurosci*, 30(4), 1363–1376.

[Citri & Malenka, 2007] Citri, A. & Malenka, R. C. (2007). Synaptic plasticity: Multiple forms, functions, and mechanisms. *Neuropsychopharmacol*, 33(1), 1301559.

[Davis, 2013] Davis, G. W. (2013). Homeostatic signaling and the stabilization of neural function. *Neuron*, 80(3), 718–728.

[Davis & Müller, 2015] Davis, G. W. & Müller, M. (2015). Homeostatic control of presynaptic neurotransmitter release. 77(1), 1–20.

[Davis et al., 1997] Davis, G. W., Schuster, C. M., & Goodman, C. S. (1997). Genetic analysis of the mechanisms controlling target selection: Target-Derived fasciclin II regulates the pattern of synapse formation. *Neuron*, 19(3), 561–573.

[Davydova et al., 2014] Davydova, D., Marini, C., King, C., Klueva, J., Bischof, F., Romorini, S., Carolina, M., Heine, M., Schneider, R., Schröder, M. S., Altrock, W. D., Henneberger, C., Rusakov, D. A., Gundelfinger, E. D., & Fejtova, A. (2014). Bassoon specifically controls presynaptic P/Q-type ca2+ channels via RIM-Binding protein. *Neuron*, 82(1), 181–194.

[de Jong & Verhage, 2009] de Jong, A. & Verhage, M. (2009). Presynaptic signal transduction pathways that modulate synaptic transmission. *Curr Opin Neurobiol*, 19(3), 245–253.

[de Jong et al., 2016] de Jong, A. P., Meijer, M., Saarloos, I., Cornelisse, L., Toonen, R. F., Sørensen, J. B., & Verhage, M. (2016). Phosphorylation of synaptotagmin-1 controls a post-priming step in PKC-dependent presynaptic plasticity. *Proc National Acad Sci*, 113(18), 5095–5100.

[Deák et al., 2004] Deák, F., Schoch, S., Liu, X., Südhof, T., & Kavalali, E. (2004). Synaptobrevin is essential for fast synaptic-vesicle endocytosis. *Nat Cell Biol*, 6(11), ncb1185.

[del Castillo & Katz, 1954] del Castillo, J. & Katz, B. (1954). Quantal components of the end plate potential. *J Physiology*, 124(3), 560–573.

[Delvendahl et al., 2016] Delvendahl, I., Vyleta, N. P., von Gersdorff, H., & Hallermann, S. (2016). Fast, Temperature-Sensitive and Clathrin-Independent endocytosis at central synapses. *Neuron*, 90(3), 492–498.

[Deng et al., 2011] Deng, L., Kaeser, P. S., Xu, W., & Südhof, T. C. (2011). RIM proteins activate vesicle priming by reversing autoinhibitory homodimerization of munc13. *Neuron*, 69(2), 317–331.

[Denker et al., 2011] Denker, A., Bethani, I., & of the …, K. K. (2011). A small pool of vesicles maintains synaptic activity in vivo. *Proceedings of the …*.

[Dietrich et al., 2003] Dietrich, D., Kirschstein, T., Kukley, M., Pereverzev, A., von der Brelie, C., Schneider, T., & Beck, H. (2003). Functional specialization of presynaptic cav2.3 ca2+ channels. *Neuron*, 39(3), 483–496.

[Dittman & Ryan, 2019] Dittman, J. S. & Ryan, T. A. (2019). The control of release probability at nerve terminals. *Nat Rev Neurosci*, 20(3), 1.

[Dobrunz & Stevens, 1997] Dobrunz, L. & Stevens, C. (1997). Heterogeneity of release probability, facilitation, and depletion at central synapses. *Neuron*.

[Dodge & Rahamimoff, 1967] Dodge, F. & Rahamimoff, R. (1967). Co□operative action of calcium ions in transmitter release at the neuromuscular junction. *J Physiology*, 193(2), 419–432.

[Dulubova et al., 2005] Dulubova, I., Lou, X., Lu, J., Huryeva, I., Alam, A., Schneggenburger, R., Südhof, T. C., & Rizo, J. (2005). A Munc13/RIM/Rab3 tripartite complex: from priming to plasticity? *Embo J*, 24(16), 2839–2850.

[Engholm-Keller et al., 2019] Engholm-Keller, K., Waardenberg, A. J., Müller, J. A., Wark, J. R., Fernando, R. N., Arthur, J. W., Robinson, P. J., Dietrich, D., Schoch, S., & Graham, M. E. (2019). The temporal profile of activity-dependent presynaptic phospho-signalling reveals long-lasting patterns of poststimulus regulation. *Plos Biol*, 17(3), e3000170.

[Ermolyuk et al., 2012] Ermolyuk, Y. S., Alder, F. G., Henneberger, C., Rusakov, D. A., Kullmann, D. M., & Volynski, K. E. (2012). Independent regulation of basal neurotransmitter release efficacy by variable ca2+ influx and bouton size at small central synapses. *Plos Biol*, 10(9), e1001396.

[Etsuko et al., 2004] Etsuko, T., Mochida, S., Inoue, E., Maki, D., Inoue, M., Ohtsuka, T., & Takai, Y. (2004). Physical and functional interaction of the active zone proteins, CAST, RIM1, and bassoon, in neurotransmitter release. *J Cell Biology*, 164(2), 301–311.

[Fatma et al., 2004] Fatma, S., Linden, D. J., & Lonart, G. (2004). Adapter protein 14-3-3 is required for a presynaptic form of LTP in the cerebellum. *Nat Neurosci*, 7(12), nn1348.

[Fatma & Lonart, 2008] Fatma, S. & Lonart, G. (2008). The role of RIM1α in BDNF-enhanced glutamate release. 55(1), 27–34.

[Fernández-Busnadiego et al., 2010] Fernández-Busnadiego, R., Zuber, B., Maurer, U., Baumeister, W., & Lucic, V. (2010). Quantitative analysis of the native presynaptic cytomatrix by cryoelectron tomography. *J Cell Biol*, 188(1), 145–56.

[Fourcaudot et al., 2008] Fourcaudot, E., Gambino, F., Humeau, Y., Casassus, G., Shaban, H., Poulain, B., & Lüthi, A. (2008). cAMP/PKA signaling and RIM1α mediate presynaptic LTP in the lateral amygdala. *Proc National Acad Sci*, 105(39), 15130–15135.

[Fowler & Staras, 2015] Fowler, M. & Staras, K. (2015). Synaptic vesicle pools: Principles, properties and limitations. *Exp Cell Res*, 335(2), 150–156.

[Fox & Stryker, 2017] Fox, K. & Stryker, M. (2017). Integrating hebbian and homeostatic plasticity: introduction. *Phil Trans R Soc B*, 372(1715), 20160413.

[Frank et al., 2006] Frank, A. C., Kennedy, M. J., Goold, C. P., Marek, K. W., & Davis, G. W. (2006). Mechanisms underlying the rapid induction and sustained expression of synaptic homeostasis. *Neuron*, 52(4), 663–677.

[Frank et al., 2010] Frank, T., Rutherford, M. A., Strenzke, N., Neef, A., Pangršič, T., Khimich, D., Fejtova, A., Fetjova, A., Gundelfinger, E. D., Liberman, C. M., Harke, B., Bryan, K. E., Lee, A., Egner, A., Riedel, D., & Moser, T. (2010). Bassoon and the synaptic ribbon organize ca2+ channels and vesicles to add release sites and promote refilling. *Neuron*, 68(4), 724–738.

[Futai et al., 2007] Futai, K., Kim, M., Hashikawa, T., Scheiffele, P., Sheng, M., & Hayashi, Y. (2007). Retrograde modulation of presynaptic release probability through signaling mediated by PSD-95-neuroligin. *Nat Neurosci*, 10(2), 186–195.

[Gerber et al., 2008] Gerber, S. H., Rah, J., Min, S., Liu, X., de Wit, H., Dulubova, I., Meyer, A. C., Rizo, J., Arancillo, M., Hammer, R. E., Verhage, M., Rosenmund, C., & Südhof, T. C. (2008). Conformational switch of syntaxin-1 controls synaptic vesicle fusion. *Science*, 321(5895), 1507–1510.

[Gersdorff & Mathews, 1994] Gersdorff, H. & Mathews, G. (1994). Dynamics of synaptic vesicle fusion and membrane retrieval in synaptic terminals. *Nature*, 367(6465), 367735a0.

[Girach et al., 2013] Girach, F., Craig, T. J., Rocca, D. L., & Henley, J. M. (2013). RIM1α SUMOylation is required for fast synaptic vesicle exocytosis. *Cell Reports*, 5(5), 1294–1301.

[Goold & Nicoll, 2010] Goold, C. P. & Nicoll, R. A. (2010). Single-Cell optogenetic excitation drives homeostatic synaptic depression. *Neuron*, 68(3), 512–528.

[Gottmann, 2008] Gottmann, K. (2008). Transsynaptic modulation of the synaptic vesicle cycle by cell□adhesion molecules. *J Neurosci Res*, 86(2), 223–232.

[Granseth et al., 2007] Granseth, B., Odermatt, B., Royle, S. J., & Lagnado, L. (2007). Clathrin-mediated endocytosis: the physiological mechanism of vesicle retrieval at hippocampal synapses. *J Physiology*, 585(3), 681–686.

[Grundke-Iqbal et al., 1986] Grundke-Iqbal, I., Iqbal, K., Tung, Y., Quinlan, M., Wisniewski, H., & Binder, L. (1986). Abnormal phosphorylation of the microtubule-associated protein tau in alzheimer cytoskeletal pathology. *Proc National Acad Sci*, 83(13), 4913–4917.

[Gui et al., 1994] Gui, J., Lane, W. S., & Fu, X. (1994). A serine kinase regulates intracellular localization of splicing factors in the cell cycle. *Nature*, 369(6482), 369678a0.

[Guo et al., 2015] Guo, J., Ge, J.-l., Hao, M., Sun, Z.-c., Wu, X.-s., Zhu, J.-b., Wang, W., Yao, P.-t., Lin, W., & Xue, L. (2015). A Three-Pool model dissecting readily releasable pool replenishment at the calyx of held. *Sci Rep*, 5, 9517.

[Han et al., 2011] Han, Y., Kaeser, P. S., Südhof, T. C., & Schneggenburger, R. (2011). RIM determines ca2+ channel density and vesicle docking at the presynaptic active zone. *Neuron*, 69(2), 304–316.

[Hanson et al., 1997] Hanson, P. I., Heuser, J. E., & Jahn, R. (1997). Neurotransmitter release - four years of SNARE complexes. *Curr Opin Neurobiol*, 7(3), 310–315.

[Harris & Cotman, 1986] Harris, E. W. & Cotman, C. W. (1986). Long-term potentiation of guinea pig mossy fiber responses is not blocked by n-methyl d-aspartate antagonists. *Neurosci Lett*, 70(1), 132–137.

[Harris & Sultan, 1995] Harris, K. & Sultan, P. (1995). Variation in the number, location and size of synaptic vesicles provides an anatomical basis for the nonuniform probability of release at hippocampal CA1 synapses. 34(11), 1387–1395.

[Helassa et al., 2018] Helassa, N., Dürst, C. D., Coates, C., Kerruth, S., Arif, U., Schulze, C., Wiegert, S. J., Geeves, M., Oertner, T. G., & Török, K. (2018). Ultrafast glutamate sensors resolve high-frequency release at schaffer collateral synapses. *Proc National Acad Sci*, 115(21), 5594–5599.

[Henry et al., 2012] Henry, F. E., McCartney, A. J., Neely, R., Perez, A. S., Carruthers, C. J., Stuenkel, E. L., Inoki, K., & Sutton, M. A. (2012). Retrograde changes in presynaptic function driven by dendritic mTORC1. *J Neurosci*, 32(48), 17128–17142.

[Hong et al., 2012] Hong, Y., Chan, C., Kwon, I., Li, X., Song, M., Lee, H., Liu, X., Sompol, P., Jin, P., Lee, H.-g., Yu, S., & Ye, K. (2012). SRPK2 phosphorylates tau and mediates the cognitive defects in alzheimer's disease. *J Neurosci*, 32(48), 17262–17272.

[Houy et al., 2013] Houy, S., Croisé, P., Gubar, O., Sylvette, C., Petra, T., Bailly, Y., Ory, S., Bader, M., & Gasman, S. (2013). Exocytosis and endocytosis in neuroendocrine cells: Inseparable membranes! *Front Endocrinol*, 4, 135.

[Huang & Kandel, 1994] Huang, Y. & Kandel, E. (1994). Recruitment of long-lasting and protein kinase A dependent long-term potentiation in the CA1 region of hippocampus requires repeated tetanization. *Learn Mem Cold Spring Harb N Y*, 1(1), 74–82.

[Ibata et al., 2008] Ibata, K., Sun, Q., & Turrigiano, G. G. (2008). Rapid synaptic scaling induced by changes in postsynaptic firing. *Neuron*, 57(6), 819–826.

[Imig et al., 2014] Imig, C., Min, S., Krinner, S., Arancillo, M., Rosenmund, C., Südhof, T., Rhee, J., Brose, N., & Cooper, B. (2014). The morphological and molecular nature of synaptic vesicle priming at presynaptic active zones. *Neuron*, 84(2), 416–431.

[Inagaki et al., 2008] Inagaki, T., Begum, T., Reza, F., Horibe, S., Inaba, M., Yoshimura, Y., & Komatsu, Y. (2008). Brain-derived neurotrophic factor-mediated retrograde signaling required for the induction of long-term potentiation at inhibitory synapses of visual cortical pyramidal neurons. *Neurosci Res*, 61(2), 192–200.

[Jackman et al., 2014] Jackman, S. L., Beneduce, B. M., Drew, I. R., & Regehr, W. G. (2014). Achieving High-Frequency optical control of synaptic transmission. *J Neurosci*, 34(22), 7704–7714.

[Jaffe & Johnston, 1990] Jaffe, D. & Johnston, D. (1990). Induction of long-term potentiation at hippocampal mossy-fiber synapses follows a hebbian rule. *J Neurophysiol*, 64(3), 948–60.

[Jahn & Fasshauer, 2012] Jahn, R. & Fasshauer, D. (2012). Molecular machines governing exocytosis of synaptic vesicles. *Nature*, 490(7419), 201.

[Jiang et al., 2010] Jiang, X., Litkowski, P., Taylor, A., Lin, Y., Snider, B., & Moulder, K. (2010). A role for the Ubiquitin–Proteasome system in Activity-Dependent presynaptic silencing. *J Neurosci*, 30(5), 1798–1809.

[Johnson et al., 2009] Johnson, E., Fetter, R., & Davis, G. (2009). Negative regulation of active zone assembly by a newly identified SR protein kinase. *Plos Biol*, 7(9), e1000193.

[Johnson & Barford, 2003] Johnson, L. & Barford, D. (2003). The effects of phosphorylation on the structure and function of proteins. *Annu Rev Bioph Biom*, 22(1), 199–232.

[Johnson et al., 2003] Johnson, S., Halford, S., Morris, A. G., Patel, R. J., Wilkie, S. E., Hardcastle, A. J., Moore, A. T., Zhang, K., & Hunt, D. M. (2003). Genomic organisation and alternative splicing of human RIM1, a gene implicated in autosomal dominant cone-rod dystrophy (CORD7). *Genomics*, 81(3), 304–314.

[Jung et al., 2014] Jung, J., Loy, K., Schilling, E., Röther, M., Brauner, J., Huth, T., Shloetzer-Schrehardt, U., Alzheimer, C., Kornhuber, J., Welzel, O., & Groemer, T. (2014). The antidepressant fluoxetine mobilizes vesicles to the recycling pool of rat hippocampal synapses during high activity. *Mol Neurobiol*, 2, 916–30.

[Kaeser et al., 2012] Kaeser, P., Deng, L., Fan, M., & Südhof, T. (2012). RIM genes differentially contribute to organizing presynaptic release sites. *Proc National Acad Sci*, 109(29), 11830–11835.

[Kaeser et al., 2011] Kaeser, P. S., Deng, L., Wang, Y., Dulubova, I., Liu, X., Rizo, J., & Südhof, T. C. (2011). RIM proteins tether ca2+ channels to presynaptic active zones via a direct PDZ-Domain interaction. *Cell*, 144(2), 282–295.

[Kaeser et al., 2008a] Kaeser, P. S., Kwon, H., Blundell, J., Chevaleyre, V., Morishita, W., Malenka, R. C., Powell, C. M., Castillo, P. E., & Südhof, T. C. (2008a). RIM1α phosphorylation at serine-413 by protein kinase a is not required for presynaptic long-term plasticity or learning. *Proc National Acad Sci*, 105(38), 14680–14685.

[Kaeser et al., 2008b] Kaeser, P. S., Kwon, H., Chiu, C. Q., Deng, L., Castillo, P. E., & Südhof, T. C. (2008b). RIM1α and RIM1β are synthesized from distinct promoters of the RIM1 gene to mediate differential but overlapping synaptic functions. *J Neurosci*, 28(50), 13435–13447.

[Kapur et al., 1998] Kapur, A., Yeckel, M. F., Gray, R., & Johnston, D. (1998). L-Type calcium channels are required for one form of hippocampal mossy fiber LTP. *J Neurophysiol*, 79(4), 2181–2190.

[Kato et al., 1994] Kato, K., Clark, G. D., Bazan, N. G., & Zorumski, C. F. (1994). Platelet-activating factor as a potential retrograde messenger in CA1 hippocampal long-term potentiation. *Nature*, 367(6459), 367175a0.

[Kavalali & Jorgensen, 2013] Kavalali, E. T. & Jorgensen, E. M. (2013). Visualizing presynaptic function. *Nat Neurosci*, 17(1), 10–16.

[Kavalali et al., 1999] Kavalali, E. T., Klingauf, J., & Tsien, R. W. (1999). Properties of fast endocytosis at hippocampal synapses. *Philosophical Transactions Royal Soc Lond B Biological Sci*, 354(1381), 337–346.

[Kazemipour et al., 2018] Kazemipour, A., Novak, O., Flickinger, D., Marvin, J. S., King, J., Borden, P., Druckmann, S., Svoboda, K., Looger, L. L., & Podgorski, K. (2018). Kilohertz frame-rate two-photon tomography. *Biorxiv*, (pp. 357269).

[Kim & Hayashi, 2014] Kim, K. & Hayashi, Y. (2014). CaMKII: the swiss army knife of synaptic plasticity. *J Physiology*, 592(22), 4807–4808.

[Kim & Neuron, 2010] Kim, S. & Neuron, R. T. (2010). CDK5 serves as a major control point in neurotransmitter release. *Neuron*.

[Kiyonaka et al., 2007] Kiyonaka, S., Wakamori, M., Miki, T., Uriu, Y., Nonaka, M., Bito, H., Beedle, A. M., Mori, E., Hara, Y., Waard, M., Kanagawa, M., Itakura, M., Takahashi, M., Campbell, K. P., & Mori, Y. (2007). RIM1 confers sustained activity and neurotransmitter vesicle anchoring to presynaptic ca2+ channels. *Nat Neurosci*, 10(6), nn1904.

[Klingauf et al., 1998] Klingauf, J., Kavalali, E., & Tsien, R. (1998). Kinetics and regulation of fast endocytosis at hippocampal synapses. *Nature*, 394(6693), 29079.

[Köhrmann et al., 1999] Köhrmann, M., Haubensak, W., Hemraj, I., Kaether, C., Leßmann, V. J., & Kiebler, M. A. (1999). Fast, convenient, and effective method to transiently transfect primary hippocampal neurons. *J Neurosci Res*, 58(6), 831–835.

[Körber & Kuner, 2016] Körber, C. & Kuner, T. (2016). Molecular machines regulating the release probability of synaptic vesicles at the active zone. *Frontiers Synaptic Neurosci*, 8, 5.

[Lachamp et al., 2009] Lachamp, P. M., Liu, Y., & Liu, S. (2009). Glutamatergic modulation of cerebellar interneuron activity is mediated by an enhancement of GABA release and requires protein kinase A/RIM1α signaling. *J Neurosci*, 29(2), 381–392.

[Lazarenko et al., 2017] Lazarenko, R. M., E, D. C., Strothman, C. E., & Zhang, Q. (2017). Ammonium chloride alters neuronal excitability and synaptic vesicle release. *Sci Rep-uk*, 7(1), 5061.

[Lazarevic et al., 2013] Lazarevic, V., Pothula, S., Maria, A., & Fejtova, A. (2013). Molecular mechanisms driving homeostatic plasticity of neurotransmitter release. *Front Cell Neurosci*, 7, 244.

[Lazarevic et al., 2011] Lazarevic, V., Schöne, C., Heine, M., Gundelfinger, E., & Fejtova, A. (2011). Extensive remodeling of the presynaptic cytomatrix upon homeostatic adaptation to network activity silencing. *J Neurosci*, 31(28), 10189–10200.

[Lee et al., 2000] Lee, A., Scheuer, T., & Catterall, W. A. (2000). Ca2+/Calmodulin-Dependent facilitation and inactivation of P/Q-Type ca2+ channels. *J Neurosci*, 20(18), 6830–6838.

[Lee et al., 2002] Lee, A., Westenbroek, R. E., Haeseleer, F., Palczewski, K., Scheuer, T., & Catterall, W. A. (2002). Differential modulation of ca(v)2.1 channels by calmodulin and ca2+-binding protein 1. *Nat Neurosci*, 5(3), 210–7.

[Lee et al., 1999] Lee, A., Wong, S. T., Gallagher, D., Li, B., Storm, D. R., Scheuer, T., & Catterall, W. A. (1999). Ca2+/calmodulin binds to and modulates P/Q-type calcium channels. *Nature*, 399(6732), 20194.

[Leenders & Sheng, 2005] Leenders, A. & Sheng, Z. (2005). Modulation of neurotransmitter release by the second messenger-activated protein kinases: Implications for presynaptic plasticity. *Pharmacol Therapeut*, 105(1), 69–84.

[Llinas et al., 1992] Llinas, R., Sugimori, M., & Silver, R. (1992). Microdomains of high calcium concentration in a presynaptic terminal. *Science*, 256(5057), 677–679.

[Lonart et al., 2003] Lonart, G., Schoch, S., Kaeser, P., Larkin, C., Südhof, T., & Linden, D. (2003). Phosphorylation of RIM1α by PKA triggers presynaptic Long-Term potentiation at cerebellar parallel fiber synapses. *Cell*, 115(1), 49–60.

[Looger et al., 2018] Looger, L. L., Marvin, J. S., Shimoda, Y., Magloire, V., Leite, M., Kawashima, T., Jensen, T. P., Knott, E. L., Novak, O., Podgorski, K., Leidenheimer, N. J., Rusakov, D. A., Ahrens, M. B., & Kullmann, D. M. (2018). A genetically encoded fluorescent sensor for in vivo imaging of GABA. *Biorxiv*, (pp. 322578).

[Lu et al., 2006] Lu, H., Butts, D. A., Kaeser, P. S., She, W., Janz, R., & Crair, M. C. (2006). Role of efficient neurotransmitter release in barrel map development. *J Neurosci*, 26(10), 2692–2703.

[Lučić et al., 2008] Lučić, V., Greif, G. J., & Kennedy, M. B. (2008). Detailed state model of CaMKII activation and autophosphorylation. *Eur Biophys J*, 38(1), 83.

[Maciejewski et al., 1995] Maciejewski, P. M., Peterson, F. C., Anderson, P. J., & Brooks, C. L. (1995). Mutation of serine 90 to glutamic acid mimics phosphorylation of bovine prolactin. *J Biol Chem*, 270(46), 27661–27665.

[Mahdokht et al., 2016] Mahdokht, K., Chua, J. J., Urlaub, H., Jahn, R., & Czernik, D. (2016). Analysis of protein phosphorylation in nerve terminal reveals extensive changes in active zone proteins upon exocytosis. *Elife*, 5, e14530.

[Marra et al., 2012] Marra, V., Burden, J., Thorpe, J., Smith, I., & Neuron, S. S. (2012). A preferentially segregated recycling vesicle pool of limited size supports neurotransmission in native central synapses. *Neuron*.

[Marvin et al., 2013] Marvin, J., Borghuis, B., Tian, L., Cichon, J., Harnett, M., Akerboom, J., Gordus, A., Renninger, S., Chen, T., Bargmann, C., Orger, M., Schreiter, E., Demb, J., Gan, W., Hires, S., & Looger, L. (2013). An optimized fluorescent probe for visualizing glutamate neurotransmission. *Nat Methods*, 10(2), 162.

[Marvin et al., 2018] Marvin, J. S., Scholl, B., Wilson, D. E., Podgorski, K., Kazemipour, A., Müller, J. A., Schoch, S., Quiroz, F., Rebola, N., Bao, H., Little, J. P., Tkachuk, A. N., Cai, E., Hantman, A. W., Wang, S., J, D. V., Borghuis, B. G., Chapman, E. R., Dietrich, D., A, D. D., Fitzpatrick, D., & Looger, L. L. (2018). Stability, affinity, and chromatic variants of the glutamate sensor iGluSnFR. *Nat Methods*, 15(11), 936–939.

[Maximov et al., 2007] Maximov, A., Shin, O., Liu, X., & Südhof, T. C. (2007). Synaptotagmin-12, a synaptic vesicle phosphoprotein that modulates spontaneous neurotransmitter release. *J Cell Biology*, 176(1), 113–124.

[Meis et al., 2012] Meis, S., Endres, T., & Lessmann, V. (2012). Postsynaptic BDNF signalling regulates long□term potentiation at thalamo□amygdala afferents. *J Physiology*, 590(1), 193–208.

[Michel et al., 2015] Michel, K., Müller, J. A., Oprişoreanu, A. M., & Schoch, S. (2015). The presynaptic active zone: A dynamic scaffold that regulates synaptic efficacy. *Exp. Cell Res.*, 335(2), 157–64.

[Miesenböck et al., 1998] Miesenböck, G., Angelis, D. A., & Rothman, J. E. (1998). Visualizing secretion and synaptic transmission with pH-sensitive green fluorescent proteins. *Nature*, 394(6689), 192–195.

[Miller & Heuser, 1984] Miller, T. & Heuser, J. (1984). Endocytosis of synaptic vesicle membrane at the frog neuromuscular junction. *J Cell Biology*, 98(2), 685–698.

[Mittelstaedt et al., 2010] Mittelstaedt, T., Elena, A., & Schoch, S. (2010). RIM proteins and their role in synapse function. *Biol Chem*, 391(6), 599–606.

[Mozhayeva et al., 2002] Mozhayeva, M. G., Sara, Y., Liu, X., & Kavalali, E. T. (2002). Development of vesicle pools during maturation of hippocampal synapses. *J. Neurosci.*, 22(3), 654–65.

[Müller et al., 2015] Müller, M., Genç, Ö., & Davis, G. W. (2015). RIM-Binding protein links synaptic homeostasis to the stabilization and replenishment of high release probability vesicles. *Neuron*, 85(5), 1056–1069.

[Müller et al., 2012] Müller, M., Liu, K., Sigrist, S., & Davis, G. (2012). RIM controls homeostatic plasticity through modulation of the Readily-Releasable vesicle pool. *J Neurosci*, 32(47), 16574–16585.

[Müller et al., 2011] Müller, M., Pym, E., Tong, A., & Davis, G. W. (2011). Rab3-GAP controls the progression of synaptic homeostasis at a late stage of vesicle release. *Neuron*, 69(4), 749–762.

[Murthy & Nature, 1998] Murthy, V. & Nature, S. C. (1998). Synaptic vesicles retain their identity through the endocytic cycle. *Nature*.

[Murthy et al., 2001] Murthy, V. N., Schikorski, T., Stevens, C. F., & Zhu, Y. (2001). Inactivity produces increases in neurotransmitter release and synapse size. *Neuron*, 32(4), 673–682.

[Nakagawa et al., 2005] Nakagawa, O., Arnold, M., Nakagawa, M., Hamada, H., Shelton, J. M., Kusano, H., Harris, T. M., Childs, G., Campbell, K. P., Richardson, J. A., Nishino, I., & Olson, E. N. (2005). Centronuclear myopathy in mice lacking a novel muscle-specific protein kinase transcriptionally regulated by MEF2. *Genes Dev*, 19(17), 2066–2077.

[Nicoll & Schmitz, 2005] Nicoll, R. A. & Schmitz, D. (2005). Synaptic plasticity at hippocampal mossy fibre synapses. *Nat Rev Neurosci*, 6(11), nrn1786.

[Nieratschker et al., 2009] Nieratschker, V., Schubert, A., Jauch, M., Bock, N., Bucher, D., Dippacher, S., Krohne, G., Asan, E., Buchner, S., & Buchner, E. (2009). Bruchpilot in Ribbon-Like axonal agglomerates, behavioral defects, and early death in SRPK79D kinase mutants of drosophila. *Plos Genet*, 5(10), e1000700.

[Nimmervoll et al., 2013] Nimmervoll, B., Flucher, B., & Obermair, G. (2013). Dominance of P/Q-type calcium channels in depolarization-induced presynaptic fm dye release in cultured hippocampal neurons. *Neuroscience*, 253, 330–340.

[Nishi et al., 2011] Nishi, H., Hashimoto, K., & Panchenko, A. R. (2011). Phosphorylation in Protein-Protein binding: Effect on stability and function. *Structure*, 19(12), 1807–1815.

[Nolen et al., 2004] Nolen, B., Taylor, S., & Ghosh, G. (2004). Regulation of protein kinases controlling activity through activation segment conformation. *Mol Cell*, 15(5), 661–675.

[Ohtsuka et al., 2002] Ohtsuka, T., Etsuko, T., Inoue, E., Inoue, M., Takeuchi, M., Matsubara, K., Maki, D., Satoh, K., Morimoto, K., Nakanishi, H., & Takai, Y. (2002). Cast a novel protein of the cytomatrix

at the active zone of synapses that forms a ternary complex with RIM1 and munc13-1. *J Cell Biology*, 158(3), 577–590.

[Okumoto et al., 2005] Okumoto, S., Looger, L. L., Micheva, K. D., Reimer, R. J., Smith, S. J., & Frommer, W. B. (2005). Detection of glutamate release from neurons by genetically encoded surface-displayed FRET nanosensors. *P Natl Acad Sci Usa*, 102(24), 8740–8745.

[Opazo & Rizzoli, 2014] Opazo, F. & Rizzoli, S. O. (2014). The fate of synaptic vesicle components upon fusion. *Commun Integr Biology*, 3(5), 427–429.

[Patriarchi et al., 2018] Patriarchi, T., Cho, J., Merten, K., Howe, M. W., Marley, A., Xiong, W., Folk, R. W., Broussard, G., Liang, R., Jang, M., Zhong, H., Dombeck, D., von Zastrow, M., Nimmerjahn, A., Gradinaru, V., Williams, J. T., & Tian, L. (2018). Ultrafast neuronal imaging of dopamine dynamics with designed genetically encoded sensors. *Science*, 360(6396), eaat4422.

[Pelkey et al., 2008] Pelkey, K. A., Topolnik, L., Yuan, X., Lacaille, J., & J, M. C. (2008). State-Dependent cAMP sensitivity of presynaptic function underlies metaplasticity in a hippocampal feedforward inhibitory circuit. *Neuron*, 60(6), 980–987.

[Penney et al., 2012] Penney, J., Tsurudome, K., Liao, E. H., Elazzouzi, F., Livingstone, M., Gonzalez, M., Sonenberg, N., & Haghighi, P. A. (2012). TOR is required for the retrograde regulation of synaptic homeostasis at the drosophila neuromuscular junction. *Neuron*, 74(1), 166–178.

[Pérez-Otaño & Ehlers, 2005] Pérez-Otaño, I. & Ehlers, M. (2005). Homeostatic plasticity and NMDA receptor trafficking. *Trends Neurosci*, 28(5), 229–238.

[Petersen et al., 2000] Petersen, S. A., Fetter, R. D., Noordermeer, J. N., Goodman, C. S., & Aaron, D. (2000). Genetic analysis of glutamate receptors in drosophila reveals a retrograde signal regulating presynaptic transmitter release. *Neuron*, 19(6), 1237–1248.

[Pfenninger et al., 1972] Pfenninger, K., Akert, K., Moor, H., & Sandri, C. (1972). The fine structure of freeze-fractured presynaptic membranes. *Journal of neurocytology*.

[Prange & Murphy, 1999] Prange, O. & Murphy, T. H. (1999). Correlation of miniature synaptic activity and evoked release probability in cultures of cortical neurons. (pp. 6427–6438).

[Rafael et al., 2001] Rafael, F., Königstorfer, A., Gerber, S. H., García, J., Matos, M. F., Stevens, C. F., Brose, N., Rizo, J., Rosenmund, C., & Südhof, T. C. (2001). Synaptotagmin i functions as a calcium regulator of release probability. *Nature*, 410(6824), 41.

[Ramirez & Kavalali, 2011] Ramirez, D. & Kavalali, E. (2011). Differential regulation of spontaneous and evoked neurotransmitter release at central synapses. *Curr Opin Neurobiol*, 21(2), 275–282.

[Regehr, 2012] Regehr, W. G. (2012). Short-Term presynaptic plasticity. *Csh Perspect Biol*, 4(7), a005702.

[Rizzoli et al., 2003] Rizzoli, S. O., Richards, D. A., & Betz, W. J. (2003). Monitoring synaptic vesicle recycling in frog motor nerve terminals with FM dyes. *J Neurocytol*, 32(5-8), 539–549.

[Rosenmund et al., 1993] Rosenmund, C., Clements, J., & Westbrook, G. (1993). Nonuniform probability of glutamate release at a hippocampal synapse. *Science*, 262(5134), 754–757.

[Rozental et al., 2000] Rozental, R., Giaume, C., & Spray, D. (2000). Gap junctions in the nervous system. *Brain Res Rev*, 32(1), 11–15.

[Rubén et al., 2013] Rubén, F., Asano, S., Oprisoreanu, A., Sakata, E., Doengi, M., Kochovski, Z., Zürner, M., Stein, V., Schoch, S., Baumeister, W., & Lučić, V. (2013). Cryo–electron tomography reveals a critical role of RIM1α in synaptic vesicle tethering. 201(5), 725–740.

[Ryan et al., 1996] Ryan, T., Smith, S., & Reuter, H. (1996). The timing of synaptic vesicle endocytosis. *Proc National Acad Sci*, 93(11), 5567–5571.

[Sakamoto et al., 2018] Sakamoto, H., Ariyoshi, T., Kimpara, N., Sugao, K., Taiko, I., Takikawa, K., Asanuma, D., Namiki, S., & Hirose, K. (2018). Synaptic weight set by munc13-1 supramolecular assemblies. *Nat Neurosci*, 21(1), 41–49.

[Salin et al., 1996] Salin, P. A., Malenka, R. C., & Nicoll, R. A. (1996). Cyclic AMP mediates a presynaptic form of LTP at cerebellar parallel fiber synapses. *Neuron*, 16(4), 797–803.

[Sambataro & Pennuto, 2017] Sambataro, F. & Pennuto, M. (2017). Post-translational modifications and protein quality control in motor neuron and polyglutamine diseases. *Front Mol Neurosci*, 10, 82.

[Sara et al., 2002] Sara, Y., Mozhayeva, M. G., Liu, X., & Kavalali, E. T. (2002). Fast vesicle recycling supports neurotransmission during sustained stimulation at hippocampal synapses. *J. Neurosci.*, 22(5), 1608–17.

[Sara et al., 2005] Sara, Y., Virmani, T., Deák, F., Liu, X., & Kavalali, E. T. (2005). An isolated pool of vesicles recycles at rest and drives spontaneous neurotransmission. 45(4), 563–573.

[Scharf et al., 2002] Scharf, M. T., Woo, N. H., Lattal, M. K., Young, J. Z., Nguyen, P. V., & Abel, T. (2002). Protein synthesis is required for the enhancement of Long-Term potentiation and Long-Term memory by spaced training. *J Neurophysiol*, 87(6), 2770–2777.

[Schikorski & Stevens, 1997] Schikorski, T. & Stevens, C. (1997). Quantitative ultrastructural analysis of hippocampal excitatory synapses. *J Neurosci*, 17(15), 5858–67.

[Schneggenburger & Neher, 2000] Schneggenburger, R. & Neher, E. (2000). Intracellular calcium dependence of transmitter release rates at a fast central synapse. *Nature*, 406(6798), 889.

[Schoch et al., 2002] Schoch, S., Castillo, P., Jo, T., Mukherjee, K., Geppert, M., Wang, Y., Schmitz, F., Malenka, R., & Südhof, T. (2002). RIM1α forms a protein scaffold for regulating neurotransmitter release at the active zone. *Nature*, 415(6869), 321.

[Schoch & Gundelfinger, 2006] Schoch, S. & Gundelfinger, E. (2006). Molecular organization of the presynaptic active zone. *Cell Tissue Res*, 326(2), 379–391.

[Schoch et al., 2006] Schoch, S., Mittelstaedt, T., Kaeser, P. S., Padgett, D., Feldmann, N., Chevaleyre, V., Castillo, P. E., Hammer, R. E., Han, W., Schmitz, F., Lin, W., & Südhof, T. C. (2006). Redundant functions of RIM1α and RIM2α in ca2+□triggered neurotransmitter release. 25(24), 5852–5863.

[Scimemi & Diamond, 2012] Scimemi, A. & Diamond, J. S. (2012). The number and organization of ca2+ channels in the active zone shapes neurotransmitter release from schaffer collateral synapses. *J Neurosci*, 32(50), 18157–18176.

[Scimemi et al., 2009] Scimemi, A., Tian, H., & Diamond, J. S. (2009). Neuronal transporters regulate glutamate clearance, NMDA receptor activation, and synaptic plasticity in the hippocampus. *J Neurosci*, 29(46), 14581–14595.

[Serulle et al., 2007] Serulle, Y., Sugimori, M., & Llinás, R. (2007). Imaging synaptosomal calcium concentration microdomains and vesicle fusion by using total internal reflection fluorescent microscopy. *Proc National Acad Sci*, 104(5), 1697–1702.

[Sharpless, 1975] Sharpless, S. (1975). Supersensitivity-like phenomena in the central nervous system. *Faseb J*, 34(10), 1990–7.

[Sheng et al., 2012] Sheng, J., He, L., Zheng, H., Xue, L., Luo, F., Shin, W., Sun, T., Kuner, T., Yue, D. T., & Wu, L. (2012). Calcium-channel number critically influences synaptic strength and plasticity at the active zone. *Nat Neurosci*, 15(7), 998.

[Shibasaki et al., 2004] Shibasaki, T., Sunaga, Y., Fujimoto, K., Kashima, Y., & Seino, S. (2004). Interaction of ATP sensor, cAMP sensor, ca2+ sensor, and voltage-dependent ca2+ channel in insulin granule exocytosis. *J Biol Chem*, 279(9), 7956–7961.

[Simon & Llinás, 1985] Simon, S. & Llinás, R. (1985). Compartmentalization of the submembrane calcium activity during calcium influx and its significance in transmitter release. *Biophys J*, 48(3), 485–498.

[Skehel et al., 1995] Skehel, P., Martin, K., Kandel, E., & Bartsch, D. (1995). A VAMP-binding protein from aplysia required for neurotransmitter release. *Science*, 269(5230), 1580–1583.

[Smart & Paoletti, 2012] Smart, T. & Paoletti, P. (2012). Synaptic Neurotransmitter-Gated receptors. *Csh Perspect Biol*, 4(3), a009662.

[Smillie & Cousin, 2012] Smillie, K. J. & Cousin, M. A. (2012). Akt/PKB controls the activity□dependent bulk endocytosis of synaptic vesicles. *Traffic*, 13(7), 1004–1011.

[Söllner et al., 1993] Söllner, T., Bennett, M. K., Whiteheart, S. W., Scheller, R. H., & Rothman, J. E. (1993). A protein assembly-disassembly pathway in vitro that may correspond to sequential steps of synaptic vesicle docking, activation, and fusion. *Cell*, 75(3), 409–418.

[Sossin, 2007] Sossin, W. S. (2007). Isoform specificity of protein kinase cs in synaptic plasticity. *Learn Memory*, 14(4), 236–246.

[Spangler et al., 2013] Spangler, S. A., Schmitz, S. K., Kevenaar, J. T., de Graaff, E., de Wit, H., Demmers, J., Toonen, R. F., & Hoogenraad, C. C. (2013). Liprin-□2 promotes the presynaptic recruitment and turnover of RIM1/CASK to facilitate synaptic transmission. 201(6), 915–928.

[Stevens & Neuron, 1998] Stevens, C. & Neuron, S. J. (1998). Regulation of the readily releasable vesicle pool by protein kinase c. *Neuron*.

[Stevens & Tsujimoto, 1995] Stevens, C. & Tsujimoto, T. (1995). Estimates for the pool size of releasable quanta at a single central synapse and for the time required to refill the pool. *Proc National Acad Sci USA*, 92(3), 846–9.

[Südhof, 2004] Südhof, T. (2004). The synaptic vesicle cycle. *Annu Rev Neurosci*, 27(1), 509–547.

[Südhof & Rizo, 2011] Südhof, T. & Rizo, J. (2011). Synaptic vesicle exocytosis. *Csh Perspect Biol*, 3(12), a005637.

[Südhof, 2012a] Südhof, T. C. (2012a). Calcium control of neurotransmitter release. *Csh Perspect Biol*, 4(1), a011353.

[Südhof, 2012b] Südhof, T. C. (2012b). The presynaptic active zone. *Neuron*, 75(1), 11–25.

[Sutton et al., 1998] Sutton, B. R., Fasshauer, D., Jahn, R., & Brunger, A. T. (1998). Crystal structure of a SNARE complex involved in synaptic exocytosis at 2.4 å resolution. *Nature*, 395(6700), 347.

[Sutton et al., 2006] Sutton, M. A., Ito, H. T., Cressy, P., Kempf, C., Woo, J. C., & Schuman, E. M. (2006). Miniature neurotransmission stabilizes synaptic function via tonic suppression of local dendritic protein synthesis. *Cell*, 125(4), 785–799.

[Sutton et al., 2007] Sutton, M. A., Taylor, A. M., Ito, H. T., Pham, A., & Schuman, E. M. (2007). Postsynaptic decoding of neural activity: eEF2 as a biochemical sensor coupling miniature synaptic transmission to local protein synthesis. *Neuron*, 55(4), 648–661.

[Sutton et al., 2004] Sutton, M. A., Wall, N. R., Aakalu, G. N., & Schuman, E. M. (2004). Regulation of dendritic protein synthesis by miniature synaptic events. *Science*, 304(5679), 1979–1983.

[Takahashi et al., 2003] Takahashi, M., Itakura, M., & Kataoka, M. (2003). New aspects of neurotransmitter releasee and exocytosis: Regulation of neurotransmitter release by phosphorylation. *J Pharmacol Sci*, 93(1), 41–45.

[Takamori et al., 2006] Takamori, S., Holt, M., Stenius, K., Lemke, E. A., Grønborg, M., Riedel, D., Urlaub, H., Schenck, S., Brügger, B., Ringler, P., Müller, S. A., Rammner, B., Gräter, F., Hub, J. S., Groot, B. L., Mieskes, G., Moriyama, Y., Klingauf, J., Grubmüller, H., Heuser, J., Wieland, F., & Jahn, R. (2006). Molecular anatomy of a trafficking organelle. *Cell*, 127(4), 831–846.

[Tang et al., 2016] Tang, A., Chen, H., Li, T. P., Metzbower, S. R., D, M. H., & Blanpied, T. A. (2016). A trans-synaptic nanocolumn aligns neurotransmitter release to receptors. *Nature*, 536(7615), 210.

[Tang et al., 2006] Tang, J., Maximov, A., Shin, O., Dai, H., Rizo, J., & Südhof, T. C. (2006). A Complexin/Synaptotagmin 1 switch controls fast synaptic vesicle exocytosis. *Cell*, 126(6), 1175–1187.

[Thiagarajan et al., 2005] Thiagarajan, T. C., Lindskog, M., & Tsien, R. W. (2005). Adaptation to synaptic inactivity in hippocampal neurons. *Neuron*, 47(5), 725–737.

[Tomás & Ryan, 2004] Tomás, F. & Ryan, T. A. (2004). The kinetics of synaptic vesicle pool depletion at CNS synaptic terminals. *Neuron*, 41(6), 943–953.

[Tsuriel et al., 2009] Tsuriel, S., Fisher, A., Wittenmayer, N., Dresbach, T., Garner, C., & Ziv, N. (2009). Exchange and redistribution dynamics of the cytoskeleton of the active zone molecule bassoon. *J Neurosci*, 29(2), 351–358.

[Turrigiano, 2011] Turrigiano, G. (2011). Too many cooks? intrinsic and synaptic homeostatic mechanisms in cortical circuit refinement. *Neuroscience*, 34(1), 89–103.

[Turrigiano, 2012] Turrigiano, G. (2012). Homeostatic synaptic plasticity: Local and global mechanisms for stabilizing neuronal function. *Csh Perspect Biol*, 4(1), a005736.

[Turrigiano et al., 1998] Turrigiano, G. G., Leslie, K. R., Desai, N. S., Rutherford, L. C., & Nelson, S. B. (1998). Activity-dependent scaling of quantal amplitude in neocortical neurons. *Nature*, 391(6670), 36103.

[Tzounopoulos et al., 1998] Tzounopoulos, T., Janz, R., Südhof, T. C., Nicoll, R. A., & Malenka, R. C. (1998). A role for cAMP in Long-Term depression at hippocampal mossy fiber synapses. *Neuron*, 21(4), 837–845.

[Uriu et al., 2010] Uriu, Y., Kiyonaka, S., Miki, T., Yagi, M., Akiyama, S., Mori, E., Nakao, A., Beedle, A. M., Campbell, K. P., Wakamori, M., & Mori, Y. (2010). Rab3-interacting molecule γ isoforms lacking the rab3-binding domain induce long lasting currents but block neurotransmitter vesicle anchoring in voltage-dependent P/Q-type ca2+ channels. *J Biol Chem*, 285(28), 21750–21767.

[van Loo et al., 2019] van Loo, K. M., Rummel, C. K., Pitsch, J., Müller, J., Bikbaev, A. F., Chavez, E., Blaess, S., Dietrich, D., Heine, M., Becker, A. J., & Schoch, S. (2019). Calcium channel subunit α2δ4 is regulated by early growth response 1 and facilitates epileptogenesis. *J Neurosci*, (pp. 1731–18).

[van Loo et al., 2012] van Loo, K. M., Schaub, C., Pernhorst, K., Yaari, Y., Beck, H., Schoch, S., & Becker, A. J. (2012). Transcriptional regulation of t-type calcium channel CaV3.2 bi-diretionality by early grwoth response1 (Egr1) and repressor alement 1 (RE-1) protein-silencing transcription factor (REST). *J Biol Chem*, 287(19), 15489–15501.

[Varoqueaux et al., 2002] Varoqueaux, F., Sigler, A., Rhee, J., Brose, N., Enk, C., Reim, K., & Rosenmund, C. (2002). Total arrest of spontaneous and evoked synaptic transmission but normal synaptogenesis in the absence of munc13-mediated vesicle priming. *Proc National Acad Sci*, 99(13), 9037–9042.

[Varoqueaux et al., 2005] Varoqueaux, F., Sons, M. S., Plomp, J. J., & Brose, N. (2005). Aberrant morphology and residual transmitter release at the Munc13-Deficient mouse neuromuscular synapse†. *Mol Cell Biol*, 25(14), 5973–5984.

[Verstegen et al., 2014] Verstegen, A. M., Tagliatti, E., Lignani, G., Marte, A., Stolero, T., Atias, M., Corradi, A., Valtorta, F., Gitler, D., Onofri, F., Fassio, A., & Benfenati, F. (2014). Phosphorylation of synapsin i by Cyclin-Dependent kinase-5 sets the ratio between the resting and recycling pools of synaptic vesicles at hippocampal synapses. *J Neurosci*, 34(21), 7266–7280.

[Vyleta & Jonas, 2014] Vyleta, N. P. & Jonas, P. (2014). Loose coupling between ca2+ channels and release sensors at a plastic hippocampal synapse. *Science*, 343(6171), 665–670.

[Vyleta & Smith, 2011] Vyleta, N. P. & Smith, S. M. (2011). Spontaneous glutamate release is independent of calcium influx and tonically activated by the Calcium-Sensing receptor. *J Neurosci*, 31(12), 4593–4606.

[Wadel et al., 2007] Wadel, K., Neher, E., & Sakaba, T. (2007). The coupling between synaptic vesicles and ca2+ channels determines fast neurotransmitter release. *Neuron*, 53(4), 563–575.

[Wang et al., 1998] Wang, H., Lin, W., Dyck, J. A., Yeakley, J. M., Songyang, Z., Cantley, L. C., & Fu, X. (1998). SRPK2: a differentially expressed SR protein-specific kinase involved in mediating the interaction and localization of Pre-mRNA splicing factors in mammalian cells. *J Cell Biology*, 140(4), 737–750.

[Wang et al., 2008] Wang, L., Neher, E., & Taschenberger, H. (2008). Synaptic vesicles in mature calyx of held synapses sense higher nanodomain calcium concentrations during action Potential-Evoked glutamate release. *J Neurosci*, 28(53), 14450–14458.

[Wang et al., 1997] Wang, Y., Okamoto, M., Schmitz, F., Hofmann, K., & Südhof, T. C. (1997). RIM is a putative rab3 effector in regulating synaptic-vesicle fusion. *Nature*, 388(6642), 593–598.

[Wang & Südhof, 2003] Wang, Y. & Südhof, T. C. (2003). Genomic definition of RIM proteins: evolutionary amplification of a family of synaptic regulatory proteins. *Genomics*, 81(2), 126–137.

[Wang et al., 2000] Wang, Y., Sugita, S., & Südhof, T. C. (2000). The RIM/NIM family of neuronal c2 domain proteins interactions with rab3 and a new class of src homology 3 domain proteins. *J Biol Chem*, 275(26), 20033–20044.

[Wang, 2008] Wang, Z. (2008). Regulation of synaptic transmission by presynaptic CaMKII and BK channels. *Mol Neurobiol*, 38(2), 153–166.

[Watanabe et al., 2013] Watanabe, S., Rost, B. R., Marcial, C., Davis, W. M., Berit, S., Rosenmund, C., & Jorgensen, E. M. (2013). Ultrafast endocytosis at mouse hippocampal synapses. *Nature*, 504(7479), 242.

[Waters & Smith, 2000] Waters, J. & Smith, S. (2000). Phorbol esters potentiate evoked and spontaneous release by different presynaptic mechanisms. *J Neurosci*, 20(21), 7863–70.

[Watt et al., 2000] Watt, A. J., van Rossum, M., M, M. K., Nelson, S. B., & Turrigiano, G. G. (2000). Activity coregulates quantal AMPA and NMDA currents at neocortical synapses. *Neuron*, 26(3), 659–670.

[Weisskopf et al., 1994] Weisskopf, M., Castillo, P., Zalutsky, R., & Nicoll, R. (1994). Mediation of hippocampal mossy fiber long-term potentiation by cyclic AMP. *Sci New York N Y*, 265(5180), 1878–82.

[Wilhelm et al., 2010] Wilhelm, B. G., Groemer, T. W., & Rizzoli, S. O. (2010). The same synaptic vesicles drive active and spontaneous release. (pp. 1454).

[Wilhelm et al., 2014] Wilhelm, B. G., Mandad, S., Truckenbrodt, S., Kröhnert, K., Schäfer, C., Rammner, B., Koo, S., Claßen, G. A., Krauss, M., Haucke, V., Urlaub, H., & Rizzoli, S. O. (2014). Composition of isolated synaptic boutons reveals the amounts of vesicle trafficking proteins. *Science*, 344(6187), 1023–1028.

[Williams et al., 1989] Williams, J., Errington, M., Lynch, M., & Bliss, T. (1989). Arachidonic acid induces a long-term activity-dependent enhancement of synaptic transmission in the hippocampus. *Nature*, 341(6244), 739–742.

[Willig et al., 2006] Willig, K. I., Rizzoli, S. O., Westphal, V., Jahn, R., & Hell, S. W. (2006). STED microscopy reveals that synaptotagmin remains clustered after synaptic vesicle exocytosis. *Nature*, 440(7086), 935.

[Woitecki et al., 2016] Woitecki, A. M., Müller, J. A., van Loo, K. M., Sowade, R. F., Becker, A. J., & Schoch, S. (2016). Identification of synaptotagmin 10 as effector of NPAS4-Mediated protection from excitotoxic neurodegeneration. *J. Neurosci.*, 36(9), 2561–70.

[Wostrack & Dietrich, 2009] Wostrack, M. & Dietrich, D. (2009). Involvement of group II mGluRs in mossy fiber LTD. *Synapse*, 63(12), 1060–1068.

[Xin & Radivojac, 2012] Xin, F. & Radivojac, P. (2012). Post-translational modifications induce significant yet not extreme changes to protein structure. *Bioinformatics*, 28(22), 2905–2913.

[Yang et al., 2010] Yang, X., Yea, K., Pang, Z. P., Xu, W., & Südhof, T. C. (2010). Complexin clamps asynchronous release by blocking a secondary ca2+ sensor via its accessory α helix. *Neuron*, 68(5), 907–920.

[Yang & Calakos, 2010] Yang, Y. & Calakos, N. (2010). Acute in vivo genetic rescue demonstrates that phosphorylation of RIM1α serine 413 is not required for mossy fiber Long-Term potentiation. *J Neurosci*, 30(7), 2542–2546.

[Yea et al., 2013] Yea, K., Younts, T. J., Yang, X., Zhou, P., Wu, D., Castillo, P. E., & Südhof, T. C. (2013). Synaptotagmin-12 phosphorylation by cAMP-Dependent protein kinase is essential for hippocampal mossy fiber LTP. *J Neurosci*, 33(23), 9769–9780.

[Yokoi et al., 1996] Yokoi, M., Kobayashi, K., Manabe, T., Takahashi, T., Sakaguchi, I., Katsuura, G., Shigemoto, R., Ohishi, H., Nomura, S., Nakamura, K., Nakao, K., Katsuki, M., & Nakanishi, S. (1996). Impairment of hippocampal mossy fiber LTD in mice lacking mGluR2. *Science*, 273(5275), 645–647.

[Yoshida & Goedert, 2006] Yoshida, H. & Goedert, M. (2006). Sequential phosphorylation of tau protein by cAMP-dependent protein kinase and SAPK4/p38delta or JNK2 in the presence of heparin generates the AT100 epitope. *J Neurochem*, 99(1), 154–64.

[Zalutsky & Nicoll, 1990] Zalutsky, R. & Nicoll, R. (1990). Comparison of two forms of long-term potentiation in single hippocampal neurons. *Science*, 248(4963), 1619–1624.

[Zhu et al., 2009] Zhu, Y., Xu, J., & Heinemann, S. F. (2009). Two pathways of synaptic vesicle retrieval revealed by Single-Vesicle imaging. *Neuron*, 61(3), 397–411.

[Ziv & Arava, 2014] Ziv, N. E. & Arava, F. (2014). Presynaptic and postsynaptic scaffolds: dynamics fast and slow. *Neuroscientist*, 20(5), 439–52.

11 Publications

Parts of this thesis were published in or presented on the following papers and conferences.

11.1 Journal Articles

an Loo KMJ, Rummel CK, Pitsch J, **Müller JA**, Bikbaev AF, Martinez Chavez E, Blaess S, Dietrich D, Heine M, Becker AJ, Schoch S. *Calcium channel subunit $\alpha 2\delta 4$ is regulated by early growth response 1 and facilitates epileptogenesis.* Journal of Neuroscience 2019; [Epub ahead of print]

Engelholm-Keller K, Waardenberg AJ, **Müller JA**, Wark JR, Fernando RN, Arthur JW, Robinson PJ, Dietrich D, Schoch S, Graham ME. *The temporal profile of activity-dependent presynaptic phosphosignalling reveals long-lasting patterns of poststimulus regulation.* PLoS Biology 2019; 17(3): e3000170

Pitsch J, Kuehn JC, Gnatkovsky V, **Müller JA**, van Loo KMJ, de Curtis M, Vatter H, Schoch S, Elger CE, Becker AJ. *Anti-epileptogenic and Anti-convulsive Effects of Fingolimod in Experimental Temporal Lobe Epilepsy.* Molecular Neurobiology 2019; 56(3): 1825-1840

Marvin JS, Scholl B, Wilson DE, Podgorski K, Kazemipour A, **Müller JA,** Schoch S, Quiroz FJU, Rebola N, Bao H, Little JP, Tkachuuk AN, Cai E, Hantman AW, Wang SS, DePiero VJ, Borghuis BG, Chapman ER, Dietrich D, DiGregorio DA, Fitzpatrick D, Looger LL. *Stability, affinity, and chromatic variants of the glutamate sensor iGluSnFR*. Nature Methods 2018; 15(11): 936-939

Pitsch J, Becker AJ, Schoch S, **Müller JA**, de Curtis M, Gnatkovsky V. *Circadian clustering of spontaneous epileptic seizures emerges after pilocarpine-induced status epilepticus.* Epilepsia 2017; 58(7): 1159-1171

Woitecki AM*, **Müller JA***, van Loo KMJ, Sowade RF, Becker AJ, Schoch S. *Identification of Synapto-*

tagmin 10 as Effector of NPAS4-Mediated Protection from Excitotoxic Neurodegeneration. Journal of Neuroscience 2016; 36(9): 2561-2570; ***equal contribution**

Michel K, **Müller JA**, Oprisoreanu AM, Schoch S. *The presynaptic ative zone: A dynamic scaffold that regulates synaptic efficacy.* Experimental Cell Research 2015; 335(2): 157-164

11.2 Book Chapters

Schoch S, **Müller JA***, Schönhense EM, Betzin J. *Liprins, ELKS and RIM-BP Proteins.* Reference Module in Biomedical Sciences 2018

11.3 Poster Presentations

Only first author presentations are listed.

Müller JA, Betzin J, Oprinsoreanu AM, Engelholm-Keller K, Waardenberg AJ, Becker AJ, Graham ME, Dietrich D, Schoch S. *A novel presynaptic kinase, SRPK2, bi-directionally modifies transmitter release in a RIM1/2-dependent manner.* Gordon Meeting. Synaptic Transmission, 2018

Müller JA, Marvin J, Becker AJ, Looger LL, Dietrich D, Schoch S. *Sub-µm Localization of Quantal Glutamate Release with High Temporal Fidelity Based on a Low-Affinity iGluSnFR.* BonnBrain^3, 2018

Müller JA, Engelholm-Keller K, Dietrich D, Graham ME, Schoch S. *Synaptic function of RIM1a: role of phosphorylation sites.* Society of Neuroscience. Anual Meeting, Washington, 2017

Müller JA, Oprinsoreanu AM, Engelholm-Keller K, Graham ME, Dietrich D, Schoch S. *Presynaptic function of RIM1a: role of phosphorylation sites.* BonnBrain^3, 2017

Müller JA, Oprinsoreanu AM, Dietrich D, Schoch S. *Presynaptic function of RIM1a: role of phosphorylation sites.* BonnBrain^{3}2016

Müller JA, Oprinsoreanu AM, Dietrich D, Schoch S. *RIM1a and synaptic plasticity: How to unravel the molecular enigma?.* BonnBrain^3, 2015

12 Acknowledgements

Becoming a Ph.D. is a long, sometimes a very frustrating, but overall a very fulfilling process. A very nice circumstance is the fact, that you meet a lot of amazing people, without whom the preparation of such a thesis simply would be impossible. Here are some words of gratitude to the special people I met during my long journey to where I am today...

My deepest gratitude goes to Professor Dr. Susanne Schoch McGovern. Thank you for being such an exceptional mentor since the beginning of my studies in Neuroscience. Thank you for helping me not only in scientific question, but also when despair, frustration and self-doubt threatened to overhelm me. Many times I would have been lost, without your motivation and your comforting words. It was a real pleasure to perform my Ph.D. studies in your lab and I really am looking forward to stay for another two years to go on with my research.

I am deeply grateful to Prof. Dr. Thorsten Lang, who agreed to be the second refree of this thesis. Moreover, I would like to thank him for our annual meetings to discuss the progress of the project and his helpful questions, critics, comments and suggestions.

A very big influence and impact on my scientific path had and still has Prof. Dr. Dirk Dietrich. Your meticulously way to approach scientific questions, your tremendous amout of knowledge in neuroscientific topics and your sheer endless thirst for knowledge is sometimes simply astonishing. I really want to thank you for supporting me in all the time of my Ph.D. studies.

I cordially thank Prof. Dr. Albert Haas for agreeing to become part of my thesis committee. It is a funny coincidence, that he is now part of my committee (where the graduation journey ends), since it was also him, who left one of the first scientific impressions, when I started to study biology in Bonn (where the journey started).

Moreover, I am grateful to all my colleagues in the AG Schoch/Becker, who contributed to the funny days in the lab and helped me with my problems whenever I got stuck. Especially, I want to thank you for the primary neurons (Sabine Opitz), the adeno-associated viruses, primers and all the mouse work (Lioba, Vivi, Anna, Silke, Pia).

Wirklich phantastisch an so einer Doktorarbeit ist, dass man auch wirklich gute neue Freunde findet:
Indra, vielen Dank für unsere “Montag-morgens-Gespräche” mit den neuesten Updates, Klatsch und Tratsch vom (Fußball)Wochenende. Danke für die eine oder andere spendierte Cola und die ganzen gemeinsamen Mittagessen. Schade, dass wir uns kein Büro mehr teilen....
Katrin, vielen Dank für unsere Diskussionen über wissenschaftliche und alle nicht-wissenschaftlichen Themen. Ich war wirklich traurig als ihr nach Boston gezogen seid. Umso mehr freut es mich, dass ihr nun beide (du und Tony) hier in Bonn arbeitet, sodass wir zumindest noch etwas Zeit gemeinsam verbringen können. Ich wünsche euch nur das beste für die Zukunft zu dritt. Vielen Dank nochmal für die Unerkunft bei meinem Besuch in Boston.
Jule, vielen Dank fürs Zuhören, wenn ich mal wieder Frust loswerden musste. Herzlichen Dank auch für die Einladungen zum Schlittenfahren und zu den Geburtstagen. An dieser Stelle auch einen großen Dank dafür, dass du dich um all die Tierversuchsanträge kümmerst und damit eigentlich erst die Arbeit in unserem Labor ermöglichst.
Anne und Silvia, danke, dass ihr die besten “roommates” seid, die man sich wünschen kann und mich mit Kaugummies am leben haltet.

Ich möchte mich von tiefstem Herzen bei meinen Eltern und bei meinen Geschwistern bedanken. Mama und Papa, ich danke euch, dass ihr mir beigebracht habt “resilient” zu sein. Ich glaube, dass diese die Grundeigenschaft ist, die jeder Wissenschaftler braucht.
Besonders möchte ich mich bei meiner Schwester Melanie bedanken, da ich viele Stunden gar nicht hätte im Labor arbeiten können, wenn sie nicht auf meine Kinder aufgepasst hätte.

Zuletzt, aber auch am wichtigsten, möchte ich meiner Frau und meinen Kinder “Danke” sagen. Marie, Mia und Lukas, ich danke euch für all die Entbehrungen, all die Zeit die man nicht gemeinsam verbringen konnte, all die Samstage, Sonntage, Feiertage an denen ich im Labor war. Danke, für euer Verstädnis jedes Mal, wenn ich frustriert war, wenn ich Kummer hatte, wenn ich es eilig hatte....Ich danke euch für all eure Aurmerksamkeit, für eure Liebe und für euer Vertrauen. Danke, dass ihr für mich die Sonne, der Mond und die Sterne seid.